HYBRID PASSIVE CONTROL SYSTEM FOR SEISMIC RESPONSE MITIGATION OF STEEL FRAME STRUCTURES

MOHAMMAD HOSSEIN MEHRABI

FACULTY OF ENGINEERING
UNIVERSITY OF MALAYA
KUALA LUMPUR

2020

HYBRID PASSIVE CONTROL SYSTEM FOR SEISMIC RESPONSE MITIGATION OF STEEL FRAME STRUCTURES

MOHAMMAD HOSSEIN MEHRABI

THESIS SUBMITTED IN FULFILMENT OF THE REQUIREMENTS FOR THE DEGREE OF DOCTOR OF PHILOSOPHY

FACULTY OF ENGINEERING
UNIVERSITY OF MALAYA
KUALA LUMPUR

2020

UNIVERSITY OF MALAYA
ORIGINAL LITERARY WORK DECLARATION

Name of Candidate: Mohammad Hossein Mehrabi

Matric No: KHA140024

Name of Degree: Doctor of Philosophy, PhD

Title of Thesis: Hybrid passive control system for seismic response mitigation of steel frame structures

Field of Study: Earthquake Engineering, Structural Engineering

I do solemnly and sincerely declare that:

(1) I am the sole author/writer of this Work;
(2) This Work is original;
(3) Any use of any work in which copyright exists was done by way of fair dealing and for permitted purposes and any excerpt or extract from, or reference to or reproduction of any copyright work has been disclosed expressly and sufficiently and the title of the Work and its authorship have been acknowledged in this Work;
(4) I do not have any actual knowledge nor do I ought reasonably to know that the making of this work constitutes an infringement of any copyright work;
(5) I hereby assign all and every rights in the copyright to this Work to the University of Malaya ("UM"), who henceforth shall be owner of the copyright in this Work and that any reproduction or use in any form or by any means whatsoever is prohibited without the written consent of UM having been first had and obtained;
(6) I am fully aware that if in the course of making this Work I have infringed any copyright whether intentionally or otherwise, I may be subject to legal action or any other action as may be determined by UM.

Candidate's Signature Date:

Subscribed and solemnly declared before,

Witness's Signature Date:

Name:

Designation:

HYBRID PASSIVE CONTROL SYSTEM FOR SEISMIC RESPONSE MITIGATION OF STEEL FRAME STRUCTURES

ABSTRACT

Large vibration forces such as from seismic excitations can cause structural damage and structural collapse in the case of intense earthquakes. A large number of novel methods and strategies for seismic retrofitting have been developed and successfully implemented. Any of these techniques has weaknesses and strengths. Several control devices demonstrate a two-step mechanism in which the structure's stiffness is initially raised, and then the dissipation energy phase is engaged upon yielding of the device. This may result in a shift of the first vibration period down to a region where the structural response is significantly increased. The main aim of this thesis is to propose a hybrid passive control system comprises of two phases for the seismic retrofit of moment-resisting steel frames. The first phase is a viscoelastic device called Rotary Rubber Brace Damper (RRBD), consisting of five steel plates and four layers of rubber. The second phase is a cable bracing system bundled with a pre-compressed spring (PCS). The transition between these two phases consists of an increasing stiffness as the system transitions from the viscoelastic RRBD to the cable bracing PCS. In order to develop and prove the effectiveness of the hybrid passive control system, this research is divided into two parts. The first part includes the characterization of rubber compounds and analytical modeling of the RRBD concept with the aim of ABAQUS software. Then, experimental testing was conducted to determine the material properties of the rubber compounds, and, finally, the most promising rubber compounds were selected for possible inclusion in the device. The RRBD functioned at early stages of lateral displacement, indicating that the system is effective for all levels of vibration. The second part of this research focuses on the PCS system. Both experimental and analytical studies were conducted, and no loosening in the cable is observed, as the cables are held in tension by the spring's force; thus, the ability of the bracing system to cause impulses is eliminated. A PCS system design procedure was developed through analytical and experimental testing and then it was used for practical implementation of the proposed system. The overall behavior of the hybrid system during testing demonstrates multi-phased behavior with the capability for energy dissipation at all deformation levels and significant energy dissipation for seismic events. It shows that the proposed hybrid system creates a unique and innovative method which enhances the strengths and offsets the weaknesses of the individual systems.

Keywords: Viscoelastic damper, Cable-braced Systems, Seismic control, Steel frames, Nonlinear response, Hybrid control system

SISTEM KAWALAN HIBRID PASIF UNTUK PENGURANGAN TINDAK BALAS SEISMIK BAGI STRUKTUR KERANGKA KELULI

ABSTRAK

Daya-daya getaran yang besar seperti dari gegaran seismik boleh menyebabkan kerusakan struktur dan keruntuhan struktut dalam kes gempa bumi yang agak tinggi. Sebilangan besar kaedah dan strategi baru untuk pemasangan semula seismik telah dibangunkan dan berjaya dilaksanakan. Sebarang teknik ini ada mempunyai kelemahan dan kekuatan. Beberapa alat peranti menunjukkan mekanisme dua-langkah di mana kekukuhan struktur pada mulanya dinaikkan, dan kemudiannya termasuk didalam fasa pengurangan tenaga semasa pengalahan peranti. Ini mungkin mengakibatkan pergeseran tempoh getaran pertama kekawasan dimana tindak balas struktur meningkat dengan ketara. Matlamat utama tesis ini adalah untuk mengemukakan satu sistem kawalan hibrid pasif yang terdiri daripada dua fasa untuk penambahbaikan seismik bagi kerangka keluli tahan-momen. Fasa pertama ialah peranti viskoelastik yang dikenali sebagai Penampan Penahan Getah Berpusing (Rotary Rubber Brace Damper - RRBD), yang terdiri daripada lima plat keluli dan empat lapisan getah. Fasa kedua ialah sistem perembatan kabel yang dibekalkan dengan spring pra-termampat (Pre-Compressed Spring - PCS). Peralihan antara kedua-dua fasa ini terdiri daripada kekukuhan yang semakin meningkat kerana peralihan sistem dari RRBD viskoelastik ke PCS perembatan kabel. Untuk membangun dan membuktikan keberkesanan sistem kawalan hibrid pasif tersebut, penyelidikan ini dibahagikan kepada dua bahagian. Bahagian pertama termasuk pencirian sebatian getah redaman yang tinggi dan analitikal. pemodelan konsep RRBD. Kemudian, ujian eksperimen dijalankan untuk menentukan sifat bahan sebatian getah, dan, akhirnya, sebatian getah yang paling terbaik telah dipilih untuk dimasukkan kedalam peranti tersebut. RRBD telah berfungsi pada tahap awal anjakan sisi, ianya menunjukkan bahawa sistem itu berkesan untuk semua peringkat getaran. Bahagian kedua kajian ini memberi tumpuan kepada sistem PCS. Kedua-dua kajian eksperimen dan analisis telah dijalankan, dan tiada kelonggaran pada kabel yang dapat diperhatikan, kerana kabel-kabel itu ditahan dalam ketegangan oleh daya spring; dengan itu, keupayaan sistem penahan untuk menyebabkan impuls telah dihapuskan. Prosedur rekabentuk sistem PCS telah dibangunkan melalui ujian analitik dan eksperimen dan kemudian digunakan untuk pelaksanaan praktikal bagi sistem yang dicadangkan. Tingkah laku keseluruhan sistem hibrid semasa ujian menunjukkan tingkah laku berbilang fasa dengan keupayaan untuk pelesapan tenaga di semua tahap ubah bentuk dan pelesapan tenaga yang signifikan untuk peristiwa seismik. Ia menunjukkan bahawa sistem hibrid yang dicadangkan mencipta kaedah yang unik dan inovatif yang meningkatkan kekuatan dan mengimbangi kelemahan bagi kedua-dua sistem individu.

Katakunci: Peredam viskoelastik, Sistem kabel-terembat, Kawalan seismik, Kerangka keluli, Sambutan tak-linear, Sistem kawalan hibrid

ACKNOWLEDGEMENT

First and foremost I would like to thank my supervisor, Associate Prof. Dr. Zainah Ibrahim, for her guidance and support throughout this thesis. Her commitment to advancing the field of structural engineering through research is an inspiration. I feel very fortunate to have been given the opportunity to work with her and to learn from her. I would like to express a great amount of gratitude and appreciation to my former supervisor and current consultant, Dr. Meldi Suhatril who have supervised and have provided assistance that are invaluable, to the success completion of this thesis.

I am, and always will be, grateful to my parents, for their love and selfless kindness despite my repeated mistakes, and for their support during the period of my studies and throughout my life.

Financial support for this project, provided by the University of Malaya, is gratefully acknowledged. Special thanks are also go to the staffs and members of the Heavy structures 2 laboratory, University of Malaya for their support and relentless help provided throughout the period of research.

TABLE OF CONTENTS

TABLE OF FIGURES

LIST OF TABLES

LIST OF SYMBOLS AND ABBREVIATIONS

F_w	Increment of the shear strength of storey using wire-rope bracing
F_s	Increment of the shear strength of storey using spring force
f_u	Tensile strength of cable
l_c	Solid height of spring
l_c	Spring length
n_a	Active coil numbers
A	Dimensional consistency
ADAS	Added damping and stiffness
AFD	Arc-surfaced Frictional Damper
AMD	Accordion metallic damper
ASCE	American Society of Civil Engineers
A_{υ}	Shear area VE layer
BF	Bare frame
BR	Butyl Rubber
BRB	Buckling-Restrained Brace
BRSPD	Buckling restrained shear panel damper
C	Creep strain rate
CCB	Cross cable bracing
C_{e}	Equivalent damping
CP	Collapse prevention
d	Wire diameter
DFMD	Dual function metallic damper
D_m	Mean diameter of the spring
DPD	Dual pipe damper
E	Elastic modulus
E_{d}	Energy dissipation
EDR	Energy Dissipation Restraint
FEA	Finite element analysis

FREI	Fiber Reinforced Elastomeric Isolators
G	Shear modulus
G_1	Storage modulus
G_2	Loss modulus
GFRP	Glass fiber-reinforced polymer
HDNR	High damping natural rubber
HDR	High Damping Rubber
HPCD	Hybrid passive control device
HPCS	Hybrid passive control system
HPMD	Highly plastic material damper
h_υ	Thickness of VE layer
I_1, I_2, I_3	Invariants
IMF	Intermediate moment frame
IO	Immediate occupancy
J_{el}	Elastic volume ratio
K	Bulk modulus
k	Spring constant
k_c	Lateral stiffness of the cable brace
k_{ci}	Cable brace stiffness
K_e	Equivalent stiffness
k_{MRFi}	Moment-resistant frame lateral stiffness
k_{sp}	Spring lateral stiffness
LRB	Lead rubber bearing
LS	Life safety
LVDT	Linear variable displacement transducer
MHD	Multi-action hybrid damper
MRPRA	Malaysian Rubber Producers' Research Association
N_t	Total Coils of spring
n_υ	Number of VE layers
OD	Outer diameter
OMF	Ordinary moment frames

p	Pitch
PCS	Pre-compression Spring
RRBD	Rotary Rubber Brace Damper
S	Stress
S_a	Cable-assembly allowable strength
SAFYD	Shear-and-flexural yielding damping
SMA	Shape-memory alloy
SMF	Special moment frame
S_{min}	Minimum breaking force
SREI	Steel Reinforced Elastomeric Isolator
SSD	Steel Slot damper
SVD	Superelastic viscous damper
TPEA	Tapered plate energy absorber
UHDNR	Ultra-high Damping Natural Rubber
VCD	Viscoelastic Coupling Damper
VE	Viscoelastic
VED	Viscoelastic damper
VEM	Viscoelastic material
VFD	Viscous fluid dampers
VPD	Visco-Plastic Device
W	Hyperelastic equation
β_L , β_R	Inclination angles of the cables
	Phase Angle
δ_s	Stretched or compressed distance of the spring
η	Loss factor
λ_m	Locking stretch
υ	Poisson ratio
Υ	Shear strain
	Circular Frequency
	Safety factor
L_o	Free length of spring
ε	Cable strain

λ	Extension ratio
τ	Torsion of spring

CHAPTER 1: INTRODUCTION

1.1 Background

Former structural design was based on elastic behavior which could result in small lateral load resistance of buildings. In other word, life safety and collapse prevention were the top priorities of late building codes in confrontation with moderate to high seismic loads. On the other hand, the fundamentals offered by recent codes are not sufficient to provide confidence against seismic risk and damage as in major earthquakes casualties are mostly far from being economic. Therefore, there is a demand for structural design capable of controlling both structural and nonstructural damages to reduce the structural damage and repair costs specifically in high seismic prone zones. A solution can be in a new design methodology, performance-based seismic design, and development of new structural systems. Performance-based earthquake engineering can provide a noticeable enhancement in many aspects of seismic performance of buildings through applying new design methodologies coupled with innovative structural elements, systems, and technologies which may result in a desirable control over inelastic deformation of buildings. The available seismic control systems have been categorized into seismic isolation, passive energy dampers, and semi-active and active control systems and these developments basically form the current strategies to withstand against earthquakes.

The structural response attenuation by the seismic control systems is based on a common principle which is generation of motion control force under vibration. Such control power has to be generated according to the mechanism of the selected control system. This is where various motion control devices differ from each other; in passive control devices, the required power is generated by the motion of points of attachments where the device is joined to the structure, hence, the governing factor of the consequent amplitude and direction of these forces is the relative motion of the attachment points. Active control systems include a controller attached to the structure to determine the motion control force via controller input data obtained through a variety of sensors. This mechanism requires an external power source to supply a large control power and this is the drawback of the active control device. The third control device is the semi-active control system which resembles the passive device mechanism in many aspects, i.e. motion force is generated by the attachment point movement, yet requires a battery source to adjust mechanical properties.

Discussing the passive dissipation system, they are grouped into two categories; displacement-dependent and velocity-dependent devices. Displacement-dependent mechanism refers to devices that are designed to yield against seismic excitation or dissipate the energy through sliding friction. Devices such as steel plate dampers and friction dampers belong to this category. The second category, velocity-dependent devices, relies on viscoelasticity to dissipate the energy and they are also called viscous fluid dampers and viscoelastic dampers (VEDs). The mechanism of energy dissipation in velocity-dependent devices is such that they provide damping and (optionally) stiffness to the structures and are suitable for whole range of excitations from weak to strong ones while displacement-dependent devices increase stiffness of structures and this makes them appropriate for moderate to strong excitations only.

According to the earlier discussion each energy dissipation system works in different way with particular strengths and weaknesses. In order to come up with a proper solution to eliminate the system weaknesses a new approach is required to take advantage of all the benefits of energy dissipation devices.

This research presents an innovative application of high damping rubber pads for seismic control of low to high-rise steel braced frames. These pads have always been in use as supplemental energy dissipation devices in structures which have their own independent seismic force resisting system. This research will discuss an investigation of rotary rubber brace damper (RRBD) device coupled with chevron brace. The proposed hybrid passive control system (HPCS) comprises of two passive control methods that form a two-stage mechanism; the first stage consists of a VE solid device equipped with high damping rubber (HDR) material suitable to perform against all deformation levels. This means that in case of minor earthquake and wind forces no structural repair is required. The second stage encompasses a bracing system with a pre-compressed spring (PCS) that bundles the wire-rope bracing members at the intersection point. This phase is set to engage during major earthquakes so as to ensure significant amount of energy dissipation as well as increase of structural stiffness to reduce displacements and provide stability. In this phase damages are localized into elements that can be replaced without affecting the core structure. Such combination of two passive control mechanism forms a unique and innovative technique that leads to enhancement of structural strength and offset of the weaknesses of each method considered individually.

1.2 Problem Statement

The primary focus of design codes such as American standards is to provide life safety and prevent collapse while preserving the integrity of the structure during seismic events is unaccounted. Nevertheless, there are valid concerns about safety and resiliency of structures as seismic events continue to attract global attention. A seismic event like the 1994 Northridge, California earthquake revealed the need of a multi-faceted design approach due to the damage costs and costly interruption in infrastructure which exceeded

$25 billion dollars even though many structures met their performance objectives (National Institute of Standards and Technology, 1994). Several control devices have been developed and demonstrated a two-step mechanism in which the stiffness of the structure is initially raised, and then the dissipation energy phase is engaged upon yielding of the device. Such a mechanism may result in shifting the first vibration period down to a region where the structural response is significantly increased. The main challenge is to develop such systems that increase the lateral resistance of the structure without increasing the structure's stiffness dramatically under low to medium earthquake excitations and yet economical.

VEDs provide extra energy dissipation to the lateral force resisting system by generating larger hysteretic damping (loss factor) and stiffness which causes reduction of storey drift of the frames and therefore retaining elasticity of structural elements.

Nevertheless, damper-equipped frames may be subjected to extremely severe earthquakes and large storey displacement. Therefore, this research is willing to present a new VED called RRBD in addition to a new bracing system for preventing large storey displacement called PCS system. The PCS mechanism applies wire ropes as brace members to entirely eliminate the brace buckling. This method allows the damper to continue dissipating energy when the PCS system engages.

1.3 Research Aim and Objectives

This research aims to develop three effective passive retrofit systems through combined experimental and analytical research. The main objectives of this research are to introduce two retrofitting strategies; VE passive energy device and cable bracing system. The VE passive energy has a controllable mechanism over its seismic performance and shares advantages of a variety of existing dampers. It is fabricated from readily available materials. The cable bracing system incorporates tension only cables and a PCS. Since the cables are permanently set in tension they begin to carry load as soon as a deformation reversal takes place creating a stable bi-linear behavior.

Development of the proposed system requires initial analyses to verify the concepts and development of design procedures. In addition, prototype has to be designed and proof-of-concept testing and design modifications have to be carried out. Therefore, the following specific objectives are to be accomplished:

1. To propose a simple novel VE damper device with low manufacturing costs by conducting finite element analysis and experiments.
2. To propose a new PCS cable bracing system capable of preventing large story displacement, and to develop an analytical model to design the PCS system.
3. To combine the PCS with RRBD and develop a hybrid passive control system and study the parameters which govern the performance of the proposed methods and investigate their influence on the response of multi-story structures under different ground excitations.

1.4 Scope of Work

Scope of this research encompasses the initial development, analysis and testing of the PCS system as well as development and analysis of RRBD device and their effects on structures which take advantage of them, alone and in combination.

Determination of the device configuration was the first step for which several designs were developed and considered. After obtaining the basic design, several highly damped rubber compounds were physically characterized statically and dynamically to find a proper HDR whose data was then utilized to create a material model in the commercial finite element analysis (FEA) program ABAQUS. The test data was applied to calibrate the analytical model. After further development of the obtained basic device configuration, a scale model was fabricated and then subjected to a test to make sure of the functionality of the concept of the device. In addition, an experimental test was conducted to check the practical applicability of the proposed cable cross system as a seismic retrofit system in steel frames.

Investigation of the performance of the proposed systems was carried out through numerical analysis of a selected frame in standard nonlinear structural analysis software. The analysis focused on parameters such as maximum base shear, roof drift, roof acceleration and residual drift. These variables were considered as the primary performance standards. Benefits of the introduced VE concept as well as influence of the cable bracing system in seismic control of structures were demonstrated under various levels of lateral loads. Furthermore, effect of some of the variables associated with the proposed systems was studied.

1.5 Significance of the Research

The research presented in this thesis has proven that, the hybrid passive control system (HPCS) concept provides a unique idea in passive control technology. The combination of the RRBD and PCS makes HPCS, which is a buckling-free element with significant energy dissipation capability and non-deteriorating hysteretic behavior. The loss factor and the dynamic stiffness of the device remained relatively unchanged throughout the tests. The overall behavior of the HPCS during testing demonstrates multi-phased behavior with the capability for energy dissipation at all deformation levels and significant energy dissipation for significant seismic events. Furthermore, the results revealed that the proposed HPCS can restrain storey drift to within the specified range under severe seismic motions. The hybrid system has a re-centering effect on the vibration center and a deformation dispersion effect along the height.

1.6 Thesis Outline

Chapters of this thesis are arranged as follows;

Chapter 1 presents an introduction to the current research through problem definition, introducing the proposed solutions along with scope of the work and the approach applied in the course of this research.

Chapter 2 gives an extensive literature review of previous researches with regard to the relative developments and conceptual changes of lateral resisting and passive control systems.

Chapter 3 provides the research methodology of this study that is under investigation in order to evaluate the proposed systems's performance with respect to their various components. The test setup and instrumentations of the experimental test along with material properties of utilized steels, wire ropes and PCSs are presented. The experimental effort is separated into three sections: tests of HDR material, producing new VE damper and its components and describing the advantages, and cyclic lateral loading of the specimen. Furthermore, a portion the study is allocated to constitutive models of rubber behavior and its analytical modeling.

Chapter 4 presents comprehensive analyses of all system combinations subjected to various seismic loads to identify the best system performance. The obtained test results are initially utilized to generate analytical models of HDR compounds and then a nonlinear finite element analysis (FEA) is employed to check functionality of the device and verify whether theoretical basis of the device can be analytically supported. Following portion of this chapter presents discussion of the results associated with nonlinear dynamic response history analysis. Design procedure of the PCS system in addition to test methods of characterizing the considered rubber compounds for practical application is presented.

Chapter 5 highlights the major findings and conclusions of this research and then finalizes this thesis with recommendations for future work.

CHAPTER 2: LITERATURE REVIEW

2.1 Introduction

Seismic design has moved forward during the last decades to provide well-performing seismic resistant structural systems. Such developments root in several reasons among which loss of lives is the top one. Technological advancements as the result of this ongoing demand came into practice to improve the buildings' dissipation capacity in addition to special detailing of plastic hinge locations to upgrade the conventional seismic design from simply satisfying the life safety limit state to the level in which multiple limit states are considered called performance based engineering. In this regard, energy dissipation devices and lateral bracing systems were designed. In the following, a brief background and a comprehensive review of the related literature is presented.

2.2 Background

Damping is defined as the ability of a structure or a material in dissipating energy and persistently reducing the vibration amplitude. Considerable research has been conducted to represent and quantify the damping nevertheless, it is a very abstract quantity. Any structure has a number of means to dissipate energy such as friction between steel connections, friction between structural and nonstructural components and opening and closing of micro-cracks in concrete. The associated mechanism of damping in a structure is mathematically represented by damping ratio. This is in fact an idealization since it is almost impossible to get to an accurate damping value unlike mass and stiffness which are obtained from dimensions and sizes of structural elements.

Building resistance against natural forces has been a challenge for structural engineering. These forces encompass a large group of loads that any structure encounters including gravity loads, i.e., live and dead loads, self-weight, human occupancy and non-structural components, snow and rain ponding and in some situations other forces like flood loads, hydrostatic and soil pressure have to be included. Other challenging loads which are critical to structural performance and safety due to resulting deformations are wind and earthquake loads. In confronting wind loads the necessitated aspect of structural resistance is stiffness of the system to attenuate both horizontal displacement and vibration down to human perception threshold. An entirely different case is seismic loads. Strengthening of structural resistance system to accomplish a merely acceptable seismic design is a simple and primary solution which is only effective in areas with low level of seismicity. However, simple strengthening is not feasible because it adds on stiffness to building and therefore its period is reduced and subsequently the inertial loads are increased. This increment of inertial loads raises the need of greater strength. The greater the strength is, the larger acceleration of building becomes and that causes severe damage to the structural and non-structural contents of building. On the other hand, an appropriate combination of stiffness, strength and ductility leads to an effective seismic design. Stiffness and strength are both in charge of reducing deformation during earthquake. Dissipation of energy is provided by ductility of the structure through yielding of structural components without collapsing. The cost of ductility however, is the structural damage beyond repair to an extent that re-occupying the building imposes significant costs.

In order to tackle this problem, several methods have been developed by engineers to control the structural response. These methods are based on new elements to be introduced in structures to absorb or redirect the input energy so that the main structure does not undergo the whole imposed forces.

2.3 Structure control system

Natural hazards and service loads create different types of dynamic loads against which structural response has to be controlled and reduced. In order to do so, structural control systems can be employed. These systems are supposed to provide the necessary strength, ductility or energy dissipation capacity for structural systems to save lives and to ward off the collapse. In addition, regardless of the hazard, any structures with embedded structural control systems should be able to withstand the external load while it is still functional with minimal repair. Although these control systems increase the up-front building construction costs, however, protection of occupants and reduction of casualty has the priority over initial investment. Structural control systems are generally categorized into four main groups; passive, active, semi-active and hybrid. This classification is according to their operating mechanisms, (cheng et al., 2001; Ikeda, 2009; symans et al., 2008). Further illustration of modern structural control systems are presented in the following.

2.3.1 Active control systems

This type of system has the ability to apply a force to the structure as a controlled response to the unpredictable vibrations induced by different dynamic loadings. Such error activated control system as proposed by Yao (1972) reduces the dynamic response for different vibration modes. These systems operate through a network of controllers, actuators and sensors and require a significant energy to counteract dynamic loadings, as shown in Figure 2.1. This means that active control systems necessarily need an energy supply which cannot be guaranteed during several natural hazards due to probable failure. On the other hand, presence of this network makes the system complicated. Controller is in charge of monitoring the applied forces and induced displacements obtained by sensors. The controller then decides the response of the system in return and determines what the actuator can do as a reaction to the external excitation to bring the building back to its undeformed condition. The sensors may be strain gages, fiber optics, accelerometers etc. The way active control systems operate has the disadvantage of pushing the structure into an undefined or unstable state, (Christenson, 2001). This system, however, is adaptive to ever-changing excitations.

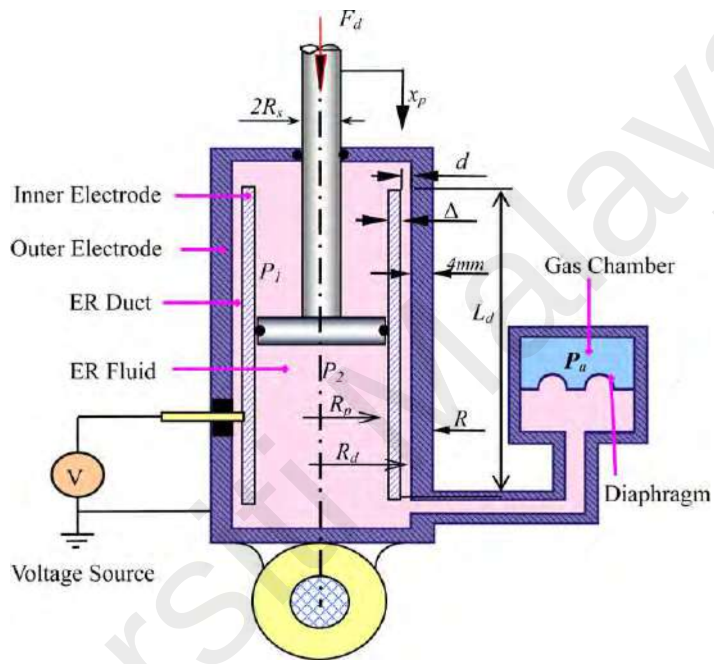

Figure 2. 1: Schematic configuration of the ER damper (Nguyen et al., 2012)

2.3.2 Semi-active control systems

Semi-active control systems share an advantage of “controllability” or “intelligence” with active control systems. Although semi-active control systems are a natural extension of passive control systems, they are adaptive systems which adjust the behavior of dampers based on the data relating to the excitation and structural response. The system encompasses sensors to measure the input and/or output, a control computer which is in charge of measuring and supplying control signal for the actuator, a control actuator to regulate performance of passive device, and a passive damping device with limited control potential. In semi-active control systems unlike the active ones, the actuator is used not to directly apply a force to the structure, but instead to control the device's properties. This demands a relatively moderate power supply which can be provided by batteries. This is an advantage over active control systems which makes this control system reliable during an earthquake. Some of semi-active control devices can be listed as electrorheological (ER) fluid, variable-orifice fluid dampers and magnetorheological (MR) fluid (Spencer and Nagarajaiah, 2003; Symans and Constantinou, 1999).

2.3.3 Hybrid control systems

Active and semi-active control systems were primarily discussed to highlight their properties. As was mentioned earlier, active and semi-active damper devices share the advantage of adaptability and intelligence, however, compared with active control systems, the capacity and intelligence of both semi-active and passive control systems are restricted. On the other side, active control systems suffer major drawbacks including the need of external power supply, sensor arrays, signal processing system and substantial force-generating equipment. This issue limits control reliability and increases the complexity and cost of the system, (Cheng et al., 2010). In order to tackle the aforementioned problems and to obtain advantages of the three control systems (passive, semi-active and active), another type of control system has been developed by combining these control systems whose impact of drawbacks is minimized. This new system is referred to as hybrid control system.

Presence of active and passive device offsets the weakness of each one by minimizing the role of active controller and maximizing the advantages of passive damper. The active controller is only effective for severe ground motions while the passive system is set to be effective during small and moderate seismic events. The passive device is in charge of achieving the bulk of the response reduction which is needed for structures to stay within the desired performance range. The active device is responsible for adjusting and tuning the structural response, e.g., to reduce deformations and accelerations to protect sensitive equipment in the building. Such combination has no large control forces, therefore, it is more reliable as it requires less energy compared to active control systems (Cruz, 2003 and Christenson, 2001). Further discussion on the benefits of hybrid control system with some of its recent applications is presented in the literature, (Love et al., 2011 and Khodaverdian et al., 2012).

2.4 Passive control systems

In order to have a reliable and accurate prediction of seismic response of a building equipped with passive damper device, a detailed analysis with parametric study concerning influence of passive damper device in controlling structural behavior is needed. Dissipation of energy through passive control devices relies on isolation and energy dissipation devices. Mechanism of the damping generation is according to local structural response, i.e., the relative movement of the structure, (Cheng et al., 2010). This control system is inherently stable and unlike the active or semi-active control systems, there is no need for external energy and response measurements to operate. Passive dampers are simple to design and construct, (Christenson, 2001).

There are various types of passive dissipation devices with multiple configurations. Two general categories of passive damper devices are namely rate-independent and rate-dependent. Mechanism of rate-independent type depends on the displacement transferred to the device from structure. Examples of this type are such as metallic yielding, friction and shape-memory alloy (SMA) damper, (Whittaker and Aiken, 1993). Those dampers that belong to rate-dependent type can be listed as viscous fluid dampers (VFD), VE solid dampers and viscous damping walls and their energy dissipation mechanism and capacity rely on both velocity across the device as well as displacement depending on which VE material is utilized.

Structural control systems were ever created and employed in civil engineering to improve the seismic resistance of buildings by reducing and dissipating detrimental dynamic loads. For structural engineering applications, as described by Uang and Bertero (1990), the classical energy conservation law has the following form:

$$E_i = E_k + E_s + E_h + E_\zeta \tag{2.1}$$

Where E_i represent energy input exerted to the system from earthquake, E_k stands for kinetic energy, E_s and E_h are the recoverable strain energy and irrecoverable energy due to dissipation by inherent damping respectively. The energy dissipated by supplemental device is shown by E_ζ. A superior solution to survive significant seismic events with no collapse is adding energy dissipation capacity into the system so that the primary structural elements designed to support gravity loads experience less damage and remain elastic. Application of supplemental dampers at the base level of buildings is called base isolation or earthquake protection systems which reduces the input energy and deflects it through decoupling the structure from the ground, (Naeim and Kelly, 1999).

Dynamic vibration absorbers are another class of control systems. Mass dampers, tuned liquid dampers and tuned liquid column dampers belong to this class. Performance mechanism of this type is based on tuning to a specific frequency, which is usually the first mode, to decrease vibrations at that specific frequency. This limits their application since the device has to remain in elastic range for optimal performance, (Constantinou, 1998). Reinforced concrete (RC) structures and steel structures have shared the major part of application of structural control systems. Compared to RC and steel structures wood structures have a higher level of inherent damping capacity, up to 15%, which may also cost inelastic damage to the structure. Wood structures were subjected to investigation by Symans et al. (2002) to study their seismic performance of these light framed timber structures equipped with passive energy dissipation and base isolation systems. Comparison between the existing passive energy dissipation systems of the time was conducted by Constantinou et al. (1998). A comprehensive review of passive damper devices was later presented by Symans et al. (2008) to highlight the merits and demerits of these dampers concerning their hysteric behavior, physical models and construction.

For better illustration, Figure 2.1 shows three levels of damping and their influence on linear acceleration-displacement response spectra whose vertical axis represents lateral acceleration associated with base shear against variation of displacement represented by horizontal axis. In the figure different periods of vibration are shown by diagonal lines expanded from the origin. Consider an original structure with fundamental period best described by the middle diagonal line and 5% damping. This pinpoints the response at point A. in case of increasing the stiffness, the period also increases and shift the point to the upper diagonal line where point B is located. Referring to the horizontal and vertical axis shows that shift results in reduction of displacement at the expense of greater intensity of base shear. Base isolation would reduce the first mode period of the structure from point A down to the point C on the lower diagonal line. As described by the figure, point C is associated with larger displacement and reduction of forces.

Other than increasing the stiffness and base isolation, adding to the damping capacity or energy dissipation can be considered as an option as well. Assuming the damping increment from 5% to 20% for the base structure yields the shift of point A to point F with less displacement and base shear. This also happens in case the base isolated structure is provided with larger damping and can be shown by the shift from point C to E. Similarly a shift from point B to D happens on the upper diagonal line associated with larger stiffness if more damping is added and consequently reduced response for both quantities can be observed. It has to be mentioned that such base shear reduction is true only if the structure remains elastic and if it enters nonlinear range the behavior would be highly unpredictable.

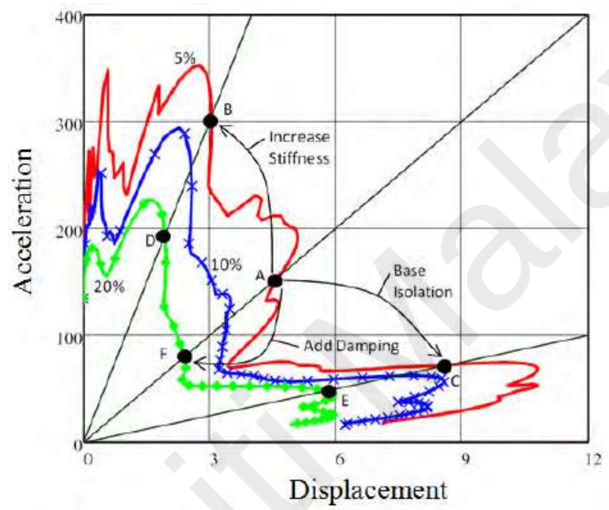

Figure 2. 2: Acceleration-Displacement Response Spectrum (Marshall, 2008)

2.4.1 Base isolation devices

A design methodology to lengthen the fundamental period of the structure as well as reducing the acceleration response is base isolation. This earthquake resistant system serves so by decoupling a structure at foundation level by installing isolating bearings which are accordingly designed to withstand the associated increased displacement contracted in the isolation layer.

As a matter of fact the challenging issue is occurrence of the resonance. This happens when a short period excitation shakes a building with a short period like low-rise buildings that are stiff. Earthquakes mostly have high frequency energy content and this energy content translates to a short period, (Gemme, 2009). That is where base isolation is a useful strategy. The effectiveness of isolation system is function of three principle feature; Firstly, sufficient lateral flexibility or in other words low lateral stiffness. This feature lengthens the building's period to sufficiently reduce the seismic demand. Secondly, a practically limited displacement of the system which is obtained by the employed isolator itself or by supplemental dampers. Thirdly, adequately high initial lateral stiffness to make sure that service loads such as wind or minor earthquakes do not adversely affect the structure, (Chen and Scawthorn, 2003).

Utilization of steel as the reinforcing element in the bearings is a cost factor of isolation system. The manufacturing process is such that steel needs to be prepared for vulcanization bonding to the rubber by cutting, sandblasting and cleaning, (Kelly and Takhirov, 2002). Presence of steel in the manufacturing process of the elastomeric bearings adds on a substantial weight which increases the cost of transportation as well as installation. Nevertheless, because of the higher level of safety provided by this system to both occupants and structures, this system is being implemented. Referring to the value in the increased level of safety, base isolation initiatives such as the one by Iran's Ministry of Housing and Urban Development are provided globally. For instance in a particular project in the towns of Parand and Hashtgerd near the capital Tehran, base isolation for entire city blocks are to be installed, (Naderzadeh, 2009).

Kelly (1999), Moon et al. (2002) and Mordini and Strauss (2008) studied application of various fiber reinforcing materials and concluded that carbon fiber can be a good replacement for steel. Kelly (1999) had formerly reported the comparable performance of fiber reinforced elastomeric isolator (FREI) and steel reinforced elastomeric isolator (SREI) bearing which has been also highlighted through experimental testing by Koh and Kelly, (1988), Moon et al. (2002), Toopchi-Nezhad et al., (2007b) and Toopchi-Nezhad et al., (2008a).

The performance mechanism of seismic isolation devices is based on deforming in shear. This means that the energy dissipation is done by the rubber alone or in conjunction with a lead core. Among the base isolation systems, elastomeric, sliding and hybrid systems are a few most widely used ones. The elastomeric bearings have the advantage of providing a restoring force with no residual deformation and displacement of the isolated building after a seismic event. During earthquake the entire base isolated structure moves at the base level like a rigid body. This is allowed by placement of a low friction material beneath the superstructure. Such solution had been formerly brought into the practice by placing materials like sand or talc beneath the structure. Combination of elastomeric and sliding bearings yields a hybrid system to obtain the desired seismic performance.

Those isolation systems that slide at early stages had an undesirable property which was permanent displacement. This problem was originated due to lack of a restoring force required to bring the isolation system back to its original position. Absence of isolation system realignment is a noticeable issue especially for utility connections of the structure below ground level. In order to tackle this problem, Friction Pendulum System (FPS) was developed by taking advantage of a concave sliding surface to provide a gravity-related restoring force for re-centering the bearings. Figure 2.2 shows a schematic of a FPS by which weight of the superstructure is carried on the concave surface while sliding isolation systems have curved surfaces on both top and bottom plates, (Myslimaj et al., 2002).

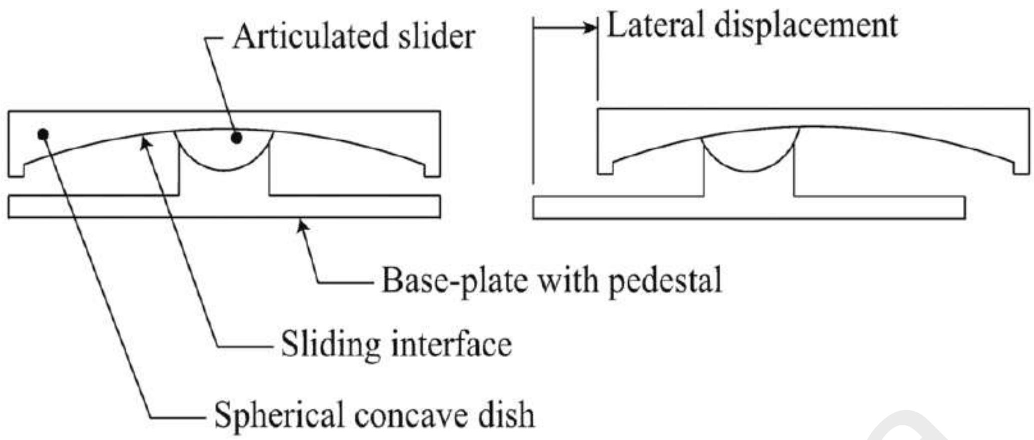

Figure 2. 3: Schematic of a friction pendulum bearing (Symans et al., 2002).

High damping natural rubber (HDNR) has been utilized as an elastomeric material laminated in the bearings to provide both horizontal flexibility and energy dissipation. The following part of the review will focus on HDNR and its implementation as a base isolation material.

Laminated bearings made with HDNR take advantage of non-linear stress-strain nature of HDNR as shown in Figure 2.3. At strains below 20%, a high initial stiffness is provided by HDNR where in strains up to 150% or 200%, there is a reduction in its stiffness providing the horizontal flexibility required for isolation. For higher ranges of strains, the HDNR shows a hyperelastic or stiffening behavior providing a stopgap against excessive displacement or failure of the bearing, (Fuller et al., 1996a). Occurrence of these levels of HDNR stiffness depends on its specific compound. Furthermore, the inherent damping of this material is beneficial as the need for a supplemental damping element to limit displacement is eliminated. This advantage helps designers for a simpler isolation system, (Derham et al., 1985). The first implementation of filled natural rubber was done by Derham, Kelly and Thomas in a ten-year study conducted in the University of California at Berkeley cooperated by the Malaysian Rubber Producers' Research Association in England. Study on the properties of HDNR compounds revealed that in shear modulus range of 480 to 1200 kPa and material loss factor over 11%, there are various compounds of carbon-black filled natural rubber. According to the test results reported by Fuller, Ahmadi and Pond, based on unfilled natural rubber bearing, over a 37-year period stiffening of 5-15% happens while due to different chemistry of HDNR, material stiffening of 20% was reported from further laboratory ageing tests. The damping and dynamic modulus were the two parameters that showed a smaller change compared to stiffness properties over time. It was also exhibited that there is a tendency of inherent damping increment above the current values, (Fuller, 1996b).

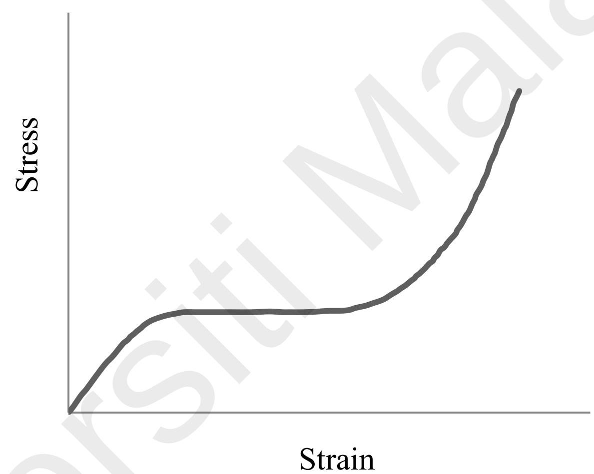

Figure 2. 4: Schematic Stress–Strain Curve For Rubber (Behnamfar et al., 2015)

The laminated elastomeric bearings with reinforcement were developed when unreinforced blocks of rubber were realized to have an adverse effect of rocking. Reinforcement is in the form of thin sheets made of steel often referred to as shims. Moon et al. (2002) discussed that fiber materials can be used as an alternative reinforcement for steel. Steel Reinforced Elastomeric Isolator (SREI) bearings have been the most common type of base isolation for several decades. This is because implementation of steel reinforcement can provide high vertical stiffness so that bulging of the bearing undertaking the weight of superstructure as well as rocking of the system as the result of lateral and vertical motions are prevented, (Naeim and Kelly, 1999). Two main types of SREI bearings include one with elastomer and steel and the second one is a lead rubber bearing (LRB). The LRB type was invented in 1975 in New Zealand. The lead cores in this type of bearing is in charge of providing an initial stiffness to resist against service loads like wind, while at the design loads the lead core(s) yield(s) to provide hysteretic damping. A regular SREI and LRB with lead core are shown in Figure 2.4.

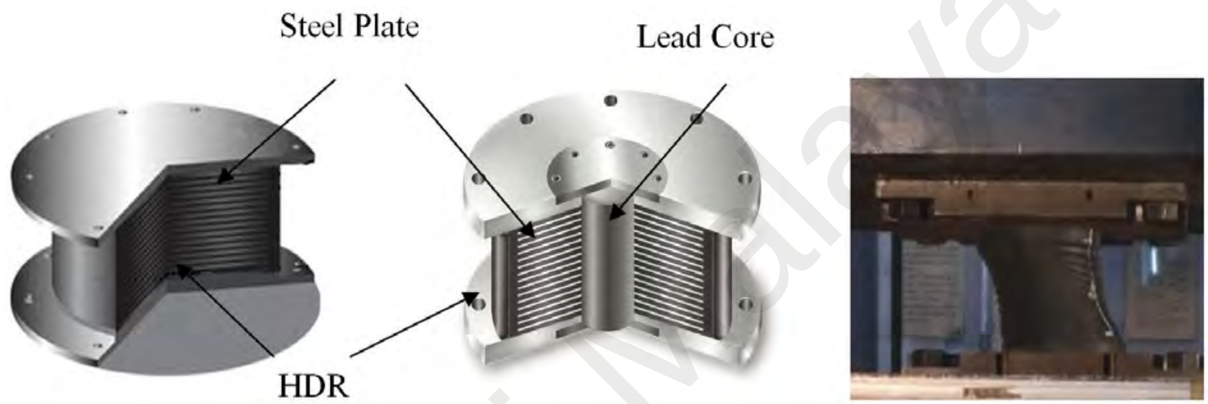

Figure 2. 5: Seismic Isolators (Shen et al., 2016)

A relatively new type of elastomeric bearing is Fiber Reinforced Elastomeric Isolators (FREI). Application of fibers gives the benefit of decreased weight and cost while FREI uses principle of low lateral stiffness similar to SREI bearings. Different types of fiber fabric reinforcement such as glass fiber are compared to steel by Mordini and Straws, (2008) and Kelly and Takhirov (2002). Kelly (1999) constructed a fiber reinforced elastomeric bearing using damping rubber with the properties of roughly 8% equivalent viscous damping at 100% shear strain. The test showed that at the same level of shear strain, the damping was 15% revealing that a larger part of energy is dissipated by the composite structure of the bearing than the rubber alone. The extra dissipation of energy was assumed to be related to the friction between individual fibers, (Kelly, 1997).

A large body of studies has been designated to physical behavior modeling of carbon filled rubbers to tackle the associated complexity. HDNR has complex material properties along with nonlinear stress-strain behavior with a continuously varying stiffness. In addition, the damping mechanism is combination of its both hysteretic and viscous features.

2.4.2 Hysteretic devices

The energy dissipation mechanism associated with this type of damper device is independent of loading rate. Metallic dampers and Friction dampers belong to this type. Metallic dampers dissipate energy by yielding of metal. Friction dampers, as the name suggests, damp the energy by dry sliding friction, (Constantinou et al., 1998). Application of these devices significantly alters dynamic behavior of structures through addition of initial stiffness and energy dissipation and may yield and deform plastically under probable extreme excitation. Mechanism of this type can help to provide protection against wind load, however, adding stiffness and shortening the period of structure can act as an earthquake attractor, though increasing the input seismic energy. Idealized rate-independent hysteresis loops of these dampers are illustrated in Figure 2.5.

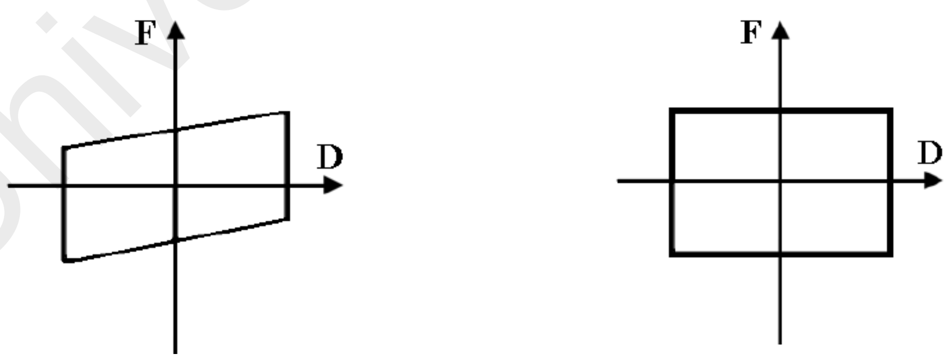

a) Metallic Damper b) Friction Damper

Figure 2. 6: Rate-Independent Idealized Hysteresis Loops (A. Chopra)

2.4.2.1 Metallic Dampers

This type of dampers takes advantage of metals' ductility to dissipate energy. The standard metal for this damper is mild steel and application of load and shape memory alloys (SMA) has been also studied by Towashiraporn et al., (2002). Di Sarno and Elnashai (2003) discussed stainless steel and aluminum alloys as contenders suitable for such seismic protection devices. Investigations over metallic yielding devices with the aim of seismic energy dissipation got started in the 1970s by Kelly et al., (1972) and Skinner et al., (1975). Some of the early presented metallic dampers were torsional beams, U-shaped plates and flexural strips. Early researches were then followed by studies over added damping and stiffness (ADAS) devices in which shaped plates were installed to dissipate energy.

2.4.2.1.(a) Added Damping and Stiffness (ADAS) Device

A series of tapered parallel plates connected to structural element like a beam at the top and attached to a chevron brace at the bottom typically form ADAS devices as shown in Figure 2.6. Plates were formerly X-shaped or hourglass, (Bergman and Goel, 1987; Whittaker et al., 1991). Triangular shaped plates are also alternative energy absorbers and were reported to be effective at dissipating energy, (Tsai and Tsai, 1995; Tsai et al., 1993). The dissipation mechanism is designed such that the most energy dissipation throughout the plates is achieved per volume of steel. The design feature of the ADAS devices allows bending about the weak axis.

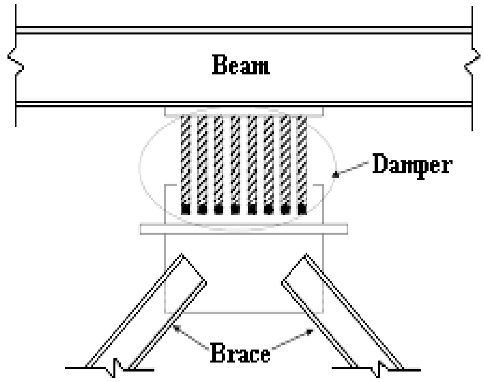

Figure 2. 7: Chevron Brace Configuration for ADAS/TPEA Device (Chan et al., 2008)

The hourglass shape of the plates with their clamped ends result in double curvature bending in addition to uniform yielding of the plates over their height. The tapered plate energy absorber (TPEA) device has clamped-pinned end conditions. The triangular shape and X-shaped plates yield over the entire plate. Geometry of ADAS and TPEA devices are shown in Figure 2.7 and 2.8 respectively.

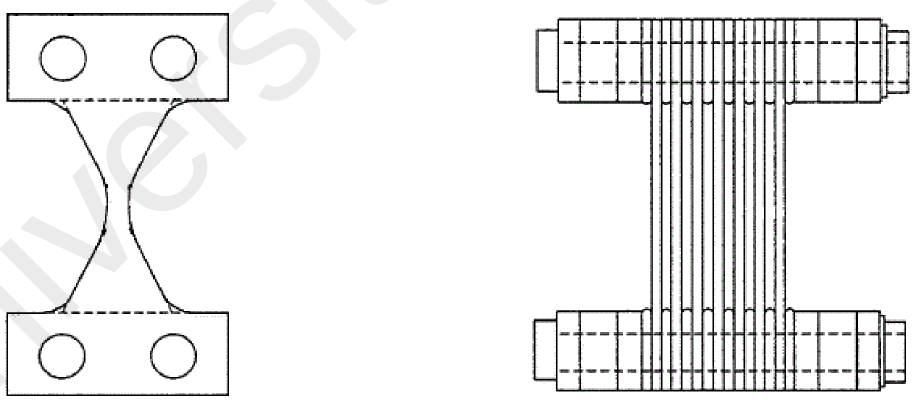

Figure 2. 8: Additional Damping and Stiffness (ADAS) Device

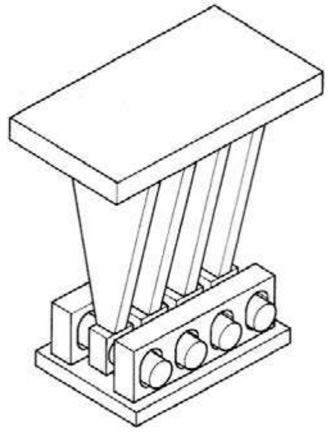

Figure 2. 9: Triangular Plate Energy Absorbing (TPEA) Device (Tsai et al., 1995)

Some of the applications and related studies of ADAS devices are discussed in the following. Among the buildings equipped with this device, there is a reinforced concrete (RC) building in Mexico City subjected to retrofitting of the peripheral structure as well as the buttresses with ADAS devices, (Martinez-Romero, 1993). Another building known as Wells Fargo Bank in San Francisco has been retrofitted due to damages from the Loma Prieta earthquakes and equipped with ADAS devices connected to chevron braces, (Perry et al., 1993). Early researches on plate dampers showed their effective applications because of reduction of displacements through additional stiffness provided. This is in addition to the resulting energy dissipation capacity supplied for structure through a stable and repeatable hysteresis.

Comparison between retrofit with ADAS device and retrofit with steel brace revealed that advantage of ADAS elements is superior to the other one when employed in a damaged building after Mexico City earthquake, (Tena-Colunga and Vergara, 1997). An exceptional dynamic behavior of a four-storey steel structure in Iran was concluded after retrofitting with ADAS device, (Tehranizadeh, 2001). Another application to be listed here is a tension only cable system with crossed cables which slip or rotate at the ends allowing the ADAS device to dissipate energy, (Phocas and Pocansch, 2003). Experiments using rhombic shape plate as an alternative to former plates along with utilization of low yield strength steel (LYS) reduced weaknesses of the original device, (see Figure 2.9). In order to maintain fixity and to achieve the prescribed condition at the centre of the plate, using symmetry is necessary in this device. Moreover greater degree of strain hardening as well as improved ductility associated with LYS compared to A36 steel lessens occurrence of failure due to fatigue and fracture under cyclic loading, (Shih et al., 2004).

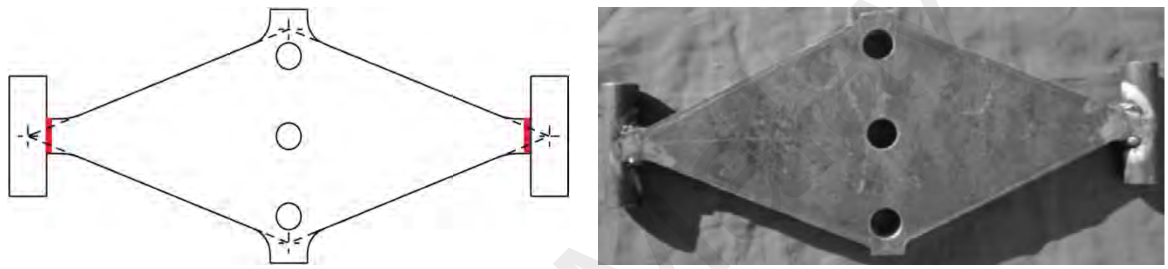

Figure 2. 10: Rhombic Low Yield Strength Steel (LYS) Plate (Han et al., 2014)

Another kind of ADAS devices is called Longitudinal ADAS (LADAS) shown in Figure 2.10. Yielding mechanism of LADAS resembles that of LYS rhombic device, however, form of installation is in diagonal or horizontal brace unlike ADAS devices that should be directly attached to a beam. Tsai et al., (2005b) discussed the reduction of seismic response of structures through implementation of LADAS device.

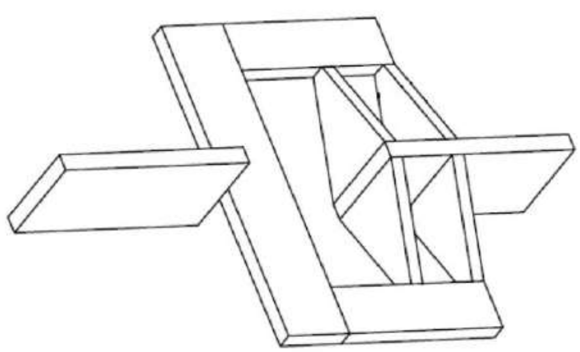

Figure 2. 11: Longitudinal Added Damping and Stiffness Device (Tsai et al., 2005)

2.4.2.1.(b) Yielding Inner Frame

According to Tyler (1985), the concept of yielding inner frame was first suggested in the late 1970s by David Smith and Robert Henry of Auckland, New Zealand. Physical form of the frame was a solid round bar shaped into rectangular. Corners of the frame were connected to each end of an X-brace, (Figure 2.11). When the frame was subjected to loading it would form like a parallelogram and therefore dissipation of energy would be provided through yielding of the system. Tyler conducted experimental test and found successful performance of the frame up to 200 cycles. Constant cross-section of the yielding component was a weakness of the primary device.

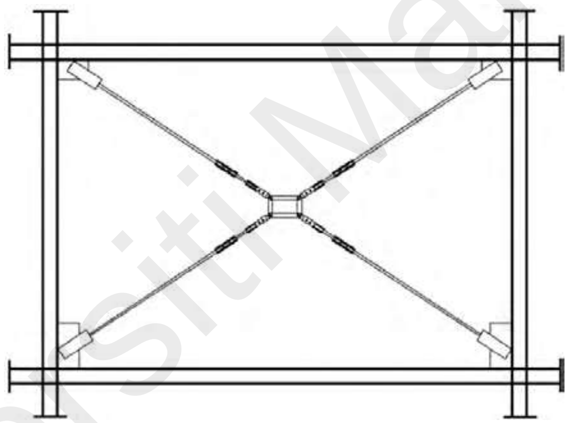

Figure 2. 12: Yielding Dissipative Bracing (Tyler, 1985)

In order to provide a larger material volume to yield, new configuration with varying cross-section was selected as was the case for ADAS and TPEA devices. To do so, the moment diagram and the cross-section were matched up by adding extra plates or tapering them, (Ciampi and Samuelli-Ferretti, 1990). Some of the sketches are provided in Figure 2.12.

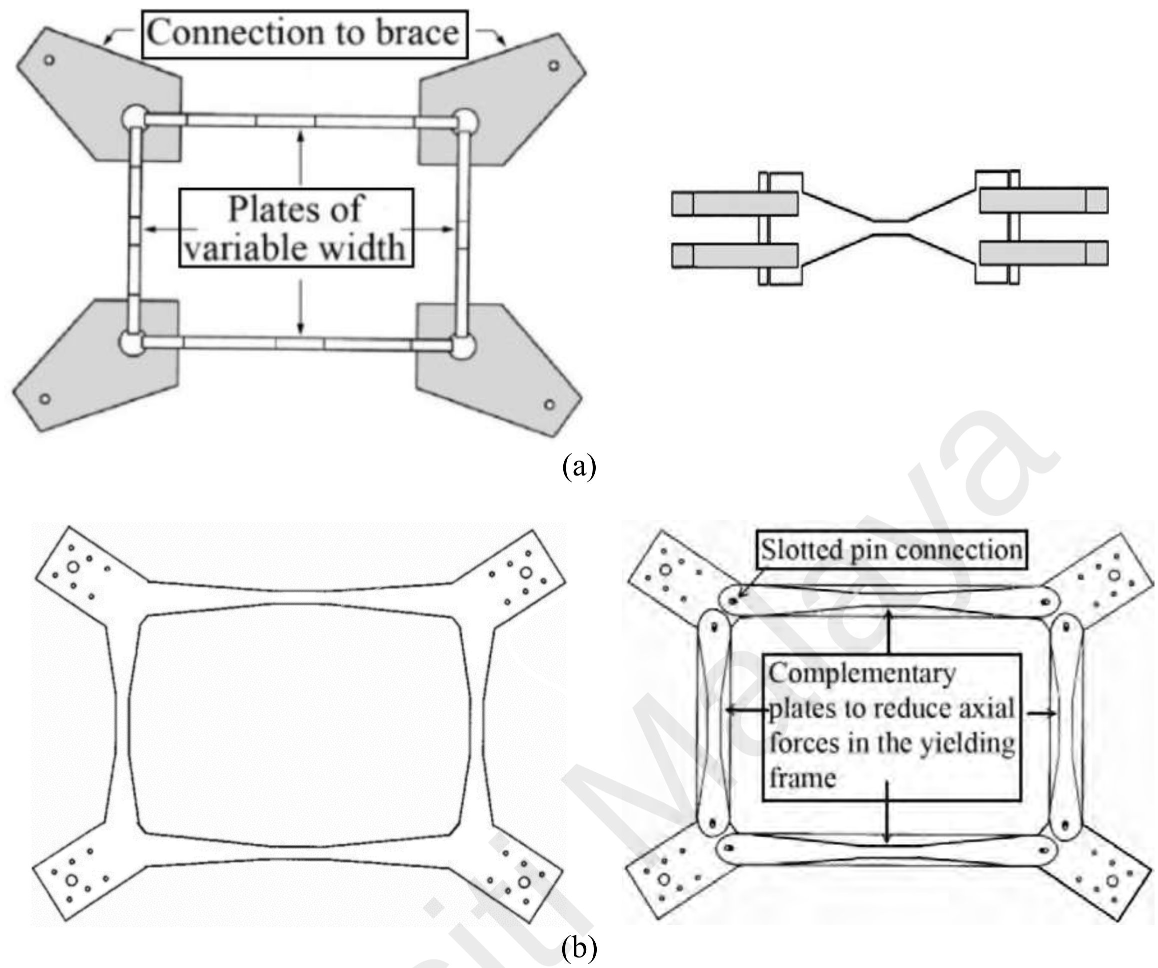

Figure 2. 13: Yielding frames with variable cross section for deployment in cross-bracings (Ciampi and Samuelli-Ferretti, 1990).

Other plate-bending metallic damper devices have E-shaped and C-shaped yield components, (Ciampi et al., 1993; Ciampi, 1995). The C-shaped elements have variable cross-section and act as curved beam-column. This design leads to nearly uniform yielding along the length of the element. As shown in Figure 2.13, these elements are installed within inverted V-braced frame whose performance is expected to be in elastic range both in tension and compression while the device is supposed to deform plastically.

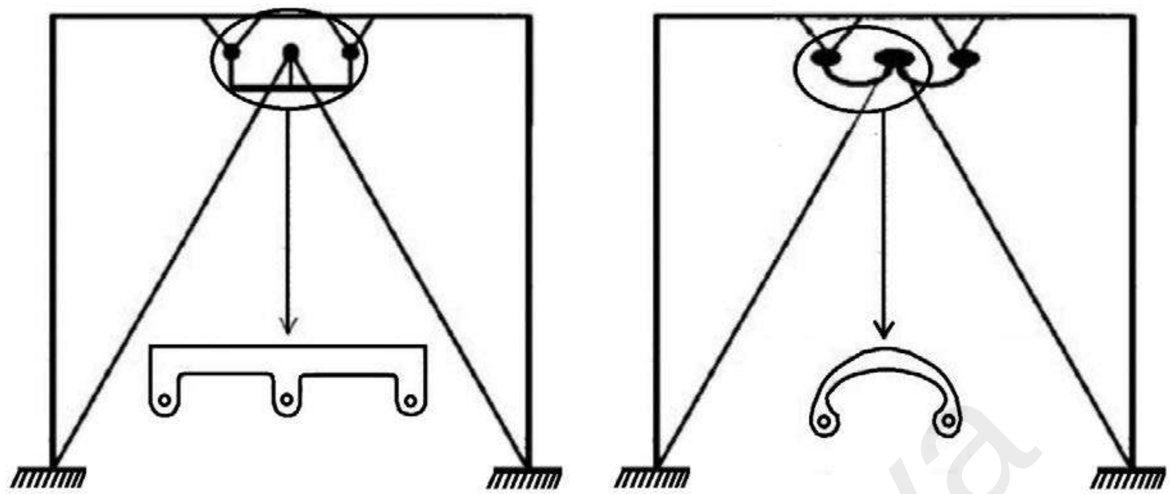

Figure 2. 14: E-shaped And C-shaped Dampers (Ciampi et al., 1993**)**

A new form of lightweight dissipative bracing system was developed at the university of Rome ‘La Sapienza’. The configuration of the bracing system is such that C-shaped damping elements are connected to a hinged rectangular frame. Corners of the frame are attached to tension-only cross bracing whose elongation or shortening under loading result in yielding of C-shaped element in addition to deformation of the frame into a trapezoid. When the frame is located at the centre of the bay, it is called the articulated quadrilateral. Figure 2.14 shows the configuration of this device. Effectiveness on this device was verified through a shaking table test conducted for a two storey steel frame, (Ciampi, 1995; Ciampi et al., 1993; Emanuele Renzi et al., 2006).

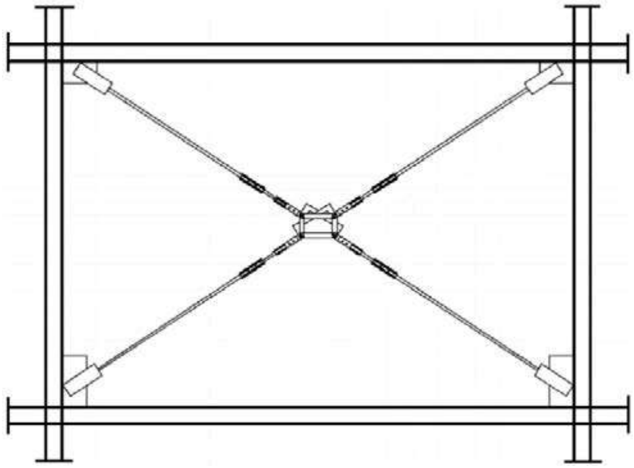

(a)

(b)

Figure 2. 15: C Shaped Dissipative Device, Test Setup Structure With Bracings, Installed On The Shaking Table (Renzi et al., 2006)

2.4.2.1.(c) Buckling-Restrained Brace (BRB)

In order to tackle the disadvantage of concentric braces which was buckling under compression, the steel core was restrained so that deforming and yielding would occur without buckling. This solution increased the ductility and energy dissipation capacity on BRBs. The hysteresis associated with a conventional and a buckling-restrained brace are shown in Figure 2.15.

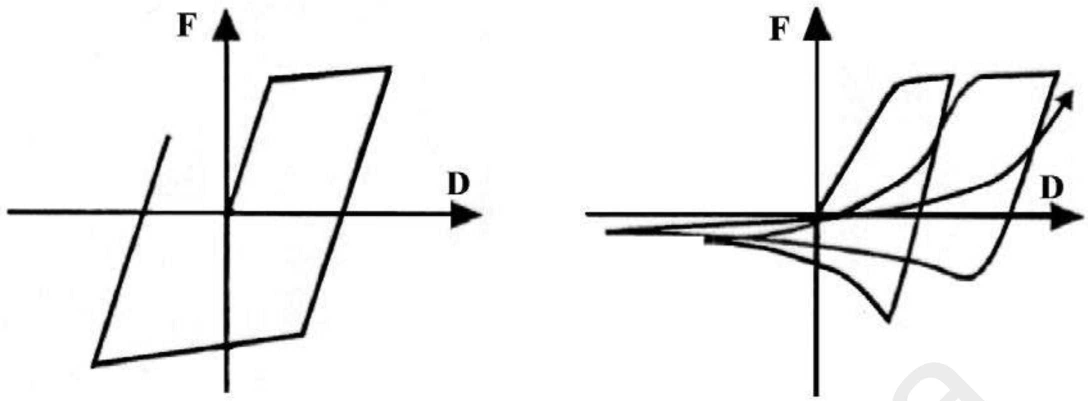

Buckling-Restrained Brace Buckling Brace

Figure 2. 16: Comparison of BRB Hysteresis and Conventional Brace Hysteresis (Sabelli, 2001)

Yoshino (1971) conducted the first research on BRBs. Two specimens consisting of a steel plate and a concrete panel casing were considered with one specimen having the steel plate and the concrete panel casing bonded and in the other one not. The specimen with debonded steel plate was reported to have larger deformation and energy dissipation capacity. Similarly, in a research done by Wakabayashi (1973), this result was further verified. These studies led the BRBs to its modern configuration in which the casing tube provides confinement and axial force is taken by the steel core. Xie, (2005) reviewed different shapes of cross-section proposed for BRBs. Figure 2.16 presents these cross-sections and further illustration is in the following.

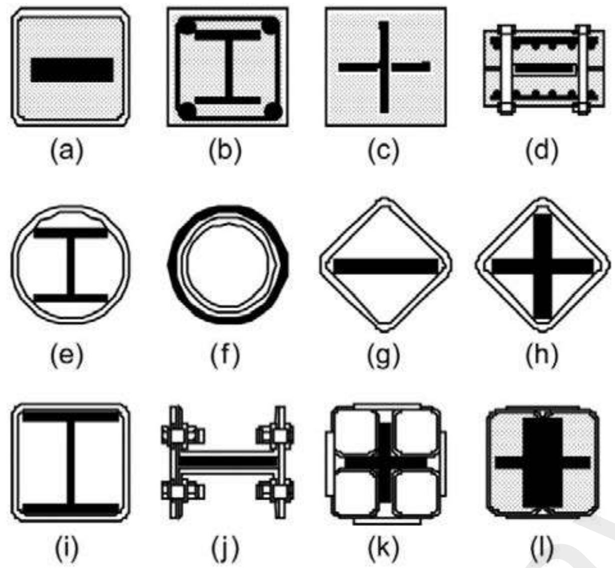

Figure 2. 17: Cross-sections of BRBs Proposed by Previous Researchers (Xie, 2005)

(a) Steel plate encased by mortar-infilled steel tube (Watanabe et al., 1988);

(b) I-shape steel brace enclosed by reinforced concrete (Nagao et al., 1988);

(c) Cruciform steel brace enclosed by steel-fiber reinforced concrete (Mase et al., 1995);

(d) Brace encased by bolt-connected precast concrete panels (Inoue et al., 1993);

(e) Wide-flange steel encased in steel tube (Suzuki et al., 1994);

(f) One inner circular steel tube encased by another exterior circular steel tube (Kuwahara et al., 1993);

(g) Steel plate encased by square steel tube (Kamiya et al., 1997);

(h) Cruciform steel brace encased by square steel tube (Shimizu et al., 1997);

(i) I-shape steel brace encased by square steel tube (Usami et al., 2001);

(j) Steel plate enclosed by bolt-connected steel plates (Isoda et al., 2001);

(k) Cruciform steel brace enclosed by four steel tubes (Narihara et al., 2000);

(l) Double T-shape steel enclosed by four steel tubes (Tsai et al., 2002).

In order to restrict buckling of the core steel component, Kailai Deng et al., (2015) proposed a new glass fiber-reinforced polymer (GFRP) steel BRB which encompasses four

GFRP pultruded tubes tied and wrapped together by layers of GFRP. Such manufacturing technique is convenient for large-scale industrialized production compared to conventional steel tube and infilled concrete as it is extremely lightweight. Although well performance of the suitably designed GFRP steel BRB was reported, nevertheless it suffers from probable local failure of wrapping GFRP components. This may be tackled by additional reinforcements. Schematic view of a GFRP profile is shown in Figure 2.17, (Kailai Deng et al., 2015).

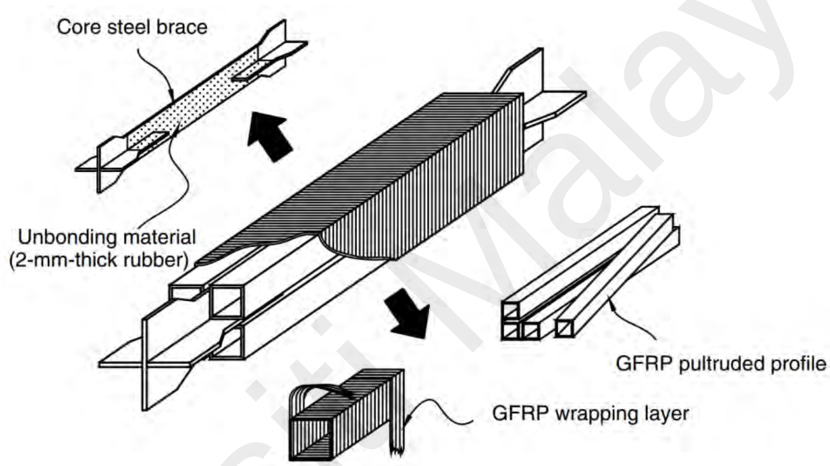

Figure 2. 18: Proposed GFRP steel BRB (Kailai et al., 2015).

2.4.2.1.(d) Other Energy Dissipaters

There are many possible configurations of damping devices developed based on the plastic deformation of metals. Higgins (2001) tested a metallic yielding device applicable for wood-frame structures in the form of diagonal bar configuration with a unique anchorage in charge of slipping in compression but instant griping in tension. Experiments reveal ideal effectiveness to ADAS device generally because of providing a larger yield surface by catching the bar at different locations. Another type of damper with a short alloy column and low yield point attached to two steel plates has been developed by Tsai et al., (2002). This multiple-direction damper was implemented in a structure between a beam and a chevron brace. In addition to low yield point, the alloy had ductility and stable hysteresis. Performance of this multiple-direction damper was tested under 20 earthquake records and satisfactory result was obtained. A highly plastic material damper (HPMD), shown in Figure 2.18, with highly nonlinear hysteresis was introduced by Tsai et al., (2003b). Combining the rate-dependent and rate-independent devices, it provided a reliable resistance to seismic loading taking advantage of both initial stiffness and energy dissipation.

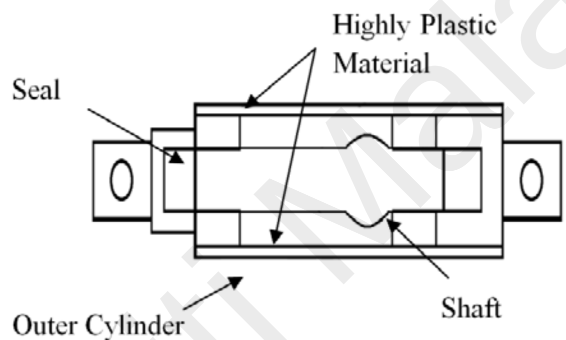

Figure 2. 19: Schematic of Highly Plastic Material Damper Schematic (Tsai et al., 2003)

Another kind of metallic yielding device known as dual pipe damper (DPD) has been developed by Maleki et al., (2013). As shown in Figure 2.19, it consists of two welded pipes loaded in shear. The function mechanism is such that the energy dissipation takes place through cyclic deformation associated with flexure of the pipe body while additional stiffness and strength are given to the structural frame by DPD at large displacements due to the induced tension in the middle of the device. A comparison between performances of a 10-storey frame equipped with DPD and TADAS was conducted and it was found that with the aid of unique secondary hardening portion in force displacement, implementation of DPD has resulted in lower structural and non-structural damage.

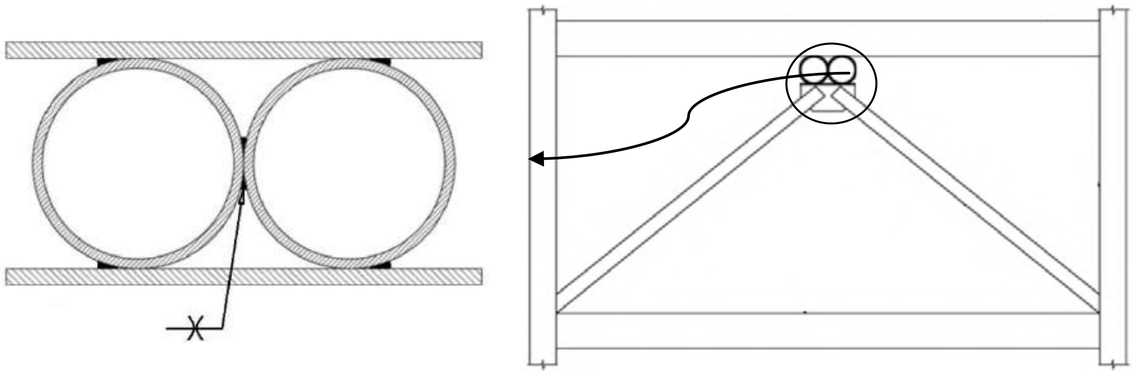

(a) (b)

Figure 2. 20: a) Dual-pipe damper configuration; and b) installation configuration for DPD. (Maleki et al., 2013)

A widely used seismic resistance system is steel shear panel dampers (SPDs). This damper often suffers from low cycle fatigue damage near to the welded stiffener and this causes weakness, (Kailai Deng et al. 2014). Kailai Deng et al., 2015 introduced a steel panel damper namely buckling restrained shear panel damper (BRSPD) which includes two main components; two restraining plates and an energy dissipation plate presented in Figure 2.20. There is no stiffener attached to energy dissipation plate. The energy dissipation plate is bolted to the two restraining plates to prevent out-of-plane buckling.

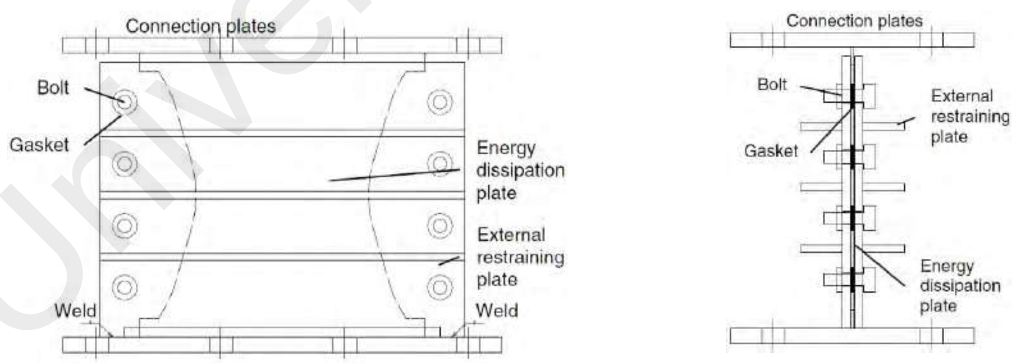

(a) Front View (b) Side View

Figure 2. 21: buckling restrained shear panel damper (BRSPD) (Pan et al., 2015).

Another effective yielding-device energy dissipater is accordion metallic damper (AMD), shown in Figure 2.21. The AMDs hysteresis loops resemble those of ADAS or TPEA devices. In an experimental test conducted by Motamedi and Nateghi-A, (2008) the AMD device stood for 70 cycles at 7 cm of deflection.

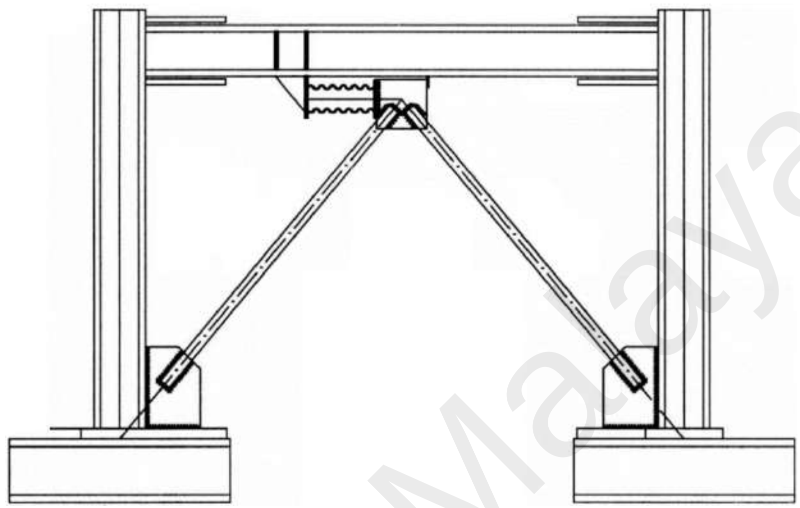

Figure 2. 22: Application of AMD In Seismic Retrofitting of Frames (Motamedi et al., 2018).

The dual function metallic damper (DFMD) dissipates energy through yielding under in-plane loads. Similar to other yielding devices, multiple shapes were proposed and tested among which double X-shaped and single roundhole shapes, presented in Figure 2.22, were found to have the best performance, (Li and Li, 2007).

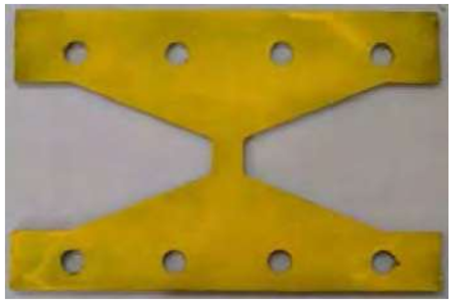

(a) X-Shaped

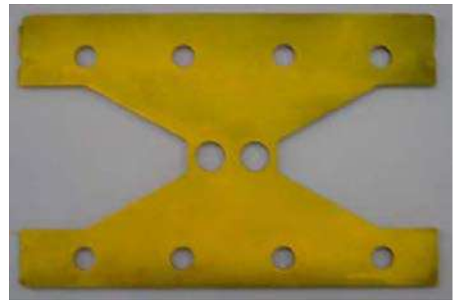

(b) Double Round Hole

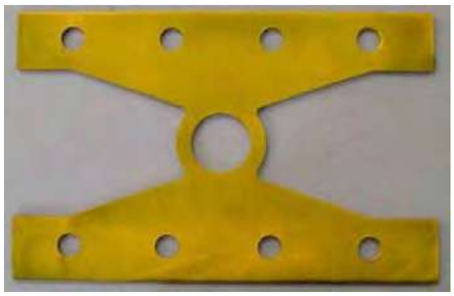

(c) Single Round Hole

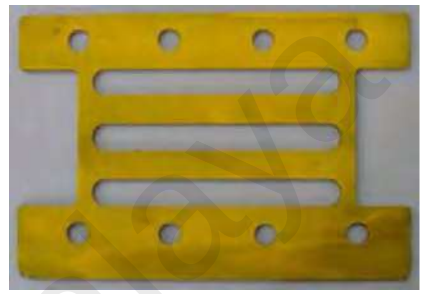

(d) Double X-Shaped

Figure 2. 23: Dual Function Metallic Damper (DFMD) (Li and Li, 2007).

Decleli and Mehta, (2007) developed an energy dissipating steel-brace frame (EEDBF) using HP section as a shear yielding element illustrated in Figure 2.23. The EEDBF implementation is ideal to TPEA and ADAS devices. Selection of HP section is because of the web thickness due to which a layer volume of material is provided for yielding and consequently greater amount of energy can be dissipated. Another merit of this device is confinement of damage to the yielding element itself which is then easy to replace in case of extreme seismic excitation. Performance of EEDBF was studied by Dicleli and Mehta in an analytical comparison to moment resisting frames and concentrically braced frames and it was observed that application of EEDBF can outperform the other two with less damage and greater lateral deformation capacity.

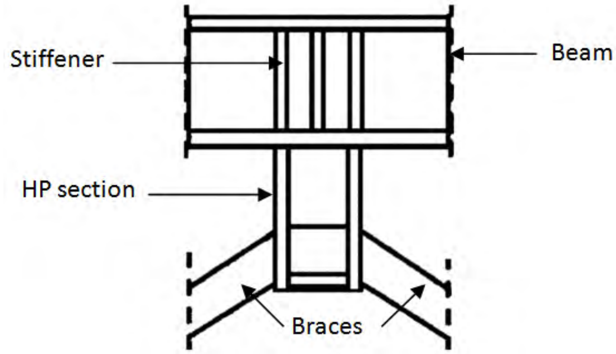

Figure 2. 24: Details of Shear Element And Connections In EEDBF (Dicleli et al., 2007)

A yielding damper device composed of a series of steel plates able to yield in both shear and flexure namely shear-and-flexural yielding damping (SAFYD) device has been investigated by Sahoo et al., (2015). Two X-configuration end plates provide damping under flexural action whereas shear yielding and associated energy dissipation is carried out by a rectangular web plate of the SAFYD presented in Figure 2.24. Sahoo and his co-researchers compared SAFYD, ADAS and shear link devices and stated that SAFYD device remarkably intensifies the lateral load carrying capacity and enlarges the energy dissipation potential.

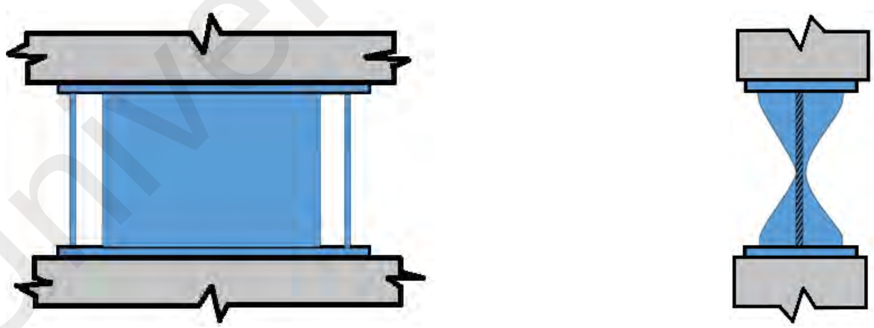

(a) Front View (b) Side View

Figure 2. 25: Schematic of SAFYD (Sahoo et al., 2015).

In order to improve the energy dissipation capacity of bottom flange connections for the weak direction of columns the weld-free Pi dampers were developed. This energy dissipating connection was named so because of configuration's similarity to the Greek capital letter. This form of connector sets off the yielding mechanism as soon as the beam section rotates about the connection's top flange. Application of Pi dampers have proven to have the anticipated energy dissipation capacity required to keep the beam and column essentially in elastic range. Configuration of Pi dampers is shown in Figure 2.25, (Koetaka et al., 2005).

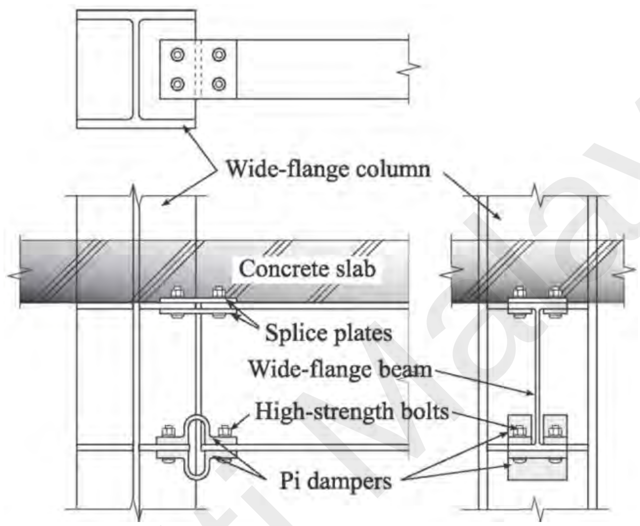

Figure 2. 26: Configuration of connection (Koetaka et al., 2005).

The Steel Slot damper (SSD) is another weld-free energy dissipation device fabricated from a standard structural wide-flange section. There are number of slits cut from the web in a vierendeel truss arrangement. Manufacturing and installation of SSD has no uncertainties and difficulty associated with in situ welding. Under inelastic cyclic excitation, the vierendeel's web member yields by flexural action and therefore dissipation of energy is provided. Chan et al., (2008) investigated the performance of the SSD through nine experimental tests and conducted a parametric study on geometrical factors affecting behavior of the device. It was observed that the SSD has well performed with stable hysteresis and remarkable energy dissipation and ductility early in a seismic test through small angular distortion. Tagawa et al., (2016) implemented the SSDs to a seesaw energy dissipation system. In order to evaluate the stability of the hysteretic property and capacity of energy dissipation, six cyclic loading tests were considered. Slit dampers were reported to yield at early stages of the test roughly at a storey rotation angle of 0.001 rad. For building structures undertaking seismic loads, such property is mostly intended to attenuate story drift. Figure 2.26 presents seesaw system with steel slit dampers.

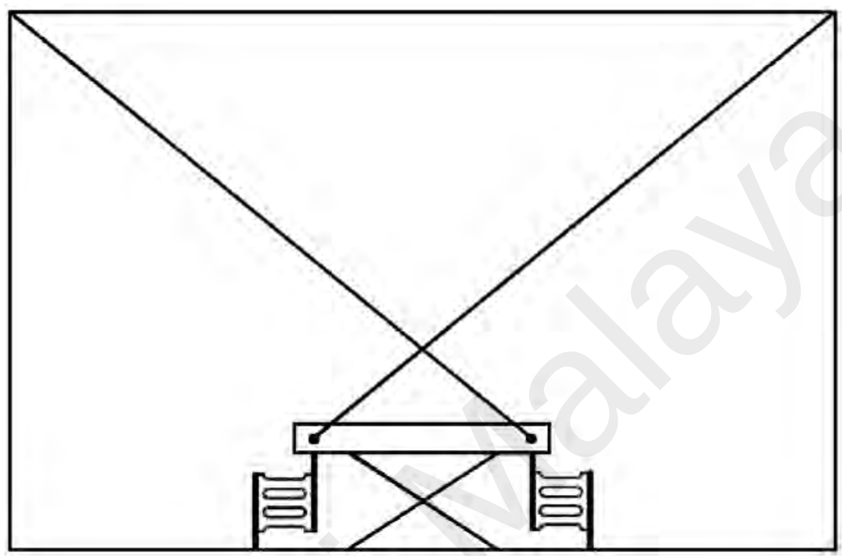

Figure 2. 27: Seesaw System With Steel Slit Dampers (Tagawa et al., 2016)

This review on metallic yielding devices highlights that the concept, energy dissipation mechanism and their overall performance fully depend on the metal properties, geometric configuration innovated by the engineering imagination and off course loading condition. Combination of these three concludes the energy dissipation capacity of the device.

2.4.2.1.(e) Shape Memory Alloy (SMA) Recentering System

This class of metallic alloys takes advantage of material's ability to return to its original shape after the stress is diminished. This characteristic feature is known as pseudo- or superelastic effect (SE). Heat can also be applied to the metal to get it back to its primary shape (shape memory effect or SME). According to Otsuka and Wayman (1998), the first performance observation of AuCD alloy was conducted by Chang and Reid in 1932. Another alloy that was found to have similar feature was an equal-atomic composition of nickel and titanium at the U.S Naval Ordinance Lab and they named the composition NiTINOL, (Jackson et al., 1972). NiTi alloy had several characteristics and those made it a beneficial alloy for aerospace, medical and civil engineering sciences. Tyber et al., (2007) discussed that properties of this alloy evolved considerable range of useful characteristics for civil engineering applications such as fatigue and high corrosion resistance, stable hysteretic behavior, biocompatibility and large recentring capability and recovering strain up to 8%. Although this alloy could be used in civil engineering field, its application has been so limited compared to other fields due to lack of knowledge in transferring the material science and implementing the developed SMAs. Lack of knowledge regarding large-scale SMA's performance and difficulty in implementation of large size SMA devices have been further discussed by McCornick et al., (2007b) and Weinert and Petzoldt, (2004), respectively. However, the last decade has witnessed dramatic grow of the knowledge of SMA's mechanical and material properties leading to a high potential for investigating and applying such robust and resilient technology to improve the sustainability of structural systems.

Recentering damper systems have been well recognized as a solution for structural response enhancement. This category of passive control systems sacrifices damping for lowering residual deformations after earthquake. The hysteretic behaviors of traditional elastoplastic system and a recentering or SMA system are presented in Figure 2.27 for comparison. Re-centering characteristic can be obtained through both using superelastic shape memory alloys (Dolce et al., 2001; McCormick et al., 2007; Sepulveda et al., 2008) or using post tensioned connections (Chowdhury, 2017; Chowdhury et al., 2019). Several researchers like Xu et al., (2019) and Dong et al., (2019) have illustrated the improved structural performance of equipped building taking residual drift as the factor of comparison to traditional passive energy dissipation devices.

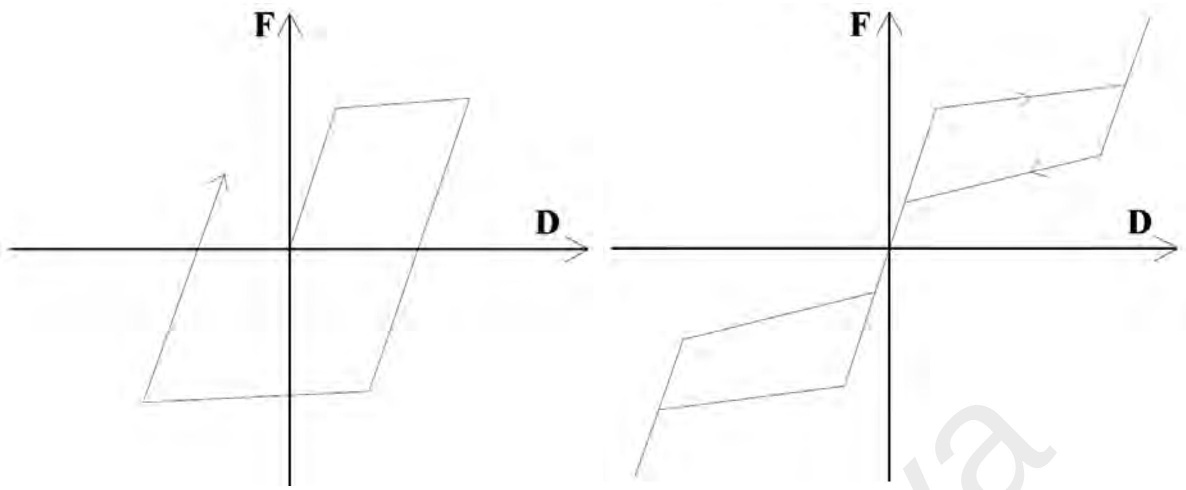

(a) Traditional Behavior (b) SMA Behavior

Figure 2. 28: Qualitative comparison between (a) a traditional system and (b) SMA system (Speicher, 2010)

Further exploration in the category of SMA devices includes analytical and experimental investigation of NiTi bracing systems conducted by a group of scientists and engineers, (Aiken et al., 1993; Cardone and Dolce, 2009; Lafortune et al., 2007; McCormick et al., 2007; Yan et al., 2007; Fang et al., 2019). Wang et al., (2015) has recently outlined the strategies for seismic retrofit of structures equipped with SMA bolts. Scheme of a recentering device is presented in Figure 2.28.

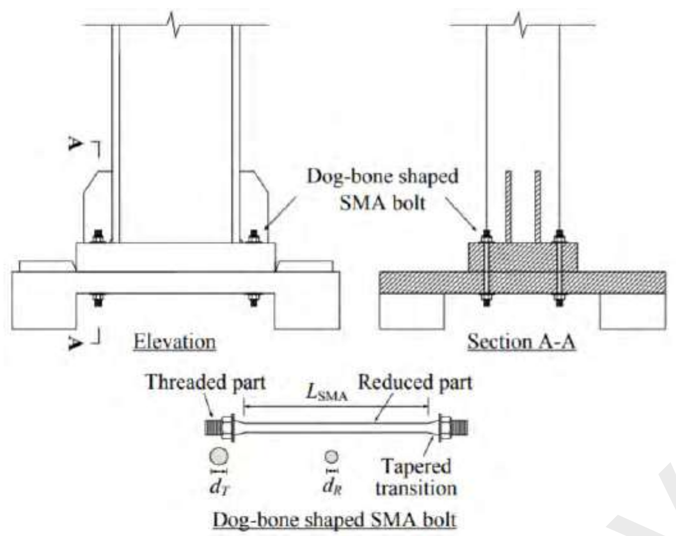

Figure 2. 29: Steel column base details: Elevation and section views and SMA bolt. (Wang et al., 2019)

2.4.2.2 Friction Dampers

Friction dampers have been noticed because of their capacity in dissipating large amount of energy which is provided by the rigid plastic behavior they have. Another performance characteristic or advantage of friction dampers is their independency to load frequency, number of load cycles or even changing temperature. Their plastic behavior and force response is modeled by coulomb friction.

Pall et al., (1982) proposed X-braced friction damper shown in Figure 2.29. Performance mechanism of friction dampers makes them applicable in moment resisting frames and it is functional in both tension and compression. When the damper is under loading, slippage is induced by the tension brace at the friction joint. Consequently, energy is dissipated in both braces.

Figure 2. 30: Pall Friction Damper (Pall et al., 1982)

In the category of bracing-damper systems in which every element has its axial and bending characteristics, the structural braces are assumed to yield in tension. In a study conducted by Filiatrault and Cherry (1987), the bending stiffness was included and elastic buckling in compression was considered while maintaining stability of the damper mechanism. It was found that minor fabrication details can crucially impact the overall performance at the friction damper.

Wu at al., (2005) developed an improved class of friction damper. In a compression between the improved Pall friction damper and the original class considering construction details, performance and damper force the improved class found to replicate the mechanical properties of the original Pall friction damper as the generated forces by both dampers were identical while the improved damper showed to be better as it could be manufactured easier. Fitzgerald et al., (1989) proposed a friction damper, known as slotted bolted damper, in which dissipation of energy is achieved through sliding of steel interface in slotted bolted connections consisting of two back to back channels, bolts with washers, cover plates and a gusset plate all shown in Figure 2.30.

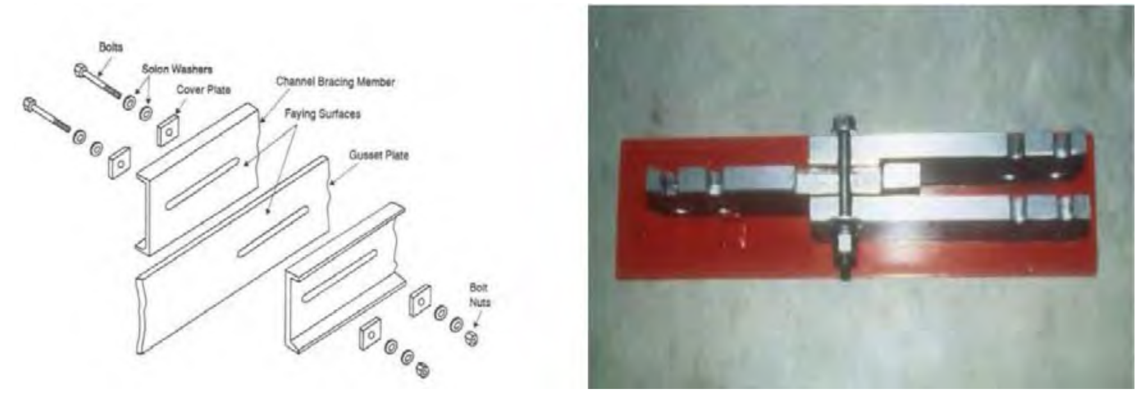

Figure 2. 31: Slotted Bolted Connections (Fitzgerald et al., 1989)

Response of these dampers has been reported to be repeatable with regular and rectangular hysteresis loops. However, reduction of displacement with this type of dampers is dependent on input ground motion due to the force threshold smaller than which the damper does not activate to dissipate energy, (Aiken and Kelly, 1990). In experimental and numerical study, conducted by Aiken and Kelly, a 1/4 –scale nine storey steel frame equipped with friction dampers and chevron brace was considered and friction damper's performance was seen remarkable with consistent hysteresis loops, roughly ideal Coulomb behavior and 60% dissipation of input energy.

Another friction damper with ideal physical appearance to Sumitomo damper was manufactured by Flour Daniel Inc. called Energy Dissipation Restraint (EDR) including an internal spring and wedges packed in a steel cylinder. However, the response characteristics were different because of some novel features which can be listed as follows:

a) friction wedges in charge of converting the axial spring force into normal pressure were made of steel and bronze.

b) in order to make the tension and compression gaps, internal stops were installed inside the cylinder.

c) variable spring length during operation could provide a dynamic friction slip force.

Wang et al. (2017) introduced an innovative type of frictional damper named Arc-surfaced Frictional Damper (AFD) whose damping force can vary with displacement as its frictional surfaces are curved. The pre-compression of applied Polyurethane Elastomer (PUE) secures the damping force of this damper. Figure 2.31 shows a schematic view of the AFD.

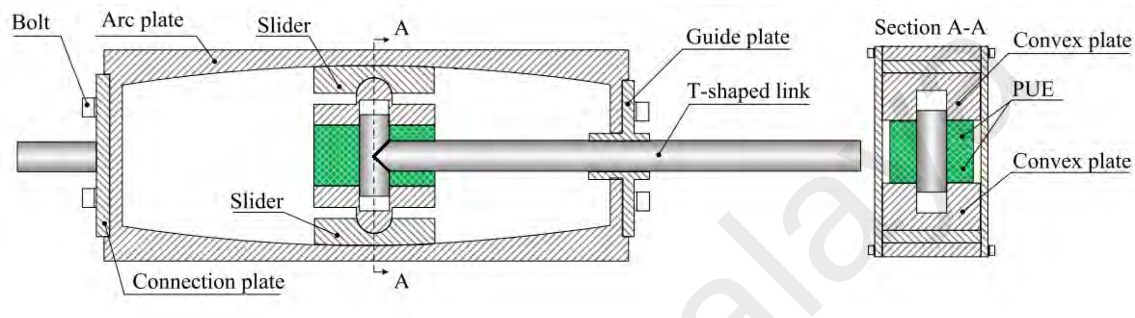

Figure 2. 32: Schematic illustrate of Arc-surfaced Frictional Damper (Wang et al., 2017)

2.4.3 Velocity Dependent Devices

As the name suggests, performance of this type of dampers is function of velocity across the device (rate dependent) and sometimes dependent on both velocity and displacement. Among this group of dampers viscous fluid dampers (VFD) and VE solid dampers can be listed. Figure 2.32 sketches idealized hysteresis loops of this group of dampers.

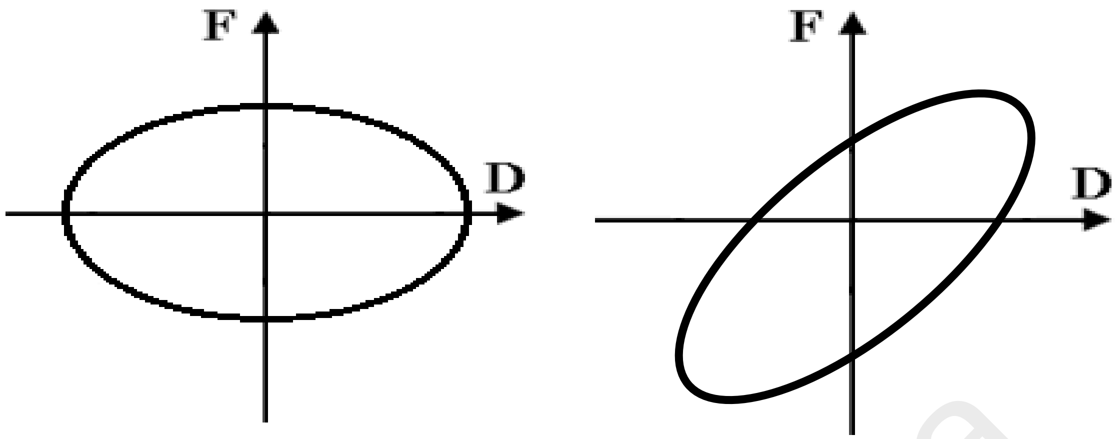

a) Linear Viscous Device b) Solid Viscoelastic Device

Figure 2. 33: Idealized Velocity-Dependent Hysteresis Loops

2.4.3.1 Viscous Fluid Dampers (VFD)

Performance mechanism of VFDs is by pressing a viscous fluid into small passages within an enclosed container, (Constantinou, et al., 1998). In order to resist motion the VFD can be placed in a bracing system such as chevron brace, as shown in Figure 2.33. Figure 2.34 illustrates an architectural display of an existing building equipped with VFD.

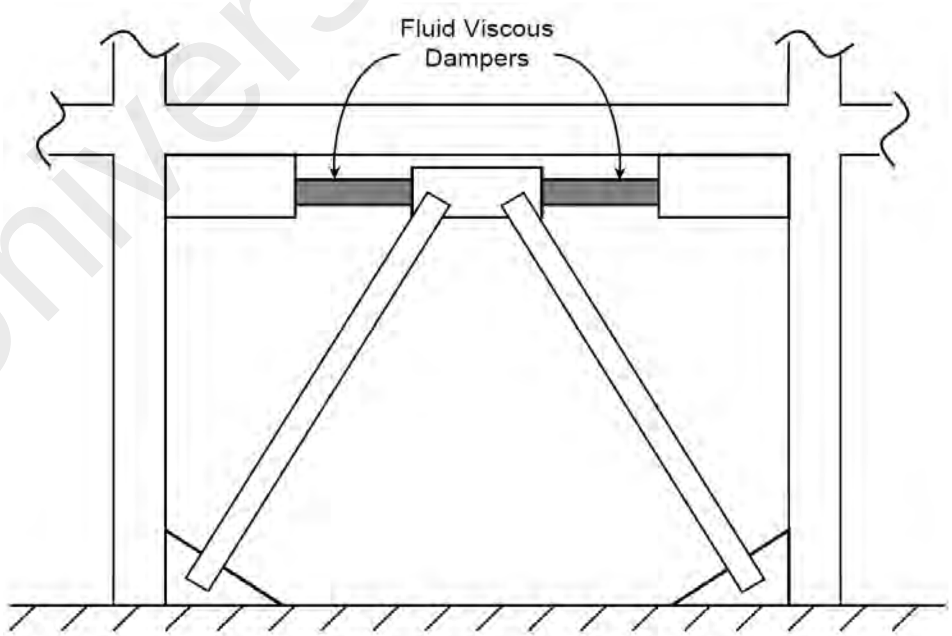

Figure 2. 34: Viscous Fluid Dampers in a Chevron Brace Configuration (Kruep, 2007)

Figure 2. 35: Viscous Fluid Dampers Exposed in a Building (Kruep, 2007)

It is notable that the VFDs have no contribution to structural stiffness. Dissipation of energy in this class of dampers relies on relative motion velocity. As Makris, (1997) discussed, this feature makes them most beneficial against high-frequency content seismic events. A given velocity develops a force which can be calculated as:

$$F = C\ sgn\left(\frac{dx}{dt}\right)\left|\frac{dx}{dt}\right|^{\alpha} \qquad (2.2)$$

In which C stands for damping, $\frac{dx}{dt}$ is the velocity, and α represents a factor which determines damper response linearity. When α is unity, the VFD is a linear damper device and Equation 2.2 reduces to:

$$F = C\ \frac{dx}{dt} \qquad (2.3)$$

Significant damages caused by Northridge earthquake in 1994 resulted in failure of many moment frames. The failures were determined to be due to brittle fractures of beam-column connections. Moment frames were designed based on the standards of the time. Subsequent studies focused on solutions to reduce the deformations that could be the origin of such brittle failures. As a remedy, passive energy dissipation devices were implemented in the building structures that were located in high seismic prone zones. Filiatrault et al.,

(2001) evaluated the ability of the VFDs in controlling structural deformations and accelerations induced by seismic vibration. A six-storey moment frame with three bays was considered as a case study. The frame was designed according to the pre-Northridge standards and equipped with chevron braces in conjunction with both linear (α =1.0) and nonlinear (α =0.5 and α =0.3) VFDs to provide 0% to 35% of damping ratios. The frame was subjected to six near-field earthquakes among which five of them were scaled to have a 10% probability of exceedance in 50 years. The considered unscaled records were El Centro from 1940 Imperial Valley earthquake and the Taft Lincoln Tunnel from 1952 Kern County earthquake. Experiments showed reduced storey drift and attenuation of peak floor accelerations while in the near-field earthquake tests, even higher levels of damping failed to prevent structural collapse and chevron braces experienced exceedingly high forces during stronger ground motions. Comparatively, the nonlinear VFDs led to slightly smaller forces but larger velocities in bracing system and negligible influence in reduction of lateral deflections. The study conducted by Filiatrault and his co-researchers investigated a wide range of damping ratios, damping exponent and seismic severity through which passive energy dissipation systems were concluded to benefit the structural frames located in regions of medium seismic activity but not sufficient to provide the desired protection against extreme seismic hazard. Furthermore, the chevron braces had buckled in the test and were never subjected to redesigning to examine the potential improvements of their tests. Besides, the tests were only limited to steel moment frames designed to meet both stiffness and strength requirements. Capacity of passive energy dissipators in controlling interstorey drift of moment frames designed only for strength was never studied.

In a similar research conducted by Miyamoto and Singh (2002) three case studies including single, five and eleven storey moment frames were considered. All frames were retrofitted by passive energy dissipation devices providing 20% of critical damping. To prevent near-fault ground motion eight seismic records, three of which exceeding the level of design recommended, were utilized in linear and nonlinear dynamic analysis in which nonlinear VFDs and linear VFDs were employed respectively. The results showed that except the three near fault motions, the models performed elastically for all the records. Interstorey drift was observed in single and five-storey models suggesting probability of little damage occurrence in case of less intense earthquakes while near-fault records would result in moderate damage. Although the drift associated with considered cases were within the limits protecting life safety, nevertheless, the immediate post-earthquake occupancy drift restrictions were exceeded due to four of the ground motions in eleven-storey frame. Inclusion of VFDs was discussed to have a disadvantage which was increased base shear. Satisfactory results motivated further study on VFD and its application in five storey frame redesigned based on strength requirements only. As the first mode period of the new frame was larger the base shear was less than that of original damped five storey frame. The strength designed frame suffered greater magnitudes of interstorey drift and plastic hinge compared to the bare frame while performance of damped frame was reported to be improved. It was also concluded that linear VFDs can affect compliance with codified drift limits.

The notable contrast between Miyamoto's and Singh's positive point of view and Filiatrault and his co-researchers' negative point of view justifies further study on the practical effects of VFDs on steal moment frame drift. In a parallel study by Oesterle (2003) nonlinearity of VFD and its impact on a nine-storey model with dampers having α of 0.5, 1.0 and 1.5 was investigated. Considered damping ratios were 5%, 10% and 20%. The model was subjected to near and far fault ground motions. Similar to formerly mentioned studies, the dampers were implemented in conjunction with chevron brace system. In addition, yielding braces were included in some of the models to observe the relation between elasticity of the braces and the varying velocity exponent. While higher exponent values resulted in suitable reduction of drifts and damage, induced forces in braces and base shear grew larger. This was especially noted for case α=1.5 since the elastic behavior of chevron brace members was determined to be in relation with the exponent.

2.4.3.2 Viscoelastic Solid Dampers

Typical configuration of this category of damper devices is such that VE materials are sandwiched between steel plates as shown in Figure 2.35. The VE material dissipates energy in shear action. Advantages of VE solid dampers are, first, they add initial stiffness to the structure, though less than metallic yielding devices, and second, VE materials provide energy dissipation for all levels of deformation. A drawback, however, is often dramatic alteration of the properties due to temperature caused by long events like hurricane. Fortunately, in confrontation with earthquake such effect is not a problem as the duration is not long enough. Nevertheless, other VE materials such as 3M material ISD-110 may suffer from this issue, (Lee et al., 2004).

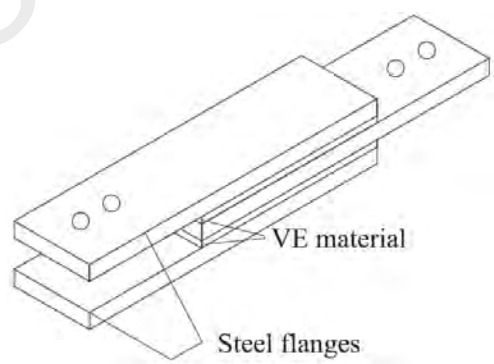

Figure 2. 36: Typical Configurations for VE Devices (Moliner et al., 2012)

Satisfactory performance of VE dampers (VEDs) standing against small deformation led to construction of several tall buildings in the United States and Japan prior to 1999, (Kareem et al., 1999). VEDs were also used in World Trade Center buildings in New York City to reduce deformations induced by wind load. Such application was also studied by Higgins and Kasai (1998) and Tan et al., (1997). A 46-storey RC residential building in Korea with a core concrete shear wall was equipped with VE dampers placed in an outrigger according to wind serviceability requirements. Steel stub beam and their adjacent columns were connected below slab. Rotation of columns would cause shear deformation of the rubber damping providing additional damping and stiffness to the structure, (Ahn et al., 2008). Figure 2.36 sketches the VE damper with a stub RC beam.

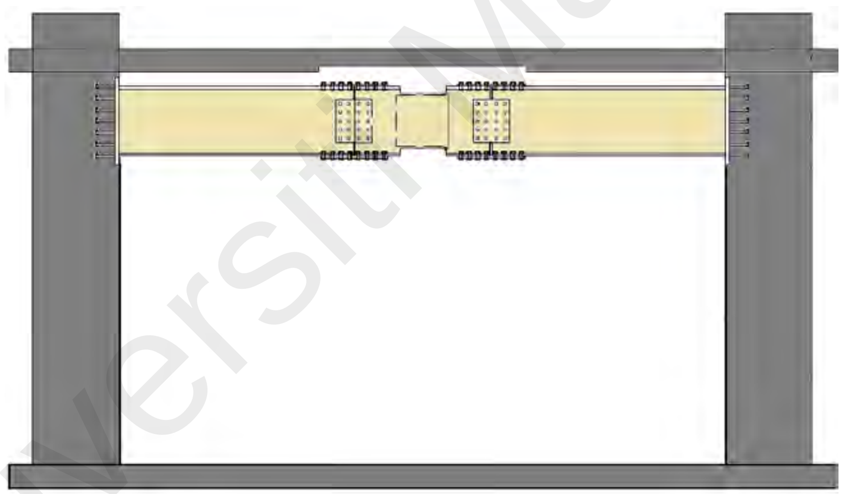

Figure 2. 37: VE Damper in Reinforced Concrete Frame (Ahn et al., 2008)

Application of VEDs set off for seismic protection in the mid to late 1980's, (Constantinou et al., 1998). Influence of temperature variation on the performance of a VED-equipped structure subjected to seismic load was studied by Tsai and Lee (1993) and reduced stresses and displacements of the considered structure were reported. Chang and Lin, (2004) and Min et al., (2004) highlighted the adverse effect of temperature increment on the VED's performance in an experimental test on an equipped five-storey steel frame.

Chang and El-natur (1993) considered minimum weight seismically designed structures in their parametric numerical study and concluded that implementation of VEDs could result in elastic behavior of structures. Shen et al., (1995) experimentally retrofitted damaged 1/3 scale RC frame and showed that the damper device is effective in attenuation of seismic response apart from considerable inherent damping of the damaged frame itself. In a series of parallel studies on experimental shaking table tests of a 2/5 scale three-storey steel frame equipped with VEDs, the corresponding dissipation of energy was illustrated to be effective while no other supplemental dissipation was added, (Chang et al., 1996; Chang et al., 1995; Lai et al., 1995).

The benefit of VEDs in reducing ductility demand of frames has been further highlighted in numerical modeling of damped steel and RC structures, (Raut et al., 2019; Vatanshenas et al., 2018; Verma et al., 2018). Connecting adjacent structures has been proposed to be another application of VEDs most suitably for cases that include connection of structures with significantly different natural frequencies, (Kim et al., 2006). Lin et al., (2006) discussed the functionality of VEDs across all levels of vibration corresponding to both seismic events and small mechanical vibrations. A 13-storey VED-equipped structure was considered and resulting response reduction was observed. A numerical research was conducted by Xu and Zhang, (2001) regarding connection damper focusing on compression and tension flanges of bolted connections improved by elastomeric pads or VE layers under shear action. It was concluded that under certain fixity connection, the considered damping configuration can be highly beneficial in controlling structural response. Behnamfar et al., (2015) reported stable hysteretic cycles of a steel beam-to-column VE connection consisting of a VE damper located under the lower flange as a lower pad on the seat angle of the connection. Connection of the bottom flange to the pad was provided by series of bolts as shown in Figure 2.37. Satisfactory hysteresis loops were observed along with no experience of damage induced by the considered strong seismic excitation at structural members, connectors and welds.

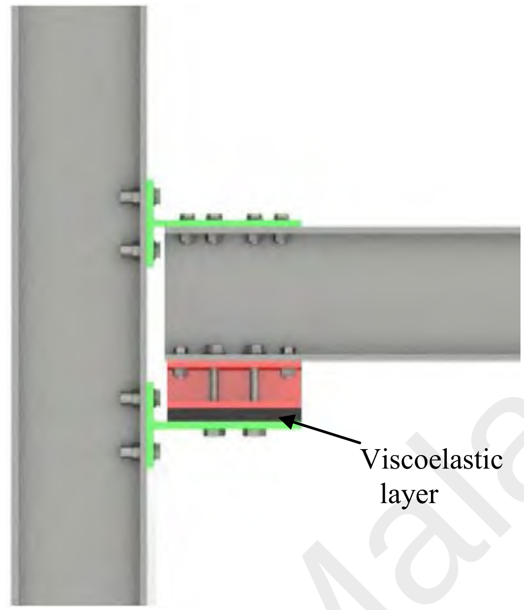

Figure 2. 38: Viscoelastic connection damper (Behnamfar et al., 2015).

A new device known as Viscoelastic Coupling Damper (VCD) has been added to VEDs category by Montgomery, (2011) at University of Toronto. The VCD takes advantage of multiple layers of VEM. Layers of steel plate are located between VE material and anchored at alternating ends as shown in Figure 2.38. Performance mechanism of VCD is dependent on shear deformation which makes it applicable to coupled core wall building. Lateral movement and the subsequent relative motion of coupled walls, induced due to wind or seismic loading, let the VCD undergoes significant shear deformations, therefore VE material provides a displacement-dependent elastic restoring force and a velocity dependent viscous force. Hence, VCDs have a significant advantage over the typical axial brace configuration of VE dampers and that is sufficient relative displacements required for effective energy dissipation of typical axial brace while for VCDs this is not the case.

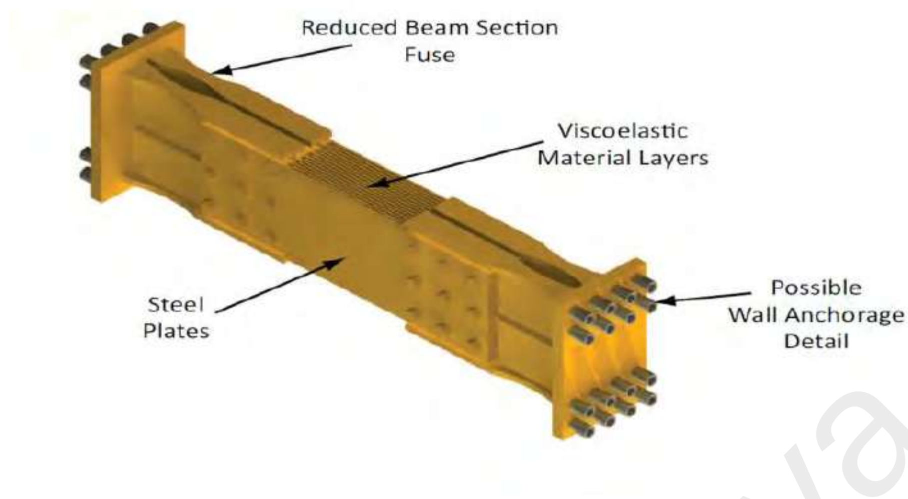

Figure 2. 39: Viscous Coupling Damper (Montgomery, 2011)

Recent improvements of VE solid devices include utilization of (HDNR). This damping material is composed of natural rubber (isoprene) manufactured through vulcanization process filled with carbon black. Performance mechanism of this class of dampers has low dependency upon both frequency and temperature and shows high energy dissipation capacity. For strains greater than 200%, a hyperelastic effect in force-deformation relationship can be seen. Depending on the amount of filler and rubber compound, this type of damper can sustain strains of up to 500% or greater without failure.

Lehigh University introduced an 'Ultra-high Damping Natural Rubber (UHDNR) structural dampers with loss factor of 0.35 and 0.4. The loss factor is defined as the ratio of the loss modulus to the storage modulus of a material. This parameter stands for amount of energy dissipated to the amount of elastic strain energy stored and released for a given cycle. Lee et al., (2004) and Sause et al., (2001) compared the dependency of UHDNR and dependency of VE material on temperature, strain level and frequency and mentioned that although such dependency exists for both cases, however, for VE material this relation is much stronger. Comparative study showed that the UHDNR damped system outperforms 3MISD110 when temperature is included in the design. Performance of the considered frame under seven ground motions was tested and it was observed that both of materials can reduce the structural response.

In an experimental research on an RC frame equipped with HDR device, up to 120% increment of inherent damping was obtained. It was stated that stable performance of the rubber damper can be achieved provided that the applied stress is in simple shear, (Bartera et al., 2004; Bartera and Giaccheti, 2004). The rubber used in the researches conducted by Lehigh University and by Bartera and his co-researchers was provided by Tun Abdul Razak Research Center (TARRC) and Malaysian Rubber Board.

2.5 Combination of Structural Control Systems

Application of the concept of performance-based design advanced the structural behavior against seismic and wind loads. Structural control systems have enhanced the structural resistance through lowering inertia forces and inter-storey drifts. However, each retrofitting system has a weakness, and to tackle structural weakness of the system, recent studies and investigations have focused on combination of various structural control systems.

Solutions for structural protection encompass combinations of passive, active and semi-active control systems. Palacios-Quinonero, et al. (2011) studied a passive-active control approach to enhance the seismic behavior of a three-adjacent-building case and to prevent inter-building pounding. Numerical study simulated a set of passive damping devices as link elements between buildings in which active control system was implemented as local damping system since superior seismic protection was required (Figure 2.39). It was concluded that application of this system can result in significant reduction of both storey drifts and inter-building pounding.

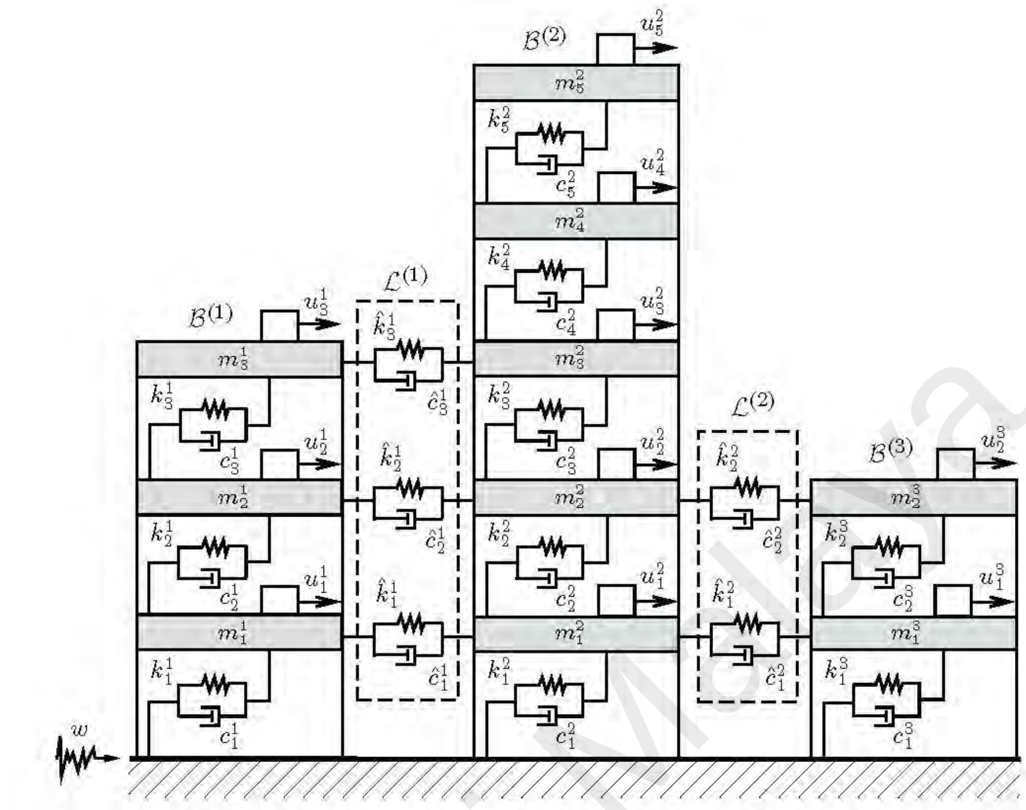

Figure 2. 40: Three-building connected system (Palacios-Quinonero, et al. 2011)

Leblouba (2007) investigated six different combinations of the most applied base isolation systems namely HDR bearing system, lead rubber bearing system (LRBs), and friction pendulum system (FPS). These combinations were applied in a three-storey reinforced concrete building as shown in Figure 2.40.

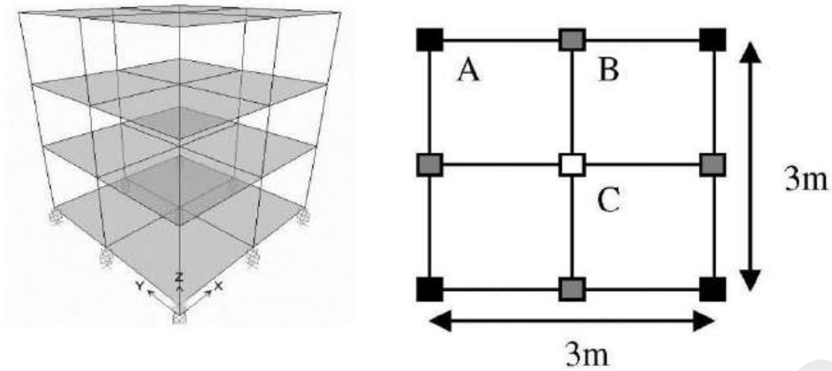

Figure 2. 41: General view of the building being isolated and location of isolators (Leblouba 2007)

A nonlinear time history analysis was conducted on the six considered combinations whose layouts are shown in Figure 2.41. Comparisons concluded that buildings equipped with different layouts of combination of LRBs and HDRB had almost similar responses. Furthermore, combination of FPS with LRBs and HDRB reduced the base shear while displacement was reported to rise. Application of HDRB isolation system was revealed to influence the seismic response of the structure in a more remarkable way compared to other combinations in addition to lowering down the cost of isolating the structural system.

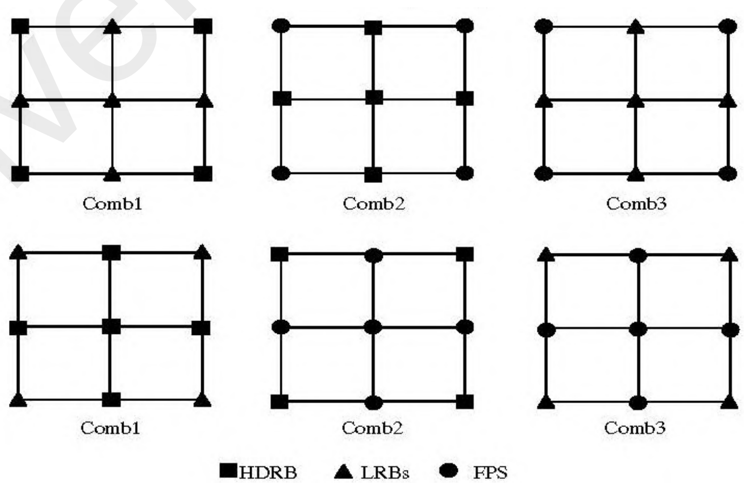

Figure 2. 42: The Different Combinations Considered (Leblouba 2007)

A passive type of damper with bent channels in its configuration is Visco-Plastic Device (VPD) which takes advantage of an elastomeric damping material sandwiched between the two bent plates as shown in Figure 2.42. In this type of damper the amplification of displacements across the rubber governs the damping process. Energy absorbing mechanism is such that upon reaching the axial-flexural yield of the steel elements, the energy absorbing capacity is increased. Furthermore, this damper's geometry provides a hyper-elastic effect under large displacements imposed by significant seismic events. This extra stiffness is added to the stiffness of structure and helps in collapse prevention (Ibrahim et al. 2007).

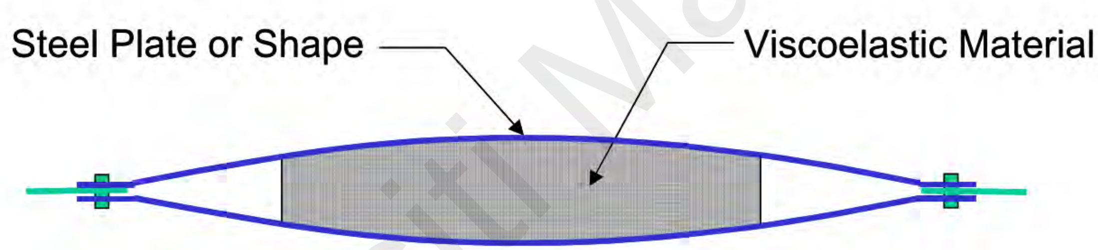

Figure 2. 43: Visco-Plastic Device (VPD) (Ibrahim et al., 2007)

In a study conducted by Marshall (2010), a hybrid passive control device (HPCD) was proposed through combination of two typical passive control devices: a buckling restrained brace and a VE damper. HPCD had a two phase damping mechanism; the first phase employed a HDR sandwich damper with a VE behavior which had advantages of simplicity in production and lock-out method design. The second phase was operated by a buckling restrained brace (BRB) which is a metallic ductile yielding device and it is famous as a lateral load resistant element. The lock-out mechanism was in charge of smooth development of a transition through slotted bolt holes and rubber pads which are demonstrated in a simple representation of the HPCD in Figure 2.43.

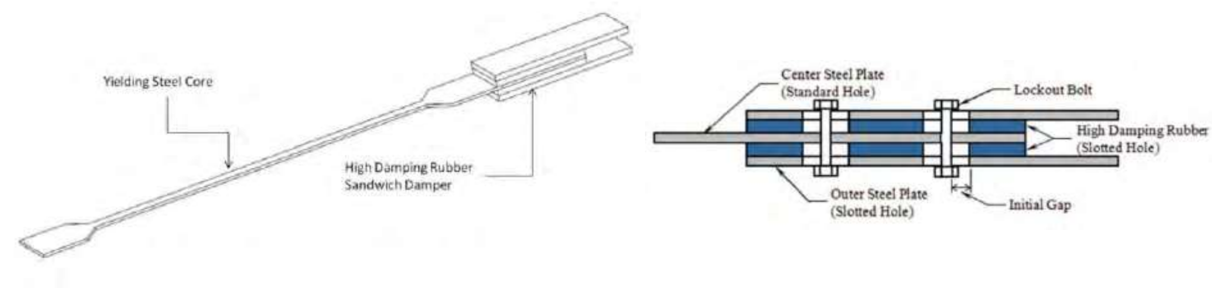

Figure 2. 44: Schematic of the hybrid passive control device (Marshall 2010)

Silwal et al. (2015) proposed a superelastic viscous damper, a hybrid type that uses shape memory alloy (SMA) cables, which have the inherent re-centering capability of shape as depicted in Figure 2.44. Study showed a superior seismic performance and energy dissipation ability by the utilized heavily damped elastomer compound named butyl compound. Buty1 was considered for the VE component of the hybrid damper and could provide a high damping at low stiffness. Interstorey drift demands and residual drifts of the considered buildings were reported significantly lower than the cases that excluded the superelastic viscous dampers when subjected to earthquakes. On the other hand, no considerable increment of peak acceleration demand was observed.

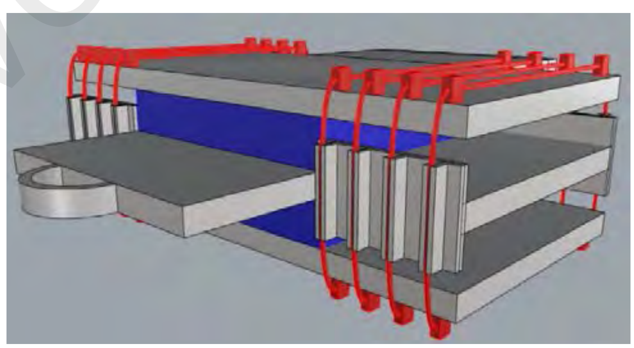

Figure 2. 45: Superelastic viscous damper (SVD) (Silwal 2015)

Roh et al. (2018) proposed a multi-action hybrid damper (MHD) consisting of friction pads, lead rubber bearings and steel plates, shown in Figure 2.45. Since the lead rubber bearing and the friction pad are in series connection, the MHD damping mechanism is such that under cyclic loads the lead rubber bearing is initially engaged until it deforms and therefore the restoring force reaches the slip load of the friction pad and then the additional deformations are damped by the friction pad. This process showed that the lead rubber bearing and the friction pad have behaved independently against amplitude of the deformation. Study investigated the performance of the MHD in a numerical analysis of a 20-storey steel structure and a 15-storey RC apartment and the obtained hysteretic curves were found very stable with no undesirable variation. It was concluded that the MHD is a suitable damping device against relatively small wind and large seismic loads.

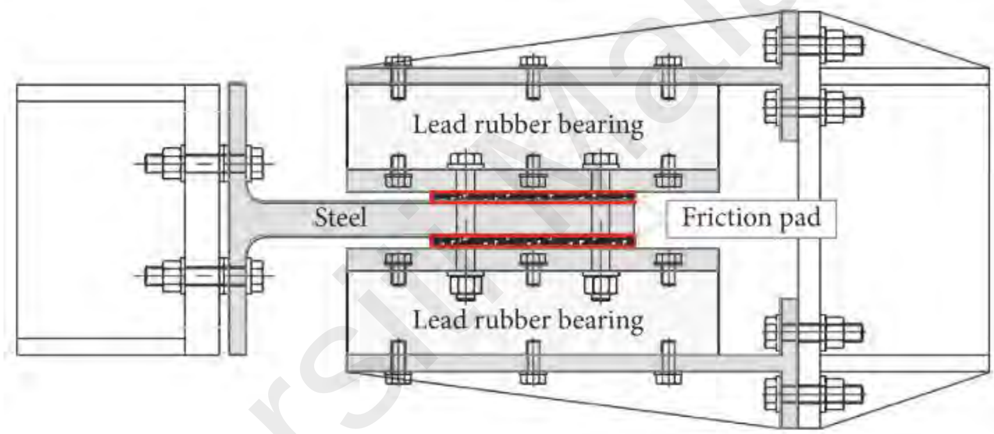

Figure 2. 46: Section of the proposed MHD (Roh et al., 2018)

Another hybrid damper is proposed by Lee et al. (2017). This device has a steel slit damper combined with rotational friction dampers as shown in Figure 2.46. An advantage of this damper was that only under small earthquakes or strong winds the applied friction damper is activated while in case of strong seismic loads both friction and slit damper play role together. Stable hysteretic behavior was reported along with satisfactory energy dissipation. Furthermore, it was revealed that in case of generation of tension field at large displacement, the post-yield stiffness of the damper was increased when vertical deflection of the specimen was restrained.

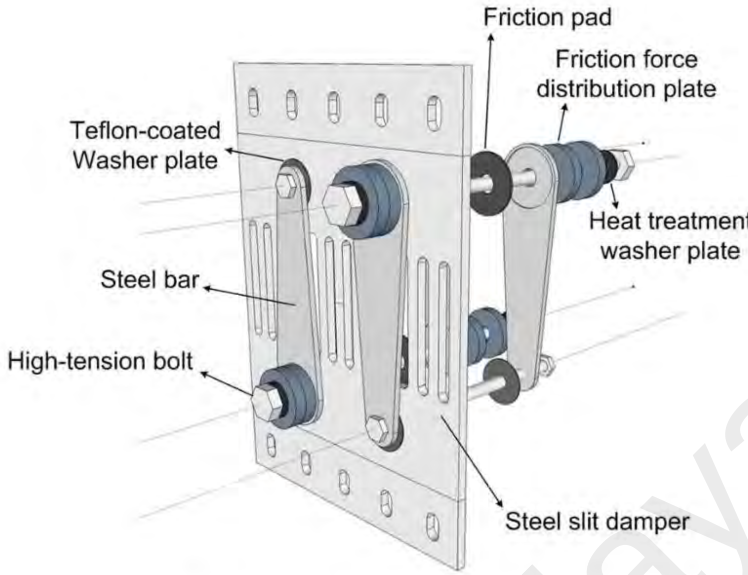

Fig. 1. Hybrid slit-friction damper.

Figure 2. 47: Hybrid slit-friction damper (Lee et al., 2017)

2.6 Tension only bracing strategies

In the seismic resistant design framework, besides varying configurations of yielding devices, other strategies regarding collapse prevention systems have been proposed to be utilized in new construction and enhancing seismic performance of existing buildings. In this regard, a "collapse prevention" system encompassing the main lateral-force resisting system which works in tandem with a pair of slack cables or loose linkages has been introduced by Judd et al. (2016). Such collapse inhibiting mechanism is capable of engaging the gravity framing and eventually preventing collapse. Combination of gravity framing and the main lateral-force resisting system has made this collapse prevention system a holistic design approach capable of supplying adequate performance when structure is subjected to low to moderate level ground motions as well as providing life safety under sever ground motions. In order to strengthen the performance under lateral excitations, additional energy dissipation device such as small viscous fluid or VE solid dampers can be added on to the collapse inhibiting mechanism. Some of the collapse prevention systems are sketched in Figure 2.47, (Judd et al., 2015).

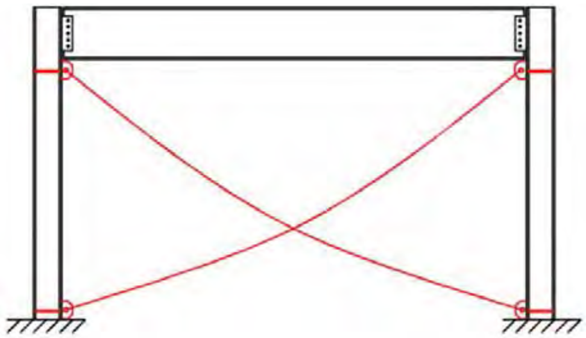

(a) Fully- Bay Slack-Cable X-Bracing

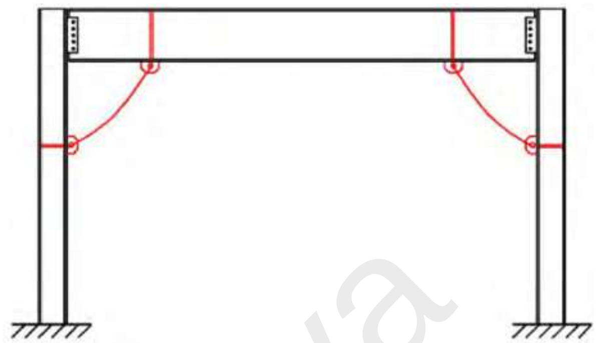

(b) Slack-Cable (SC) Knee Bracing

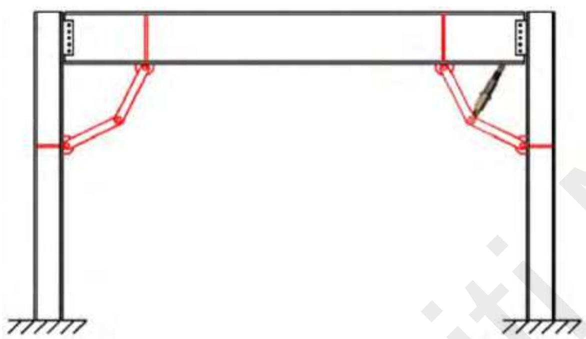

(c) Loose Linkages

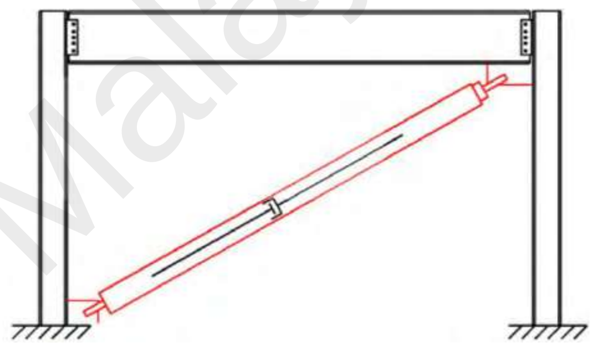

(d) Telescoping Brace; With Optional Energy Dissipation System such as High Damping Rubber

Figure 2. 48: Prototypical Collapse Inhibiting Mechanisms (Judd et al., 2015).

Hou et al. (2009) introduced a seismic retrofit method for steel moment-resisting frames. This method takes advantage of wire rope (cable) bracing to increase the lateral storey strength and to restrain the storey drift in a specified range with no reduction in ductility of the moment frame. The proposed mechanism included a cylindrical member to bundle the wire-rope bracing members at the intersection point. This study reported a large energy dissipation capacity, achieved in the tests, by delaying the brace action mechanism. The employed high-stiffness cylindrical member caused an early strain increment in the bracing members. The conducted seismic response analyses for the considered three-storey frame models retrofitted by the proposed seismic resistant system showed a restrained storey drift with no considerable increment of the storey shear force. Furthermore, residual deformation was reported to get attenuated because of the re-centering effect on the vibration center. It was discussed that the introduced deformation dispersion effect along the height had enabled avoidance of energy concentration into the local storey. Comparison between bare frame and retrofitted ones demonstrated similar compression force-time alterations in the columns and that concluded to slight influence of the proposed retrofit method on the original columns. Figure 2.48 depicts the concept of the proposed bracing system.

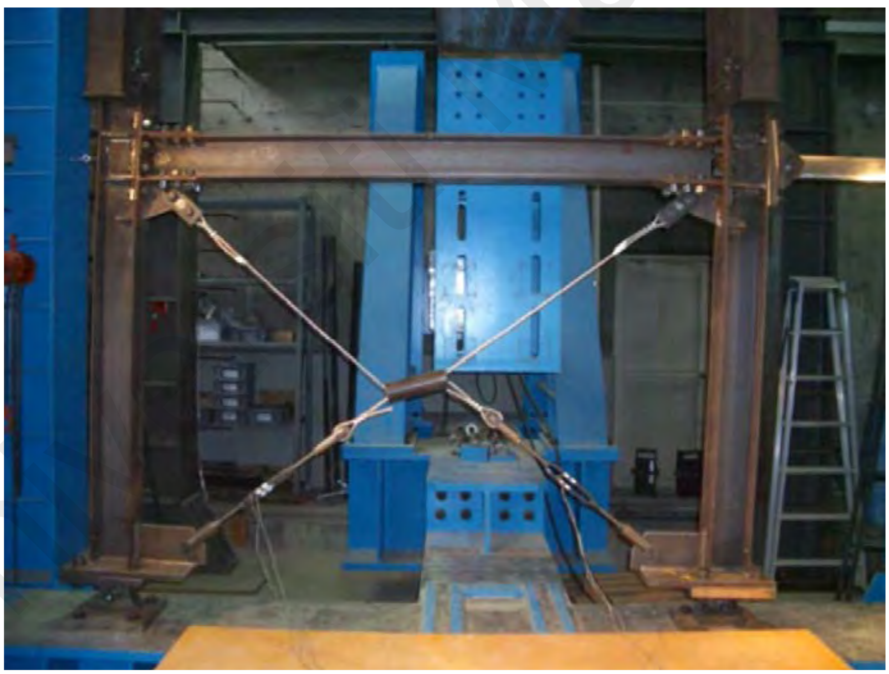

Figure 2. 49: Cable bracing system with central cylinder (Hou et al., 2009)

2.7 Concluding Remark

There has been a significant improvement in structural response by establishing performance-based seismic design. Mechanism and performance of various types of structural control systems were briefly discussed to provide a general picture of this concept applied to structural frames subjected to lateral loads. This literature review discussed a considerable portion of developments in the framework of VE dampers. VE dampers are effective in reducing vibration of structures. VEDs can be used for all levels of vibrations in addition to stiffness they provide for equipped structure although much less than stiffness which can be provided by metallic damper devices. Such volume of information is required for further innovative researches to create practical and effective VE dampers. Also, it was shown that this class of damper has significantly changed the engineers' view to the seismic-resistance based design by which immediate occupancy limit state or collapse prevention due to a large-scale event and linear elastic behavior of the structure against small- and mid-range event can be provided in addition to reduction of acceleration. These efficient performance specifications can be achieved by a properly designed hybrid system. Moreover, combination of seismic retrofit systems discussed by former researchers was outlined with expressions about better structural performances obtained in the tests. Studies of combined seismic retrofit systems also debated multiphase control system mechanisms and advantages were presented in this chapter.

Every type of seismic retrofit strategy has its strengths and weaknesses. The main challenge is to keep moving forward, develop more effective techniques, and strengthen their structural performance impact. It is crucial to know the weaknesses and strengths of the individual methods. In dampers with high initial stiffness and cross cable bracings, the increased stiffness results in reduced displacements, but with a cost of high base shear, large residual displacements, and high acceleration. This work aims to develop a highly effective combination that can be economically manufactured with minimum environmental impacts.

CHAPTER 3: MECHANICS OF VISCOELASTIC MATERIAL

3.1 Mechanics of High Damping Rubber

Family of HDRs is also called, by general term, elastomeric rubbers. In this thesis, the two terms rubber and elastomer will be used interchangeably. Rubber in its natural or raw state is a highly elastic, deformable and soft material and its behavior can be significantly affected by temperature and frequency. There are various synthetic elastomeric materials with specific properties. In order to manufacture an efficient engineering rubber appropriate additives are required and a useful rubber is made by compounding the raw rubber material with other materials like sulfur and carbon black. In this study a highly damped VEM called Butyl Rubber (BR), with synthetic rubber compound and unique combination of engineering properties, has been selected.

3.1.1 Incompressibility of Rubber

Rubber properties such as low shear modulus, G, a very high resistance to volume change under load, and a very high bulk compression modulus, K, makes it a purely incompressible material with Poisson's ratio of exactly 0.5 which is typically taken as 0.4999, (Gent, 2012). Therefore, in a not highly confined situation it is reasonable to assume that rubber is incompressible. Such nature has been utilized in many developed mathematical models of rubber. In this research, a Poisson ratio (υ) of 0.495 was assumed for rubber material.

3.1.2 Rubber Material Properties

The nonlinear nature of rubber does not guarantee a constant modulus of elasticity or shear modulus. Hence, these terms normally refer to stress at the reported typical values of either 100% or 300% strain or the strain at rupture. In this study, the typical strain value of 100% or shear strain is assumed as the considered strain unless other values are pointed out. At the 100% strain the shear modulus of rubber is generally between 0.5 and 4.8 MPa (Gent, 2012). Furthermore, rubber hardness value is considered as a modulus which falls between 30 and 80 durometer. Generally speaking, a higher hardness refers to a higher stiffness which highlights that hardness and modulus have a correlation although it is not direct.

3.1.3 High Damping Rubber

In 1982 the Malaysian Rubber Producers' Research Association (MRPRA) of the United Kingdom came up with development of HDR compounds. This was because proper rubber compounds with high damping properties have been highly in demand, Derham et al., (1985). Such need concluded the enhancement of engineering properties of natural rubber which, to become a (HDNR), has been vulcanized and mixed with carbon black and other fillers. Carbon black increases the stiffness and loss factor and fillers change the material to a rubber that has less dependency on temperature, loading and frequency. In order to manufacture a high-damping butyl rubber, similar principles are applied to raw butyl rubber which has a higher loss factor than raw natural rubber. Addition of carbon black to the butyl rubber makes it a compound with higher damping property compared to a filled natural rubber. The result of this manufacturing process is a synthetic rubber with inherent high damping nature that may reach as high as 20% at 100% shear strains. The corresponding hardness and shear modulus are 70-75 durometer and 1.4 MPa respectively. Compound of the selected synthetic buty1 rubber in this research has a high damping nature and loss factor.

3.1.4 Mechanical Behavior of Filled Rubber

Speaking of the classification of rubbers with respect to their behavior, they are categorized as both isotropic and VEMs. This adds up to the complexity of the numerical modeling of these synthetic materials's behavior. In a comparison, metals are considered as elastic solid materials with very small inherent damping which is totally in contrast with HDR with high capability of energy dissipation. Therefore, behavior of the HDR can be treated as both time independent, i.e. static force-deformation relationship, and time dependent, i.e. represented by loss modulus. These two characteristics can be observed in the stress-strain equation for VEMs shown in Equation 3.1. The complex modulus in mathematical modeling is represented by E* which is explained in two parts; first, the real part, E' and second, the imaginary part, E". Such mathematical representation can be defined in reality as such: the real part, typically called elastic modulus or storage, is in phase with the strain while the imaginary part, also called loss modulus, is 90 degrees out of phase with the strain. Considering the viscoelasticity of the rubber, this phase-oriented definition means that the maximum stress and maximum strain do not take place at the same time and have to be mathematically regarded as being out of phase.

The storage modulus is defined as the amount of strain energy which is elastically stored and released per unit volume. The loss modulus represents the energy lost per unit volume. These parameters are placed in Equation 3.2 in which η stands for the loss factor in place of the loss modulus, E". Another representation of the loss modulus is tan   which is the tangent of the phase angle between the stress and strain as given in Equation 3.3. The parameter   is the time lag between the stress and strain and strain of $\varepsilon_0$sin (t)   is what these equations are based on.

$$\sigma_0 = E^*\varepsilon_0 = (E' + \mathrm{i}E")\varepsilon_0 \tag{3.1}$$

$$\sigma_0 = E\,(1 + \mathrm{i}\eta)\varepsilon_0 \tag{3.2}$$

$$\eta = \frac{\mathrm{E}''}{\mathrm{E}} = \tan \tag{3. 3}$$

These equations can also be managed in terms of simple shear deformation by replacing E^* with G^*. Consequently, shear stress, τ, and shear strain, ϒ are used. In this case the loss factor has to be obtained through simple shear deformation versus axial tension test (Nashif et al., 1985). It has to be mentioned that for filled rubbers the loss factor is generally the same in tension and shear. Therefore, in this research the principal deformation of the rubber is considered based on simple shear and the loss factor is determined by shear.

Stress-strain relation is plotted in Figure 3.1. The loss factor differentiates the two stress traces as indicated in the legend. The phase angle which is presented by shows the difference between the cross point of the horizontal axis with stress and strain traces. The time lag between stress and strain is presented in terms of seconds. This needs to be transformed into an angle in radians. Therefore, the time lag is divided by period of the motion and then multiplied by 2π. The tangent of that angle gives the loss factor, η. The loss factor itself is defined as the ratio of the loss modulus to the storage modulus. The greater loss factor the larger lag between the stress and strain in the stress plot. Moreover, larger loss factor corresponds to a higher stress peak and that originates from the same storage stiffness of both traces while with a larger loss modulus the dynamic stiffness is larger.

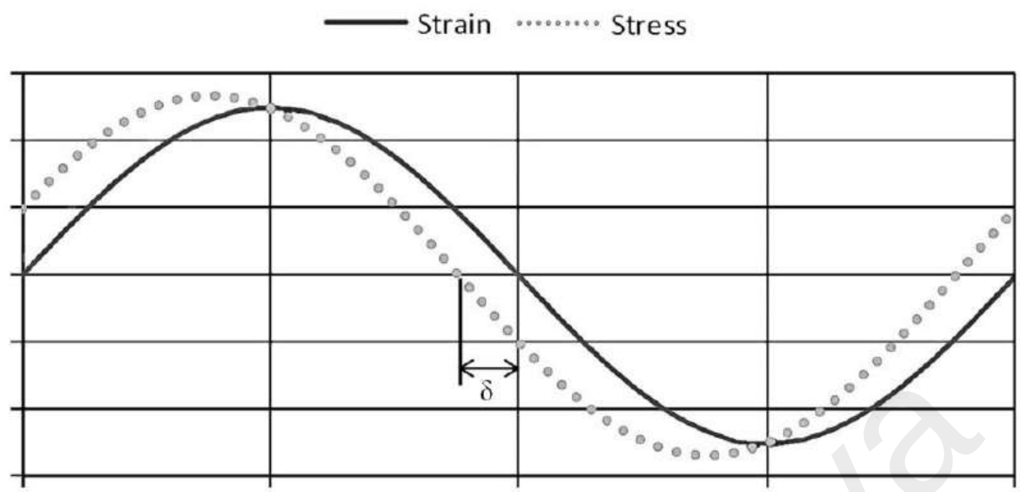

Figure 3. 1: Stress and Strain versus Time for Sinusoidal Strain (Vincent, 2012)

Cyclic pattern of a hysteresis loop is another way of obtaining amount of dissipated energy. The area under the loop divided by the elastic strain energy stored and released during a single cycle, gives the loss factor. This highlights the fact that a material with a great loss factor has a robust loop. The middle line of the plot presents zero value of the loss factor which corresponds to purely elastic response with no dissipated energy, e.g. steel when subjected to cyclic loading shows little energy loss which is generally neglected. The hysteresis loop plotted in Figure 3.2 is obtained for the same loading that was applied to plot Figure 3.1.

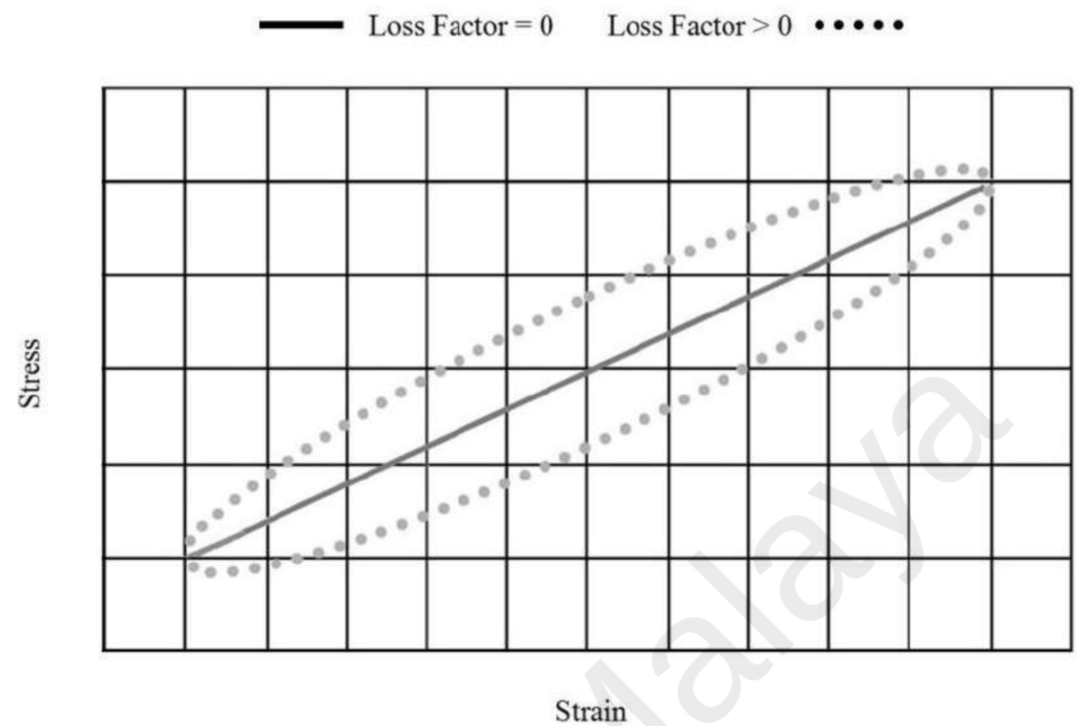

Figure 3. 2: Hysteresis Plot for Sinusoidal Strain (Vincent, 2012)

Speaking of the dual nature of the synthetic rubber, to obtain two properties namely *E*' and loss factor, the material test has to first comes up with stress-strain properties which corresponds to *E*' under static loading conditions and an additional dynamic testing has to be separately conducted to determine the loss factor or loss modulus. The behavior model development of rubber is broken into first, elasticity area and second, viscoelasticity area. It is worth mentioning that many properties of typical VEMs depend on temperature and frequency while for the case of filled rubbers such dependency is lessened to a lower degree. Temperature can be a challenge for near the glass transition temperature while for the considered HDR compounds in this research such temperature condition is well below 0º C.

3.1.5 Elasticity Material Models

The nonlinearity of the stress-strain relationship and a large capacity of rubbers for elastic deformation make the mathematical modeling of rubbers a very complicated process. For instance, rubber behaves almost according to Hooke's law at small strains like below 15%, and above this level of strain the behavior becomes highly nonlinear. Such behavioral feature is why this material is termed hyperelastic material. To tackle this complexity a strain-energy density function, W, is utilized instead of modeling behavior based on the stress-strain curve, (Muhr, 2005). The benefit of the hyperelastic curve is that it can be differentiated according to strain to determine stress. The two general approaches to specify appropriate mathematical models of these hyperelastic functions are statistical or physical based method and the second one is called phenomenological theory.

Statistical theory tries to consider properties of the long-chain molecules and their characteristics to derive a formula where highly complex mathematics is involved even in the range of small strains. However, according to related experimental verification, apart from a good first approximation, matching the actual behavior with the outcome of the statistical theory has difficulties, (Treloar, 1975). This noncompliance becomes more problematic in cases with large deformation.

The second approach, phenomenological approach, is a purely mathematical one to model the elastomers' stress-strain behavior and, unlike the statistical theory, it is not based on the actual molecular make-up. This method has made a greater success matching the test data with those of experimental verification and has been in use in commercial finite element programs. The phenomenological functions were first introduced by Mooney and later on it was developed by Rivlin in the 1940s (Freakley and Payne, 1978).

3.1.6 Viscoelastic Material Behavior

The inherent damping properties of rubber originate from VE nature of this material. VE behavior of rubber in simple shear condition for typical range of deformation is approximately linear, (Freakley and Payne, 1978). This highlights the independency of VE behavior on the stress level for the normal range of usage. Apart from the strain level, the VE characteristics of rubber can be represented by a stress relaxation curve. There are several fashions that can deal with determination of the numerical values for material damping. The loss modulus can be determined through two methods that are associated with cyclic testing. In case of plotting both stress and strain against time the lag between stress and strain gives the phase angle, , which is presented by Equation 3.4 along with stress and strain under forced harmonic loading. The phase angle is the result of multiplying the lag in seconds by the radial frequency, . This calculation is illustrated in Figure 3.3.

$$\sigma = \sigma_0 \sin(\quad t + \quad)$$
$$\varepsilon = \varepsilon_0 \sin(\quad t) \tag{3.4}$$

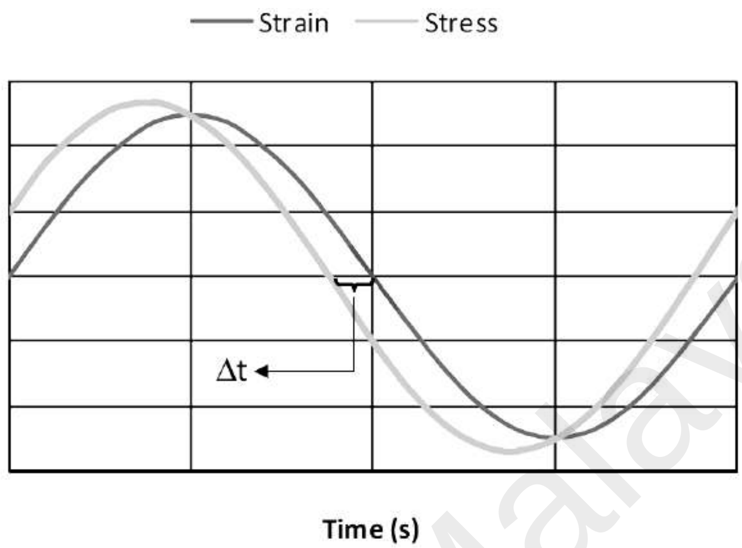

$\delta = \Delta t \times \omega = \Delta t \times 2\pi f$
$\eta = \tan(\delta)$

η: Loss Factor
δ: Phase Angle
f: Frequency (Hz)
: Circular Frequency (rad/s)

Figure 3. 3: Calculation of Loss Factor from Cyclic Stress and Strain Data (Vincent, 2012)

Another approach to determine the required properties through identical forced vibration experiment is by plotting stress on the vertical axis and strain on the horizontal axis. This plot creates elliptical hysteresis whose area shows the energy dissipated. The ratio of this area to the quantity 2π multiplied by the strain energy stored during that loop results the loss factor. In other words, the energy dissipated divided by the elastic strain energy. Figure 3.4 depicts an example of this calculation. For both aforementioned methods the experiment has to be conducted throughout both the frequency range and applicable strain levels to specify the variation.

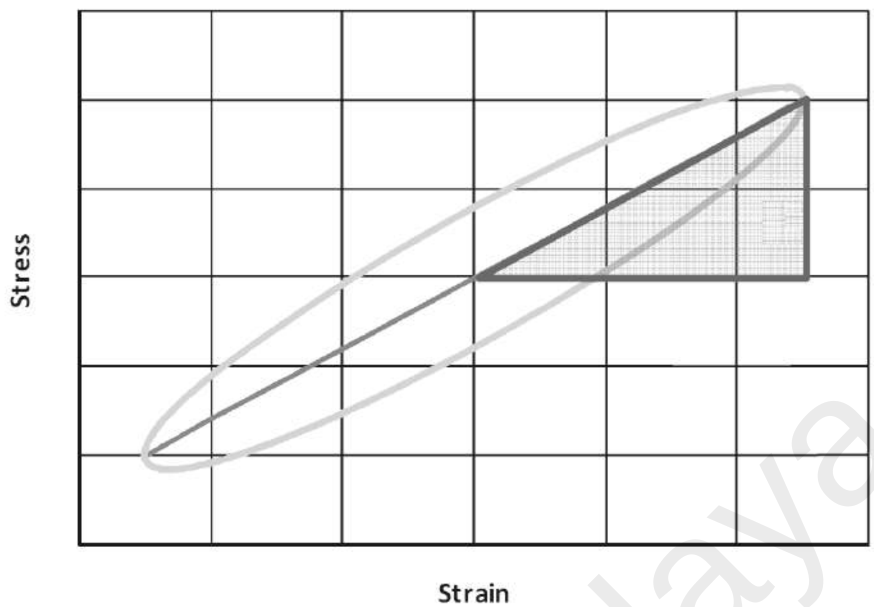

$= E_D/2\pi SE$ Elastic Strain Energy (SE), Triangular Area
Energy Dissipated (ED), Ellipse Area

Figure 3. 4: Loss Factor Determination from Hysteresis Loop (Vincent, 2012)

The key factors that reflect the characteristics of VE dampers are storage modulus G_1, the loss modulus G_2, the loss factor η and the energy dissipation E_d. Considering the sinusoidal excitation as $u_d = u_0 \sin \omega t$, in which u_0 is the amplitude and stands for circular frequency of excitations. Following this, the force-displacement relation can be expressed as follows:

$$\left(\frac{F_d - K_d u_d}{\eta K_{d1} u_0}\right)^2 + \left(\frac{u_d}{u_0}\right) = 1 \tag{3.5}$$

where F_d represents the force and u_0 is displacement of the VE damper as shown in Figure 3.5.

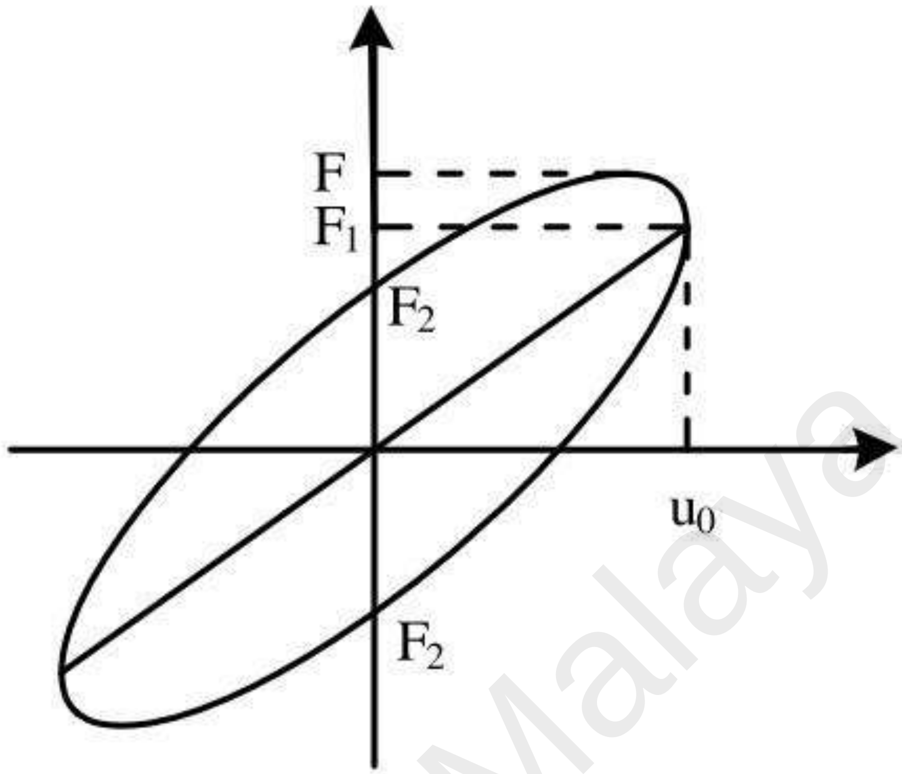

Figure 3. 5: Force-displacement hysteresis curve (Xu, 2007)

The biggest damping force of the damper is given by F, the maximum displacement is represented by u_0, the corresponding force at displacement u_0 is F_1, the corresponding force at zero displacement is F_2 and K_{d1} stands for storage stiffness. The last two parameters are expressed by Equations 3.6 and 3.7, respectively.

$$F_2 = \eta k_{d1} u_0 \tag{3.6}$$

$$k_{d1} = F_1/u_0 \tag{3.7}$$

The earthquake mitigation theory of VE devices defines the storage modulus G_1, the loss modulus G_2, the loss factor η and the energy dissipation E_d through Equations 3.8 to 3.11, (Xu, 2007).

$$G_1 = \frac{F_1 h_v}{n_v A_v u_0} \tag{3.8}$$

$$\eta = \frac{F_2}{F_1} \tag{3.9}$$

$$G_2 = \eta G_1 \tag{3.10}$$

$$E_d = \frac{\pi n_v G_2 A_v u_0^2}{h_v} \tag{3.11}$$

where F_1 and F_2 can be obtained from the hysteresis curves, n_υ stands for the number of VE layers, A_υ and h_υ represent the shear area and thickness of the VE layer, respectively. $A_{\upsilon,}$ n_υ and h_υ are known from the manufacturing process of VED. After determination of these parameters (G_1, G_2, η and $E_{d)}$ other related factors of the VED can also be calculated. The following expressions give the equivalent stiffness K_e and the equivalent damping C_e of the VED.

$$k_d = \frac{n_v G_1 A_v}{h_v} = \frac{n_v A_v}{h_v} \times \frac{F_1 h_v}{n_v A_v u_0} = \frac{F_1}{u_0} \tag{3.12}$$

$$C_d = \frac{G_2 A_v}{\omega h_v} = \frac{n_v A_v}{\omega h_v} \times \eta \times \frac{F_1 h_v}{n_v A_v u_0} = \frac{F_2}{\omega h_v} \tag{3.13}$$

3.2 Finite Element Analysis of High Damping Rubber

According to the review of the significant volume of research regarding VEM modeling, idealization of the mechanical behavior of synthetic rubber is a very complex process even if linear viscoelasticity is an appropriate assumption. In addition to highly nonlinear behavior of the rubber in the elastic range there are many options, depending on the deformation range and the material itself, provided by existing hyperelastic models. An obstacle in the VE material modeling is combination of stress-softening and its ability to recover a portion of the softening upon rest. Thanks to the software engineering efforts, many of these complex behavioral characteristics are implemented in the commercial finite element software ABAQUS (ABAQUS, 2017). In the following sections the applicable options for modeling materials like rubber and viscoelasticity are discussed.

3.2.1 Hyperelastic Functions

There are several hyperelastic models implemented in ABAQUS, generally categorized as physically based models and phenomenological models. In order to determine the suitable model which best fits the data, the curve fitting routines and the static test data are utilized for implementation of the models within the program. In general, more test data input leads to a better fit of the hyperelastic function. Following discussion clarifies the strengths and weaknesses of the various models.

3.2.1.1 Mooney and Mooney-Rivlin Model

Mooney's equation of strain energy is given in Equation 3.14, (Treloar, 1975):

$$W = C_1(\lambda_1^2 + \lambda_2^2 + \lambda_3^2) + C_2\left({}^{1}/_{\lambda_1^2} + {}^{1}/_{\lambda_2^2} + {}^{1}/_{\lambda_3^2}\right) \tag{3.14}$$

In this equation C_1 and C_2 stand for elastic material constants. The λ terms define the extension ratios for the three principal directions. The extension ratio is the difference between the original length of the body and its axially deformed shape. This ratio is equal to 1 for an unstrained sample and a 100% strain corresponds to an extension ratio of 2.

In order to find out how these functions work, a simple shear case can be taken for the Mooney's equation. Simple shear makes λ_3 equal to $1/\lambda_1$ and λ_2 equal to 1. Furthermore, Equation 3.14 shrinks to Equation 3.15. By substituting the shear strain, Υ, instead of the quantity λ_1-$1/\lambda_1$, the second part of the equation is obtained. Next is taking the derivative of W with respect to shear strain (Υ) and that concludes Equation 3.16 in which the quantity $2\times(C_1+C_2)$ is equivalent to the shear modulus G. Considering the assumption of the Mooney's formulation regarding incompressibility, the modulus of elasticity, E, is obtained by multiplying G times 3.

$$W = (C_1 + C_2) \times (\lambda_1^2 + {}^{1}/_{\lambda_1^2} - 2) = (C_1+C_2) \times \Upsilon^2 \qquad (3.15)$$

$$\tau = {}^{dW}/_{d\Upsilon} = 2 \times (C_1 + C_2) \times \Upsilon \qquad (3.16)$$

The constant in the Mooney formulation is related to the mechanical properties. This can be shown in a simple fashion. Although functionality of other hyperelastic material models is similar, nevertheless it is not as simple to understand the correlation of typical isotropic material properties to the hyperelastic constants. In order to generate these constants for hyperelastic material models, the test data obtained from pure homogeneous states of strain has to be used.

Further development of Mooney's model by Rivlin still stands on the assumption of incompressibility but there are three strain invariants (I_2, I_3, I_3) added to the model. Development of these three invariants is based on the assumption of isotropic material implying that the material has to be symmetric with respect to the three orthogonal principal strains. Equation 3.17 shows the updated mathematical model with use of these invariants. Since the rubber is assumed incompressible the third invariant, I_3, is equal to 1. Therefore, the two remaining invariants are actually independent of each other. Equation 3.18 shows the Mooney-Rivlin formulation, (Treloar, 1975). It is worth mentioning that the Mooney equation is a special case of the Mooney-Rivlin formulation.

Number of constants required in the Mooney-Rivlin formulation is summed to infinity which has mathematical expression but no physical meaning exists. For typical application of this equation values of i and j take values no more than 1 or 2 while C_{00} is set to be zero in order to maintain consistency at zero strain. Effectiveness of this model has been proven for rubber behavior prediction up to strains of 100%. Nevertheless, at strains greater than 200% this model fails to represent the increasing stiffness. There are many earlier modifications that have tried to provide a simpler model and to improve it for betterment of the physical behavior modeling. Number of these modified versions is too great to be discussed here and beyond the scope of this work.

$$\begin{aligned} I_1 &= \lambda_1^2 + \lambda_2^2 + \lambda_3^2 \\ I_2 &= \lambda_1^2\lambda_2^2 + \lambda_2^2\lambda_3^2 + \lambda_3^2\lambda_1^2 \\ I_3 &= \lambda_1^2\lambda_2^2\lambda_3^2 \end{aligned} \tag{3.17}$$

$$W = \sum_{i=0,j=0} C_{ij}(I_1 - 3)^i (I_2 - 3)^j \tag{3.18}$$

3.2.1.2 Arruda-Boyce Model

The Arruda-Boyce is a two-material-parameter and I_1 based model which is also called the eight-chain model as it was first introduced by a volume element which had eight springs emanating from the center of a cube to its corners and this was the representative element of this model.

Equation 3.19 shows the hyperelastic equation, *W*. As can be seen, this model includes small number of coefficients and this limits the ability of the model in terms of modeling shape change. Meanwhile, having only two coefficients, this model can fit well with limited test data. In this model μ is the shear modulus and D is equal to 2 times $1/K$, where K stands for the bulk modulus. λ_m represents the locking stretch which is typically set to value of 7. J_{el} is the elastic volume ratio and it depends on the level of thermal strains.

$$W = \mu\{\frac{1}{2}(I_1 - 3) + \frac{1}{20\lambda_m^2}(I_1^2 - 9) + \frac{11}{1050\lambda_m^4}(I_1^3 - 27) + \frac{19}{7000\lambda_m^6}(I_1^4 - 81) + \frac{519}{673750\lambda_m^8}(I_1^5 - 243) + \frac{1}{D}\left(\frac{J_{el}^2 - 1}{2} - \ln(J_{el})\right) \tag{3.19}$$

The eight-chain model is a physical-oriented hyperelastic model and it is grounded on non-linear representation of the strain energy density in terms of the first invariant I_1. The corresponding stress for uniaxial incompressible loading is calculated by Equation 3.20.

$$\sigma = \frac{\mu}{\lambda^{chain}} L^{-1}\left(\frac{\lambda^{chain}}{\lambda^{chain}}\right)(\lambda^2 - \frac{1}{\lambda}) \tag{3.20}$$

In this equation μ and λ are the material parameters, $\lambda^{chain} = \sqrt{(\lambda^2 + 2/\lambda)/3}$, and $L^{-1}(x)$ is the inverse Langevin function, where $L(x) = \coth(x) - 1/x$. It has to be mentioned that the Arruda-Boyce model is always unconditionally stable. Former studies have reported that this model can suitably predict large-strain multiaxial deformation states.

3.2.1.3 Van der Waals Model

The hyperelastic Van der Waals model is also known as the Kilian model and has the following form of strain-energy density function:

$$W = \mu\{-(\lambda_m^2 - 3)\,[\ln(1-\eta) + \eta] - \frac{2}{3}\alpha(\frac{\tilde{I}-3}{2})^{\frac{3}{2}}\} + \frac{1}{D}(\frac{J_{el}^2-1}{2} - \ln(J_{el}))$$

$$\tilde{I} = (1-\beta)\bar{I}_1 + \beta\bar{I}_2 \tag{3.21}$$

$$\eta = \sqrt{\frac{\tilde{I}-3}{\lambda_m^2-3}}$$

The parameter β is a linear mixture parameter that combines the parameters $\bar{I}_1$ and $\bar{I}_2$ into $\tilde{I}$. The interaction between the chains is modeled by the global interaction parameter 'a'.

$$a = \frac{2c_{01}}{3\mu} + \frac{\lambda_m^2}{\lambda_m^3 - 1} \tag{3.22}$$

3.2.1.4 Polynomial Model

The most commonly applied strain energy density function is the polynomial model of the strain energy potential. There are two classification of polynomial models; full and reduced.

3.2.1.4.(a) Mooney-Rivlin model

The full model, as seen in Equation 3.23, deals with the generalized form of the Mooney-Rivlin equation and depends on I_1 and I_2. Speaking of the full model equation, when N = 1, the standard Mooney-Rivlin model is obtained and based on former discussion, this results a good prediction for strain below 100% but not suitable for higher ranges of strain. On the other hand, utilization of a larger value of N demands a larger body of test data for fitting the corresponding 5 coefficients. ABAQUS software allows up to N=2. For this model the initial shear modulus and initial compressibility are calculated from $2\times(C_{10} + C_{01})$ and $2/D_1$ respectively. *Jel* is the same for all forms.

$$W = \sum_{i+j=1}^{N} C_{ij}(\bar{I}_1 - 3)^i(\bar{I}_2 - 3)^j + \sum_{i=1}^{N} \frac{1}{D_i}(J_{el} - 1)^{2i} \tag{3.23}$$

3.2.1.4.(b) Neo-Hookean Model

The Neo-Hookean model is a first-order, N=1, reduced polynomial model in which the dependency on I_2 is removed. This model was first developed in the 1930s and the formulation is presented in Equation 3.24. This model has limitations but yet simple in the application and effective at small strains. The initial shear modulus and initial bulk modulus are represented by C_{10} and $2/D_1$, respectively.

$$W = C_{10}(\bar{I}_1 - 3) + \frac{1}{D_1}(J_{el} - 1)^2 \tag{3.24}$$

3.2.1.4.(c) Yeoh model

The Yeoh model is a third-order reduced polynomial model, i.e. N=3, and compared to other models it covers a much wider range of deformation. Studies have reported that predictions of this model are robust (Drucker stable). Advantages of Yeoh strain energy function are listed in the following:

i. prediction of stress-strain behavior in different deformation modes via data obtained from a simple deformation mode like uniaxial tension,

ii. accurate prediction of equilibrium response of elastomers in different loading modes,

iii. predicting variation of the shear modulus along with deformation increment,

iv. ease of apply.

Equation 3.25 depicts the Yeoh model where the initial shear modulus and the initial bulk modulus are $2 \times C_{10}$ and $2/D_1$, respectively. J_{el} is the same as other forms. Calculation of reduced polynomial models can go up to N=6.

$$W = \sum_{i=1}^{3} C_{i0} \, (\bar{I}_1 - 3)^i + \sum_{i=1}^{3} \frac{1}{D_i} (J_{el} - 1)^{2i} \tag{3.25}$$

As can be seen in the equation, the strain energy density of the hyperelastic material model of Yeoh is a 3-term expansion of the first strain invariant, I_1 and it is available in all major Finite Element (FE) codes.

3.2.1.5 Ogden Model

The Ogden model has the ability of capturing upturn (stiffening) of stress-strain curve in addition to covering a large deformation range. This model is expressed in terms of the principal stretches and there is no need for the exponents to be integers. This is a unique advantage of this model. Variable N can go up to 6, nevertheless 3 is a common value. The

Ogden model's drawback is that it should not be utilized with one type of test data, especially if multiple terms are considered. Equation 3.26 shows the generalized Ogden model in which $2/D_1$ is the initial bulk compressibility and J_{el} term is the same as all the previous models. The initial shear modulus is given in Equation 3.27.

$$W = \sum_{i=1}^{N} \frac{2\mu_i}{\alpha_i^2} (\overline{\lambda_1^{\alpha i}} + \overline{\lambda_2^{\alpha i}} + \overline{\lambda_3^{\alpha i}} - 3)^i + \sum_{i=1}^{N} \frac{1}{D_i} (J_{el} - 1)^{2i} \quad (3.26)$$

$$\mu_0 = \sum_{i=1}^{N} \mu_i \quad (3.27)$$

3.2.1.6 Marlow Model

The Marlow model needs no curve fitting and its ability to capture the behavior from one test mode has been reported to be exact. This model is a general first invariant and it is ideal when only one type of test data is available. According to Equation 3.28, the Marlow model divides the strain energy into the deviatoric and volumetric parts. The former is created from inputting uniaxial tension test data and the earlier is associated with volumetric tests data or specifying the Poisson's ratio.

$$W = W_{dev}(\bar{I}_1) + W_{vol}(J_{el}) \quad (3.28)$$

3.2.2 Modulus

Generally speaking, Young's modulus is expressed as the slope of the stress-strain curve in the linear elastic range. In case of rubber compounds this linear part is associated with small strains (usually less than 15 %). For greater strains of filled rubber there are two moduli employed for stress-strain description; the modulus of first extension deals with high elongation like 300% and it is higher than that of unfilled rubber compound, and the final modulus corresponds to the extent of cross linking of stress and its corresponding strain of say 100% or 300%. According to "Mullins effect" phenomenon, carbon black vulcanizates are permanently softened in tension, (Mullins, 1969). This means that the more successive load is exerted on the rubber the more softening occurs. The filled rubber under successive stretches has a lower modulus and this may be because of secondary filler network breakdown, detachment of rubber molecules from the filler surface, aggregate movement like rotational movement and rupture of the short chains between filler particles, Donnet et al., (1993).

Application of hyperelastic models in ABAQUS provides the Mullins effect option, (ABAQUS, 2017). Although implementation of this model has provided a damage type model in ABAQUS, nevertheless application of Mullins effect cannot be done with modeling of VE nature of the rubber material.

3.2.3 Hysteresis

Studies of rubber material behavior conducted by Bergstrom and Boyce (1998; 2000; 2001) first founded the hysteresis option for rubber like materials. Along with the time-dependent element in ABAQUS, other options such as perfect elastic spring and hyperelastic material definition are available. Equation 3.29 presents the effective creep strain in the time dependent element.

$$\dot{\varepsilon}^{cr} = A(\lambda^{cr} - 1)^{C}\sigma^{m} \tag{3.29}$$

where parameter, *m,* a positive exponent, is in charge of characterizing the effective stress dependence on the effective creep strain. Parameter, *C*, is in charge of characterizing the creep strain dependence on the creep strain rate and it is restricted to values between -1 and 0. The constant, *A*, maintains dimensional consistency and must be greater than 0. In addition to the mentioned parameters the stress scaling factor, *S*, defines the ratio of stress carried by the time-dependent spring-dashpot to the elastic spring. Other terms listed below may take typical values suggested in Equation 3.30 due to absence of curve fitting for this model. That is why application of this model in ABAQUS demands a trial and error approach. The research conducted by Bergstrom and Boyce (2001) has suggestions regarding where these numbers can get started.

$$
\begin{aligned}
&S = 1.6 \\
&M = 4 \\
&C = -1.0 \\
&A = \frac{5}{\sqrt{3}^{m}}\,(sec)^{-1}(\mathrm{MPa})^{-m}
\end{aligned}
\tag{3.30}
$$

3.3 Concluding Remark

This chapter presented a comprehensive discussion of the viscoelastic material behavior. Rubbers are versatile materials and necessary for a broad range of applications. There is no doubt that a comprehensive understanding of the assumptions and models associated with hyperelastic and VE or hysteretic behavior is required to create an accurate model of synthetic rubber's dual nature. There are some key issues to be discussed regarding the modeling of rubber materials and viscoelasticity with finite element method; first, incompressibility of rubber which requires utilization of hybrid elements recommended for incompressible hyperelasticity. In this regard, the stability of the strain energy function must be verified when hyperelastic materials and automatic material evaluation are used.

CHAPTER 4: METHODOLOGY

4.1. Introduction

This chapter contains detailed description of the experimental test program. The test program is divided into five sections; (i) concept of the considered VE RRBD, (ii) concept of the cable brace system with a PCS by which wire-rope bracing members are bundled at the intersection point, (iii) describing the cyclic uniaxial tensile tests of the viscoelastic material (VEM) in which monotonic simple shear and shear stress relaxation tests are considered, (iv) cyclic quasi static tests of RRBD, and (v) details of the experimental tests including test setup of the frame specimens, instrumentations and loading procedures are presented. Furthermore, to evaluate performance of steel buildings retrofitted with proposed systems, individually and in hybrid combination, 9-storey structures with moment-resisting frame are designed.

4.2 Methodology

Material properties of VEM can be obtained through a very recognized method which is measuring the stress-strain responses for each rubber specimen. Therefore, each specimen is subjected to monotonic and cyclic uniaxial tensile tests and simple shear and shear stress relaxation tests.

The hysteretic behavior of the suggested damper was obtained and assessed via a pseudo-static test of a built prototype. Increasing amplitude of loading was considered in the test and results approved the preliminary qualification of the device as an energy absorber one. Test of reversed cyclic loading was conducted for five specimen cases including bare frame (BF), cross cable bracing (CCB), the proposed PCS system, frame with (RRBD), and combination of the two techniques (RRBD+PCS). These experimental investigations were eventually followed by the nonlinear time-history analysis of a five-bay nine-storey moment steel frame which was equipped with both devices, the RRBD and the PCS cable bracing system, to assess the contribution and resistance of these two systems against seismic ground motions.

4.3 The Concept of New Viscoelastic Damper

Configuration of the suggested damper consists of VE pads that are sandwiched between steel plates, see Figure 4.1. These rubber pads have two advantages; first, they provide enough shear resistance to ensure both stable shear force and attenuation of lateral displacement and acceleration and second, they produce the restoring force for the damping system to return to its original location. The mechanism of the damper stands on the push/pull functioning of chevron brace members combined with slight rotational shear in a way that for a horizontal displacement of the frame structure, steel plates slide along with chevron braces and allow the rubbers to be pulled and pushed as the bracings undergo tension and compression forces. The performance mechanism of the system is shown in Figure 4.2.

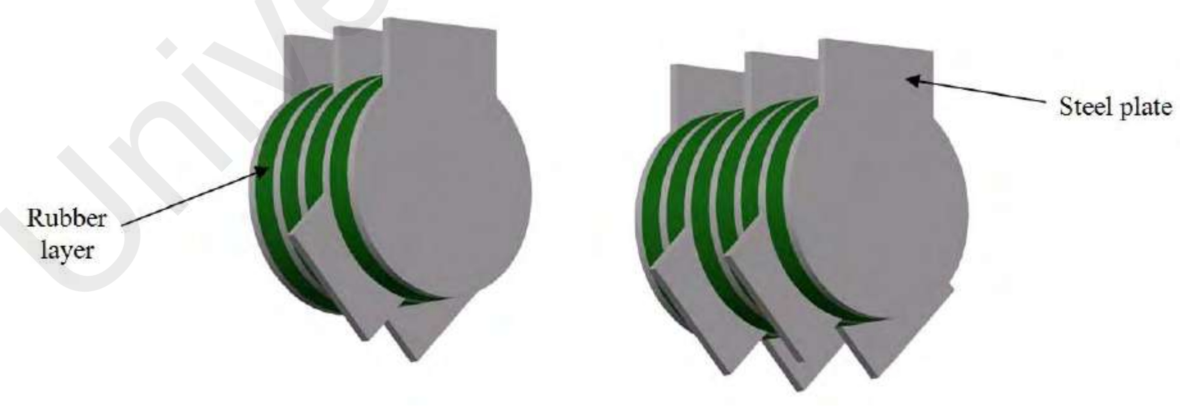

(a) 4 VE layers (b) 6 VE layers

Figure 4. 1:Rotary rubber brace damper (RRBD)

The nonlinear force-deformation relation of VE dampers provides greater stiffness at larger amounts of deformation in the structure. A very well-known material property of VE dampers is hyperelasticity which features a useful alternative compared to other damping materials like linear stiffening devices. Linear dampers increase base shear which is undesirable while hyperelastic material not only requires low strength at service loads but also it provides additional stiffness at higher displacement levels and therefore structural stability is improved.

For the employed VE material the moderate initial stiffness is associated with strains lower than 60%. Mid-range values of stiffness correspond to strains around 90% and strains in excess of 90% cause the hyperelastic effect (Roland, 2011). It has to be mentioned that such levels of stiffness change are largely dictated by the VEM compound. Next sections will discuss the incorporation of VEM stiffness behavior into the RRBD design. In order to control performance of the RRBD system the following parameters are introduced:

- Rubber thickness (T)
- Rubber diameter (D)
- Aspect ratio (D/T) of the device
- Number of rubber pads that have direct effect on the shear area
- Strength of VE material; the stiffness (k) of the VEM can be reduced by cored holes
- Different types of rubber, e.g., natural rubber, high-damping rubber
- Dynamic constitutive behavior of VEM

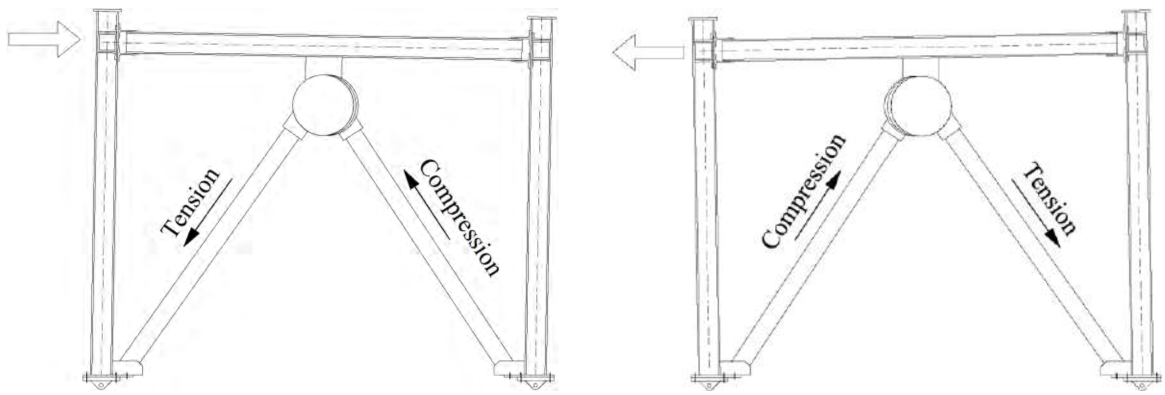

Figure 4. 2: Mechanism of action of the RRBD. Frame movement to the (a) right and (b) left.

4.4 Material Testing

Due the lack of a standard set of engineering constants and complexities the finite element analysis and design of elastomeric materials demand physical testing of the material for the required material properties. The required data for the FEA was generated by material characterization testing. This data can also be obtained from approximate values suggested by former publications or rubber manufacturers in absence of test data. Static, dynamic and time-dependent tests were performed. Static testing was consisted of uniaxial tension, and simple shear. Dynamic testing included both tension specimens and simple shear specimens considering three displacement levels and five frequencies (0.1, 0.2, 0.5, 1.0 and 1.5 Hz) of cycling. The selected frequencies are because of simulation periods of vibration in actual applications. The test of Multi-step stress-relaxation was carried out for all of the loading conditions at various strain levels.

4.4.1 Degradation test

Lifecycle of VEMs is a major factor that should be taken into consideration as it is related to the efficiency of the material as well as maintenance of the damper which causes replacement cost. One of the important degradation mechanisms takes place due to the ozone attack which causes split of carbon-carbon double bonds and consequently development of surface cracking. This phenomenon degrades the stiffness and strength over time. In order to evaluate the resistance of the VEM against the ozone attack it is very common to subject stretched strips of rubber to a higher concentration of ozone than the rubber is supposed to experience in its lifetime. This test sets the condition to a much severer condition than the real environment conditions and measures the long-term characteristics of the product within the limited time. The solution to ozone cracking is in adding anti-ozonants to the rubber compound. Therefore, specimens were tested with and without additives, based on ISO 1431, as shown in Figure 4.3.

(a) Ozone chamber

Figure 4. 3: Degradation test

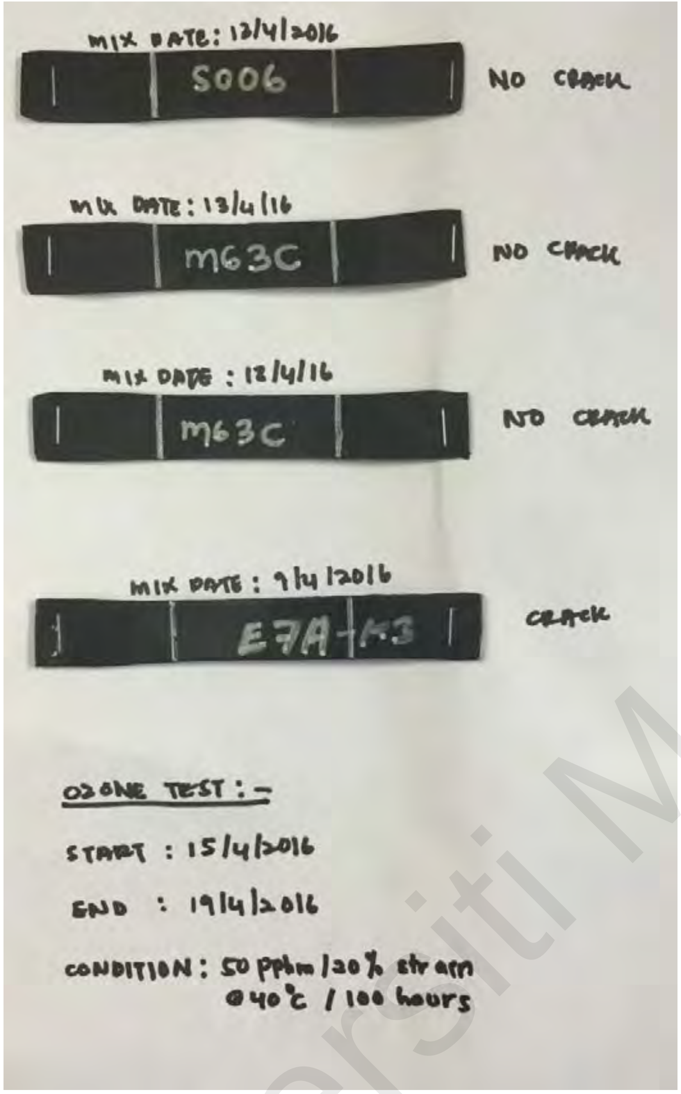

(b) Specimens

(c) Specimen dimension

(d) Specimen with cracks

Figure 4. 3: Degradation test (Cont.)

4.4.2 Hardness test

Shore (Durometer) test is the most common method to measure the empirical hardness value of VEMs. In this test, the Durometer indenter foot penetrates into the sample, as shown in Figure 4.4. It has to be mentioned that the resilience of VEMs may change the indentation reading over time, which is why the indentation time is sometimes reported along with the hardness number. Generally, the typical rubber hardness values fall between 20 and 90, and they are often given as a modulus quantity since a correlation between the hardness and modulus exists, i.e., a higher hardness indicates a higher stiffness, and often given along with the hardness value. The hardness test was carried out according to ISO 7619, and its value was ranged from 34 to 36. The selected value was the average value of 35.

Figure 4. 4: Hardness test

4.4.3 Uniaxial specimen testing

Monotonic and cyclic uniaxial tensile tests are both required, as determined in ISO37, (1995), to specify the material properties of the synthetic VEM. A tensile testing machine was utilized to measure the stress-strain response of each rubber specimen at the environmental temperature of 25˚C, shown in Figure 4.5 (b). The strain was then measured by an extensometer with clip gauges, located 20 mm from each other, and tensile grips to hold the specimen. The distance between the gauge marks were measured up to the breaking point.

According to the Malaysia Industrial standards, the tension in the monotonic uniaxial test was also exerted on the synthetic uniform 2-mm-thick dumbbell-shaped specimens until all three samples reached the failure state, see Figure 4.5 (a) in which the area clamped by the jig is shaded. Thickness of the specimens was the same with maximum difference of 0.2 mm. The gauge length (I_{exp}) and tensile force (F_{exp}) were measured in the test so that the nominal stress P_{exp} and stretch λ_{exp} could be calculated through Equation (4.1).

$$P_{exp} = \frac{F_{exp}}{t.B}, \quad \lambda_{exp} = \frac{I_{exp}}{I_0} \tag{4.1}$$

where parameter B stands for the thickness of the specimen and I_0 presents the initial gauge length.

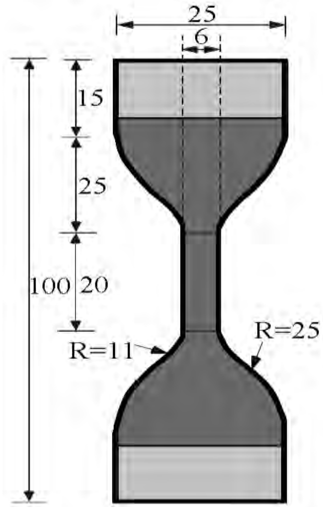

(a) Specimen sample for uniaxial tension test (mm)

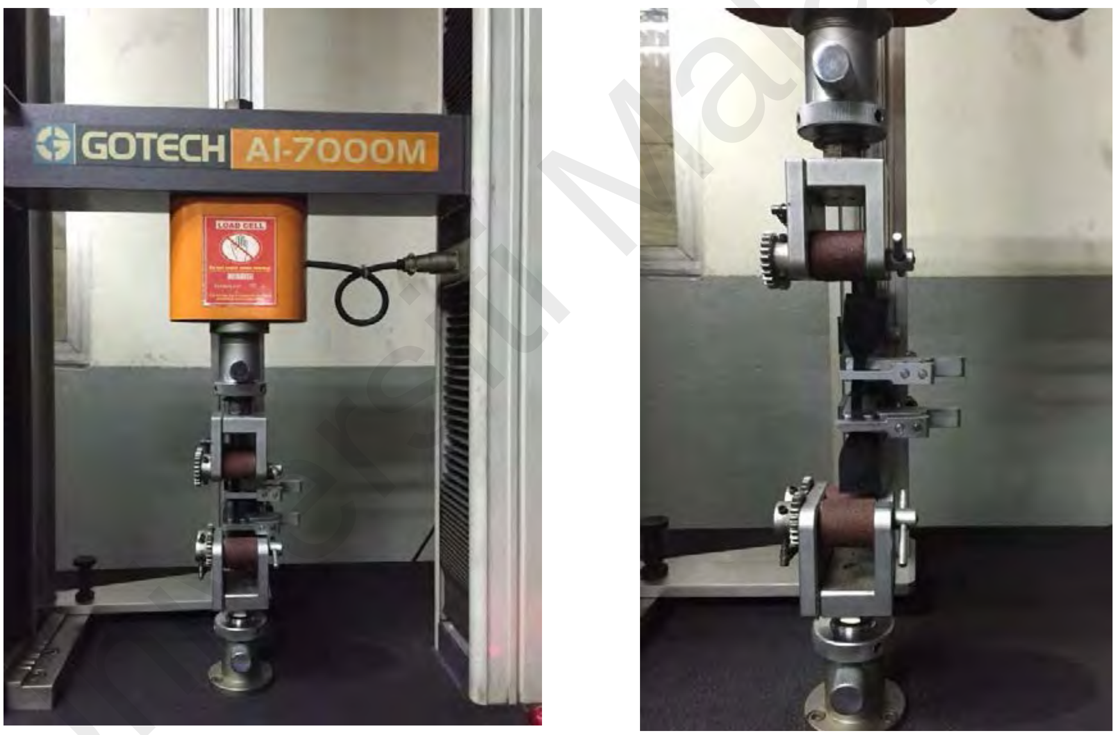

(b) Photograph of dumbbell specimen sample

Figure 4. 5: Tensile rubber test

4.4.4 Shear specimen testing

The selected shear specimen was a standard double sandwich sample whose dimensions are depicted in Figure 4.6 (a). Three steel plates and two rectangular specimens formed the sandwich construction and it was fixed to the testing machine. The stretching force was then applied by the movable clamp of the machine to the middle plate to exert the shear deformation. In order to be certain about a full bond between plate and rubber, the rubber and plate were bonded together during vulcanization process so that the bond was stronger than the rubber. The shear area was designed to be 500 mm2 and the rubber pad was 10 mm thick. Since several famous earthquakes like Northridge (USA, 1994) and the Kobe (Japan, 1995) lay within a frequency range of 0.14 – 1.12 Hz, the rate dependent performance of the sample was assessed at five test rates (0.1, 0.2, 0.5, 1.0 and 1.5 Hz) and at various strain levels including 25%, 50% and 100% of the thickness of the rubber pad, as illustrated in the shear test set-up in Figure 4.6 (b). It has to be mentioned that this data was not directly applied into ABAQUS. Nevertheless, adequacy of the finite element model was determined through making a comparison between the analytical and experimental hysteretic and cyclic plots.

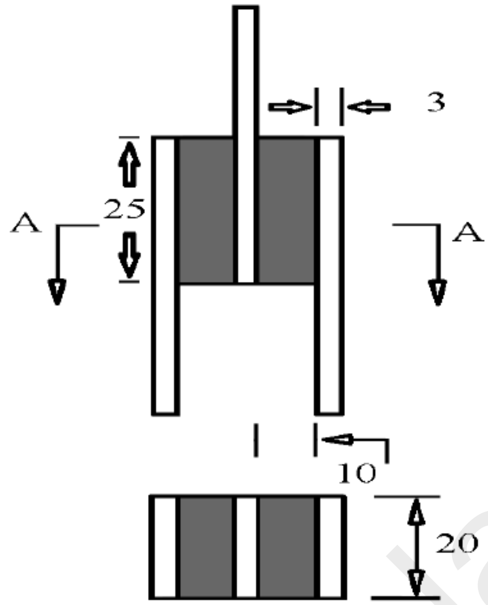

(a) Simple Shear Specimen Dimensions

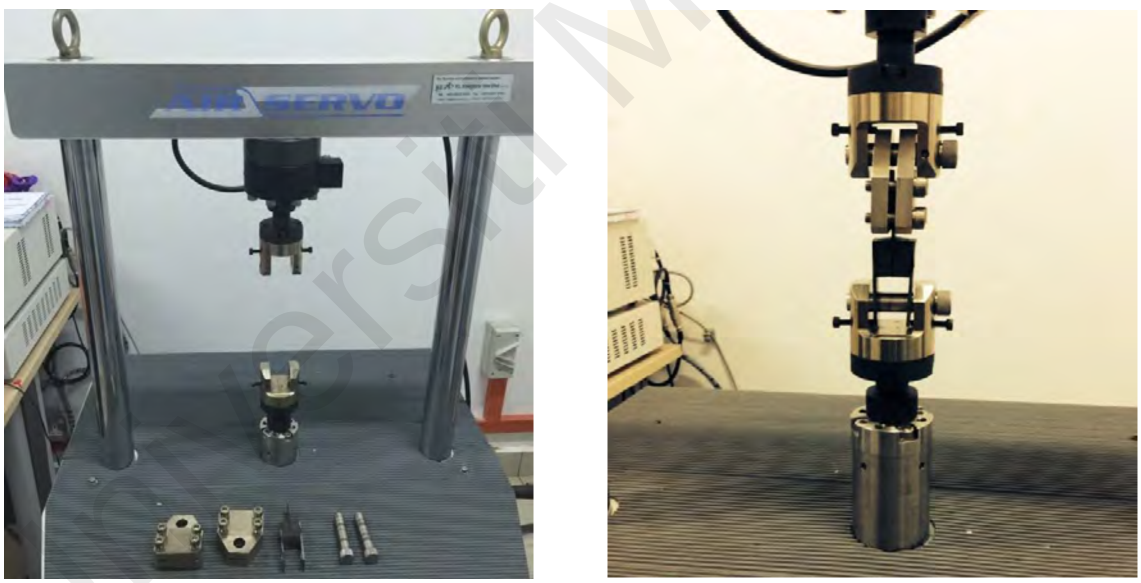

(b) Photograph of specimen sample

Figure 4. 6: Shear rubber test

4.4.5 Shear stress relaxation test on the VEM

The hyperelastic material model represents the material's nonlinear elasticity, however it is not a time dependent model. The nonlinear elastic behavior and strain-rate dependencies of a material can be modeled by the hyperelastic plus VE material model. This means that regardless of the level of the strain, the VE properties of the rubber can be presented by a single time-dependent stress relaxation curve which is the outcome of the stress relaxation test of specimen under constant strain level. This strain is instantly exerted to the middle steel plate and held constant. The considered strain rate was 30% for the stress relaxation test which was conducted for 250 seconds. Figure 4.7 depicts the design flowchart of the proposed systems.

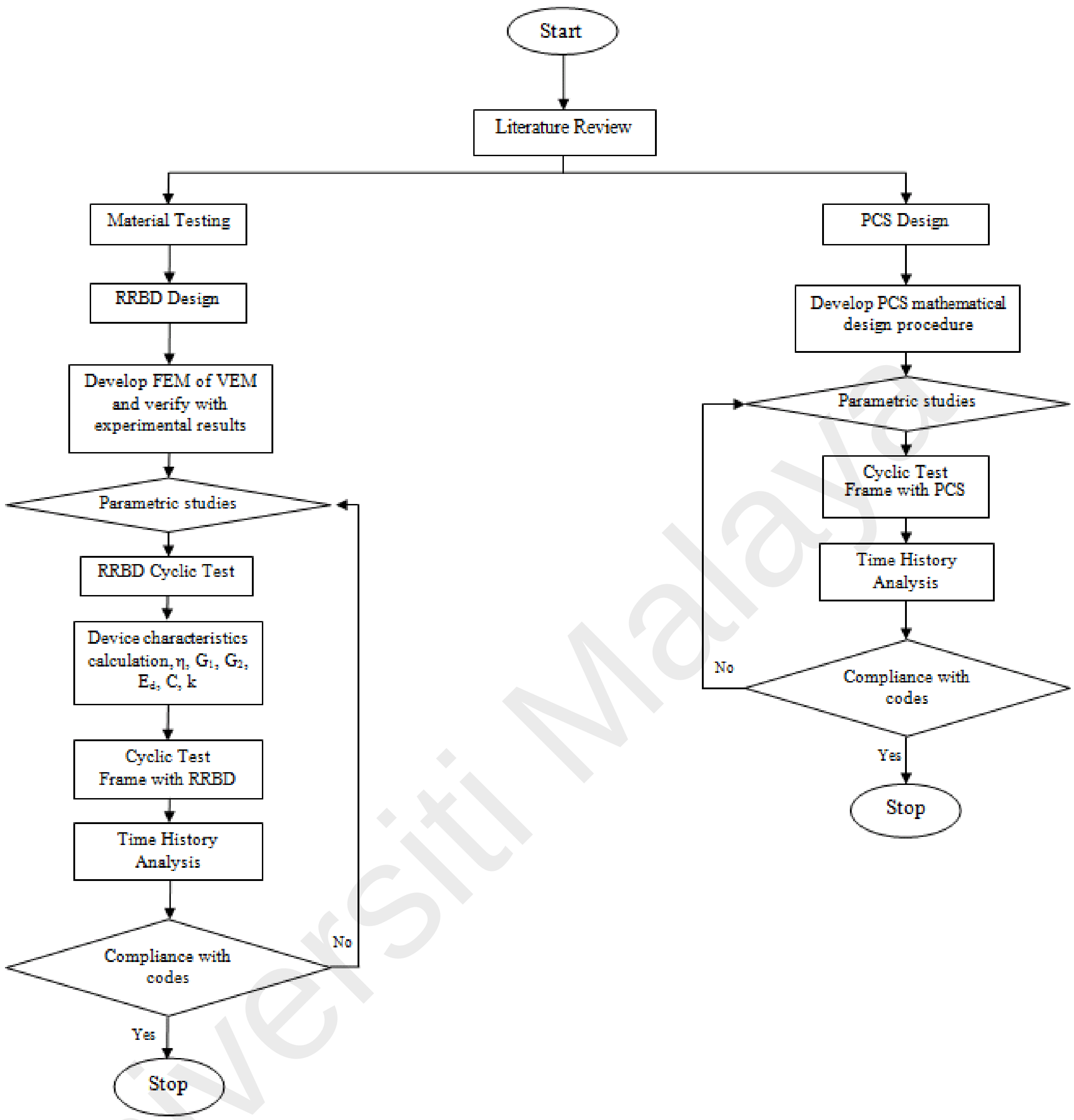

Figure 4. 7: Flowchart of research methodology

4.5 The proposed cable bracing system

The mechanism of the proposed cable bracing system allows every single cable to be crooked by the selected PCS. The PCS is in charge of bundling the wire-rope bracing members at the intersection point. This configuration sets the cables to be engaged and subsequently release their final strengths at greater lateral displacements of the frame. This considered set up for the proposed bracing system of the current research is an advanced version of an existing retrofitting method introduced for improvement of seismic behaviour of steel moment-resisting frames (Hou et al., 2009).

The steel wire ropes of the retrofitting system posses a large ultimate strength and rather small elastic modulus, hence their corresponding elastic elongation capability is a key characteristic, which causes the PCS to remain in elastic range under severe displacement demands. Furthermore, wire ropes increase the lateral stiffness and strength of the whole system. Nevertheless, they have no contribution in the energy dissipation capability. An advantage of the proposed configuration is that there is no reduction in ductility of the moment frame. The PCS function under monotonic load is depicted in Figure 4.8.

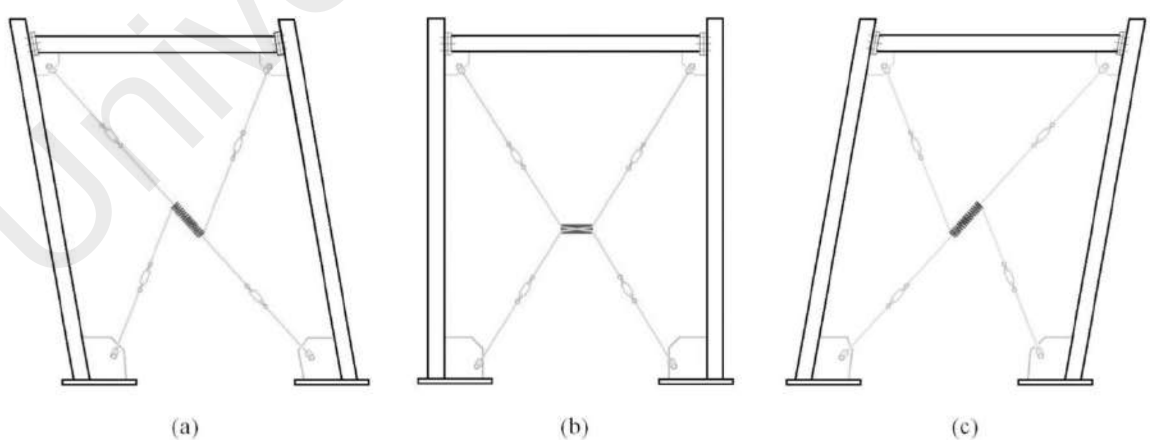

Figure 4. 8: Action of PCS System in frame: (a) right to left action of PCS; (b) imposed cyclic load; and (c) left to right action of PCS.

Figure 4.9 schematically shows the main components of the proposed retrofitting system.

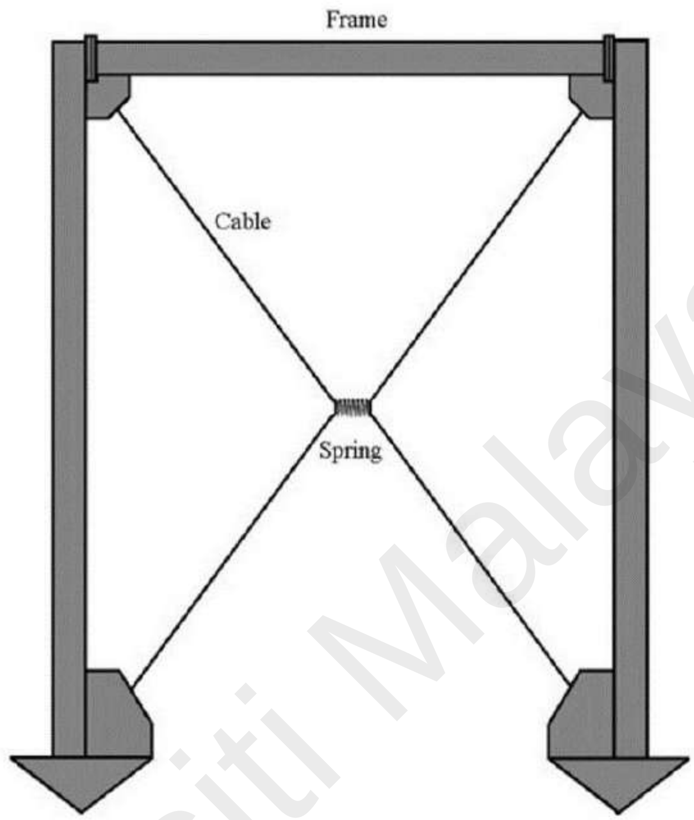

Figure 4. 9: Schematic of PCS system

The proposed bracing system takes advantage of two cables to mobilize the lateral stiffness of the structure, as both cables are held in tension by the compressed spring force. As the frame experiences lateral movement, the spring is extended, being recompressed when the frame returns to its original location. This provides additional stiffness to the frame as it returns back to the original place. This is a unique characteristic of the proposed mechanism, which is in contrast to the performance of ordinary bracing systems, such as non-prestressed and pre-stressed diagonal cable bracings, that provides the lowest stiffness when frames are in their initial position.

One of the challenges in real situation is occurrence of eccentric load. When axis of the spring does not coincide with the axis of load, hence the stress balance is disturbed. Practically, in such situation two sides of the spring undergo unequal stress during the load transfer from the cables to the spring, therefore a proper solution is to design a sliding hollow stiff shaft within the proposed PCS system as depicted in Figure 4.10.

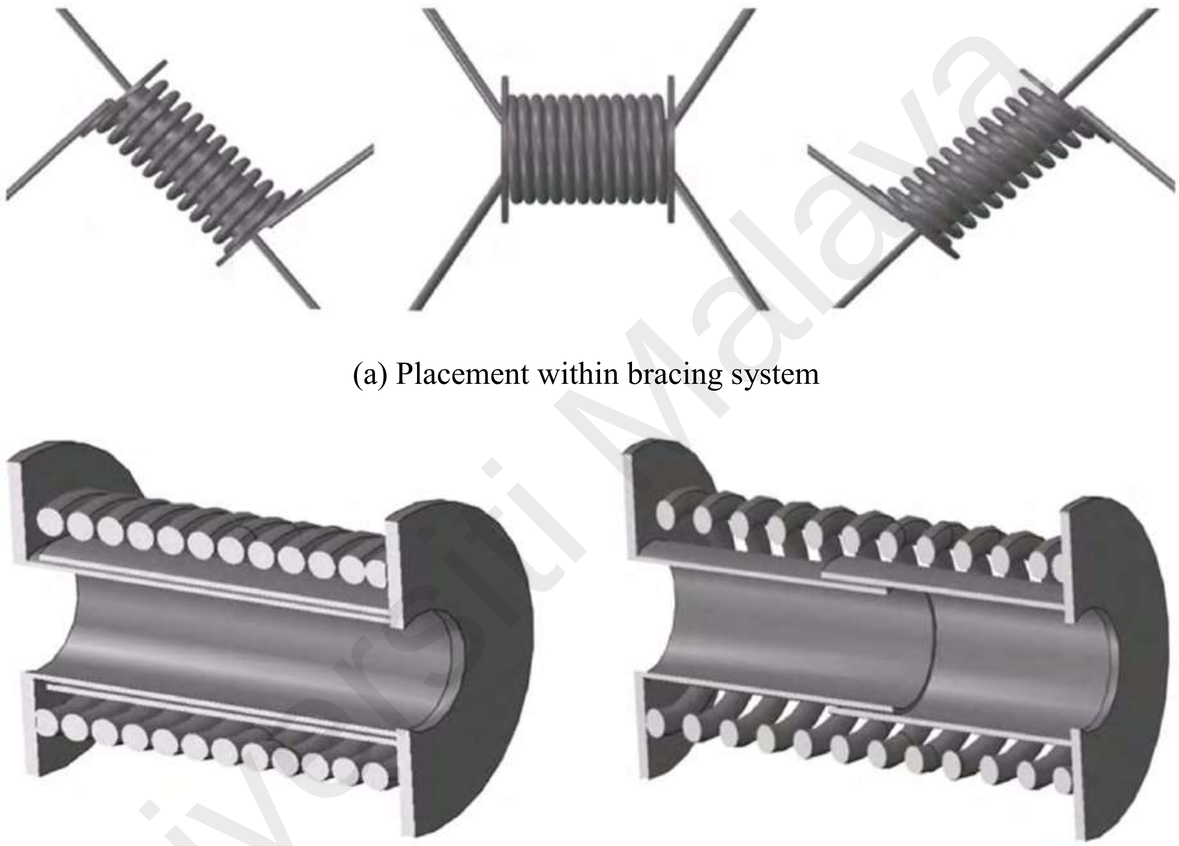

(a) Placement within bracing system

(b) Internal components

Figure 4. 10: Schematic representation of the PCS with stiff hollow shaft

4.6 Experimental Setup

4.6.1 RRBD Cyclic Test

The cyclic test of VED prototype was conducted by a 1000-kN universal testing machine in displacement control mode. The prototype was subjected to a pseudo-static test with rising amplitudes of 5mm, 10mm, and 20mm, under different frequencies of 0.1 Hz, 0.2 Hz, 0.5Hz, and 1.0 Hz to evaluate the hysteretic performance of the device. The hysteresis loops for force-displacement are distinguished by selecting the last loop among ten different cycles in each case. Three identical specimens were manufactured by MSL Rubber Company. The surface preparation for the three samples was similarly done by first removing mill scale from the steel plates and then roughening the surface with a palm sander and fine grit sandpaper. In order to clean up the grease and particles isopropyl alcohol was used on the surface which was then sanded with fine grit sandpaper. After cleaning the surface by alcohol again, both adhesive systems were utilized based on the manufacturer specifications before bonding. The test setup is displaced in Figure 4.11.

Figure 4. 11: The RRBD specimen in testing apparatus

4.6.2 Shaking Table Test

This section introduces a series of shaking table tests that simulate sinusoidal excitations of the experimental test conducted in the Structural Dynamic Laboratory at University Technology Malaysia (UTM), Figure 4.12. In the following, the experimental setup and instrumentations of the considered two-storey steel model structures equipped by the proposed damping system are explained. The two-storey steel frames are all 1.2 meters high. Model configurations include bare frame as a control for result comparison and RRBD equipped frame to assess the effectiveness and feasibility of the proposed damper in confrontation with seismic loads.

Figure 4. 12: Shaking table test frames

The main frames of the considered buildings were made by the commercially available hollow section-beam (50x30x2.5). This also made the first mode of the structure equal to the dominant frequencies of the shaking table excitation. Floor simulation was done by installing two mass blocks (60 kg each) representing the floor weight. It is worthy to note that, since the design of a single bay frame under real loads results in little sections for structural elements, the details of the RRBD were presumed, and other elements were designed proportionally to the target damping ratio of 10% of critical damping. The frames were exposed to a sinusoidal excitation with a frequency of 2.5Hz. The duration of sinusoidal harmonic excitations was 5 seconds in all cases. However, to include free vibration of structures in the study, the response measurement duration was 15 seconds. The acceleration responses and floor deflection were measured by accelerometer and linear variable displacement transducers (LVDTs), respectively. The accelerometers were installed on each floor as well as the shaking table in the direction of input ground motion. LVDTs had dynamic range of ±30 cm.

Two identical dampers were applied on the second floor, on the side frames, of the model structure. The dampers' axis coincided with the direction of shaking table motion. It has to be mentioned that optimal design of damping system for a prescribed building is still a state-of-the-art. This highlights two problematic challenges in the design of damping systems: over-design and under design of the dampers. The former case corresponds to amplification of acceleration despite a probable drastic reduction of displacement and the later leads to limited and insufficient controlling effects.

The design goal of this research was to meet simultaneous suppression of acceleration and reduction of displacement responses of the structure. To achieve this goal, dimensions of dampers were determined by a parametric study conducted through computer simulations. This preliminary study was done by a personal computer equipped with an Ethernet interface which provides fast transfer of data and post processing in other computers. The data acquisition system and the controller are depicted in Figure 4.13.

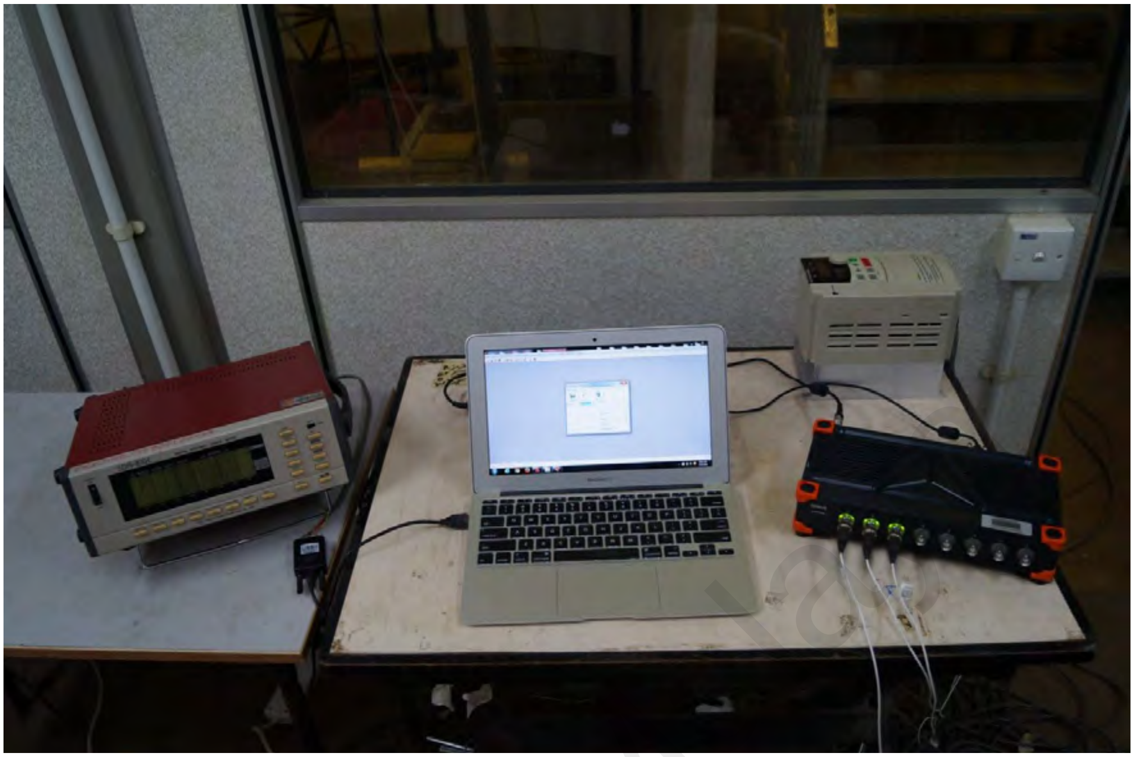

Figure 4. 13: Controller and data acquisition system

4.6.3 Test specimen details

The proposed systems were experimentally tested to evaluate their applicability and effectiveness in steel frames. The tests were conducted in the Structural Laboratory of University of Malaya. Five identical single-bay single-storey frame specimens were considered including a bare frame (BF), frame retrofitted with typical cross cable bracing (CCB), frame equipped with RRBD, frame with the PCS bracing system, and a frame equipped with hybrid passive control system (HPCS), which includes of RRBD and PCS system. Figure 4.14 presents dimensions of the specimen with wire rope (cable) bracing. The dimensions of the steel frame were 1595 × 1275 mm, measured centre-to-centre of the beams and columns. The column and beam members of H-75×75×3 (steel grade: A36) were connected using bolts, and the bottom of the columns were fixed with pin supports.

The spring was installed to the frame using a round strand with a nominal diameter of M6, 6×7 IPS IWRC bright steel wire cables, an M8 105 mm Hook and Eye turnbuckle, and steel DEE shackles.

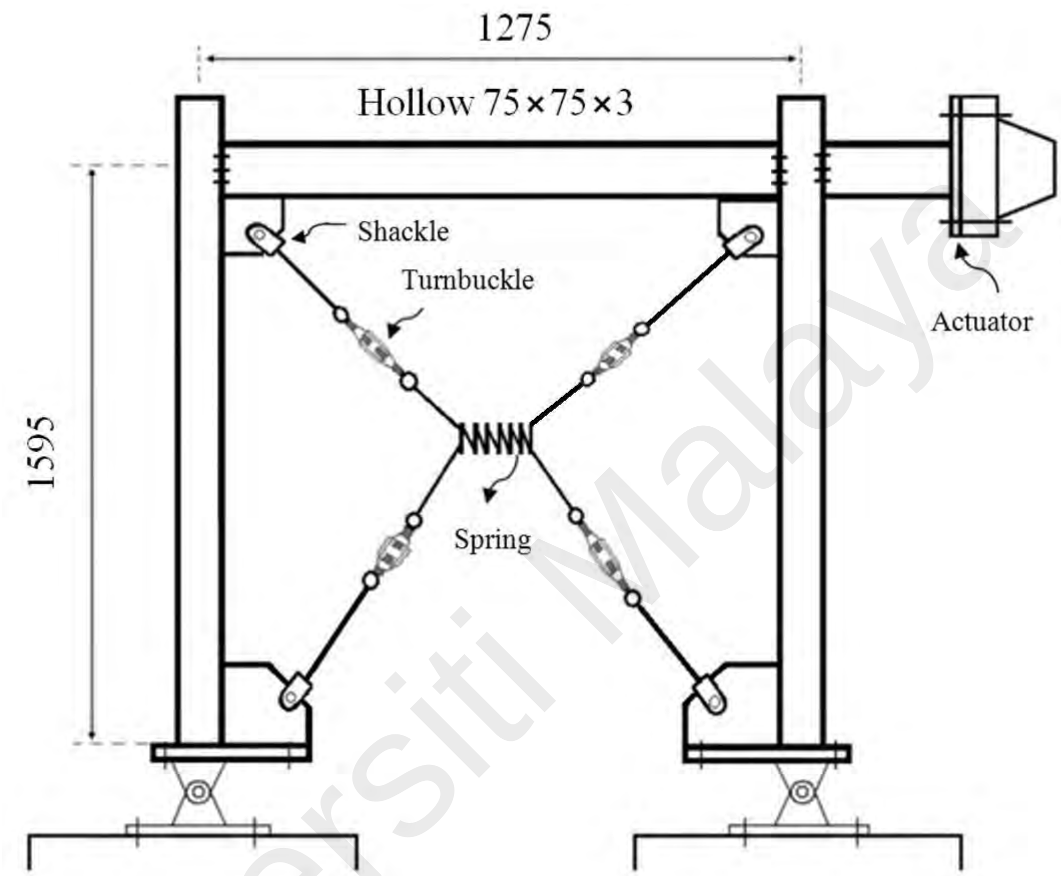

Figure 4. 14: Test specimen with loading system

Turnbuckles pull in the slack of the wire ropes. In order to record variations of the internal strains and stresses and monitor the overall performance of cable bracing, strain gauges were installed in the longitudinal direction of the turnbuckles and these were connected to the data acquisition system which had a Flextest controller and a desktop PC platform running MTS TestSuite software.

Providing large lateral strength, i.e. lower R factor, is a solution to the low inelastic deformation capacity of ordinary moment frames (OMF). This issue plays a crucial role in the design requirements of OMFs and it is why ASCE/SEI 7, (2013) has placed significant height and other limitations on their use. In order to apply strength requirements, beam-column connections have to be reinforced by cover plates or haunches attached to the beam. Noticing the minimal inelastic deformation capacity of OMF, it is clear that unlike design provisions of the intermediate moment frame (IMF) and special moment frame (SMF) systems, there is no given quantitative definition of this capacity. In fact, classification of moment frames define OMFs as moment frame systems that are difficult or impossible to qualify as IMF or SMF. For instance, moment frames with a hollow structural section (HSS) are a type of OMF. In this study, by referring to the AISC-LRFD code, (2005) and relevant seismic guidelines, three hollow structural specimens were provided. Connections of the considered specimens were strengthened by haunches. Due to the fact that the design of a single floor and single bay frame under real loads results in little sections for structural elements, the details of the RRBD were presumed and other elements were designed proportionally to the target damping ratio of 10% of critical damping. Moreover, PCS details were based on full straightening of cables at 2% drift of the column height.

In the test, magnitude of the applied load was monitored through a load cell. The wire rope used consisted of six strands laid helically over a smaller independent central core wire rope and the key mechanical properties of steel wire rope can be listed as follows: elastic stiffness is 70% of a comparable steel section (Costello, 1997), significant elastic elongation capability that helps them remain elastic under severe displacement demands and their elastic nature which makes post-yield stiffness of the whole system regulated. Table 4.1 provides the utilized mechanical characteristics of the wire rope unit in the proposed retrofitting configuration.

Table 4. 1: Mechanical properties of wire rope unit

Type	Dia. (mm)	Yield Strength (MPa)	Yield strain	Tensile strength (MPa)	Elastic modulus (GPa)	L (mm)	W (mm)
Wire rope	6	1016[a]	0.01	1765	123.5	-	-
Hook and Eye turnbuckle	8	305[b]	0.004	515	205	-	-
DEE shackles	10	305	0.004	515	205	25	13

[a] An equivalent yield stress was defined at a strain of 1% according to ASTM, as the wire rope did not exhibit a yield point.

[b] The 0.2% offset method was applied to calculate the yield strength of the turnbuckle.

4.6.4 Horizontal cyclic loading tests

In the conducted quasi-static cyclic tests, with the set-up depicted in Figure 4.15, a hydraulic jack with 500 kN capacity and 500 mm stroke were employed to impose the cyclic load. The displacement control cyclic loading protocol is depicted in Figure 4.16. The actuator had a built-in LVDT to monitor and measure the applied displacements.

(a) BF

Figure 4. 15: Experimental setup

(b) RRBD

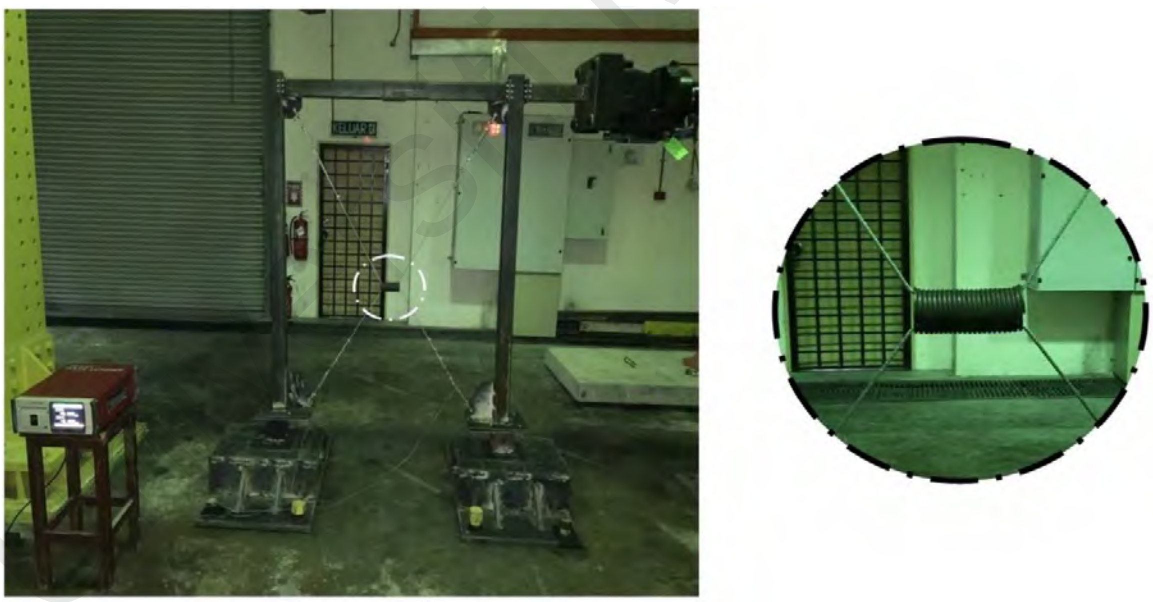

(c) PCS

Figure 4. 15: Experimental setup (Cont.)

(d) CCB

(e) PCS and RRBD

Figure 4. 15: Experimental setup (Cont.)

A hollow section member transmitted the push cyclic load of the actuator directly on to the column and the pull cycles were transferred via an attached plate installed at the top of the column. The cyclic exertion of displacement was continued in an incremental manner and then stopped as soon as the final stage of the load protocol was achieved.

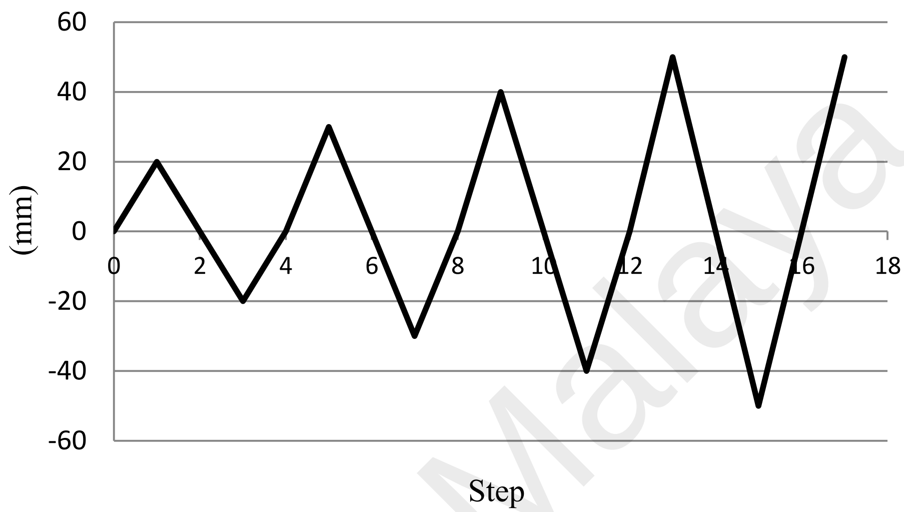

Figure 4. 16: Loading protocol used in the cyclic tests.

A tensile test was conducted on loops at its ends, in order to determine the pre-stress force required ensure that the cables were slack free. The pre-stress force was quantified to be 3.4 kN. Turnbuckles were in charge of tightening the wire rope assemblies and a cyclic inter-storey drift history was applied according to Table 4.2 (AISC, 2002).

Table 4. 2: Loading Sequence

Run number	Inter-storey drift (rad)	Number of cycles
1	0.00375	6
2	0.0050	6
3	0.0075	6
4	0.0100	4
5	0.0150	2
6	0.0200	2
7	0.0300	2
8	0.0400	2

4.7 Nonlinear Dynamic Response History of 9-Storey Steel Moment Frame Structures with Proposed Systems

Researches conducted in the area of structural control systems have concluded a great diversity in terms of specific applications and required objectives. That is why there is no common guideline to compare the results obtained from various algorithms and devices. The acceptance and proof of effectiveness of a proposed control strategy is only dependent on experimental verification in close to realistic condition which is not practical for cases like medium or high-rise structures due to both practical and economical aspects of the tests.

To tackle this issue, the American Society of Civil Engineers (ASCE) recommended an alternative to evaluate the validity of the research results. That solution is the analytical benchmark models developed by a committee of ASCE that tends to compare the results obtained from structural control algorithms in confronting with the structural control problems (Spencer et al., 1997 and Wu et al., 1997). This study tends to evaluate performance and effectiveness of the proposed systems (RRBD and PCS) individually and in hybrid combination in an existing multi-storey building under real condition and presents them as one dynamic hazard mitigation. Hence, a 9-storey steel moment frame, numbered with respect to the ground level, was selected. This structure had been designed for the SAC building project, (Gupta and Krawinkler, 1998).

4.8 Input earthquake records

In general, earthquakes have different properties such as peak acceleration, duration of strong motion and ranges of dominant frequencies and therefore have different influences on the structure. In order to ensure that the chosen mitigation procedure is effective under different types of excitations, three, well-known earthquakes records were used in this study. These were all applied for the first 20 s of their duration, during which the strong motion took place.

Duration of the strong motion and range of dominant frequencies were kept unchanged and were evaluated by Welch's method (1967) based on Fast Fourier Transform Techniques, using the computer program MATLAB software. The earthquake records, which were selected to investigate the dynamic response of the models, are depicted in Figure 4.17.

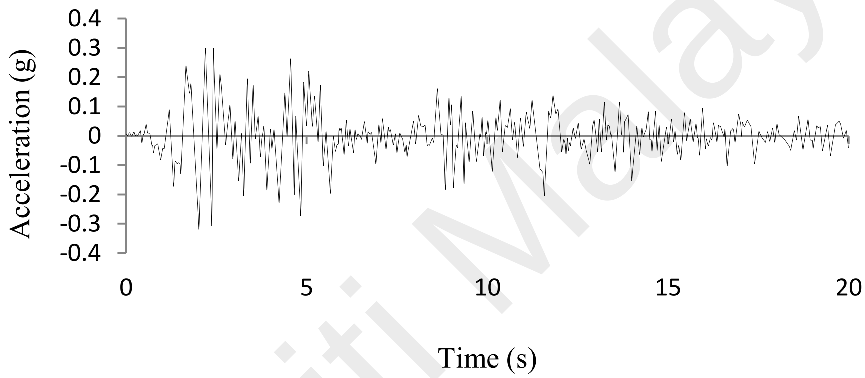

(a) El-Centro

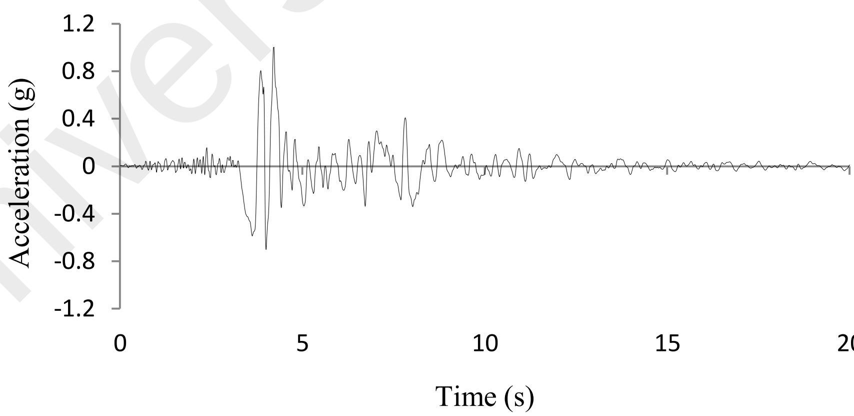

(b) Northridge

Figure 4. 17: Time histories of three earthquake records

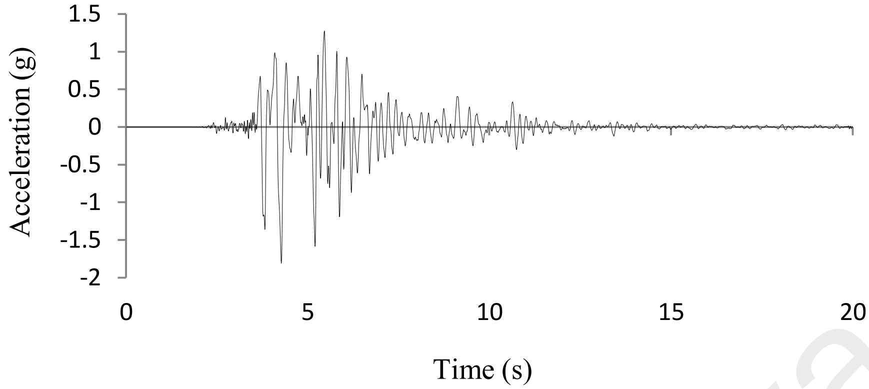

(c) Kobe

Figure 4. 17: Time histories of three earthquake records (Cont.)

The first simulation was conducted to the frame which excluded the proposed systems. The seismic responses of the structure were recorded for system identification in addition to result comparison with other frames equipped with PCS system, RRBD and combined RRBD-PCS system. Large displacement and P- effects were also considered in the analysis. Each floor equipped with one of the retrofitting systems, individually or in combination. Figure 4.18 presents the details of the frame and the penthouse is shown by shaded area. Physical dimensions of the nine-storey benchmark structure are 37.19 m in elevation and 45.73m by 45.73m in plan. The considered drift limit in these series of test was h/400, where “h” indicates the storey height.

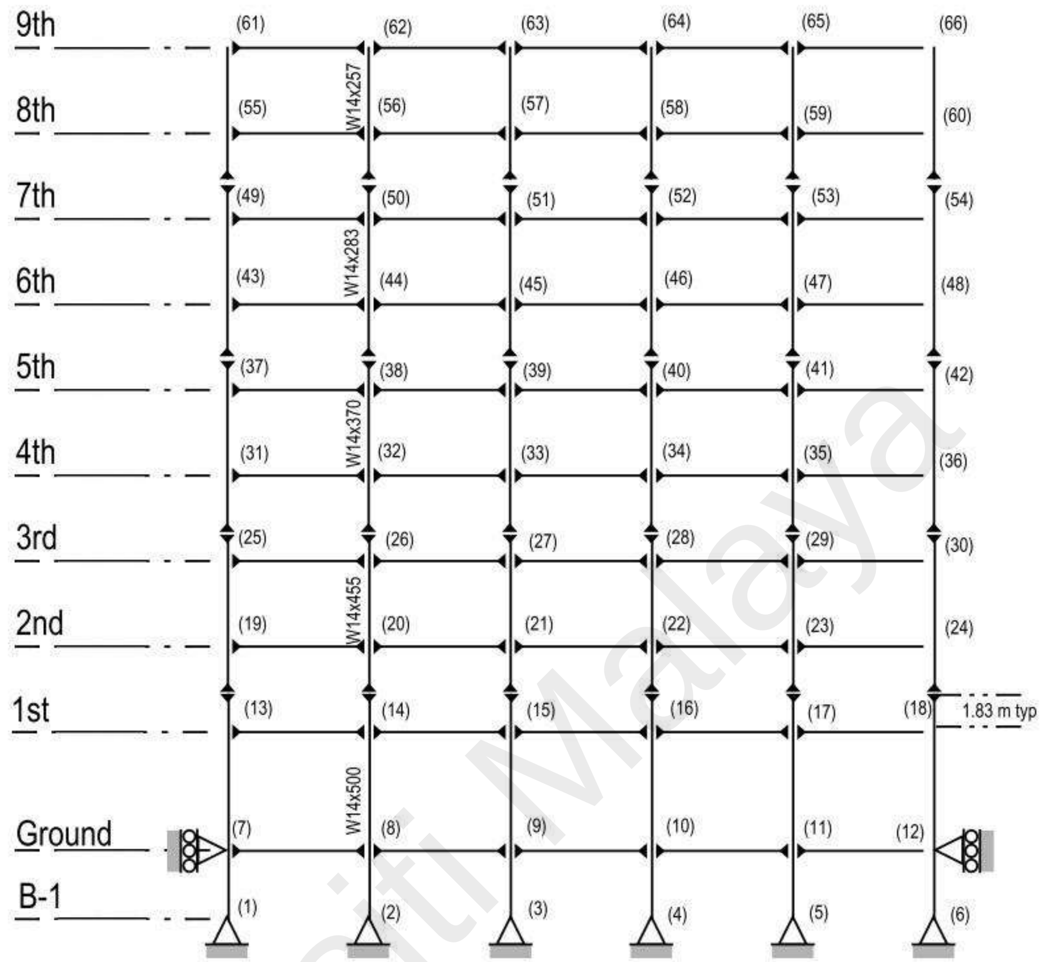

(a) Elevation

Figure 4. 18: 9-Storey Benchmark Building N-S MRF (Gupta and Krawinkler, 1999)

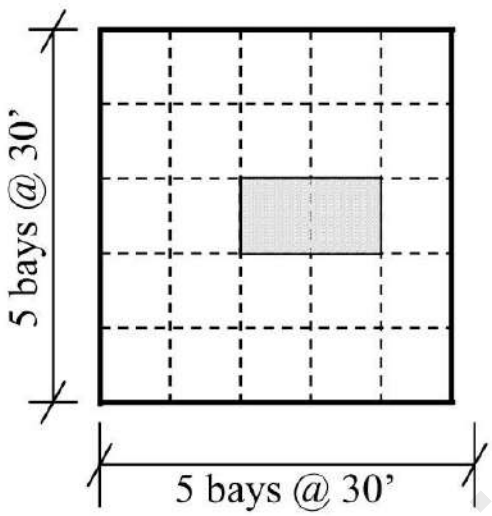

NOTES

Beams (248 MPa):
- Ground– 2nd level W36x160;
- 3rd – 6th level W36x135;
- 7th level W30x99;
- 8th level W27x84;
- 9th level W24x68.

Columns (345 MPa):
- column sizes change at splices
- corner columns and interior columns the same, respectively, throughout elevation;

Restraints:
- columns pinned at base;
- structure laterally restrained at 1st level.

Splices:
- denoted with ⊹;
- are at 1.83 m w.r.t. beam-to-column joint

Connections:
- ⤙⤚ indicates a moment resisting connection.
- – – indicates a simple (hinged) connection.

Dimensions:
- all measurements are center line;
- basement level height 3.65 m;
- Ground level height 5.49 m;
- 1st – 8th level heights 3.96 m;
- bay widths (all) 9.15 m.

Seismic Mass:
- including steel framing, for both N-S MRFs;
- Ground level 9.65×10^5 kg;
- 1st level 1.01×10^6 kg;
- 2nd – 8th level 9.89×10^5 kg;
- 9th level 1.07×10^6 kg;
- entire structure (above ground) 9.00×10^6 kg.

(b) Building plan (c) Details

Figure 4. 18: 9-Storey Benchmark Building N-S MRF (Cont.)

Design similarity of the frames in the two orthogonal directions was either identical or very similar, so that it was decided to analyze only half of the structure along the North-South (N-S) direction. The design difference lies in the gravity load effects owing to the gravity beams and sub-beams direction; they are oriented along N-S direction and this creates the gravity load difference with frame design of the East-West (E-W) direction.

This issue can be justified by considering the fact that influence of the gravity loading on the girders of the perimeter SMRF is almost negligible in the seismic response.

The structure has 5 bays in each directions and every bay is 9.15 meters long. Lateral resistance of the building is provided by steel perimeter moment-resisting frames. The furthest south E-W frame is designed as simple frame, and interior bays are all designed as simple frame with composite floors. Columns are wide-flange type and 345 MPa steel. Roof is denoted by the ninth floor and basement is referred by B-1. Floor heights are typically 3.96 m which is measured from center to center of beam. The basement and first level floor-to-floor height are 3.65 m and 5.49 m, respectively.

Two-tier construction was employed for columns with monolithic pieces which are connected every two levels from the first floor. The seismic tension splices of the columns are located on the levels one, three, five and seven at 1.83 m above the center-line of beam-column connection. These splices stand against bending and uplift forces. Assumptions regarding the restrains are first, bases of the columns which are modeled as pin at level B-1 and second, the horizontal displacement of the ground floor which is being held by the surrounding soil and concrete foundation walls.

Wide flange beams of 248 MPa steel were used for the floor system. Half of the seismic mass of the structural and non-structural components such as floor slabs, mechanical/electrical, ceiling/flooring, partitions, roofing and the penthouse are resisted by the frame. Speaking of the seismic mass, the ground level has 9.65×10^5 kg, the first floor has 1.01×10^6 kg, the second up to eighth floors have 9.89×10^5 kg and the ninth floor which is the penthouse has 1.07×10^6 kg of seismic mass. Therefore, the seismic mass of the entire frame above the ground level is 9×10^6 kg. 3% critical damping was assumed as the inherent damping of the structure. SAP2000 program was employed for this analysis. The damping device has a damping constant and spring stiffness which were considered in the analysis.

In order to fulfill the performance objective of the building design, the dynamic characteristics of structure equipped with additional retrofitting systems have to be carefully analyzed. This is due to the lack of a general rule for all types of structures. Furthermore, finding the most effective location for device installation is another issue which should be tackled by analyzing higher modes that contribute to the structural seismic response. It has to be noted that the best reduction of response is not necessarily guaranteed by adding the largest damping. There is a common practice within damper producers that tends to apply the maximum damping which does not always result in the most effective design. In order to conduct a comprehensive parametric study and to evaluate the efficiency of the proposed control systems and their location influence, variety of retrofitting systems placements were considered which are depicted in Figure 4.19.

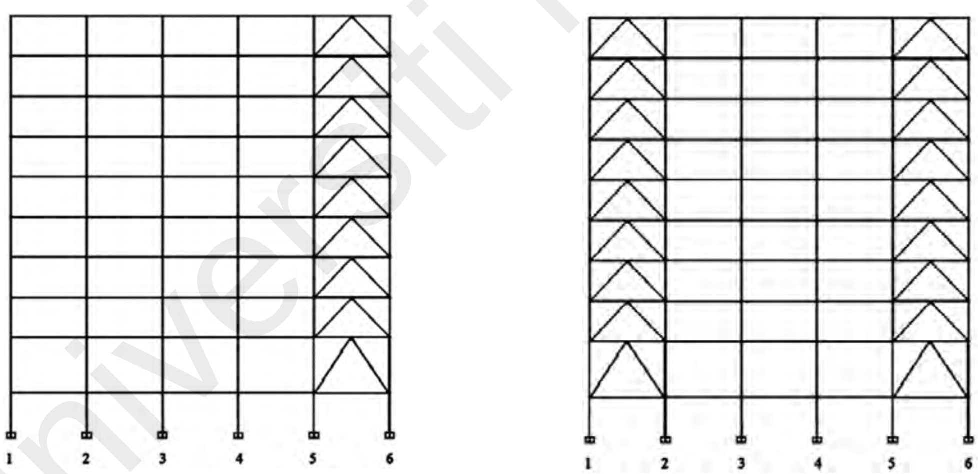

(a) RRBD

Figure 4. 19: Placement of RRBD and PCS systems within 9-storey frames

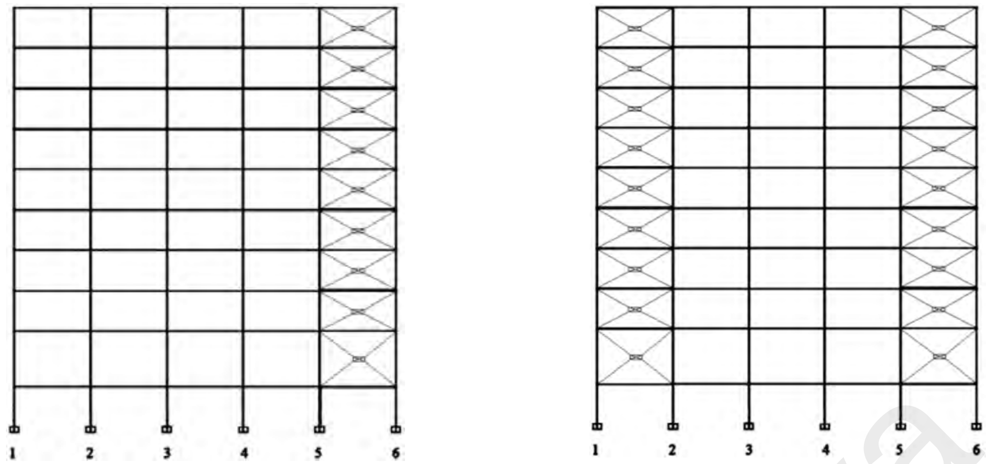

(b) PCS

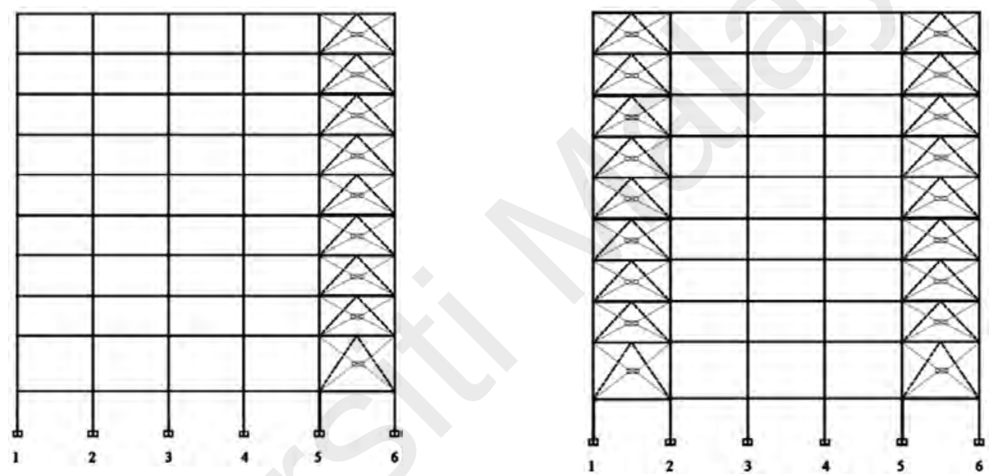

(c) Hybrid

Figure 4. 19: Placement of RRBD and PCS systems within 9-storey frames (Cont.)

The spring types employed in the RRBD and PCS system configuration are illustrated in Figure 4.20. Idealization of the VED was done by utilizing an elastic spring which was in parallel with a linear viscous damper. Cable element was used to model the PCS unites with a presumed constant pre-stress force equivalent to the spring force. Time-history analysis in SAP2000 is not able to model size variation of the spring although this alteration is negligible. Another considered control system configuration in this parametric study was placing RRBD and a cable brace element parallel together.

The RRBD is modeled using a multilinear elastic spring in parallel with a linear viscous damper. A multilinear elastic spring provides the capability to have several legs with different elastic stiffness. The proposed cable bracing system has a two-phase mechanism and to implement this mechanism, a gap element was placed in series with the cable bracing. One benefit of this configuration is that the damper can continue to be effective when the PCS cable bracing is engaging. The gap element is a multi-linear elastic element with initial stiffness equal to the spring constant. An initial stiffness of 90 N/mm was used to represent friction between the cables moving inside the spring. As was mentioned before, this mechanism provides further energy dissipation due to the cable bracing's delayed action, which provides a ductile behavior to the system for absorbing energy. The PCS bracing system has been designed in such a way that the cables fully straighten before 2% drift of the column height. In this arrangement a multi-linear link and linear damper were employed to model the RRBD device. This idealization presents the hyperelastic nature of the VED by the second leg of the spring.

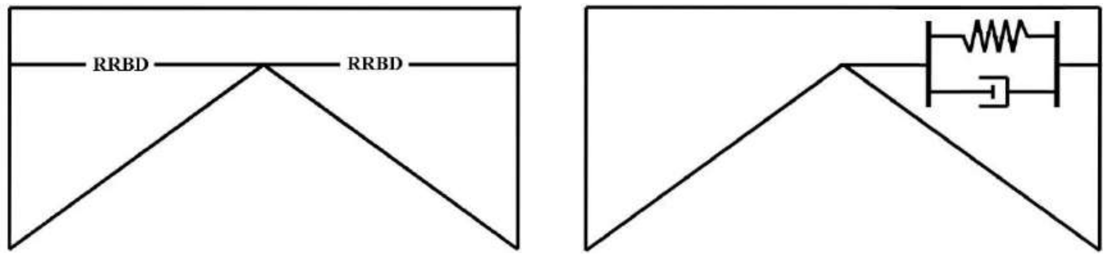

(a) Rotary rubber brace damper RRBD

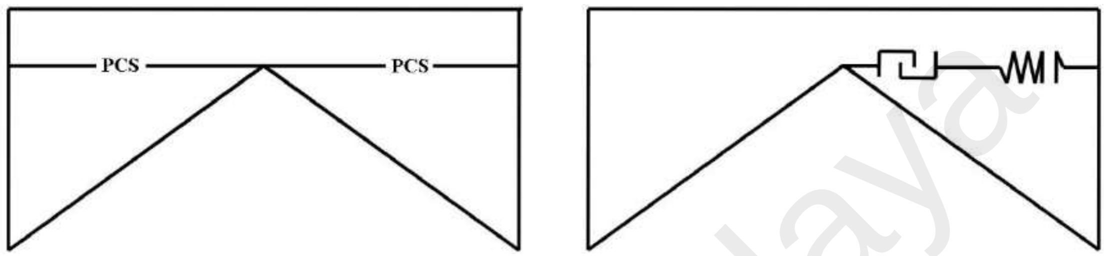

(c) Pre-compressed spring brace system

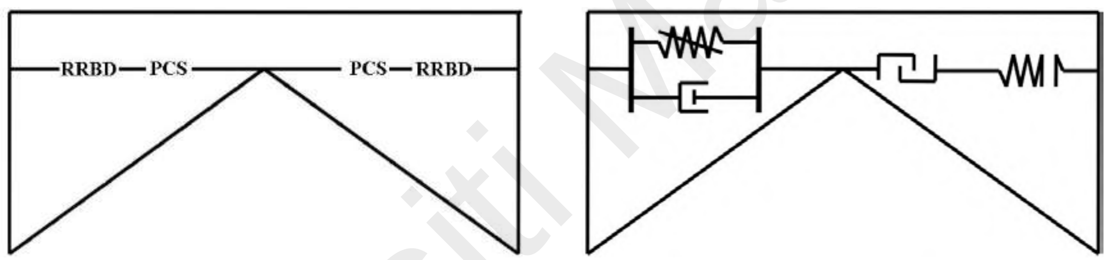

(d) Hybrid system

Legend:

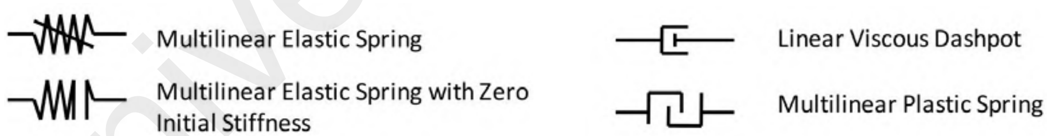

Figure 4. 20: System arrangements

The gap backbone curve performance is shown in Figure 4.21. At any level of the building the maximum tension and compression forces are presumed to be 125% of the cable tension forces of that level.

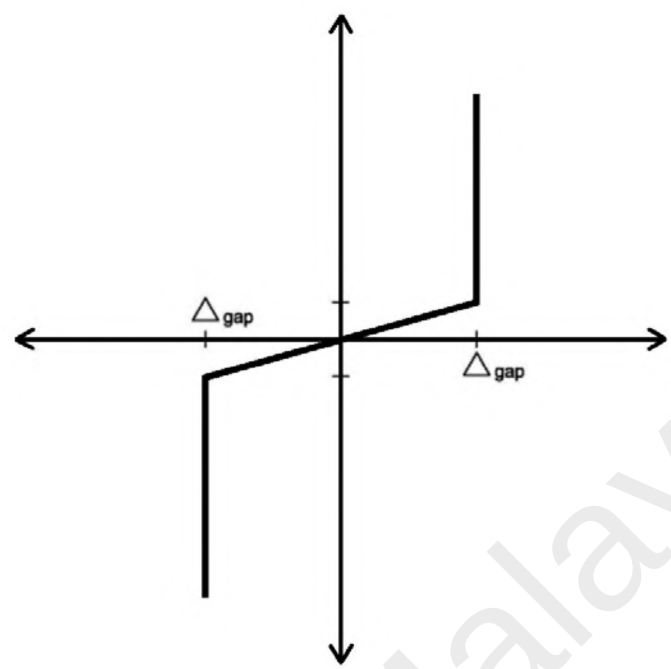

Figure 4. 21: Gap Backbone Curve

4.9 Seismic retrofit of an example structure

In order to model beams and columns of the frame, frame element with yielding plastic hinges was selected idealizing ASTM A992 steel. At each end of beams plastic hinge with strain hardening about the strong axis was considered. Performance of columns was assumed with no probable occurrence of yielding but at each end of columns an interacting axial load-bending moment plastic hinge was modeled. Since this frame model required some spliced columns, therefore they were modeled with two frame elements per storey and the interacting hinge was placed at the nearest column ends to the beam-column joint. The selected seismic excitations for numerical analyses were El Centro, Kobe and Northridge earthquakes. This was along with considering large displacement and P- effects throughout the analyses. Behavior of the proposed systems as well as the relative performance of structural system was monitored.

There were four different seismic retrofitting systems considered for the current numerical analyses. The first case was a special steel moment resisting frame (SMRF) which was a bare steel frame and its corresponding energy dissipation capability is totally associated with formation of plastic hinges at beams. Other considered configurations had identical frame but retrofitted with PCS, RRBD and hybrid passive control system (HPCS) types of systems. The frame and the proposed systems arrangement are depicted in Figure 4.22.

The approximate damping target was 10% based on which size of the RRBD was selected. This percentage included the Rayleigh proportional inherent damping of 2% in the first and fifth modes. Iterative approach was assigned to determine the VE damper size and a linear free vibration analysis was conducted to determine the first-mode damping by applying a sinusoidal acceleration at the base of the structure. Excitation was applied at the first modal frequency for a few cycles and then frame was let free and motion was decayed. The modal mass participation of the building is more than 90%. Log decrement method was employed to calculate the damping and eventually the size of damper was finalized through equations 3.8 to 3.13.

Design of the PCS elements was done using the design procedure described at part 5.9. The PCSs were designed in such a way that the cables become straighten before 2% drift of a storey. The reason behind it is due to the elastic modulus of the cables. HPCS was the last system configuration consisting of a rubber damper in series with a PCS. Due to the delay action of the cable bracing, which can be considered as a gap, the rubber damper deforms prior to the engagement of the cable brace. It permits the behavior of the initial phase of the device with the rubber damper providing energy dissipation at low displacements. In addition to dynamic analysis, nonlinear static pushover (SPO) analysis with p-delta effects was conducted and obtained results were expected to conclude the best overall performance analysis of the considered cases.

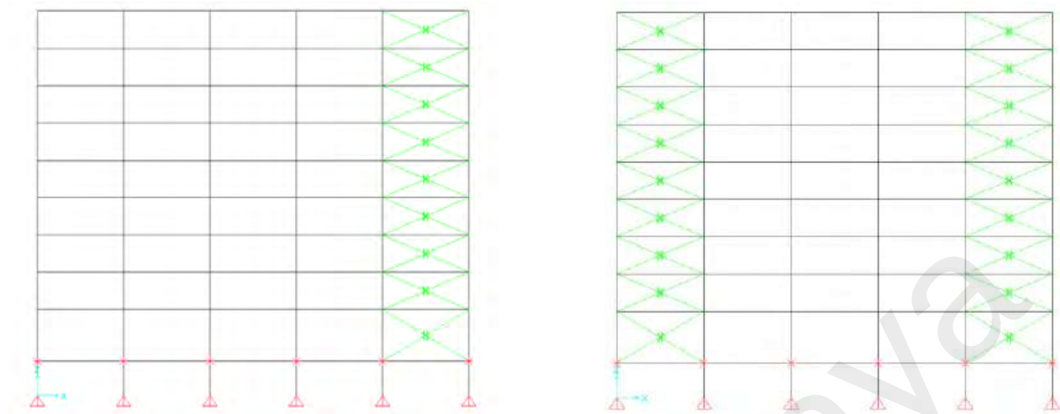

(a) PCS

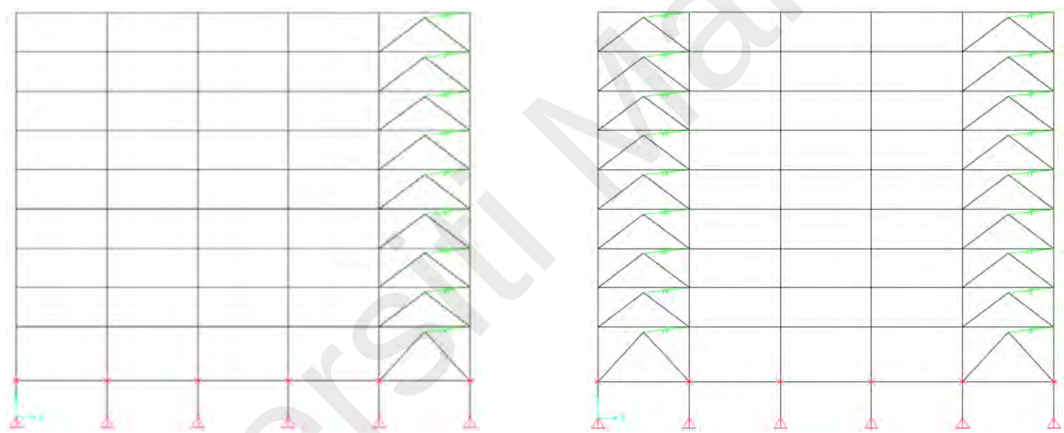

(b) RRBD

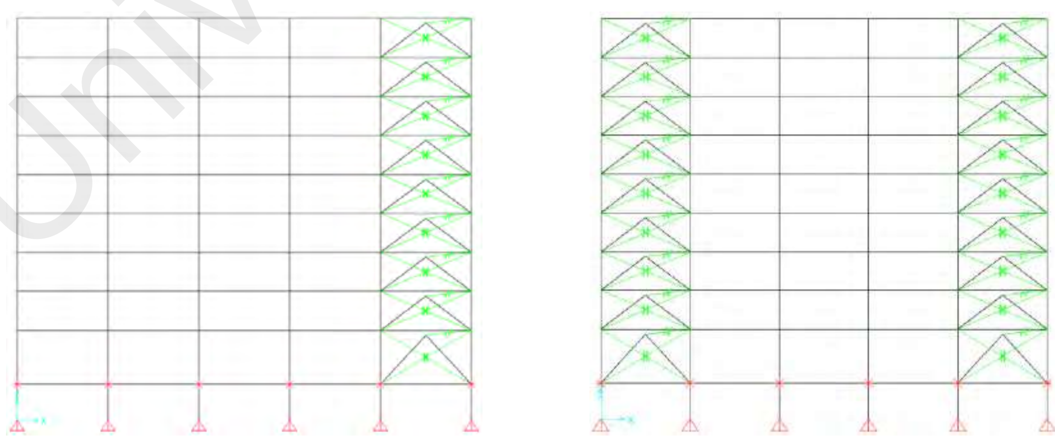

(c) HPCS

Figure 4. 22: Model of the analyzed nine-storey steel frame with the systems (See Figure 4. 18 for details of the MRF)

4.10 Concluding Remark

This chapter presented a discussion regarding the parametric development, study plan, detailing of the proposed retrofit systems and the possibilities available for the suggested systems. In addition, the parameters and factors considered for analysis were explained. The experimental plan consisting of the instrumentation, component layout, and load cases was clarified. Finite element method was discussed to highlight its capabilities in idealization of the VE nature of rubber. Moreover, match of the test data with those of unit cube tests is a critical process to be conducted. Analytical modeling of the RRBD requires adequate and appropriate assumptions and models for the material properties. This chapter focused on development of the device concept by presenting basic knowledge and information for testing, designing and analyzing synthetic rubber materials. Furthermore, this research targeted the development of a cable bracing system namely PCS cable brace. Performance of ordinary cable bracing was shown to be improved by inserting a PCS at intersection point of the X-cable bracing. Cyclic lateral tests were conducted to evaluate influence of the introduced cable bracing system. Totally, five steel moment frames with pinned bases including bare frame (BF), frame with RRBD, frame with PCS system, frame with X-cable (cross cable) brace and frame equipped with HPCS, which includes of RRBD and PCS system were considered for the study.

A nine storey moment steel structure equipped with the proposed systems was subjected to seismic analysis. For placement of the proposed control systems various locations across the height of the structure were assessed. The single-phase and multi-phase systems arrangement and their combination were illustrated in this chapter. Confirmation of the structural performance was done via finite element modelling in the SAP2000 software.

Next chapter will present in detail the outcome of the proposed cable bracing technique, VED and multi-phase hybrid system.

CHAPTER 5: RESULTS AND DISCUSSION

Part I. RRBD device

5.1 Introduction

This chapter, which consists of three main sections, describes the results of an extensive study on the inelastic seismic response of steel buildings equipped with the proposed systems. In the first part, a finite element model considering nonlinearity, large deformation, and material damage is developed to conduct a parametric study on different damper sizes under pushover cyclic loading. The fundamental characteristics of this VED system are clarified by analyzing building structures under cyclic loading. Additionally, by using a sinusoidal shaking table test, the effectiveness of the RRBD to manage the response displacement and acceleration of steel frames is considered and the results are presented. In the second part the PCS system has been examined. Both experimental and analytical studies are conducted and the equations involved in the proposed technique are discussed before being verified using finite element (FE) solutions based on ABAQUS analysis. And in the final part, nonlinear dynamic response history analysis was conducted in SAP2000 software for the systems individually and in hybrid combination and the results are presented, accompanied by an extensive discussion.

5.2 Material testing

Design of a VED requires properties identification. Performance of rubber as a VEM is associated with properties such as loss factor η, storage modulus G_1 and loss modulus G_2. Commercially available rubbers are not supplied along with adequate technical specifications therefore some specific tests are needed to be considered, such as uniaxial tension tests and shear tests for determination of G_1, G_2, and η.

Specimens underwent different material testing programs including monotonic, cyclic and time dependent testing. The uniaxial tension test of similar specimens considered monotonic and cyclic loads and for simple shear test static, cyclic and stress relaxation conditions were applied. Selection of frequencies and strain levels was based on expected ranges in typical structures. These data were then used for calibration with finite element analysis (FEA) in ABAQUS. Cyclic test applied sinusoidal load at frequencies of 0.1, 0.2, 0.5, 1.0 and 1.5 Hz. This test measured the dependency level of both dynamic stiffness and loss factor on frequency. Influence of shear strain magnitude on material behavior was investigated by considering various levels of displacement amplitude for the shear specimens. The data obtained from uniaxial tension determined the best hyperelastic model to be used in ABAQUS software, and the data taken from the stress relaxation and cyclic tests were utilized to develop hysteretic properties of the rubber material.

Evaluation of stress softening of the samples was another purpose of the developed testing protocol and for that, specimens were statically cycled up to 10 cycles within the desired deformation range to achieve a steady-state static property. It has to be mentioned that due to inability of current FEA software in accounting for both the Mullins effect and the inherent material damping, the mechanical conditioning was used. The steady-state response data obtained from later cycles of the static tests was used for FEA. Permanent set of the stress–strain curves associated with the steady-state cycles in uniaxial and simple shear tests had to be calculated in advance which was then followed by determination of the mean properties. Average of stress at a given strain was measured from polynomial curve fits of the individual curves of each cycle whose permanent set was removed primarily. Other parameters including material storage modulus, loss modulus, loss factor and energy dissipation of VEM associated with the range of frequencies and strain levels are expressed in next sections. Figure 5.1 depicts the specimens under uniaxial tension and simple shear tests.

(a) Specimen sample under uniaxial tension test

(b) Dumbbell specimen sample after test

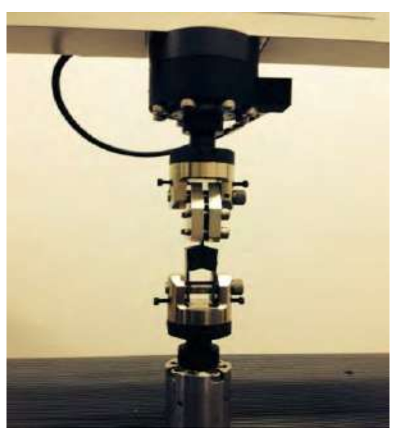

(c) Rubber specimen under shear test

Figure 5. 1: Tensile and shear rubber tests

Figure 5.2 shows the tested specimens. Dog bone specimens were subjected to cyclic tension tests with the steady rate of elongation at 1mm/s. It is noteworthy that the measurement of relationship between the actual strain in the center area of the specimen and the grip travel may experience uncertainty due to the compliance existing in the loading cables and the material flowing from the grips. The rubber residue largely remained on both bonded section of the steel plates indicates the tearing that originates from the rubber failure, Figure 5.2 (c).

Tensile test results present the stress-elongation relationship of the four samples, Figures 5.3. Graph depicts the nonlinear stress-strain behavior and hyperelastic property of the synthetic rubber compounds. In addition, synthetic rubber materials exhibit stress softening which is also known as the Mullins effect. Stress softening or Mullins effect is defined as reduction in the stiffness for subsequent cycles at a formerly reached deformation. The softening behavior observed in uniaxial static tension test is presented in Figure 5.3(b).

(a) Monotonic

(b) Cyclic

(c) Simple shear

Figure 5. 2: Rubber specimens tested

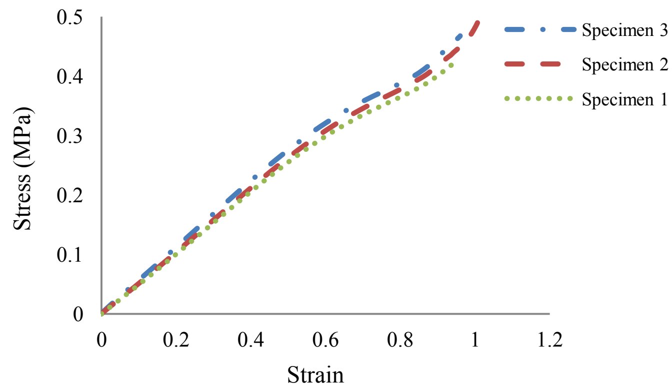

(a) Monotonic

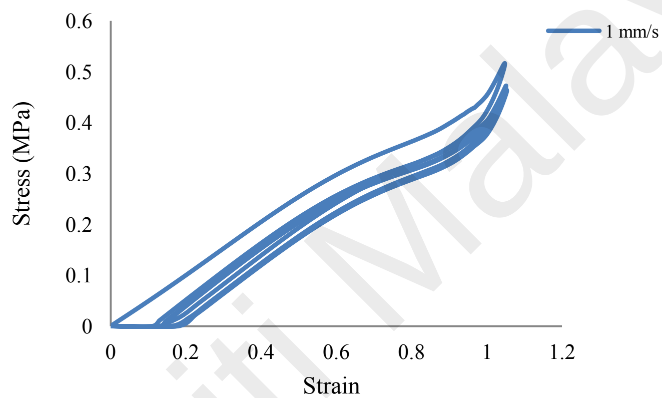

(b) Cyclic

Figure 5. 3: Uniaxial experimental stress–strain curve results

5.3 Finite element modeling

Selection of appropriate hyperelastic model is the first step for creation of rubber properties required to model the (RRBD) and this step is associated with inputting the obtained static stress–strain data. Material modeling cannot be completed unless the time dependent nature of VEM is considered and for that purpose two options are available; the finite strain viscoelasticity model and the Hysteresis model.

Predicted behavior made by the chosen hyperelastic or VEM model in ABAQUS can be evaluated by a convenient option known as "Evaluate". This option uses the strain energy potential specified in the material definition by researchers to measure the material's response according to the formerly gathered experimental data. Reports of the test should include strain energy potential coefficients and material instability. A single data set along with its specified constants obtained from experimental data evaluation is presented in Table 5.1.

Table 5. 1: Reduced polynomial model (Yeoh) material constants

Rubber material	C_{10}	0.3524
properties	C_{20}	-0.02091

The material's nonlinear elasticity is represented by hyperelastic material model but no time dependence. The overall material behavior in terms of nonlinear elastic and strain-rate dependencies can be predicted by the hyperelastic plus VEM model, that is to say, a single stress relaxation curve can present the VE properties of the synthetic rubber regardless of the strain level. The time dependent stress response is measured in a stress relaxation test under constant strain level of specimen.

Tension inputs are the only set of data used in ABAQUS to determine the hyperelastic function. Figure 5.4 presents the data gathered from relaxation test. Meanwhile, it has to be noted that simple shear is the probable damper state and accurate idealization of the shear behavior is critical. The stress-strain curves presented by Figure 5.5 (a-c) are associated with various rates and cyclic strains of $\pm 25\%$, $\pm 50\%$ and $\pm 100\%$. Full ellipse of the hysteresis curves proves proper energy dissipation capacity of the chosen VEM. Moreover, different degrees of slope and plump curve associated with the considered excitation rates and amplitudes highlight the fact that stiffness and damping variation of the VEM take effect from excitation rate and amplitude. Figure 5.5 (a-c) shows the direct correlation between excitation rate and both enveloping area, i.e. energy dissipation capacity, and tilt angle, i.e. stiffness, of the hysteresis curve.

Evaluation of the stress softening in the samples concluded that strain in negative direction had a softening effect in the positive direction. Figure 5.5 (d) demonstrates that increment of displacement amplitude resulted in reduction of the tilt angle and expansion of the enveloping area of the hysteresis curve. This highlights the comparison between hysteresis loops obtained from the simulation and those of the test at 0.5 Hz. Hysteresis loops at strain level of 25% and 50% showed the best fit and similarity of those associated with remaining strain levels appeared to be reasonable. Among the gathered test data the most deviation happened for the case corresponding to 100% displacement level in which, according to Figure 5.5 (d), the correlation level required for analysis was not attained. Therefore, the damping device will be designed in such a way that in case of maximum frame displacement the damper will never experience more than this strain level. Furthermore, data of finite element analysis and experimental test coincided while the only discrepancy took place for dynamic stiffness, see Figure 5.5 (d). This originates from the rough linear fit of the hyperelastic model stiffness. Dependency of the hysteresis loops on both displacement and driving frequency is shown in the graphs and as it can be seen, for a given range of frequency the energy dissipation magnitude is higher at higher displacement.

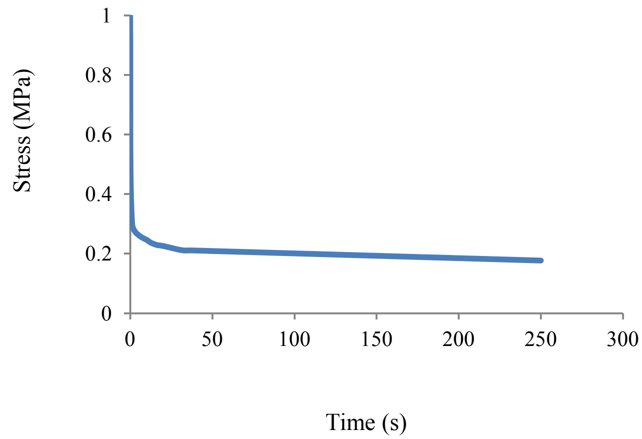

Figure 5. 4: Relaxation shear test result

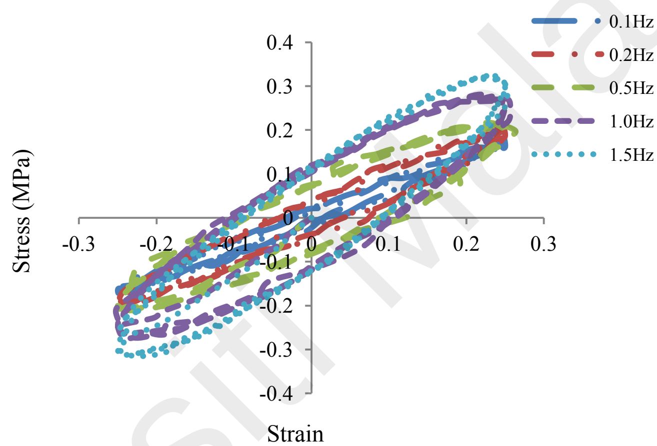

(a) 25% strain

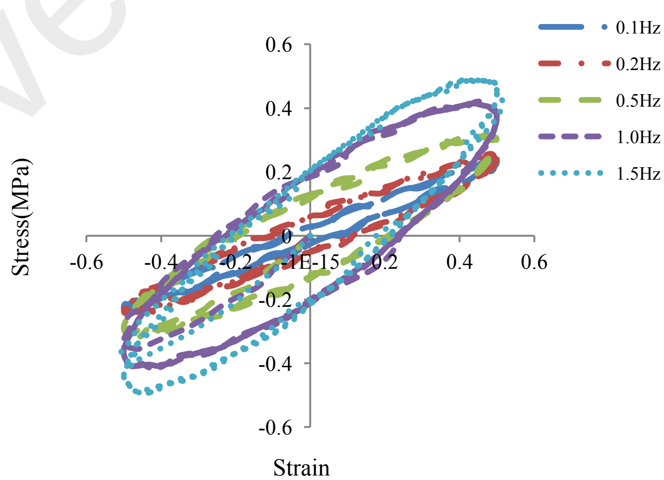

(b) 50% strain

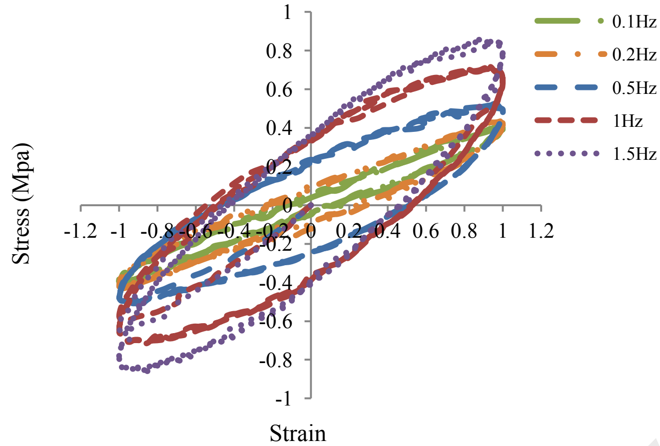

(c) 100% strain

Figure 5. 5: Experimental shear test results at various rates

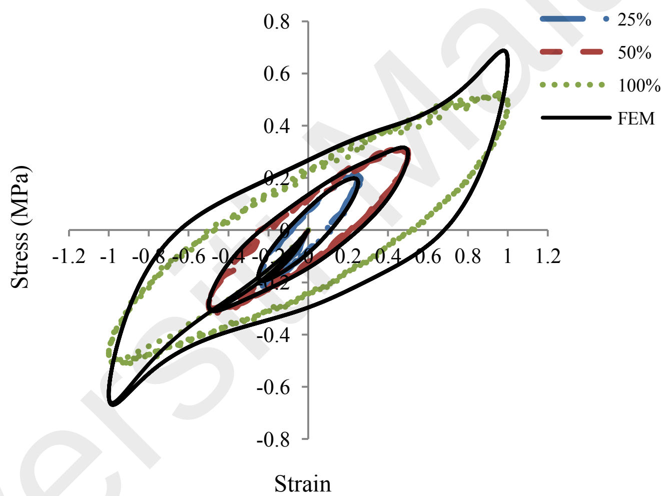

(d) Comparison of shear test results and FEM at 0.5Hz

Figure 5. 5: Experimental shear test results at various rates (Cont.)

5.4 Cyclic tests of the damper

The cyclic test included different test conditions, excitation frequencies and amplitudes to plot hysteresis curves and subsequently determine the VE damper characteristics such as the energy dissipation per cycle E_d, the loss factor η, the storage modulus G_1 and the loss modulus G_2. The device under cyclic test is shown in Figure 5.6.

(a) VED under compression (b) VED under tension

Figure 5. 6: RRBD under cyclic test

The force-displacement hysteresis loops associated with various excitation frequencies and amplitudes are distinguished by selecting the last loop as the single steady cycle among 10 considered cycles for each case. Figure 5.7 illustrates force-displacement hysteresis curves under different excitation frequencies at the excitation amplitudes of 5mm, 10mm and 20mm and Figure 5.8 depicts the force-displacement hysteresis curves obtained from excitation frequencies of 0.1 Hz, 0.2 Hz, 0.5Hz and 1.0 Hz under different excitation amplitudes. Figures 5.7 and 5.8 show varying slope and plump degrees of these hysteresis curves with respect to different excitation frequencies and amplitudes. Such variation is because slope and plump degree are correlated with device stiffness and energy dissipation, respectively. Further discussion with respect to these effects is presented in the subsection 5.5.

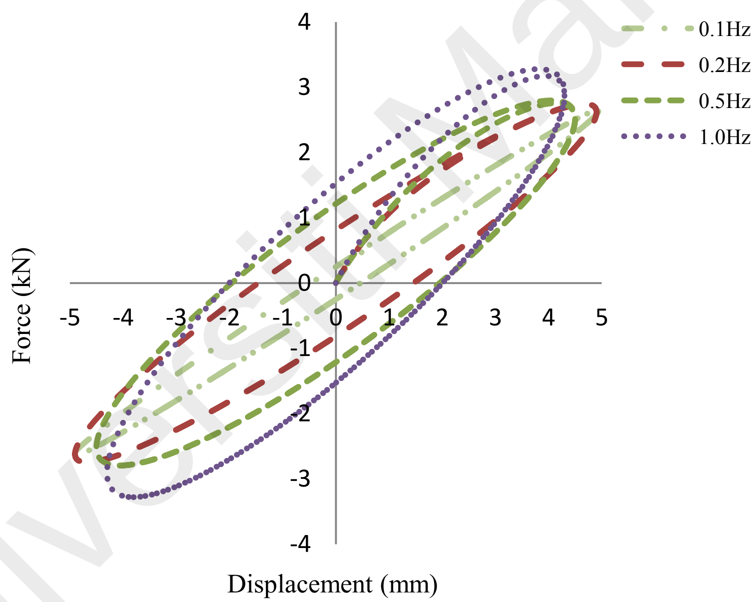

(a) 5mm

Figure 5. 7: Hysteresis curves under different amplitudes and frequencies

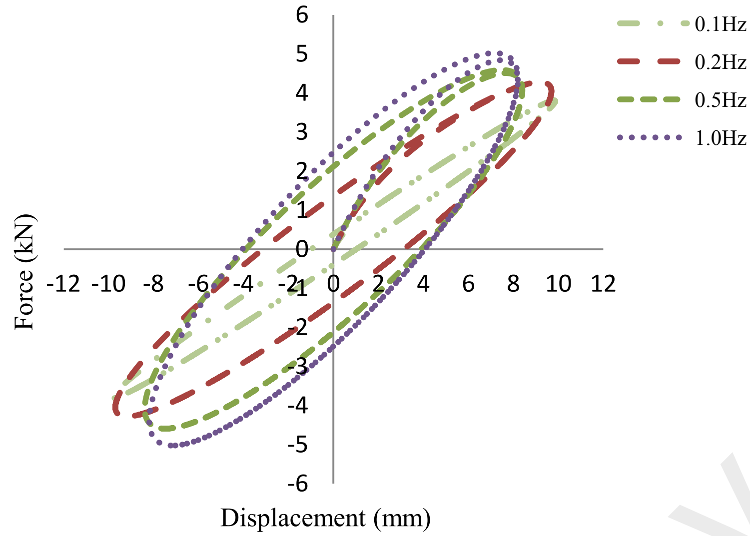

(b) 10mm

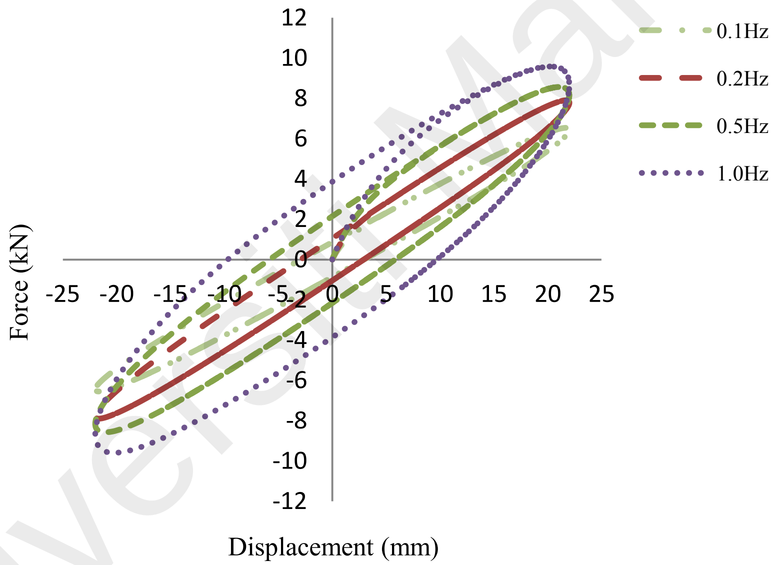

(c) 20mm

Figure 5. 7: Hysteresis curves under different amplitudes and frequencies (Cont.)

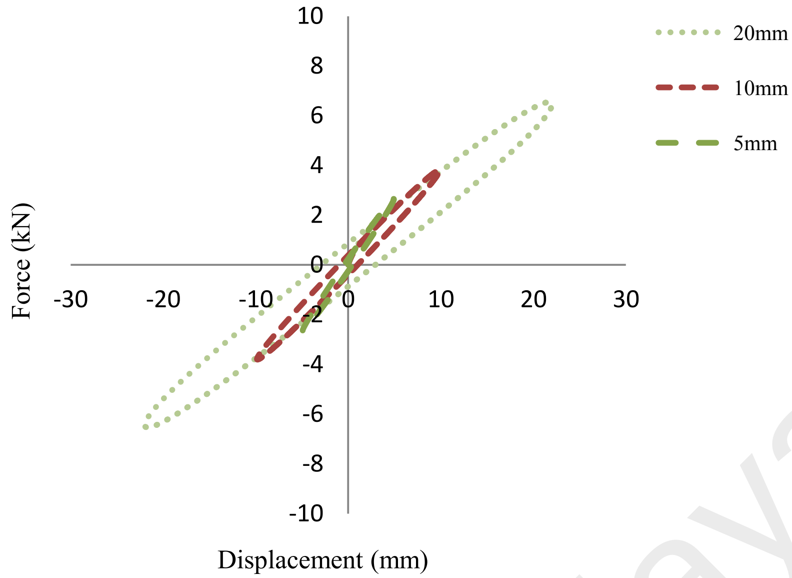

(a) f = 0.1 Hz

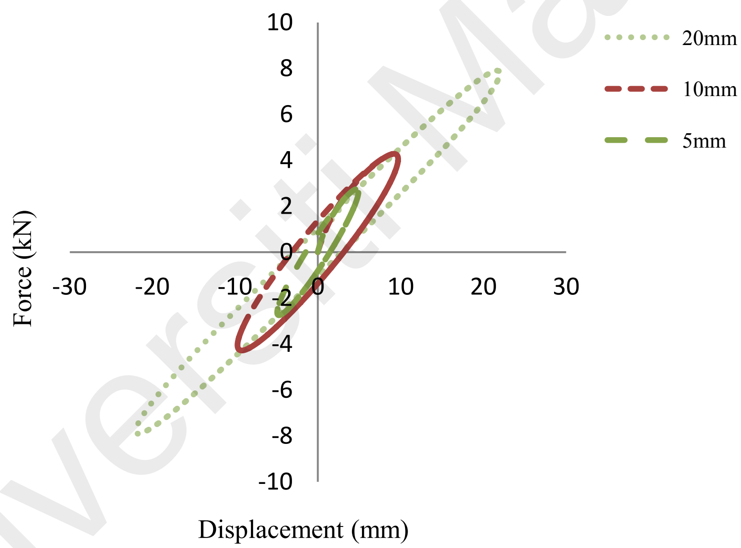

(b) f = 0.2 Hz

Figure 5. 8: The hysteresis curves at the same frequency with different displacements

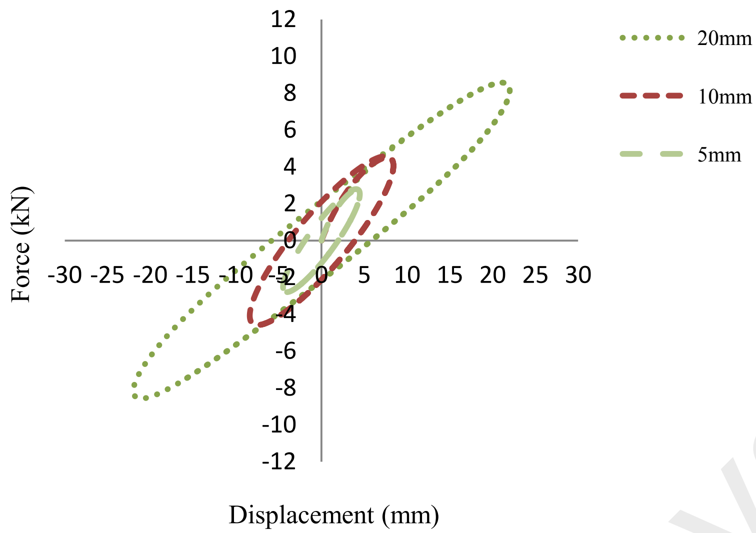

(c) f = 0.5Hz

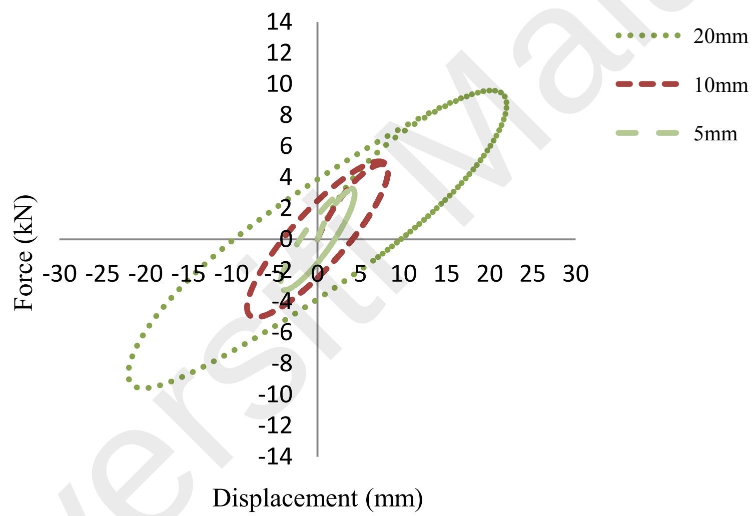

(d) f = 1.0 Hz

Figure 5. 8: The hysteresis curves at the same frequency with different displacements (Cont.)

Table 5.2 and 5.3 contain the detailed results of the equations (3.5) to (3.13) in chapter 3 which discussed calculation of the storage modulus G_1, the loss modulus G_2, the loss factor η, equivalent damping C_e, the equivalent stiffness K_e and the energy dissipation E_d of the VE damper with regard to different frequencies and displacement amplitudes. The influence of parameters such as excitation frequency, excitation amplitude, and fatigue on the properties of the VED will be expressed in the following subsections.

Table 5. 2: Parameters of the RRBD device under different conditions

Frequency (Hz)	Amplitude (mm)	Loss factor (η)	Storage modulus G_1 (MPa)	Loss modulus G_2 (MPa)	Energy dissipation E_d (N·m)
0.1	5	0.110	0.177	0.019	3.454
	10	0.109	0.162	0.018	12.56
	20	0.107	0.160	0.017	48.984
0.2	5	0.367	0.217	0.080	14.130
	10	0.350	0.177	0.062	43.96
	20	0.154	0.172	0.027	75.36
0.5	5	0.509	0.234	0.119	21.195
	10	0.490	0.186	0.091	64.684
	20	0.286	0.173	0.049	138.16
1.0	5	0.533	0.265	0.141	25.1
	10	0.516	0.210	0.092	76.9
	20	0.433	0.199	0.086	245

Table 5.3 presents the equivalent stiffness and damping obtained under different loading cases.

Table 5. 3: Equivalent stiffness and damping of the RRBD device under different conditions

Frequency (Hz)	Amplitude (mm)	Equivalent damping C (Ns/m)	Equivalent stiffness k (N/m)
0.1	5	93.0	400.0
	10	109.0	366.0
	20	74.0	361.4
0.2	5	90.0	490.0
	10	85.0	400.0
	20	38.0	390.0
0.5	5	75.0	530.0
	10	64.0	420.0
	20	32.0	385.0
1.0	5	46.0	600.0
	10	39.0	475.0
	20	30.0	450.0

5.5 Effect of excitation frequency

Study of the influence of frequency and displacement amplitude variation on the characteristic parameters of VE material (G_1, G_2, η, E_d, K_e and C_e) showed that the characteristic factors change with the rise of frequency at the considered displacement amplitude limits. Variation trend is plotted in Figure 5.9 (a-d). Plots depict that at the displacement amplitude limit of 10mm the characteristic factors such as η, G_1, G_2 and E_d rise while their increments are smaller at higher frequencies especially for the loss factor η and the energy dissipation per cycle E_d. In case of 20mm displacement amplitude, considering three different increment ranges of frequency; 0.1Hz~0.2 Hz, 0.2Hz~0.5Hz and

0.5Hz~1.0 Hz, the corresponding increases of the storage modulus were 7.5%, 0.5% and 15%, for loss modulus were 58.8%, 81.4% and 75.5%, for the loss factor were 43.9%, 85.7% and 51.3% and for the energy dissipation were 53.8%, 83.3% and 77.3%, respectively.

The variation trends of the characteristic factors G_1, G_2, η and E_d associated with displacement amplitude of 20mm, however, were different from those at other displacement amplitudes which is due to the fact that displacement amplitude of 20mm causes large shear deformation condition and subsequently the VE layers experiences tiny cracks. These cracks have detrimental effect on the damping capacity of the VE damper.

Figure 5.9 (e) presents variation of the equivalent stiffness K_e versus variation of frequency. Obviously, at the same displacement amplitude, K_e increased with the increase in frequency. For instance consider 10mm excitation amplitude case, for the frequency variation ranges of 0.1Hz~0.2 Hz, 0.2Hz~0.5Hz and 0.5Hz~1.0Hz the respective increment of K_e, were 9.2%, 5.0% and 11.9%, respectively.

Variation trend of equivalent damping C_e, however, showed a gently reducing tendency in exchange for increase in frequency. This was even more pronounced during the excitation frequency range of 0.1Hz~0.2 Hz. Consider the 5mm excitation amplitude case, for the excitation frequency areas of 0.1Hz~0.2 Hz, 0.2Hz~0.5Hz and 0.5Hz~1.0Hz, reduction percentages of C_e were 3.2%, 16.6% and 38.6%, respectively. A can be seen; the RRBD characteristics are highly affected by frequencies, that means the higher the frequency, the higher the loss factor, storage modulus, loss modulus, energy dissipation, and equivalent stiffness, but on the other hand, less equivalent damping.

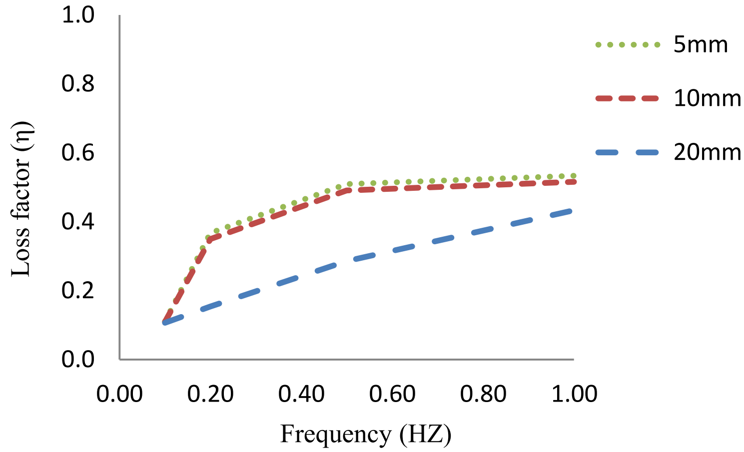

(a) Loss factor

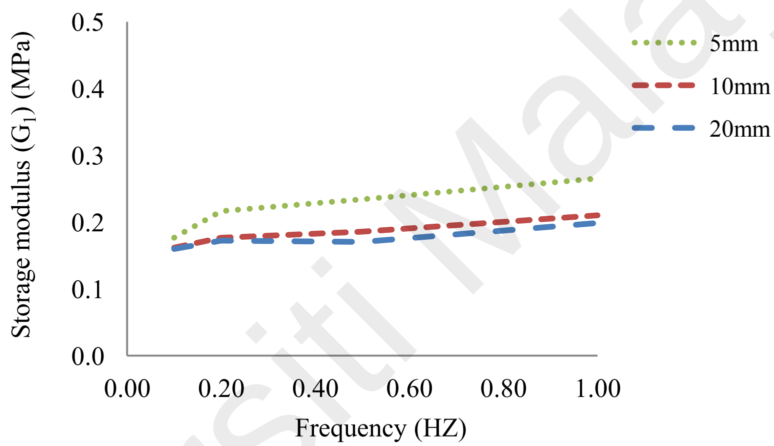

(b) Storage modulus

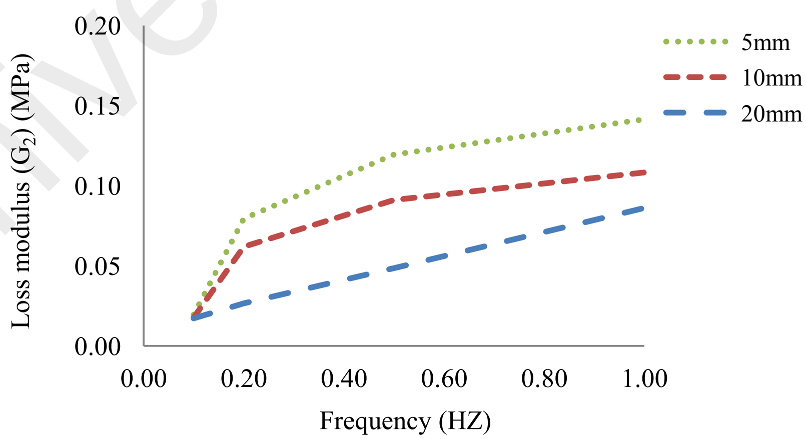

(c) Loss modulus

Figure 5. 9: Dynamic parameters change with excitation frequency

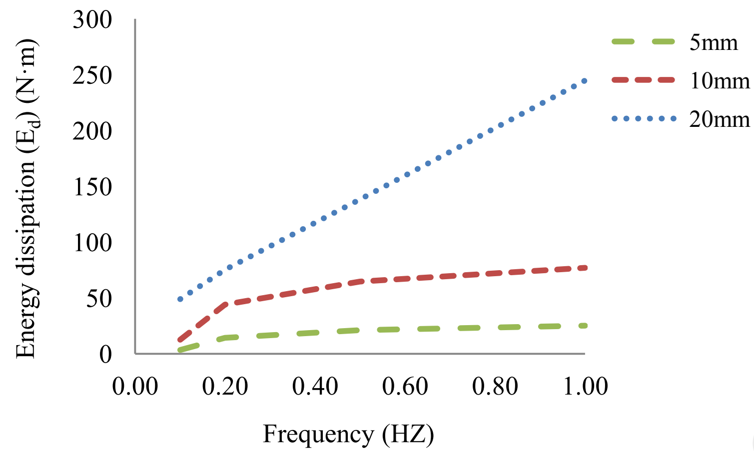

(d) Energy dissipation

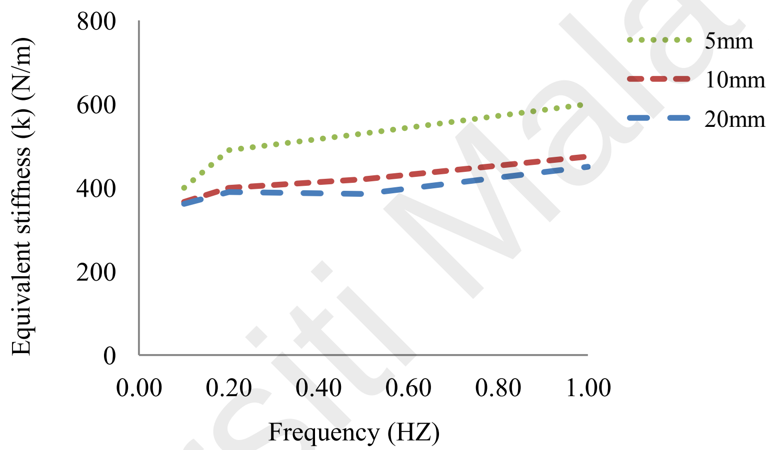

(e) Equivalent stiffness

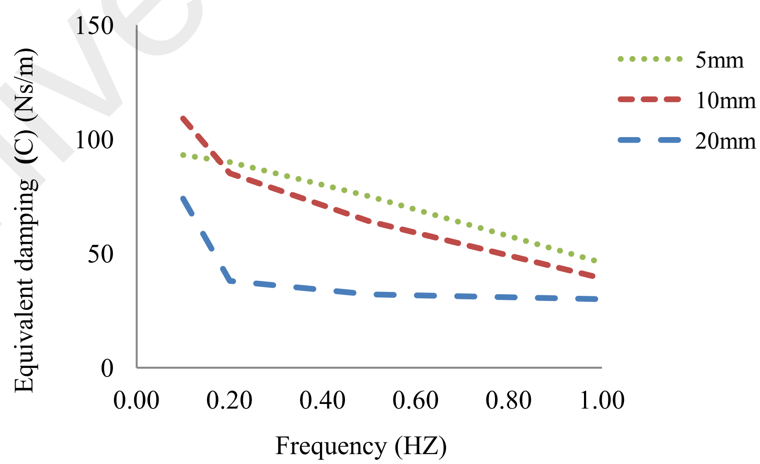

(f) Equivalent damping

Figure 5. 9: Dynamic parameters change with excitation frequency (Cont.)

5.6 Effect of displacement amplitude

Comparison of the loss factor against variation of displacement amplitude revealed slight reduction of η as depicted in Figure 5.10 (a). This highlights the steady property of damping under different displacement amplitudes at the same frequency. According to Figures 5.10 (b) and (c), for range of 5mm~10mm displacement at frequency of 1.0 Hz, G_1 and G_2 tended to quick reduction by 15% and 34.7% respectively, while these percentages changed to 20.5% and 23.5% for the same range of displacement but at frequency of 0.5 Hz. G_1 and G_2 were observed to vary gently at other frequencies. Furthermore, increase of displacement amplitude led to quick increase of energy dissipation (E_d) as it is proportional to the square of displacement as shown in Figure 5.10 (d). This issue was discussed in equation 3.11 of chapter 3.

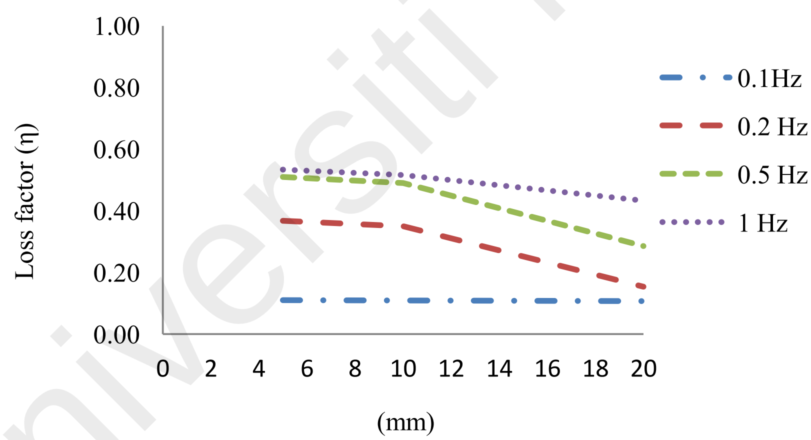

(a) Loss factor

Figure 5. 10: Dynamic parameters change with displacement amplitude

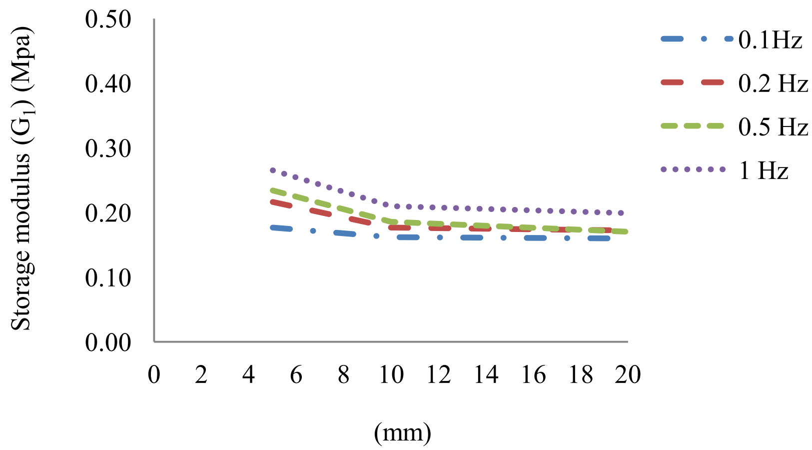

(b) Storage modulus

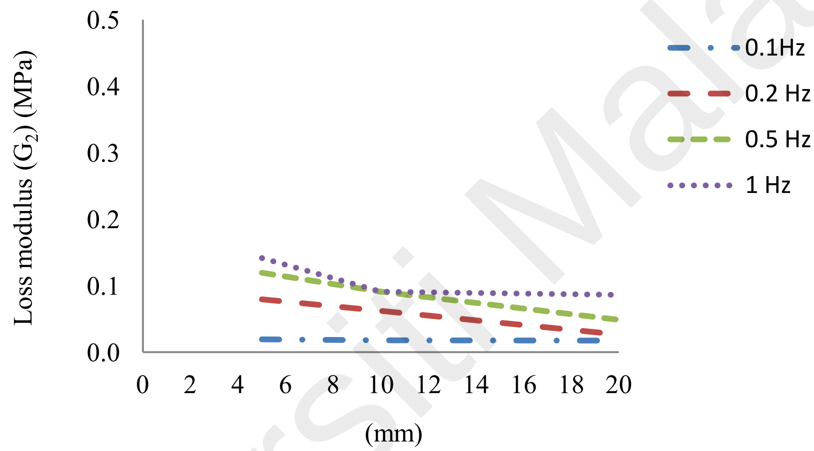

(c) Loss modulus

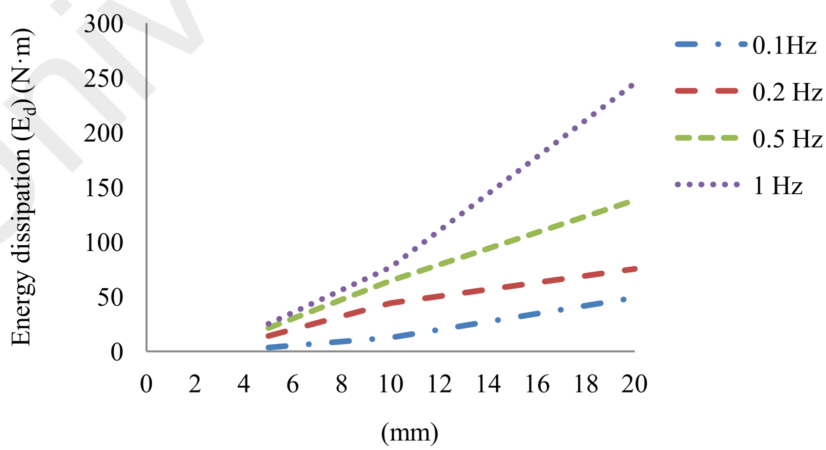

(d) Energy dissipation

Figure 5. 10: Dynamic parameters change with displacement amplitude (Cont.)

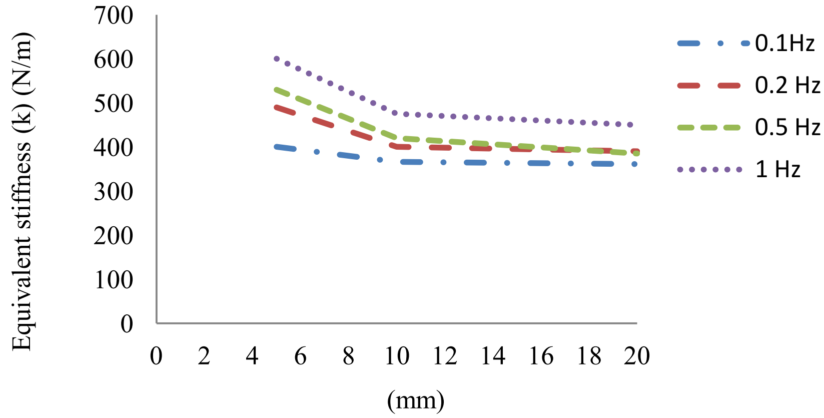

(e) Equivalent stiffness

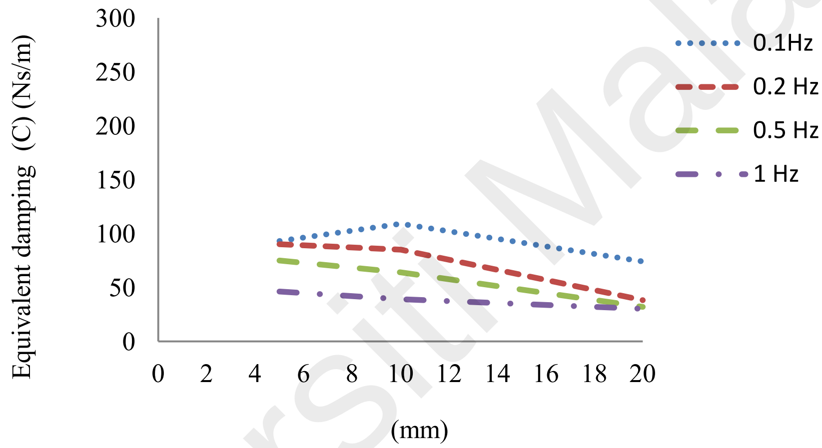

(f) Equivalent damping

Figure 5. 10: Dynamic parameters change with displacement amplitude (Cont.)

Moreover, variation trends of equivalent stiffness K_e and the equivalent damping C_e versus frequency and displacement change are presented in Figure 5.10 (e) and (f). It can be seen that, except C_e at frequency of 0.1Hz, change of displacement amplitude has small effect which accentuates the insignificant effect of displacement amplitude on the VE damper properties. As Figure 5.10 shows, the effect of the displacement amplitude changes on RRBD's characteristics shows that loss factor, storage modulus, and shear modulus decreased against an increase in displacement amplitudes in contrast to the increasing energy dissipation trend.

5.7 Shaking table test

The shaking table tests carried out simulated sinusoidal excitation of two-storey steel frames with different configurations; BF as the control for comparison and frame equipped with the RRBD, see Figure 5.11. The considered input motion was a five-second harmonic displacement after which frames were left to vibrate freely. Frame storey height was 1.2 meters and the variables including acceleration responses of the structures and floor deflections were measured in the direction of input ground motion by three accelerometers and three linear variable displacement transformers (LVDTs), respectively.

Figure 5. 11: Shaking table test frames

Deflection and acceleration results of the shaking table test are depicted in Figure 5.12. It was observed that installation of RRBD was effective as displacement response of the top floor was mitigated from 13.12mm to 6.05 mm which is 53.89%, Figure 5.12(a). In addition, the re-centering ability of the damper and subsequently the efficiency in preventing any residual deformation was observed. Results of the acceleration responses indicated slight increase of top floor acceleration from 1.38 m/s^2 to 1.71 m/s^2 which can be justified by increase of stiffness, Figure 5.12 (b). This originates from increment of structural stiffness and damping provided by the RRBD. Plots depict a disturbance at time zero and five seconds of load exertion. Inspection revealed that disturbance recorded by sensitive accelerometer was because of sudden movement and stoppage of shaking table that appeared at point A and similarly at points B and C.

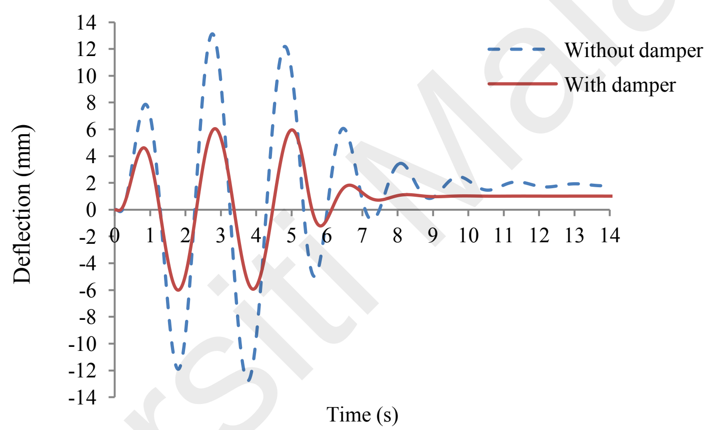

(a) Deflection

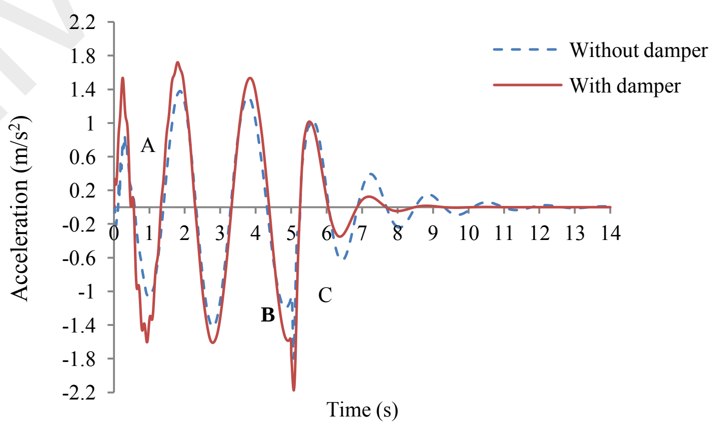

(b) Acceleration

Figure 5. 12: Comparison between the BF and frame with damper under sinusoidal excitation

Other performance-related properties of RRBD such as displacement reduction, deformation capacity ratio, initial stiffness level, etc., are listed in Table 5.4 along with those of common passive dampers for sake of comparison. This comparison remarks the satisfying performance of the RRBD apart from benefit of the low cost of this damper.

Table 5. 4: Properties of RRBD and major types of passive dampers

Parameter	Damper Type			
	VED RRBD	Metal damper (Slit) [d]	Viscous fluid damper (VFD) [e]	Friction damper [f]
Displacement reduction	116%	74%	50-70%	50%
Initial stiffness level	Low	High	Vey low	Moderate
Deformation capacity ratio	500%	12%	Stroke restriction	Stroke restriction
Construction cost (US Dollar) (bracing included)	1600 [a]	2,000	14,000 -18,500	6,800
Coverage of vibration level	ALV [b]	MHV [c]	ALV	MHV
Idealized hysteresis behavior	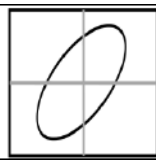	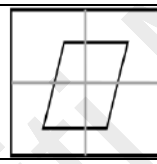	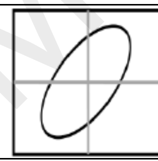	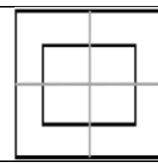

[a] Based on Malaysian market;
[b] ALV: all level of vibration;
[c] MHV: moderate and high level of vibration
[d] Chan et al., (2008), Pimiento et al., (2015), Kim et al., (2017)
[e] Miyamoto et al., (2003)
[f] Pall et al.

Part II. PCS System

5.8 Preliminary analyses

In order to determine the relationship between spring dimensions and frame response, a series of analytical simulations with finite element method were conducted using FEA software and various PCSs were considered. Results were then used for experimental verification. The configuration design of the spring primarily targeted the determination of physical properties of the spring such as length and internal diameter. The preliminary dimension of the spring has been chosen in such a way that at 2% drift of the column height the cables would fully straighten. Table 5.5 lists the frame details considered in the numerical simulation.

Table 5. 5: Details of frames used for finite element preliminary analysis.

Frame label	Spring length (mm)	Spring diameter (mm)
L7	70	40
L8	80	40
L9	90	40
L10	100	40
Ø2	80	20
Ø3	80	30
Ø4	80	50

Performance of a building during a seismic excitation takes influence from both structural and non-structural components. Building codes which have described the allowable limits of structural and non-structural damages in standard-based rehabilitated buildings are such as SEI/ASCE 7 (Clause 9.5.2.8) (ASCE/SEI 7-10, 2013) and FEMA code in Table C1-2 (Clause 1.5) (FEMA, 2000). In confrontation with earthquake, different levels of structural performance are illustrated by the given typical drift values. In this regard, the considered drift to be applied to the frames was 3%. Based on the available seismic design guidelines for braced frames, this value is 1.5 times greater than the allowable storey drift (ASCE, 1997; FEMA, 2000).

Figure 5.13 shows the stress distribution on the frame and the functionality of both cables along with demonstration of direction of exerted loads on cables by the compressed spring. Resultant stress distribution showed stress concentration at the top of column in BF case and also revealed the same overall capacity in both frames which underlines the similar performances of the BF and the cable braced frame during initial stages of loading. Speaking of the cable-spring mechanism, it was observed that the stress was developed throughout the cable length. No occurrence of slack cable condition was seen because of the spring pre-compression force. Therefore, apart from the resembling behaviors of the considered frames, the expected sequence in the functionality of the pretension mechanism of cables which were firstly set to experience the pretension force and secondly become fully straight under the external load was proved.

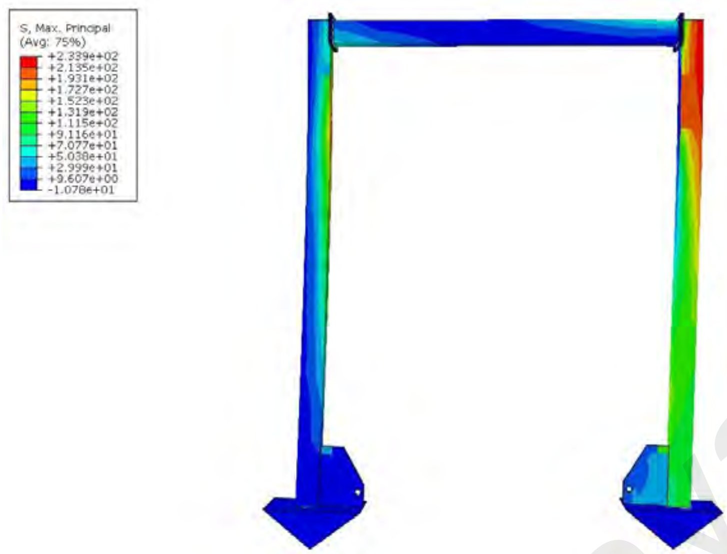

(a) BF

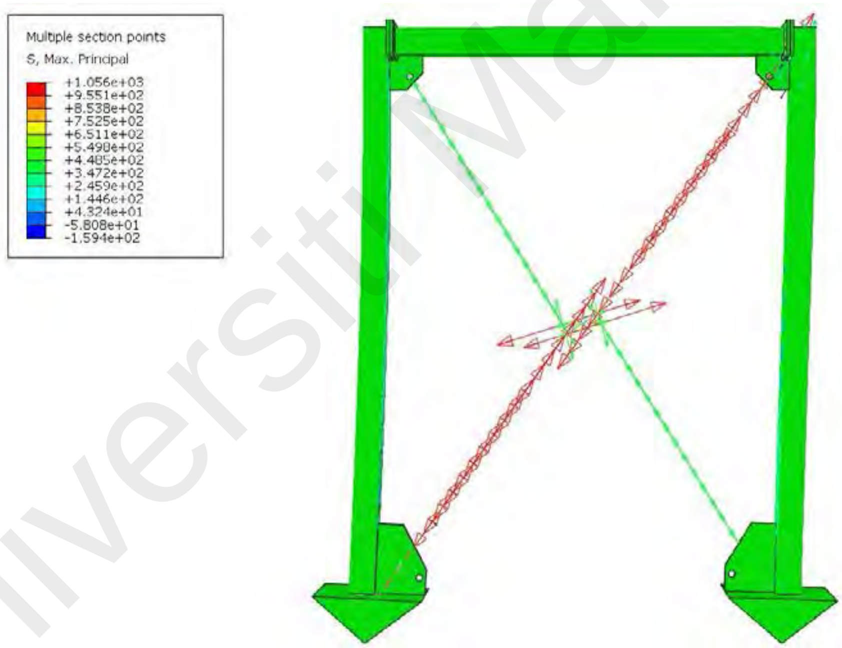

(b) Frame with pre-compressed spring

Figure 5. 13: Contours of Von-Mises Stress

Figures 5.14 and 5.15 illustrate the efficiency of the PCS length and diameter on the overall behavior of the frame, respectively. A crucially important issue in the modeling of the spring is appropriate determination of the geometry. It was formerly mentioned that the target frame lateral displacement ( ) in this study corresponded to 2% drift. This means that at this range of lateral displacement, one of the cables straightens while in case of larger values the cable in the compression diagonal was not expected to become slack and loose its initial tension completely because of the spring expansion. Meanwhile, these are the mechanical and geometrical (length and diameter) properties of the spring which govern the tension force in the compression diagonal cable. The mechanism is such that at the target frame drift the spring expands to its maximum and the tension force along the compression diagonal cable diminishes to zero; otherwise the tension force in the cable is equal to the spring force.

Results revealed that variation of PCS length and diameter had significantly influenced the frame strength or in other words system capacity. It was observed that with the constant spring diameter of 40 mm, increase of spring length caused the frame strength to decline and subsequently led the cables to reach their yielding limit and strengthening at larger displacements, see Figure 5.14. Furthermore, the curves of PCSs with longer lengths are under the curves of those with shorter lengths. This result appeared to be similar to that of the performance of the spring with a constant length of 80 mm but with a reduced internal diameter, see Figure 5.15. Further observations of the plots showed that curves associated with shorter lengths of PCS are above those associated with longer lengths. The action mechanism of the bracing had a delay which can be justified by longer length and smaller diameter of the PCS. The observed delay in the action mechanism of the bracing happened due to the smaller diameter and the longer length of the PCS. Hence, an adequately determined wire rope unit is crucial to improve the structural performance.

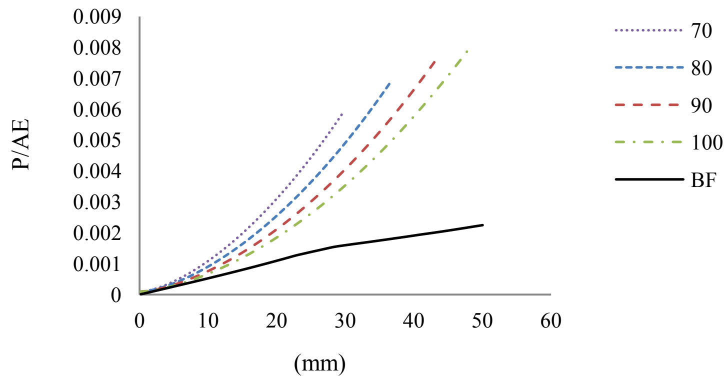

Figure 5. 14: Relationship between frame strength and the spring length

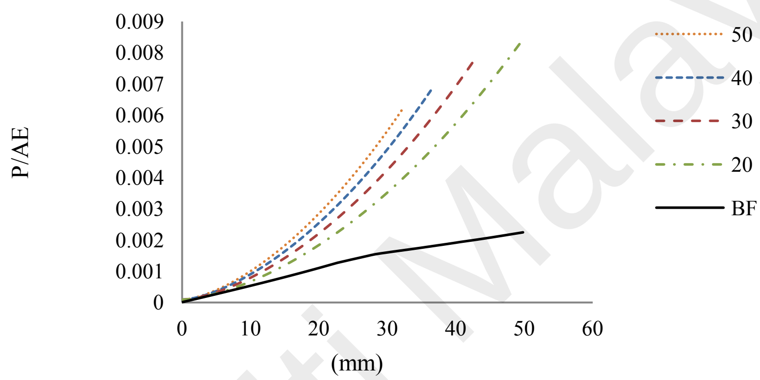

Figure 5. 15: Relationship between frame strength and internal diameter of the spring

5.9 Constitutive model

The analytical model defines the relation between lateral frame displacement to spring expansion (L) and spring rotation (θ). More specifically, by considering the resultant stress and strain on cables, expansion and compression of the spring and frame displacement and force, this relationship involves equations that develop a mathematical model.

5.9.1 Elastic spring design

Generally speaking, springs are simple tools and there are plenty of purposes for which they are designed. Development of the ideal linear spring requires background of the involved parameters that have influence on the spring action. Performance of a linear spring mostly depends on how far it is stretched and this mechanism is expressed by the well-known linear Hooke's law. Consider δ_s as the amount of spring extension from its initial position. According to the Hooke's law the force required for the extension is determined by $F_s = k\delta_s$. In this equation, k stands for the spring constant which is a quality particular to each spring. δ_s represents the stretched or compressed distance of the spring. It is worth mentioning that k is function of material's shear modulus, G, and the spring geometry.

$$k = \frac{Gd^4}{8D^3 n_a} \tag{5.1}$$

where G is obtained from material's elastic modulus E and Poisson ratio υ,

$$G = \frac{E}{2(1+\upsilon)} \tag{5.2}$$

and D represents the mean diameter of the spring (center to center of the wire cross-sections),

$$D = D_{outer} - d \tag{5.3}$$

In helical springs, however, the mechanism is such that the spring, either compressed or extended, is stressed in torsion and therefore the basic equations applied for round wire springs are as follows:

$$\tau = \frac{8FD}{\pi d^3} \tag{5.4}$$

$$\delta_s = \frac{8FD^3 n_a}{Gd^4} \tag{5.5}$$

Action mechanism of the helical spring takes advantage of a so called "memory" whose function is associated with the shape of the coils and the pitch in between them. When the spring is deflected in compression and its diameter expands, this memory creates a certain amount of energy to be stored. In other words, this energy corresponds to deformation of the spring. As soon as the load is removed this mechanism allows the spring to expand slightly. Since this action and reaction is the backbone of the spring mechanism, hence, it has to be precisely reflected by the targeted analytical model. Assuming a coil spring with one side fixed, as shown in Figure 5.16, the formula required to deal with the spring function is derived from equation (5.6),

$$OD_{exp} = (\sqrt{D_m^2 + \frac{p^2 - d^2}{\pi^2}} + d) - OD \tag{5.6}$$

where D_m is mean diameter, p represents pitch, d stands for wire diameter, and OD is original outer diameter.

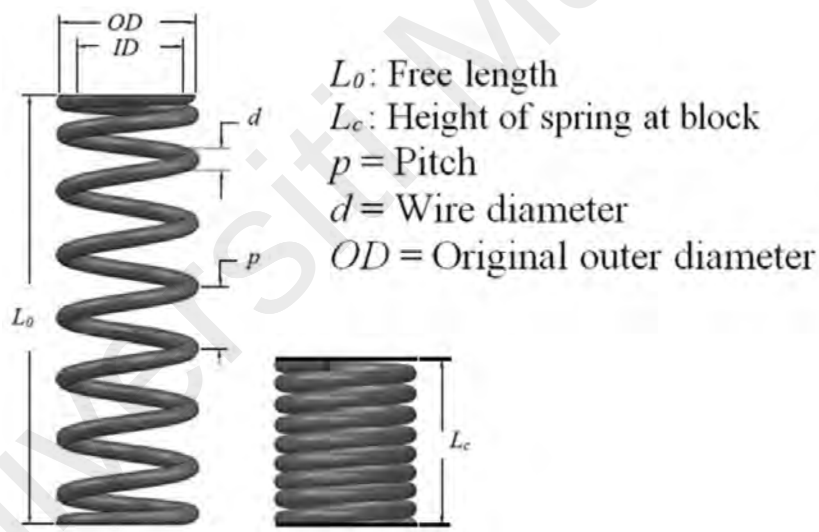

Figure 5. 16: Schematic diagram of a spring

In order to provide a safe material stress originated by the carried load, determination of two key parameters is crucial; spring diameter and wire size. The spring rate which is defined by the stiffness in Newton per millimeter of spring movement is function of required number of coils or number of active turns. This stiffness relies on the amount of free movement available for the spring. Bearing in mind that calculating the stress is starting point of the spring design, there are three variables that have to be involved for mathematical modeling of the spring; spring diameter (D); wire diameter (d); and number of active coils (n_a).

One of the challenges that calculation of the spring length has to deal with is buckling. For this reason, a critical length has to be defined and that says; when the free length of a compression spring L_o is greater than four times its mean diameter D_m, the spring has to be checked for buckling. This issue becomes important because of the reduction that takes place for length of the helical spring under axial load. This reduction however may be continued such that the spring reaches laterally flexing condition which is called buckling and corresponding length is named the buckling critical length L_k. In order to comply with target drift in case of large frame spans longer spring is required and therefore the chance of buckling becomes even more critical.

One challenging issue in the action mechanism of the spring is presence of eccentric load. Whenever the force action does not coincide with the spring axis, the subsequent performance of the spring amplifies the stress on one side and lowering it on the other side of the spring and therefore the stress balance is disturbed and spring experiences a less safe load and stiffness. Due to the movement of cables within the proposed PCS system for transferring the load to the spring, eccentric loading is imminent and therefore, a solution for this problem is utilization of a sliding hollow stiff shaft.

There are four types of compression spring ends; open, closed, open and ground, and closed and ground. Each of these end types has effects on spring characteristics; pitch, free length, total coils and solid height. Ease of installation and stability were the reasons to select the closed and ground type. This end type provides a larger area for the spring to exert its force. Calculation of dimensional characteristics (D_m and d) of the compression spring with closed and ground end type requires equations which are given in Table 5.6.

Table 5. 6: Formulas for dimensional characteristics

Spring Characteristic	Pitch (p)	Solid Height (l_c)	Total Coils (N_t)	Free Length (L_0)
Closed and Ground	$\frac{L-2d}{n_a}$	$d \times N_t$	$n_a + 2$	$(p \times n_a) + 2d$

Equation 5.7 is used to calculate the number of active turns (coils),

$$n_a = \frac{Gd^4\delta s}{8FD^3} \tag{5.7}$$

Mechanism of the spring is highly affected by the calculated number of active coils (n_a). This is a number that has to be checked with the solid height of the spring when applying the given data. Therefore, the following condition should be met:

$$d \times (n_a + 2) \equiv l_c \tag{5.8}$$

5.9.2 PCS system design

In order to define the drive relation between frame displacement and cable forces, it is necessary to balance the coordinates of the PCS system. Figure 5.17 depicts the balanced coordinates.

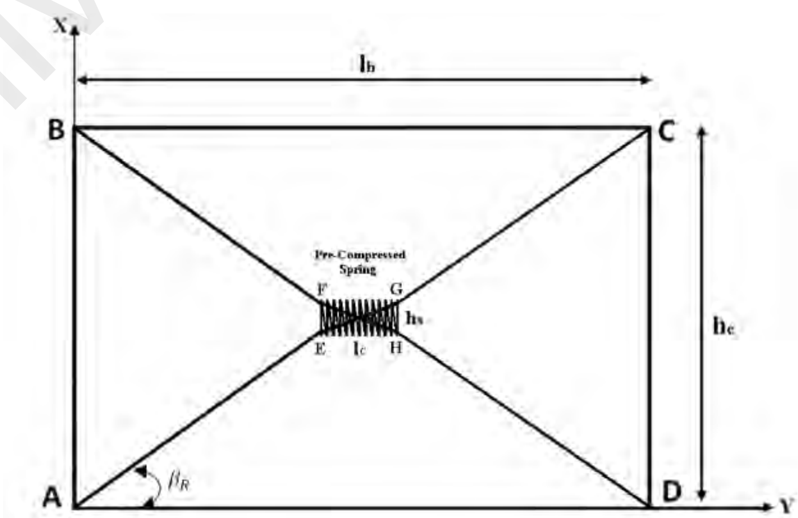

Figure 5. 17: Frame with its coordinate axes orientation

Equations 5.9 to 5.13 respectively express the length of the external parts of the cables ($2l_B$), diagonal of the solid spring or sliding hollow shaft (d_p), variation of the spring length (l_c), target storey drift ( ) where the tensioned bracing member becomes straight, and the loosened length of the compression-prone cable (∂I_s):

$$l_B = \sqrt{\left(\frac{l_b - l_c}{2}\right)^2 + \left(\frac{h_c - h_s}{2}\right)^2} \tag{5.9}$$

$$d_p = \sqrt{{l_c}^2 + (h_s - \emptyset_c)^2} \tag{5.10}$$

$$= \sqrt{(2l_B + d_p)^2 - {h_c}^2} - l_b \tag{5.11}$$

$$l_c = \sqrt{\left(d_p + \partial I_s\right)^2 - (h_s - \emptyset_c)^2} - l_c \tag{5.12}$$

$$\partial I_s = \sqrt{{h_c}^2 + {l_b}^2} - \sqrt{{h_c}^2 + (l_b - \ )^2} \tag{5.13}$$

Figure 5.18 illustrates configuration of the simply supported frame with the spring placed at intersection point of the cables. The model excluded the cables as depicted in the figure while cables were replaced by vertical and horizontal components of cable forces.

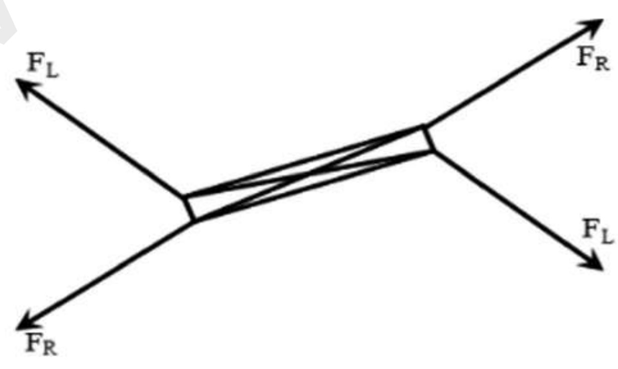

Figure 5. 18: Free body diagram of pre-compressed spring

According to the coordinate axes of the frame, slope of the cables AE and GC were all the same, as are those for cables BF and HD. The spring was located at the center of the frame. In order to obtain the lateral displacement of the frame ( ), the frame coordinates were converted into a matrix coordinate system and the moment equilibrium equation was then applied considering the following dimensional parameters; l_b as length of the beam, h_c as height of column, l_o as original length of spring, $\emptyset_c$ as cable diameter, and h_s as inner diameter of spring.

$$A:\begin{bmatrix}0\\0\end{bmatrix}\quad B:\begin{bmatrix}\delta\\h_c\end{bmatrix}\quad C:\begin{bmatrix}l_b\\h_c\end{bmatrix}\quad D:\begin{bmatrix}l_b\\0\end{bmatrix}$$

Length of the spring varies according to the frame displacement. Therefore, development of the matrix of coordinates requires considering both the corresponding extension/compression of the spring and variations of the spring diameter.

$$E:\frac{1}{2}\begin{bmatrix}(l_b+\delta)-\cos\theta(l_o-\frac{8F_sD^3n_a}{Gd^4})+\sin\theta(h_s-\sqrt{D_m^2+\frac{p^2-d^2}{\pi^2}}+d-OD)\\ h_c-\sin\theta(l_o-\frac{8F_sD^3n_a}{Gd^4})-\cos\theta(h_s-\sqrt{D_m^2+\frac{p^2-d^2}{\pi^2}}+d-OD)\end{bmatrix} \tag{5.14}$$

$$F:\frac{1}{2}\begin{bmatrix}(l_b+\delta)-\cos\theta(l_o-\frac{8F_sD^3n_a}{Gd^4})-\sin\theta(h_s-\sqrt{D_m^2+\frac{p^2-d^2}{\pi^2}}+d-OD)\\ h_c-\sin\theta(l_o-\frac{8F_sD^3n_a}{Gd^4})+\cos\theta(h_s-\sqrt{D_m^2+\frac{p^2-d^2}{\pi^2}}+d-OD)\end{bmatrix} \tag{5.15}$$

$$G:\frac{1}{2}\begin{bmatrix}(l_b+\delta)+\cos\theta(l_o-\frac{8F_sD^3n_a}{Gd^4})-\sin\theta(h_s-\sqrt{D_m^2+\frac{p^2-d^2}{\pi^2}}+d-OD)\\ h_c+\sin\theta(l_o-\frac{8F_sD^3n_a}{Gd^4})+\cos\theta(h_s-\sqrt{D_m^2+\frac{p^2-d^2}{\pi^2}}+d-OD)\end{bmatrix} \tag{5.16}$$

$$H:\frac{1}{2}\begin{bmatrix}(l_b+\delta)+\cos\theta(l_o-\frac{8F_sD^3n_a}{Gd^4})+\sin\theta(h_s-\sqrt{D_m^2+\frac{p^2-d^2}{\pi^2}}+d-OD)\\ h_c+\sin\theta(l_o-\frac{8F_sD^3n_a}{Gd^4})-\cos\theta(h_s-\sqrt{D_m^2+\frac{p^2-d^2}{\pi^2}}+d-OD)\end{bmatrix} \tag{5.17}$$

$$O:\frac{1}{2}\begin{bmatrix}(l_b+\delta)\\h_c\end{bmatrix} \tag{5.18}$$

It is worthy to note that two parameters l_b and h_c in equations (5.14-5.18) are predefined physical properties that are depend on the building's architectural drawings. The other two variables l_o and h_s are spring configurations. It was previously mentioned that the moment equilibrium equation has to be employed for the spring to formulate the relationship between spring rotation and the lateral displacement of the frame. On the other hand, definition of the spring rotation should be such that at the spring location the generated moment of the cables reduces to zero. The moment equilibrium equation of spring can be presented as:

$$\sum M = 0 : \; F_R \times \frac{|\overrightarrow{\mathrm{AE}} \times \overrightarrow{\mathrm{EG}}|}{|\overrightarrow{\mathrm{AE}}|} = F_L \times \frac{|\overrightarrow{\mathrm{DH}} \times \overrightarrow{\mathrm{FH}}|}{|\overrightarrow{\mathrm{DH}}|} \tag{5.19}$$

Then, because of equal lengths of cables this equation can be re-written in terms of elongation:

$$\sum M = 0 : \; (\Delta_{AE} + \frac{\mathrm{F_S} L_t}{2AE}) \times \frac{|\overrightarrow{\mathrm{AE}} \times \overrightarrow{\mathrm{EG}}|}{|\overrightarrow{\mathrm{AE}}|} = (\Delta_{DH} + \frac{\mathrm{F_S} L_t}{2AE}) \times \frac{|\overrightarrow{\mathrm{DH}} \times \overrightarrow{\mathrm{FH}}|}{|\overrightarrow{\mathrm{DH}}|} \tag{5.20}$$

where the forces of the right- and left-hand cables are represented by F_R and F_L respectively. F_S stands for the spring force applied to the cables and L_t is the total length of each cable. It is worth mentioning that equation (5.20) takes influence from initial lengths of cables, stretching of cables, and cross product of the directions of cables. These parameters are functions of the lateral displacement of the frame combined with the dimensions and rotation of the spring, which can be written in the following forms:

$$\overrightarrow{\mathrm{AE}} = \frac{1}{2}\begin{bmatrix} (l_b + \delta) - \cos\theta(l_o - \frac{8\mathrm{F_s D^3 n_a}}{\mathrm{Gd^4}}) + \sin\theta(\mathrm{h_s} - \sqrt{D_m^2 + \frac{p^2 - d^2}{\pi^2}} + d - OD) \\ \mathrm{h_c} - \sin\theta(l_o - \frac{8\mathrm{F_s D^3 n_a}}{\mathrm{Gd^4}}) - \cos\theta(\mathrm{h_s} - \sqrt{D_m^2 + \frac{p^2 - d^2}{\pi^2}} + d - OD) \end{bmatrix} \tag{5.21}$$

$$\overrightarrow{\mathrm{DH}} = \frac{1}{2}\begin{bmatrix} (-l_b + \delta) + \cos\theta(l_o - \frac{8\mathrm{F_s D^3 n_a}}{\mathrm{Gd^4}}) + \sin\theta(\mathrm{h_s} - \sqrt{D_m^2 + \frac{p^2 - d^2}{\pi^2}} + d - OD) \\ \mathrm{h_c} + \sin\theta(l_o - \frac{8\mathrm{F_s D^3 n_a}}{\mathrm{Gd^4}}) - \cos\theta(\mathrm{h_s} - \sqrt{D_m^2 + \frac{p^2 - d^2}{\pi^2}} + d - OD) \end{bmatrix} \tag{5.22}$$

$$\overrightarrow{\mathrm{EG}} = \begin{bmatrix} \cos\theta(l_o - \frac{8F_sD^3n_a}{Gd^4}) - \sin\theta(h_s - \sqrt{D_m^2 + \frac{p^2 - d^2}{\pi^2}} + d - OD) \\ \sin\theta(l_o - \frac{8F_sD^3n_a}{Gd^4}) + \cos\theta(h_s - \sqrt{D_m^2 + \frac{p^2 - d^2}{\pi^2}} + d - OD) \end{bmatrix} \tag{5.23}$$

$$\overrightarrow{\mathrm{FH}} = \begin{bmatrix} \cos\theta(l_o - \frac{8F_sD^3n_a}{Gd^4}) + \sin\theta(h_s - \sqrt{D_m^2 + \frac{p^2 - d^2}{\pi^2}} + d - OD) \\ \sin\theta(l_o - \frac{8F_sD^3n_a}{Gd^4}) - \cos\theta(h_s - \sqrt{D_m^2 + \frac{p^2 - d^2}{\pi^2}} + d - OD) \end{bmatrix} \tag{5.24}$$

Substitution of the introduced cross products of the vectors into equation (5.20), gives the following equations:

$$\begin{aligned} |\overrightarrow{\mathrm{AE}} \times \overrightarrow{\mathrm{EG}}| = \frac{1}{2}\ &|(l_b + \delta)(\sin\theta(l_o - \frac{8F_sD^3n_a}{Gd^4}) + \cos\theta(h_s - \sqrt{D_m^2 + \frac{p^2 - d^2}{\pi^2}} + d - OD)) \\ &-h_c(\cos\theta(l_o - \frac{8F_sD^3n_a}{Gd^4}) - \sin\theta(h_s - \sqrt{D_m^2 + \frac{p^2 - d^2}{\pi^2}} + d - OD))\ | \end{aligned} \tag{5.25}$$

$$\begin{aligned} |\overrightarrow{\mathrm{DH}} \times \overrightarrow{\mathrm{FH}}| = \frac{1}{2}\ &|(-l_b + \delta)(\sin\theta(l_o - \frac{8F_sD^3n_a}{Gd^4}) - \cos\theta(h_s - \sqrt{D_m^2 + \frac{p^2 - d^2}{\pi^2}} + d - OD)) \\ &-h_c(\cos\theta(l_o - \frac{8F_sD^3n_a}{Gd^4}) + \sin\theta(h_s - \sqrt{D_m^2 + \frac{p^2 - d^2}{\pi^2}} + d - OD))\ | \end{aligned} \tag{5.26}$$

$$|\overrightarrow{\mathrm{AE}}| = \frac{1}{2}\sqrt{\begin{aligned} &((l_b + \delta) - \cos\theta(l_o - \frac{8F_sD^3n_a}{Gd^4}) + \sin\theta(h_s - \sqrt{D_m^2 + \frac{p^2 - d^2}{\pi^2}} + d - OD))^2 \\ &+(h_c - \sin\theta(l_o - \frac{8F_sD^3n_a}{Gd^4}) - \cos\theta(h_s - \sqrt{D_m^2 + \frac{p^2 - d^2}{\pi^2}} + d - OD))^2 \end{aligned}} \tag{5.27}$$

$$|\overrightarrow{\mathrm{DH}}| = \frac{1}{2}\sqrt{\begin{aligned} &((-l_b + \delta) + \cos\theta(l_o - \frac{8F_sD^3n_a}{Gd^4}) + \sin\theta(h_s - \sqrt{D_m^2 + \frac{p^2 - d^2}{\pi^2}} + d - OD))^2 \\ &+(h_c + \sin\theta(l_o - \frac{8F_sD^3n_a}{Gd^4}) - \cos\theta(h_s - \sqrt{D_m^2 + \frac{p^2 - d^2}{\pi^2}} + d - OD))^2 \end{aligned}} \tag{5.28}$$

$$\Delta_{AE} = \frac{1}{2}\sqrt{\begin{array}{l}((l_{\mathrm{b}} + \delta) - \cos\theta(l_{\mathrm{o}} - \frac{8F_{\mathrm{s}}\mathrm{D}^3 n_{\mathrm{a}}}{\mathrm{Gd}^4}) + \sin\theta(h_{\mathrm{s}} - \sqrt{D_m^2 + \frac{p^2 - d^2}{\pi^2}} + \mathrm{d} - \mathrm{OD}))^2 \\ +(h_{\mathrm{c}} - \sin\theta(l_{\mathrm{o}} - \frac{8F_{\mathrm{s}}\mathrm{D}^3 n_{\mathrm{a}}}{\mathrm{Gd}^4}) - \cos\theta(h_{\mathrm{s}} - \sqrt{D_m^2 + \frac{p^2 - d^2}{\pi^2}} + \mathrm{d} - \mathrm{OD}))^2\end{array}} - \frac{1}{2}\sqrt{(l_{\mathrm{b}} - l_{\mathrm{s}})^2 + (h_{\mathrm{c}} - h_{\mathrm{s}})^2} \tag{5.29}$$

$$\Delta_{DH} = \frac{1}{2}\sqrt{\begin{array}{l}((-l_{\mathrm{b}} + \delta) + \cos\theta(l_{\mathrm{o}} - \frac{8F_{\mathrm{s}}\mathrm{D}^3 n_{\mathrm{a}}}{\mathrm{Gd}^4}) + \sin\theta(h_{\mathrm{s}} - \sqrt{D_m^2 + \frac{p^2 - d^2}{\pi^2}} + \mathrm{d} - \mathrm{OD}))^2 \\ +(h_{\mathrm{c}} + \sin\theta(l_{\mathrm{o}} - \frac{8F_{\mathrm{s}}\mathrm{D}^3 n_{\mathrm{a}}}{\mathrm{Gd}^4}) - \cos\theta(h_{\mathrm{s}} - \sqrt{D_m^2 + \frac{p^2 - d^2}{\pi^2}} + \mathrm{d} - \mathrm{OD}))^2\end{array}} \\ - \frac{1}{2}\sqrt{(l_{\mathrm{b}} - l_{\mathrm{s}})^2 + (h_{\mathrm{c}} - h_{\mathrm{s}})^2} \tag{5.30}$$

β_L and β_R stand for the inclination angles of the cables with respect to horizontal direction and can be calculated as follows:

$$\cos\beta_R = \frac{(l_b + \delta) - \cos\theta(l_{\mathrm{o}} - \frac{8\mathrm{F_s D^3 n_a}}{\mathrm{Gd}^4}) + \sin\theta(\mathrm{h_s} - \sqrt{D_m^2 + \frac{p^2 - d^2}{\pi^2}} + d - OD)}{\sqrt{\begin{array}{l}((l_{\mathrm{b}} + \delta) - \cos\theta(l_{\mathrm{o}} - \frac{8F_{\mathrm{s}}\mathrm{D}^3 n_{\mathrm{a}}}{\mathrm{Gd}^4}) + \sin\theta(h_{\mathrm{s}} - \sqrt{D_m^2 + \frac{p^2 - d^2}{\pi^2}} + \mathrm{d} - \mathrm{OD}))^2 \\ +(h_{\mathrm{c}} - \sin\theta(l_{\mathrm{o}} - \frac{8F_{\mathrm{s}}\mathrm{D}^3 n_{\mathrm{a}}}{\mathrm{Gd}^4}) - \cos\theta(h_{\mathrm{s}} - \sqrt{D_m^2 + \frac{p^2 - d^2}{\pi^2}} + \mathrm{d} - \mathrm{OD}))^2\end{array}}} \tag{5.31}$$

$$\cos\beta_L = \frac{-(-l_b + \delta) + \cos\theta(l_{\mathrm{o}} - \frac{8\mathrm{F_s D^3 n_a}}{\mathrm{Gd}^4}) + \sin\theta(\mathrm{h_s} - \sqrt{D_m^2 + \frac{p^2 - d^2}{\pi^2}} + d - OD)}{\sqrt{\begin{array}{l}((-l_{\mathrm{b}} + \delta) + \cos\theta(l_{\mathrm{o}} - \frac{8F_{\mathrm{s}}\mathrm{D}^3 n_{\mathrm{a}}}{\mathrm{Gd}^4}) + \sin\theta(h_{\mathrm{s}} - \sqrt{D_m^2 + \frac{p^2 - d^2}{\pi^2}} + \mathrm{d} - \mathrm{OD}))^2 \\ +(h_{\mathrm{c}} + \sin\theta(l_{\mathrm{o}} - \frac{8F_{\mathrm{s}}\mathrm{D}^3 n_{\mathrm{a}}}{\mathrm{Gd}^4}) - \cos\theta(h_{\mathrm{s}} - \sqrt{D_m^2 + \frac{p^2 - d^2}{\pi^2}} + \mathrm{d} - \mathrm{OD}))^2\end{array}}} \tag{5.32}$$

The relationship between frame lateral displacement and rotation and expansion of the spring can be implicitly obtained by horizontal static equilibrium equation of the frame:

$$\sum F_x = 0 \rightarrow P = F_R\cos\beta_R - F_L\cos\beta_L = \frac{AE}{L_{OB}}(\Delta_{AE} + \frac{F_S L_t}{2AE})\cos\beta_R$$
$$- \frac{AE}{L_{OD}}(\Delta_{DH} + \frac{F_S L_t}{2AE})\cos\beta_L = \frac{AE}{\frac{1}{2}L_t}(\Delta_{AE} + \frac{F_S L_t}{2AE})\cos\beta_R \tag{5.33}$$
$$- \frac{AE}{\frac{1}{2}L_t}(\Delta_{DH} + \frac{F_S L_t}{2AE})\cos\beta_L = \frac{2AE}{L_t}((\Delta_{AE} + \frac{F_S L_t}{2AE})\cos\beta_R - (\Delta_{DH} + \frac{F_S L_t}{2AE})\cos\beta_L)$$

where L_t stands for the total length of each cable and F_R and F_L denote the right- and left-hand cables' forces respectively. Substitution of equations (5.31) and (5.32) into equation (5.33) gives the following equation:

$$P = \frac{2AE}{L_t}\left[(\Delta_{AE} + \frac{F_S L_t}{2AE}) \times \frac{(l_b + \delta) - \cos\theta(l_o - \frac{8F_s D^3 n_a}{Gd^4}) + \sin\theta(h_s - \sqrt{D_m^2 + \frac{p^2 - d^2}{\pi^2}} + d - OD)}{\sqrt{\begin{array}{c}((l_b + \delta) - \cos\theta(l_o - \frac{8F_s D^3 n_a}{Gd^4}) + \sin\theta(h_s - \sqrt{D_m^2 + \frac{p^2 - d^2}{\pi^2}} + d - OD))^2 \\ +(h_c - \sin\theta\left(l_o - \frac{8F_s D^3 n_a}{Gd^4}\right) - \cos\theta(h_s - \sqrt{D_m^2 + \frac{p^2 - d^2}{\pi^2}} + d - OD))^2\end{array}}}\right.$$
$$+ (\Delta_{DH} + \frac{F_S L_t}{2AE}) \tag{5.34}$$
$$\left.\times \frac{(-l_b + \delta) + \cos\theta(l_o - \frac{8F_s D^3 n_a}{Gd^4}) + \sin\theta(h_s - \sqrt{D_m^2 + \frac{p^2 - d^2}{\pi^2}} + d - OD)}{\sqrt{\begin{array}{c}((-l_b + \delta) + \cos\theta(l_o - \frac{8F_s D^3 n_a}{Gd^4}) + \sin\theta(h_s - \sqrt{D_m^2 + \frac{p^2 - d^2}{\pi^2}} + d - OD))^2 \\ +(h_c + \sin\theta(l_o - \frac{8F_s D^3 n_a}{Gd^4}) - \cos\theta(h_s - \sqrt{D_m^2 + \frac{p^2 - d^2}{\pi^2}} + d - OD))^2\end{array}}}\right]$$

This equation can only be applied when the PCS is placed at the intersection point of the diagonal cables. After having the PCS combined with a sliding hollow stiff shaft and eliminating the influence of outer diameter expansion (equation 5.6), equation 5.36 is developed. It has to be noted that two issues have to be considered: firstly, cables always pass through the hollow shafts and secondly, shafts are assumed to be stiff, with a constant diameter. Equation (5.36) includes the mean of minimum to maximum variation range of the spring length and l_{o} is replaced by l_{c} :

$$\overline{P} = \frac{1}{l_{ci\,max}} \sum_{l_{ci}=0}^{l_{ci\,max}} P_i \tag{5.35}$$

where P_i is,

$$P_i = \frac{2AE}{L_t} \left[\begin{array}{c} (\Delta_{AE} + \frac{\mathrm{F_S} L_t}{2AE}) \times \frac{(l_b + \delta) - \cos\theta(l_c + \; l_c\,) + \sin\theta(\mathrm{h_s})}{\sqrt{\begin{array}{c}((l_\mathrm{b} + \delta) - \cos\theta(l_\mathrm{c} + \; l_c\,) + \sin\theta(h_\mathrm{s}))^2 \\ +(h_\mathrm{c} - \sin\theta(l_\mathrm{c} + l_c\,) - \cos\theta(h_\mathrm{s}))^2\end{array}}} + (\Delta_{DH} + \\ \frac{\mathrm{F_S} L_t}{2AE}) \times \frac{(-l_b + \delta) + \cos\theta(l_c + \; l_c\,) + \sin\theta(\mathrm{h_s})}{\sqrt{\begin{array}{c}((-l_\mathrm{b} + \delta) + \cos\theta(l_c + l_c\,) + \sin\theta(h_\mathrm{s}))^2 \\ +(h_\mathrm{c} + \sin\theta(l_\mathrm{c} + l_c\,) - \cos\theta(h_\mathrm{s}))^2\end{array}}} \end{array} \right] \tag{5.36}$$

Frame displacement is related to the cable strain and this relation is expressed by three factors known as the elongation of cables, axial rigidity of each cable, and spring force:

$$\varepsilon = \frac{\Delta L}{L} = \frac{F_S L_t / AE}{L_t} = \frac{F_S}{AE} \tag{5.37}$$

$$\varepsilon_R = \frac{2\Delta_{AE}}{L_t} + \frac{\mathrm{F_s}}{AE} \tag{5.38}$$

$$\varepsilon_L = \frac{2\Delta_{DH}}{L_t} + \frac{\mathrm{F_s}}{AE} \tag{5.39}$$

Calculation of the lateral stiffness at each floor is conducted by the following equation:

$$k_i = k_{MRFi} + \left[k_{ci} + k_{sp}\right] \tag{5.40}$$

in which $\mathrm{k_i}$ represents total lateral stiffness, and $\mathrm{k_{ci}}$, $\mathrm{k_{sp}}$ and $\mathrm{k_{MRFi}}$ are cable brace, spring and moment-resistant frame lateral stiffness at each storey, respectively. The following equation calculates the lateral stiffness of the cable brace:

$$k_c = \frac{2AE}{\delta L_t}\left[(\Delta_{AE} + \frac{F_S L_t}{2AE})cos\beta_R + (\Delta_{DH} + \frac{F_S L_t}{2AE})cos\beta_L\right] \quad (5.41)$$

where k_c is lateral stiffness of the cable brace (both cables included).

5.9.3 Cable design

The required seismic resistance load of the steel cables has to be calculated based on ASCE 19 (ASCE/SEI, 1997). The cable-assembly allowable strength, S_a, is obtained as following:

$$S_a = {S_{min}}/{\Omega} \quad (5.42)$$

where S_{min} is minimum breaking force and stands for safety factor whose quantity is equal to 2.2 (ASCE/SEI, 1997).

The wire ropes' maximum resistance is reached when one of the cables approaches its tensile capacity. The resistance level is obtained by equation (5.43):

$$f_u A_c cos\alpha \quad (5.43)$$

where f_u is the tensile strength of the cable material.

It has to be noted that the spring force should be considered in the allowable strength of the cable in the PCS system. Therefore, to simplify the calculations the following issues are considered: firstly, parameter of length variation (l_c') is ignored to consider the most critical scenario for design purpose. This elimination provides more safety as well. Secondly, full compression of spring is assumed and thirdly, cables are presumed to experience the maximum loads. The acceptance criterion of the cable elements is as follows:

$$A_c \geq \Omega\left(\frac{F_w + F_s \cos\alpha}{f_u \cos\alpha}\right) \tag{5.44}$$

where, F_w, and F_s stand for the increment of the shear strength of storey using wire-rope bracing and spring force respectively.

5.10 Numerical simulation

ABAQUS software was utilized to model the cyclic response of the proposed retrofitted structural systems. Reviewed literature and similar numerical simulations suggested second-order solid elements to model complex geometric and stress displacement. Nevertheless, the current study involves contact pressure calculations between contact members and this makes the suggested numerical element an invalid one (Lu et al., 2009). On the other hand, for three-dimensional modeling of rectangular elements such as beam and column application of a first-order hexahedral (brick) element was suggested by ABAQUS documentation (ABAQUS, 2017). In comparison with triangles or tetrahedra elements which are less sensitive to initial element shape, the hexahedral elements provide accurate results for the minimum cost.

One issue to be considered in numerical modeling is keeping the balance between accuracy and computational time since a higher mesh density leads to increased accuracy up to a certain level beyond which there is no more positive effect gained by increasing mesh density and refinement. Another issue to be noted is mesh convergence whose failure is mostly due to modeling deficiencies which have to be resolved prior to accuracy controls. Solution control parameters are normally applied to all active fields by default.

In order to minimize the required time for FE analysis execution and to make sure of convergence and accuracy, a mesh refinement study is required to determine the mesh size and accordingly, a trade-off between time and accuracy was conducted (CEN, 2005). Mesh size was decided according to occurrence possibility of element distortions and inelastic deformations throughout the structure. Locations such as cables, spring, gusset plates and haunches with high chance were modeled by fine meshing while other regions with limited plastic deformations like beam and columns were modeled with coarser and more uniform meshing. Hence, this idealization was expected to provide accurate results.

Investigation of the available elements for FE modeling of current reduced integration analysis procedure concluded the selection of a first-order 3D solid element briefly known as C3D8R which denotes 3-dimensional 8-node linear brick reduced integration with hourglass control element. This element was expected to behave stiffer behavior with a slow convergence rate while mesh locking and complexity had lower chance to take place. Furthermore, incorporation of material properties nonlinearity, geometric nonlinearity, and displacement-controlled loading were other advantages of the model. Eventually, the model was completed with total of 2055 elements whose analysis results were anticipated to correlate with the experimental results. The 3D FE meshing, boundary conditions (BCs) and displacement loading are depicted in Figure 5.19.

In order to solve nonlinear equations, it was decided to choose a technique with the advantage of savings on computational cost. Therefore, quasi-Newton technique was selected. The assigned convergence criterion was 0.005 with maximum allowed number of cutbacks for each increment to be 5. The penalty friction formulation was assumed to govern the contact between cables and spring whose static coefficient of friction was set to be 0.3. For the normal direction an augmented Lagrange method was employed which would allow separation after contact. Although the 3D model of the spring could be more realistic, nevertheless it was modeled in 2D to reduce the need for spring-cables contact analysis and its pre-compressed load was idealized through applying a pretension force on wire rope cables in the time history analysis. Thus, at the mid-point of the truss element, which modeled cables, a bolt load was calibrated and then exerted through the "adjust length" option. Simulation of cyclic displacement loading along with cyclic behavior of the frames under considered quasi static FE analyses was conducted through displacement control scheme rather than load control. Loading of the model was conducted in the static steps with the default amplitude function and BCs associated with each other. Identical loading history was utilized in all considered FE analyses and of course it was the same as the loading used in the experimental tests. Displacement loading was applied smoothly to achieve a better reflect of the total history data. To improve the beam-column contact simulation and to increase the accuracy of the analyses, displacements and rotations of the beams and columns were limited on normal direction besides the exertion of load on both tips of columns. The deformed configuration of the specimens is shown in Figure 5.20.

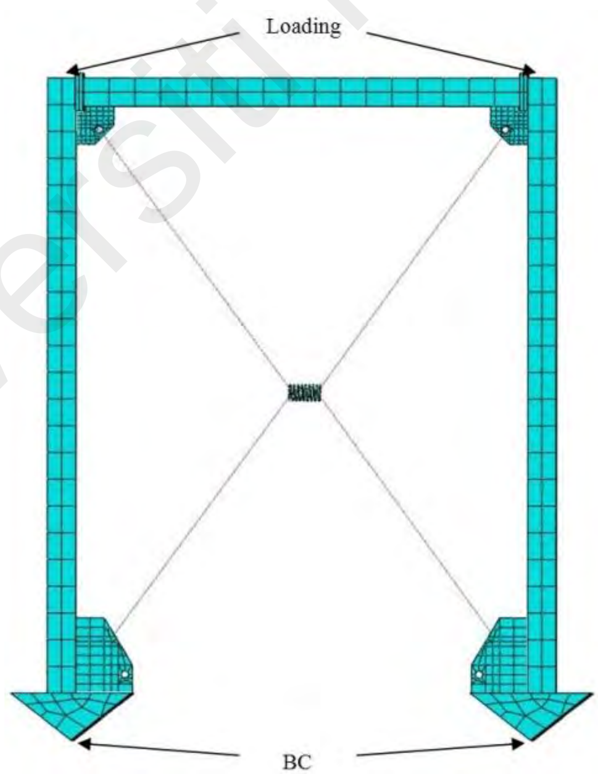

Figure 5. 19: One-bay steel frame model in ABAQUS, loading and BCs

(a) BF

Figure 5. 20: Deformed configuration of the specimens

(b) PCS

Figure 5.20: Deformed configuration of the specimens (Cont.)

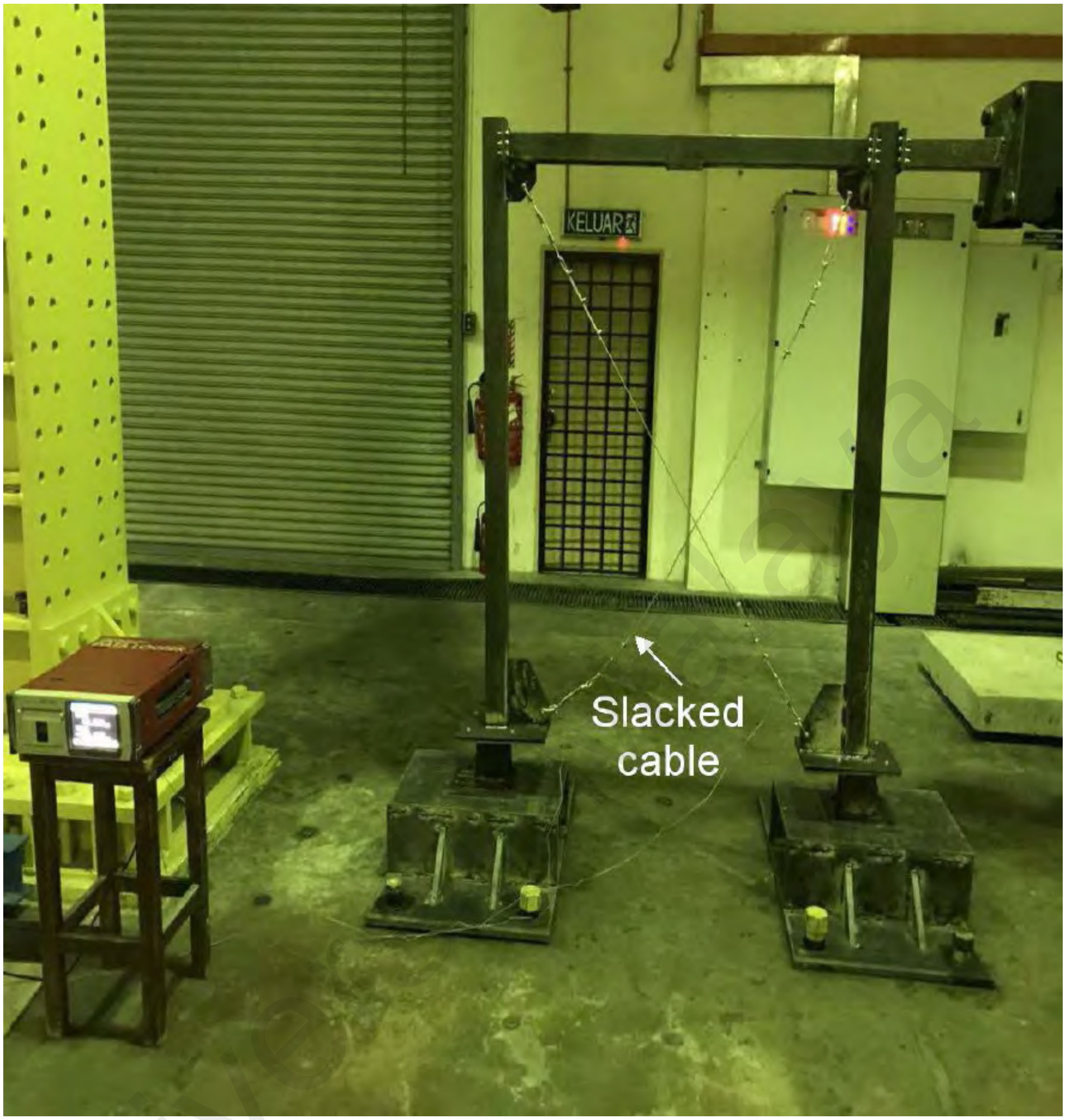

(c) CCB

Figure 5.20: Deformed configuration of the specimens (Cont.)

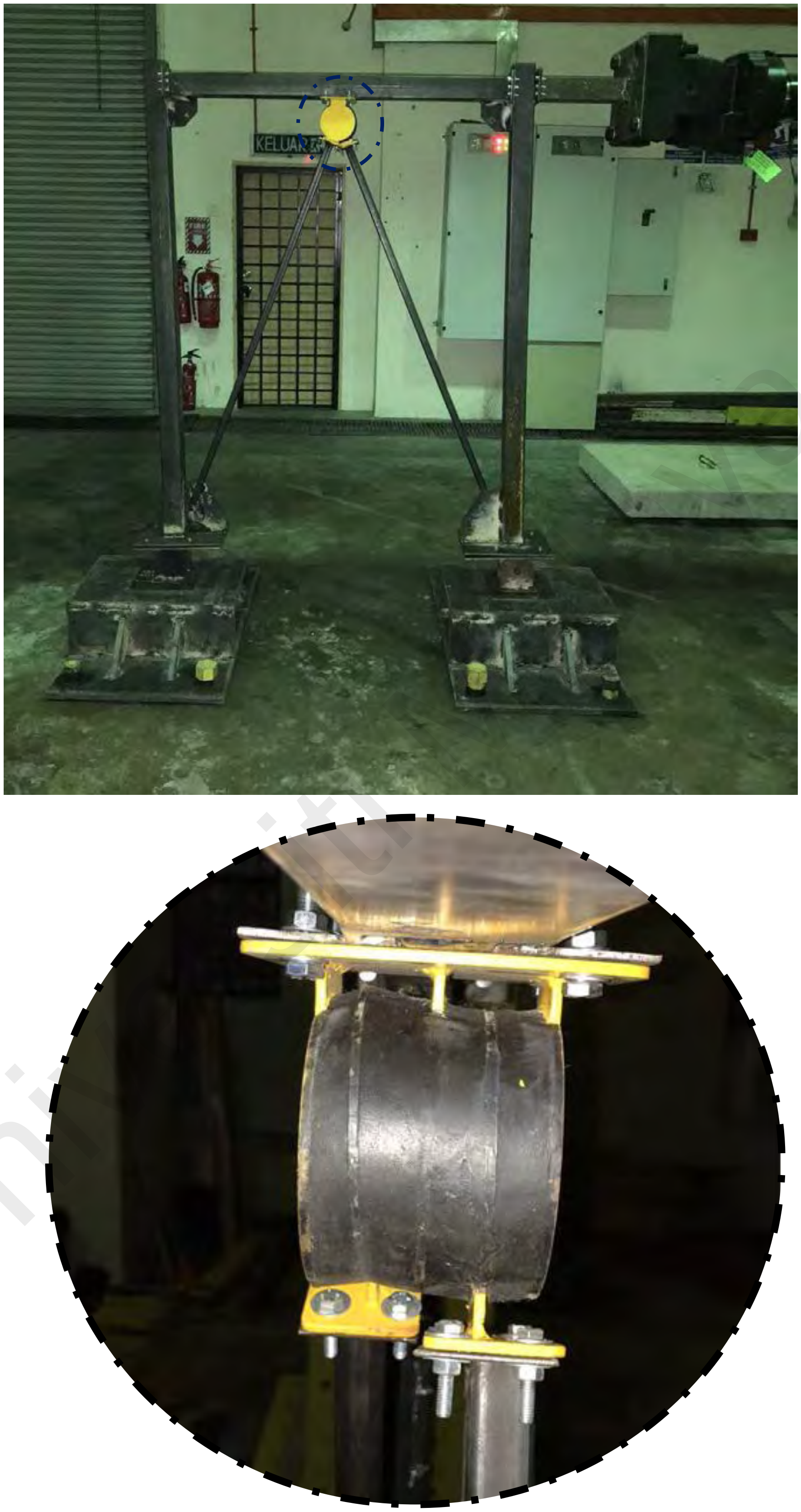

(d) RRBD

Figure 5.20: Deformed configuration of the specimens (Cont.)

(e) PCS and RRBD

Figure 5.20: Deformed configuration of the specimens (Cont.)

5.11 Static horizontal cyclic analysis

The reverse-cyclic loading of the PCS, and CCB bracing systems were conducted and the force-displacement behaviors of the equipped frames were plotted along with that of the bare frame (BF). It was observed that the general responses of the frames showed continued resistance in confrontation of additional load with no much observed damage. The loading and the corresponding structural behavior of the specimens are discussed hereafter. Two aspects of the obtained behaviors are illustrated in Figure 5.21; left panel depicts the lateral load versus storey deflection at the top of the columns and the right panel demonstrates the relationship between energy dissipation and storey deflection. The pre-compressed spring effect is shown more clearly in the magnified Figure 5.21 (c), which implies the gradual increase in stiffness when the frame goes back to its original position. As can be seen, the energy dissipated is the lowest for the BF and highest for the HPCS-equipped frame.

The obtained analysis curves of load versus lateral displacements were in a remarkable agreement with those of experiments. The force-displacement hysteretic loops of the BF model are shown in Figure 5.21 (a). One key aspect of the obtained behavior was the interaction type behavior generated by the pre-stressing force between the PCS and cables. In addition, interaction behavior caused by sliding of cables on the spring under lateral movement of the frame was neglected as it was modeled in 2D to minimize the computational cost. A way to present the specimens' response under cyclic loading was to use a join with rotation connector element to join the cables as they were assumed separate elements. This selection may cause slight differences with the experimental results, nevertheless it is still a true representation of the frame behavior.

According to the left panel, maximum shear forces obtained from experimental specimens were 11.1, 44.9, and 45.1 kN and those gathered from FE models were 12.1, 42.3, and 44.6 kN for BF, PCS, and CCB bracing systems, respectively. A simple comparison suggests 5.7% of deviation.

The ultimate strength of the cable according to Equation (5.43) is calculated as follows:

$$\alpha = \tan^{-1}\left(\frac{1557.5}{1200}\right) = 52.4^{\circ}$$

$$f_u A_c cos\alpha = \ 1765\ (32) cos\ (52.4) = 34.5kN$$

This value is in good agreement with that of test data.

Results of shear gradient associated with frames equipped with PCS bracing system are shown in Figure 5.21 (c). Obviously, the shear gradient climbs up with increase of displacement. Measurements of the capacity developed by the frame equipped with the proposed PCS and the frame equipped with CCB revealed similar capacity in withstanding against the load at 3.0% lateral drift. This drift value corresponded to 50 mm lateral deflection. This could be originated by fully straightened wire ropes at this lateral drift level. Application of PCS system resulted in high deformation capacity and unlike CCB-equipped frame the shear gradient in PCS-equipped frame experienced gradual increment.

The force-displacement hysteretic loops of the HPCS-equipped frame are depicted in Figure 5.21 (d). This hybrid system enhances the strengths and offsets the weaknesses of the individual systems. Initially, the bracing member didn't act. Hence, the initial stiffness of RRBD and HPCS-equipped frames are almost identical. This strategy has the benefits of both systems, high energy dissipation, and increased lateral resistance at large displacement due to the RRBD and PCS implementation, respectively.

Figure 5.21(e) presents the force-displacement curve of the frame equipped with CCB in FE analysis. This figure shows a sudden increase of force caused by the instant action of CCB. It is worth mentioning that high stress in the cables from one side and poor elongation capacity from another side raise the probability of an early fracture of the steel cables. In the mechanism of wire rope unit, no gradual functioning was observed due to ambiguities in the accurate modeling of the shackles and slippage of the wire rope thorough the grips upon straightening, which increased the complexity of the interaction. From these obstacles it can be concluded that solid element is not the proper element to idealize the behavior. Nevertheless, comparisons between FE analyses and experiments show acceptable modeling of FE and yet prove it as a reliable tool to predict the structural response.

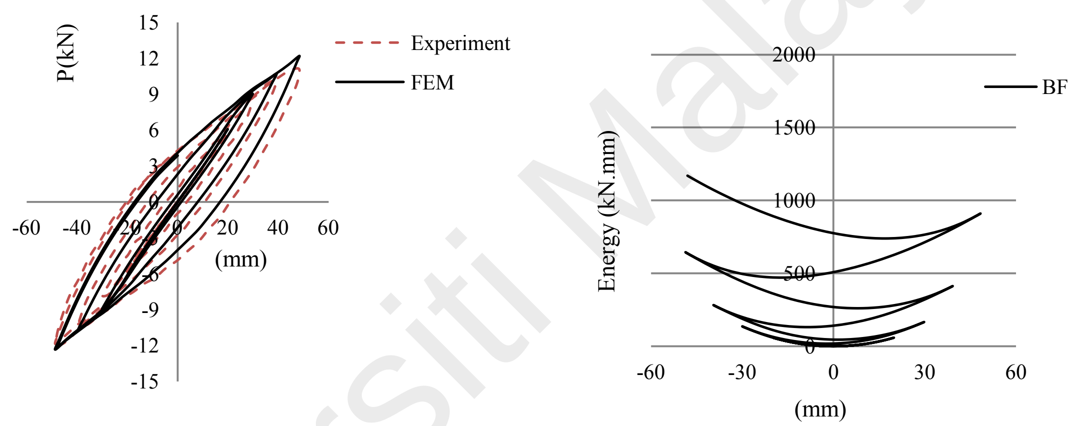

(a) BF

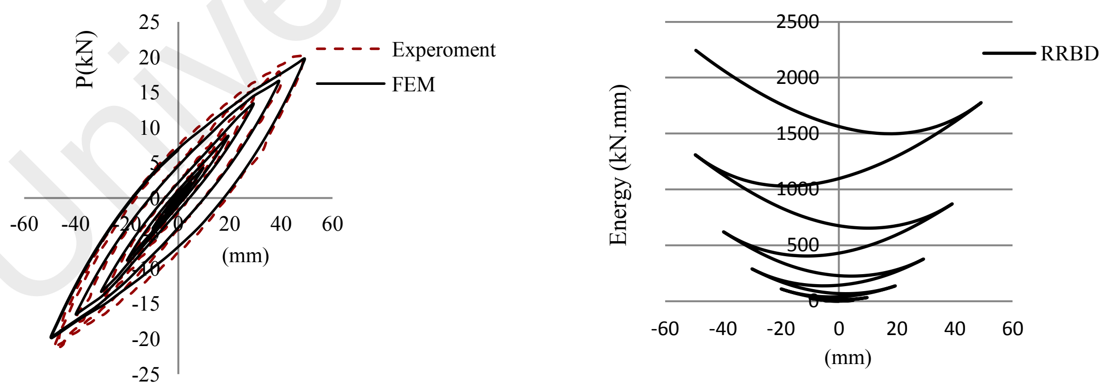

(b) RRBD

Figure 5. 21: Cyclic behavior of specimens

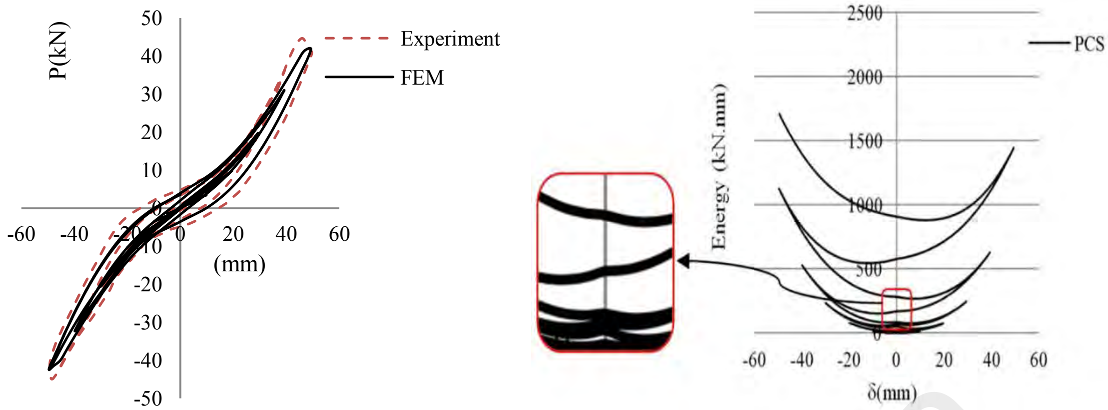

(c) PCS

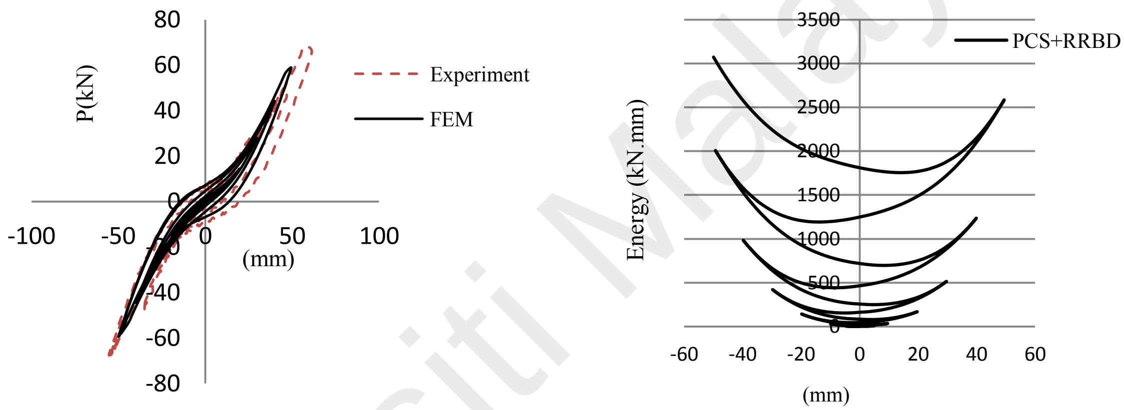

(d) HPCS

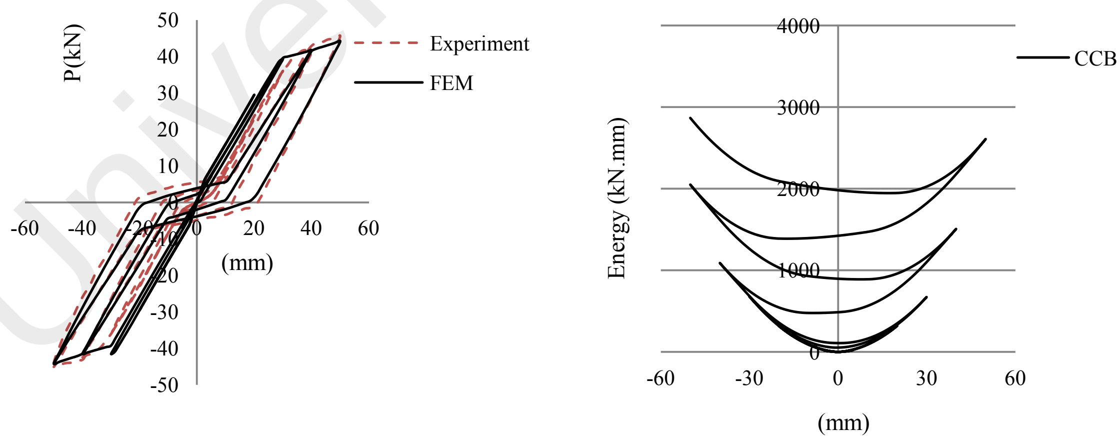

(e) CCB

Figure 5. 21: Cyclic behavior of specimens (Cont.)

In order to specify contribution level of diagonal cables in lateral load resistance of the frame and to determine the loading stage at which the cable along the compression diagonal becomes slack, strain variation was observed and plotted in Figure 5.22. The resulted strain data underlined existence of additional stiffness which was generated and added to the frame by the spring force at initial stage of loading. Loss of the initial tension generated by the PCS was observed along the compression diagonal cable while action of the wire rope in the direction of tension diagonal continued standing against significant lateral forces.

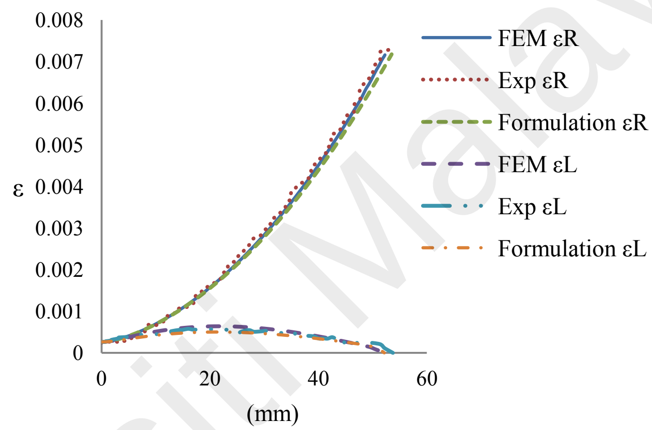

Figure 5. 22: Strain-displacement curve

Changes of brace strain in the proposed PCS bracing system was under observation from the onset of the loading and its trend was found to be in contrast with that of the cable cylindrical bracing case (Hou et al., 2008). Brace strain alteration associated with the later case is dependent on the frame size, cylinder length, and inner diameter and is reported to rise after the specific displacement of 20 mm is reached. However, the cable in the direction of tension diagonal continued resisting significant lateral forces.

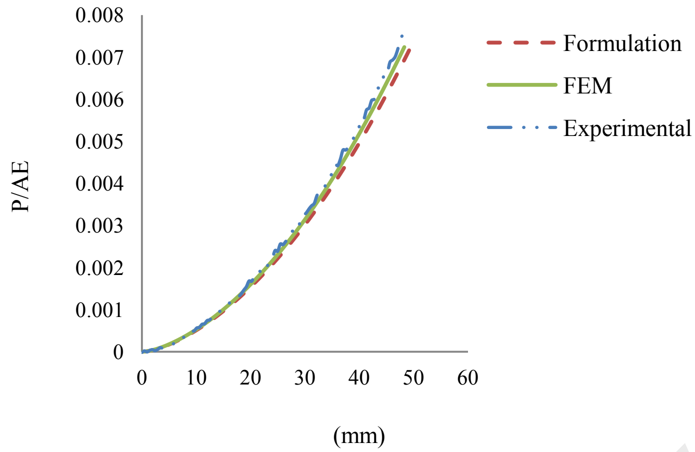

Figure 5. 23: Force–displacement curve

According to Figures 5.22 and 5.23, numerical analyses and experimental results very well coincided with each other. As shown in Figure 5.23, stiffness of the PCS system was not constant during load exertion; stiffness started from zero at the very beginning after which it started to climb up in line with frame lateral displacement.

5.12 Parametric study of rubber thickness and rubber diameter under cyclic loading

This section focuses on the influence of the proposed RRBD system on the frame performance under cyclic load and discusses the effect of rubber thickness and diameter on the performance of the whole system. Theoretically speaking, there is no application limit in number and dimension of VE pads to design an RRBD system with various stiffness and energy dissipation values. However, the key and challenging issue is how to design a proper RRBD with no chance of buckling when subjected to external load. In other words, it is a necessity to design the RRBD in such a way that buckling stiffness of the brace is greater than the total stiffness of the whole damper. This also provides further stability to the frame. To achieve this safety level in performance of the damping system the buckling point of the brace has to be initially identified and ensure that even at maximum frame displacement this threshold is not reached.

Resulting diagrams acquired from performance of all considered frames are presented in Figure 5.24. Left panels include the lateral load-displacement hysteresis diagram and in right panels the corresponding energy dissipation and storey rotation angle relationship are presented. Plots indicate functionality of dampers in both relatively small and large displacements. All dampers showed stable hysteresis loops in confronting large displacements. Application of rubber pads with different thickness resulted in varying cyclic load-displacement relationship; reduction of the VEM thickness resulted in substantial increase of the energy dissipated by the system, Figure 5.24 (a). Moreover, for 10mm-pad-thickness and 120mm-pad-diameter case the hysteresis curve of the RRBD-equipped frame has the force value of approximately 2 times that of BF at maximum displacement. The large area under hysteresis loop of RRBD system indicated high energy dissipation capability of the proposed damping system.

Figures 5.24 (c-d) demonstrate effect of the pad diameter variation on the energy dissipation capability of the damper. It was observed that increase of diameter resulted in higher energy dissipation and larger shear area. In addition, there is a notable rise in the corresponding force needed for the same amount of frame lateral displacement. This exhibits higher stiffness of the RRBD. Another aspect of the performance nature of VEMs observed in the results was larger stiffness and strength of the damper when subjected to greater deformation. This phenomenon roots in the unique nature of this type of material which shows larger stiffness values at higher levels of strain. Other dampers such as frictional and metallic dampers have not such advantage. Frictional dampers do not exhibit any stiffness upon sliding, and in most metallic dampers, stiffness either decreases or remains the same at larger displacements. Such natural property ensures the reliability of equipped structures against severe seismic loads as by increasing the structural stiffness at extra-large displacements structural collapse is prevented.

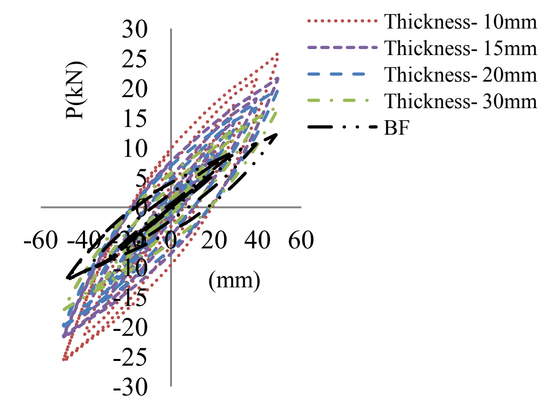

(a) Effects of rubber thickness (RT)

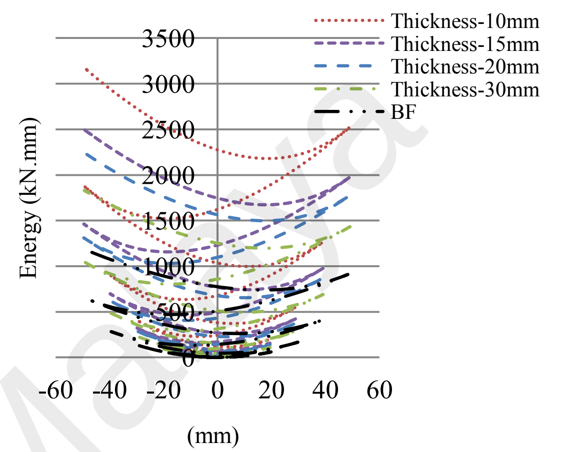

(b) Dissipated energy vs. rotation

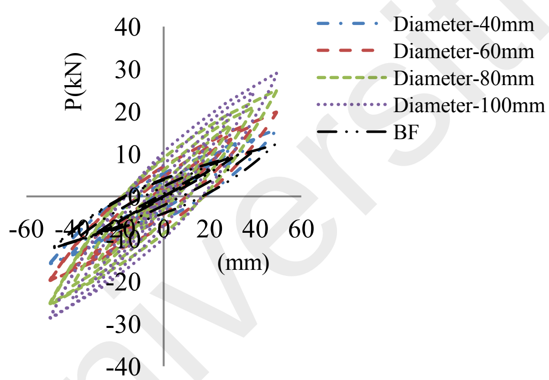

(c) Effects of diameter of rubber pad (D)

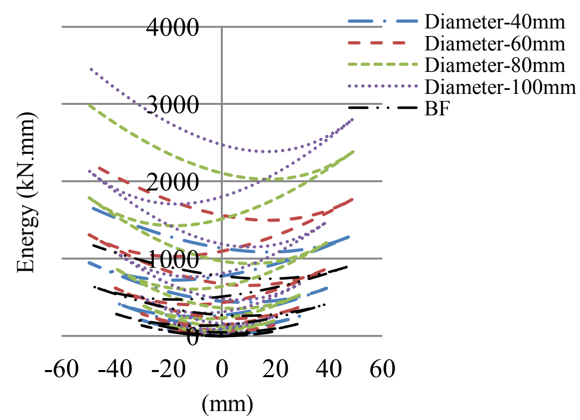

(d) Dissipated energy vs. rotation

Figure 5. 24: Cyclic behavior of BF and frame with damper

Table 5.7 categorizes the FEA results according to the geometrical and mechanical properties of frames and compares them with those of the BF based on the initial stiffness (k), maximum load (P_{max}), energy dissipation (E_D), and ratios of each value. Stiffness is measured as the average slope of the displacement-force hysteresis loop and dissipated energy per cycle is defined as the area of displacement-force hysteresis loop:

$$E_D = \int f_d dx \tag{5}$$

It has to be mentioned that variation of VEM volume associated with increase in the thickness and diameter subsequently affects functional parameters of VEM including stiffness, maximum load, and energy dissipation of the damper. For instance, an increase in the VEM thickness, as opposed to an increase in the diameter, can result in a reduction in the maximum induced load and stiffness.

Table 5. 7: Mechanical properties of parametric study models

Model no.	D (mm)	t (mm)	D/t	k (kN/mm)	k/k_A	P_{max} (kN)	P_{max}/P_{max}^{BF}	E_D (kJ)	E_D/E_{BF}
BF	N/A	N/A	N/A	2.4	1	12	1	3.96	1
1	120	10	12	5.14	2.14	25.7	2.14	9.76	2.4
2	120	15	8	4.36	1.81	21.8	1.81	7.84	1.9
3	120	20	6	3.96	1.65	19.8	1.65	7.12	1.7
4	120	30	4	3.4	1.41	17	1.41	5.95	1.5
5	200	20	10	5.8	2.41	29	2.41	9.86	2.5
6	160	20	8	5	2	25	2	5	1.26
7	80	20	4	3.14	1.31	15.7	1.31	5.1	1.28

N/A: not available

5.13 Time history analysis

After experimental testing and justifying the FE models, the proposed systems modelled and analyzed in SAP2000 for time history simulation. Results of the time history analysis are presented for BF, as the baseline, PCS-, RRBD- and the HPCS retrofitted frame in this section. Measurements of time history and SPO analyses are presented in multiple types of graphs and are generally grouped in two subsections; one retrofit system per storey and two retrofit systems per storey. Damage measurements were conducted by focusing on maximum displacement, maximum roof drifts and acceleration, residual deformations and maximum base shear and plotted on the x-axis with the elevation plotted on the y-axis.

5.13.1 One retrofit system per storey

Proposed systems were placed at the exterior spans of each storey. Analyses were conducted and results of time-history analysis for the three considered seismic motions are presented in Figures 5.25 to 5.32. Factors of the seismic response of the frame included base shear, roof acceleration and roof displacement. In addition, plots obtained from nonlinear SPO analysis demonstrated a nonlinear force-displacement trend of the structural performance. Measurements of the structural damages revealed that the SMRF structure with no damping device had the weakest performance whereas frames equipped with RRBD and PCS cable performed much better. For ease of comparison and simplicity, all symbols used to compare the plots of considered cases were remained constant. According to Figure 5.25, application of the proposed hybrid system resulted in significant degradation of roof displacement.

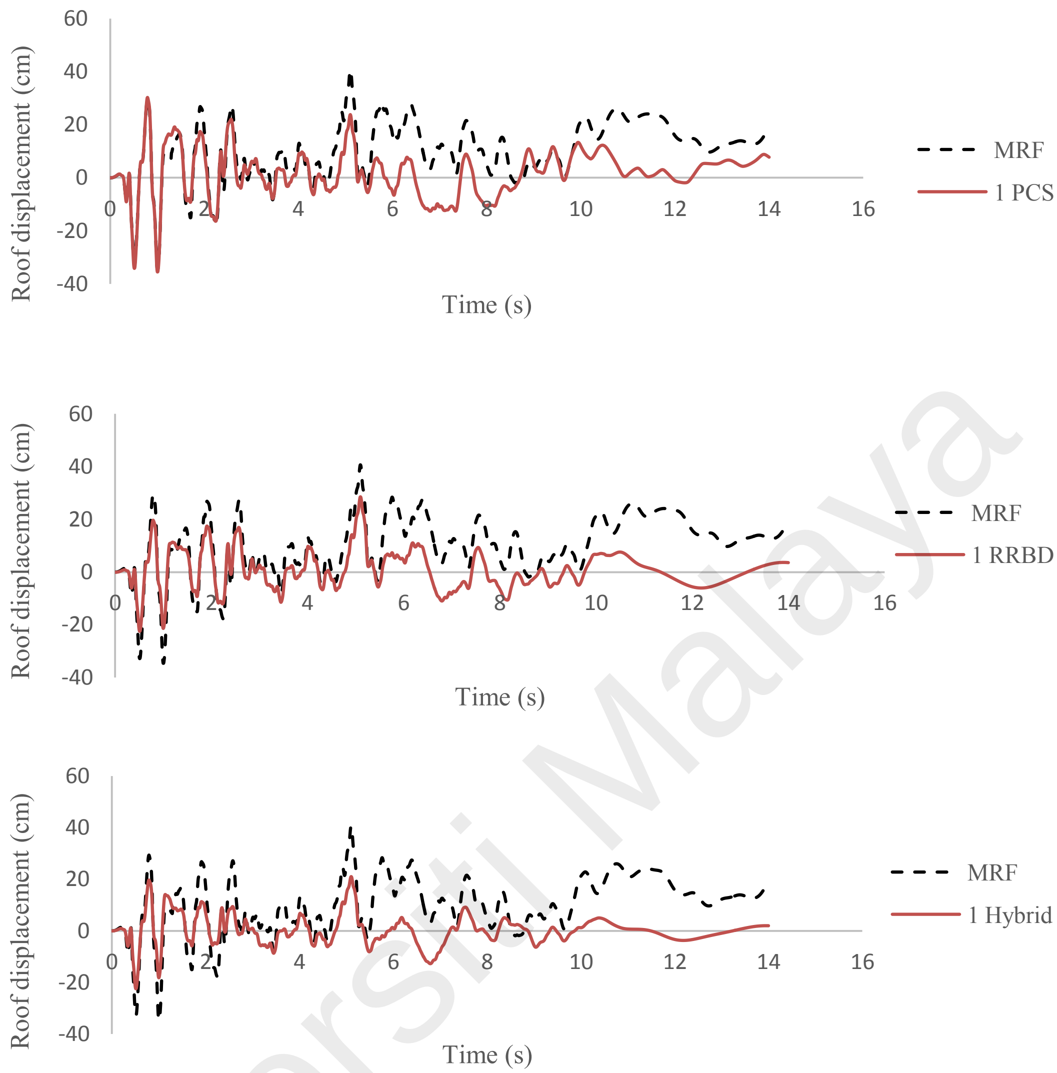

(a) El Centro

Figure 5. 25: Roof displacement

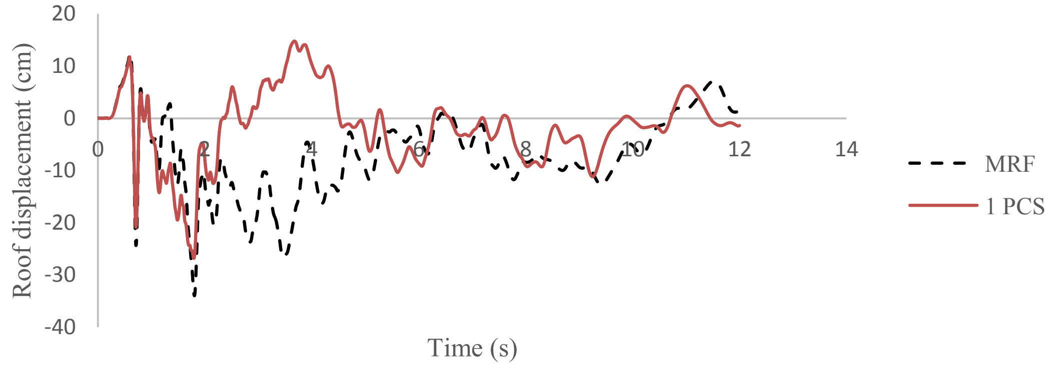

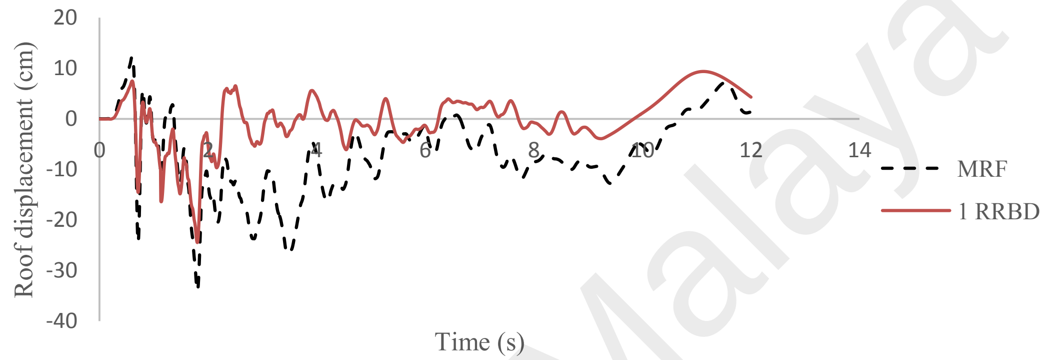

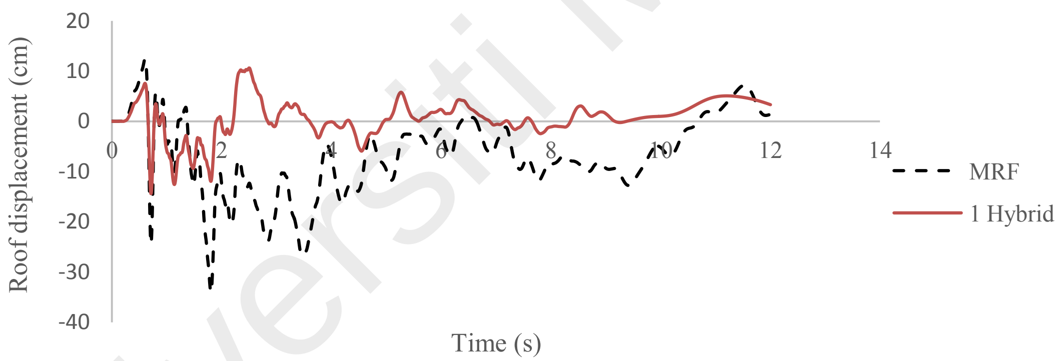

(b) Northridge

Figure 5. 25: Roof displacement (Cont.)

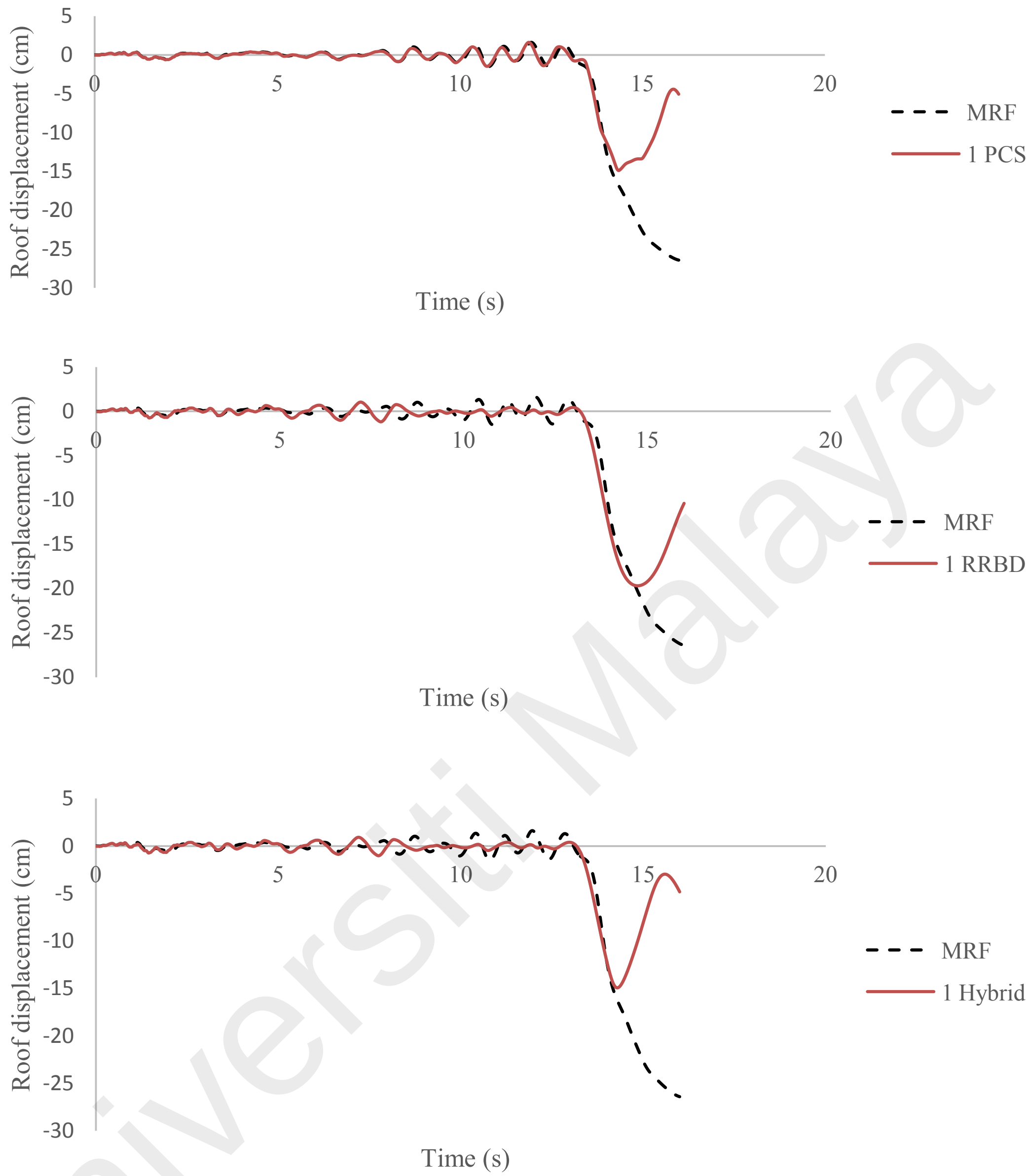

(c) Kobe

Figure 5. 25: Roof displacement (Cont.)

Bearing in mind that presence of PCS system provides extra stiffness to the structure and subsequently creates larger roof acceleration, application of RRBD, however, caused the lowest base shears and accelerations yet at the expense of larger deformations. Plots of structural drift highlighted the drift alteration from low to larger values for bottom to top floors, respectively. Observation of drift variation along the height of the frame showed intense drift variation of lower floors compared to that of upper floors. This issue underlines both larger displacement response of the frame and consequently higher risk of damage caused by loss of storey stiffness at lower and intermediate stories.

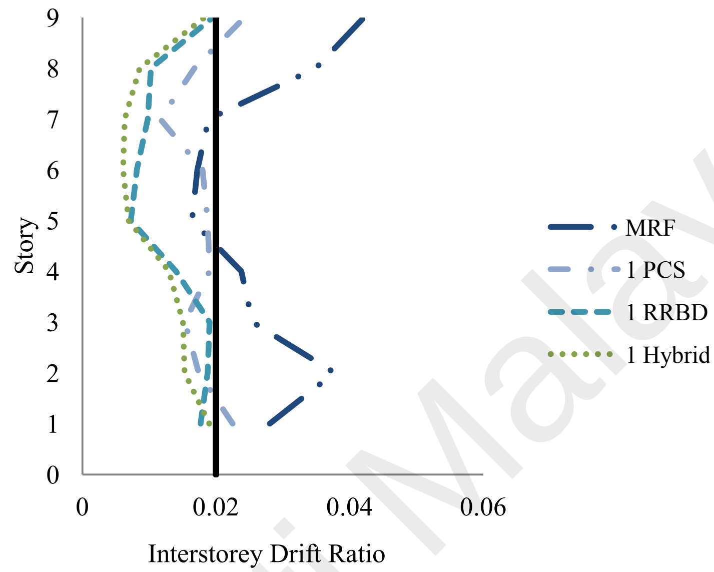

(a) El Centro

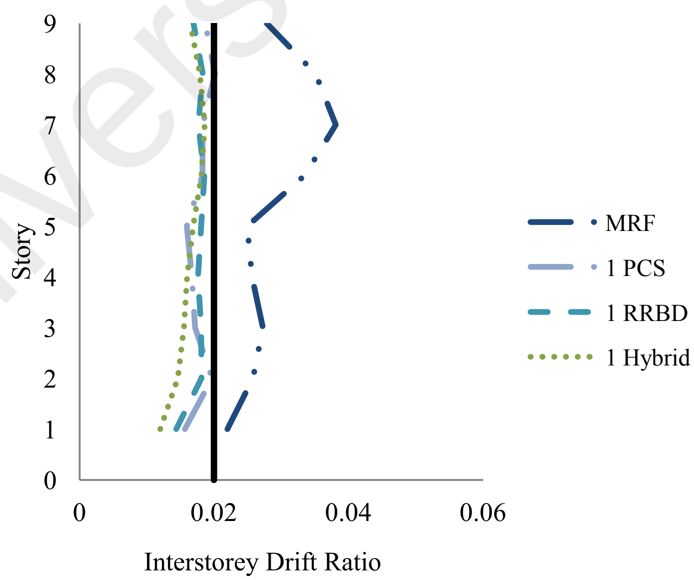

(b) Northridge

Figure 5. 26: Maximum Storey Drifts

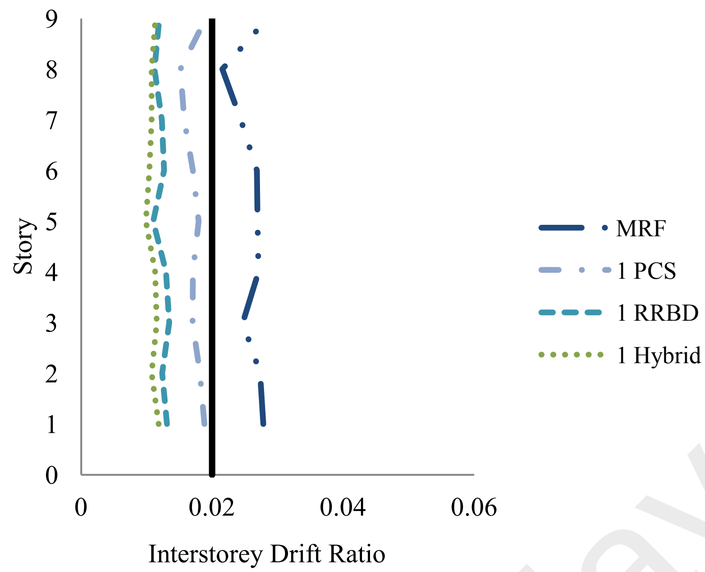

(c) Kobe

Figure 5. 26: Maximum Storey Drifts (Cont.)

Comparison of the drift variation between two cases of SMRF and PCS-equipped frame revealed that the case with PCS system experienced significantly less drift, Figure 5.26. This means that installation of PCS bracing can result in significant attenuation of the inter-storey deflection and consequently degradation of seismic damage. Apart from the correlation between drift alteration along the height of buildings and the seismic hazard level, this analysis showed that retrofitted frames with no significant reduction of the tip displacement experienced drift reduction. Nevertheless, the PCS system did not prevent exceed of 2% structural drift under El Centro earthquake load case.

In order to further evaluate the performance level of the braced steel frames FEMA acceptance criteria was considered in the conducted nonlinear analysis procedures. According to the FEMA, three performance levels are defined; immediate occupancy (IO), life safety (LS) and collapse prevention (CP). For instance, if only one structural member is not able to satisfy the CP performance level, thus the whole structure and its entire performance level is considered as failed. This means that the acceptance criteria are not met. In this regard, there was a limit state value assigned for each performance level; 0.5%, 1.5% and 2.0% of the storey height, respectively. The considered SMRF structure retrofitted with the proposed damping systems was analyzed and results approved that this structural system satisfied the collapse CP objective defined by FEMA and thus had sufficient capacity to sustain design-level seismic load. This was totally in contrast with damage-oriented measurements of the SMRF case as it performed poorly and exceeded the given standard drift limits for all earthquakes. Meanwhile, it has to be mentioned that 25% of increase on drift limits is allowed for nonlinear response history analysis by ASCE 7-05. Comparison suggests the HPCS-equipped frame as the best performer while the SMRF structure was the worst. Although the PCS and RRBD-equipped frames experienced low magnitudes of drift, trend of drifts along the height were more erratic than HPCS frame. It was further observed that the highest drift ratios took place near the bottom of the structure. The respective plot of the SMRF demonstrated a typical drift diagram of a structure experiencing significant yielding as there were several formations of column hinges that almost created a collapse mechanism.

Reduction of deformations associated with the proposed HPCS system was found more pronounced compared to other considered cases. This is in addition to the fact that almost all the retrofitted structures had passed the FEMA code requirement of 0.02. Attenuation of roof accelerations was another advantage of the HPCS over both PCS-equipped frame and BF. This highlights probable detrimental effect of additional stiffness provided by PCS. Frame with the proposed hybrid system however performed different as soon as the second phase was started by the PCS cable bracing being engaged; in second phase stiffness ascended because of parallel functioning of the RRBD with the PCS cable bracing and therefore acceleration continued to rise.

Figures 5.27 - 5.29 show the comparison between the nodal acceleration of the proposed systems and the MRF at the roof. Large acceleration magnitudes were attributed by the PCS-equipped frame, which may have been caused by an increase in the structure's stiffness. On the other hand, RRBD had the lowest acceleration response.

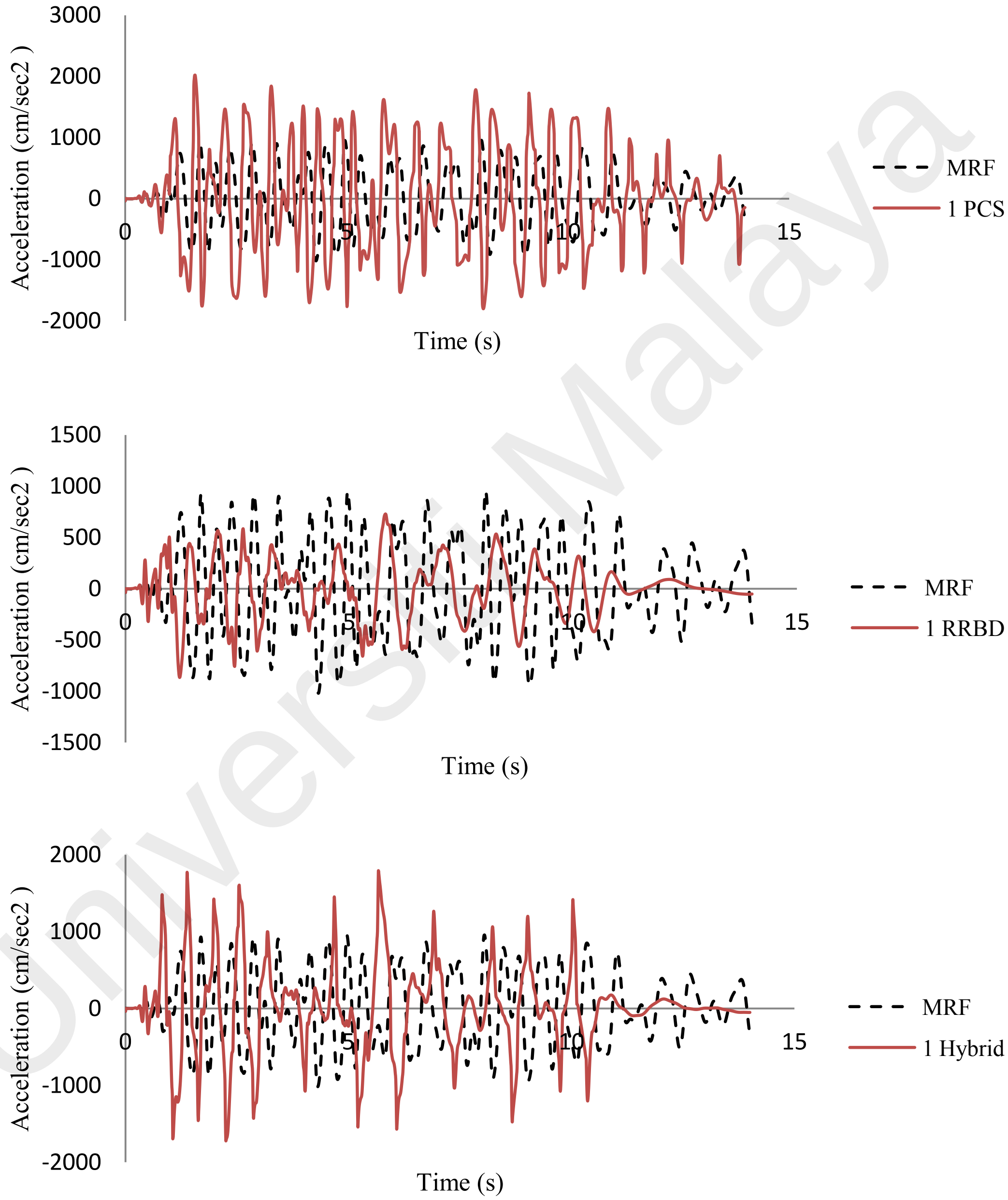

Figure 5. 27: Roof acceleration: El Centro

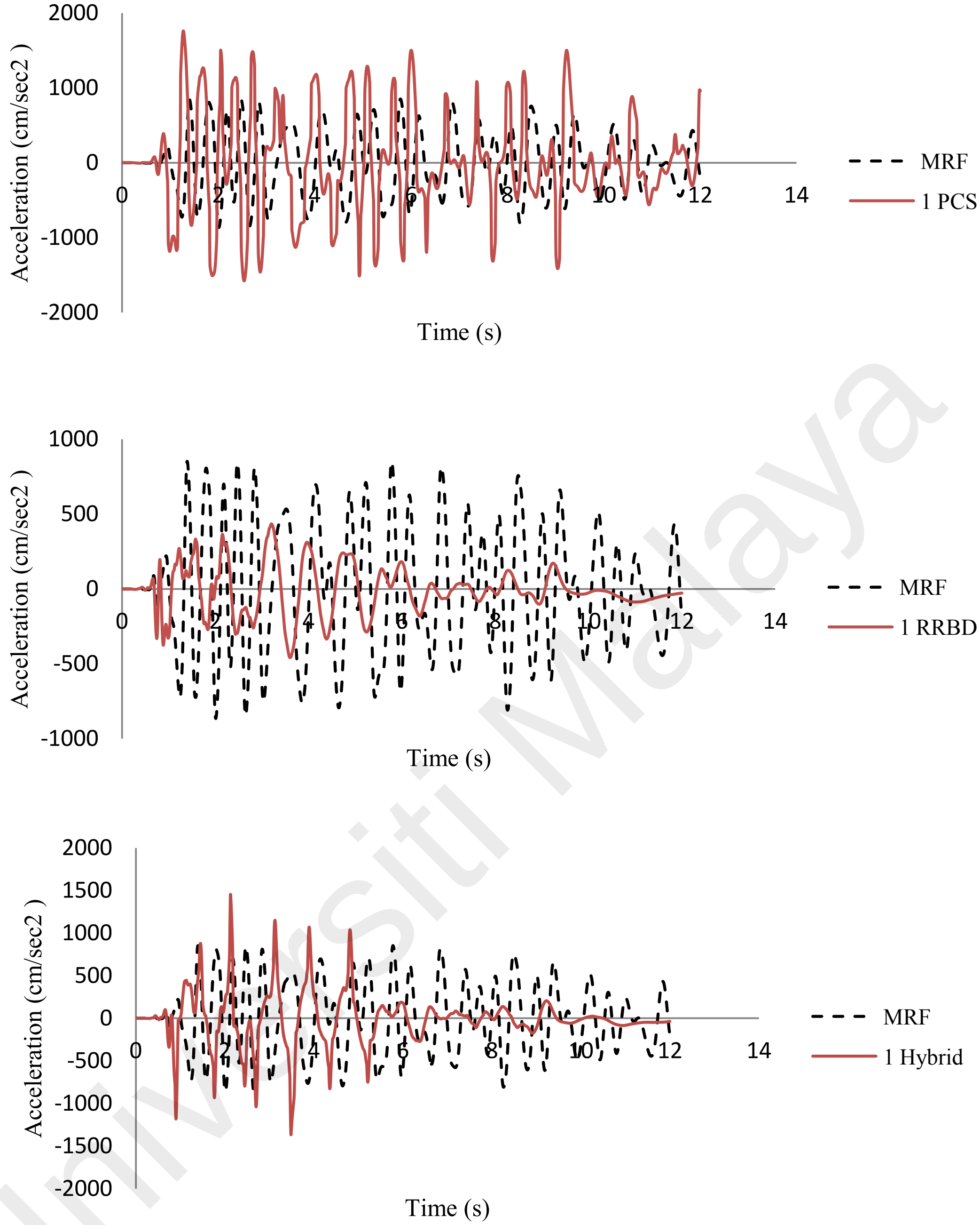

Figure 5. 28: Roof acceleration: Northridge

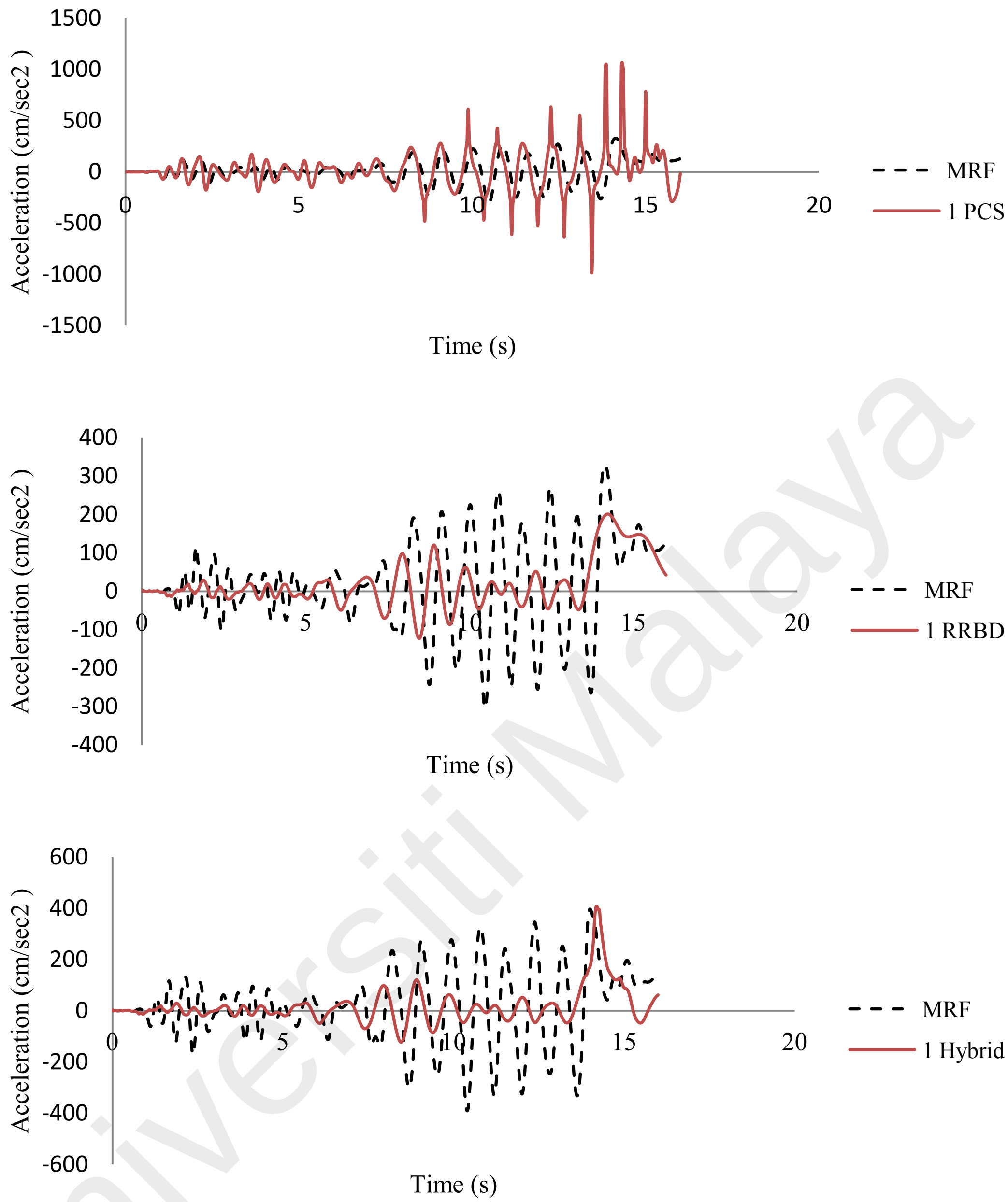

Figure 5. 29: Roof acceleration: Kobe

Residual displacements are depicted in Figure 5.30, which numerically and visually show where the structures are at the end of the seismic loading duration. The HPCS-equipped frame had the lowest residual drift problem or relatively small residual drift while the SMRF had a poor performance. These results underlined three major issues regarding application of the proposed hybrid system that contributed to the resultant low residual deformations; firstly, the damper's self-centering force which provides enough capacity for large elastic deformation and acts as a restoring force. Secondly, inherent elastic stiffness of the VE material by which a great amount of seismic force is absorbed. Thirdly, delay action of the PCS system that attenuates the dispersion of the deformations along the height of the frame through the re-centering mechanism.

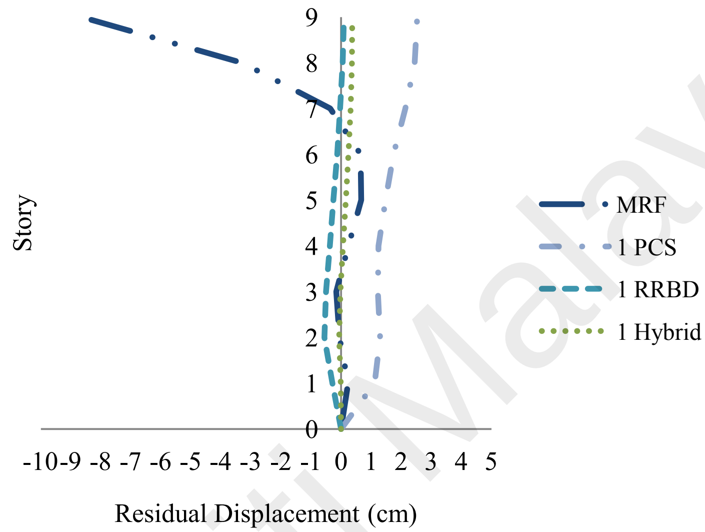

(a) El Centro

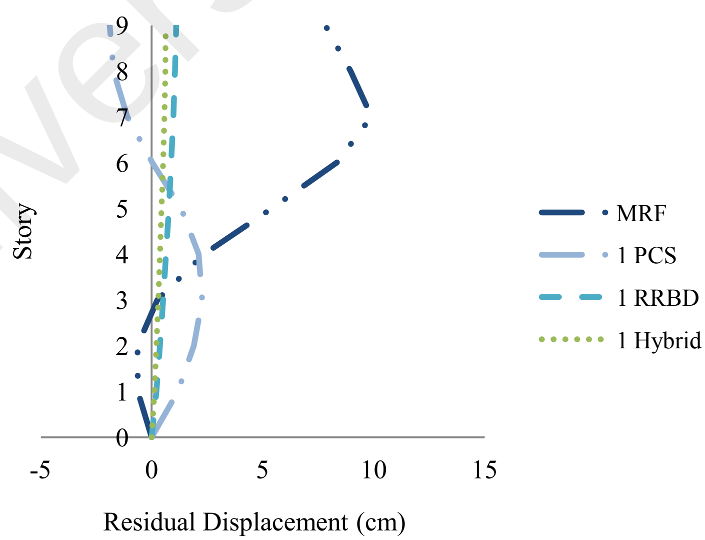

(b) Northridge

Figure 5. 30: Residual displacement

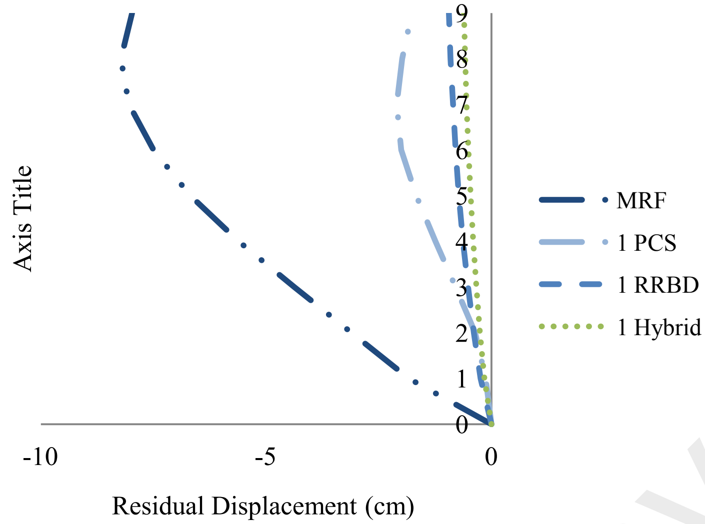

(c) Kobe

Figure 5. 30: Residual displacement (Cont.)

Results of shear highlighted the effects of the proposed systems. In HPCS frame, as depicted in Figure 5.31, due to parallel action of RRBD and cable bracing, i.e. when gap mechanism is engaged a stiffer system is created, there exists a large increase in base shear at early stage of load exertion compared to SMRF while this trend changed for the latter part and shear and number of cycles decreased. The base shear results at the early stage of loading indicated nearly identical fashion of behavior. Furthermore, The maximum base shear of the frame with PCS system is resemble the bare frame at the early portion in the earthquake due to the delay action of the cable bracing.

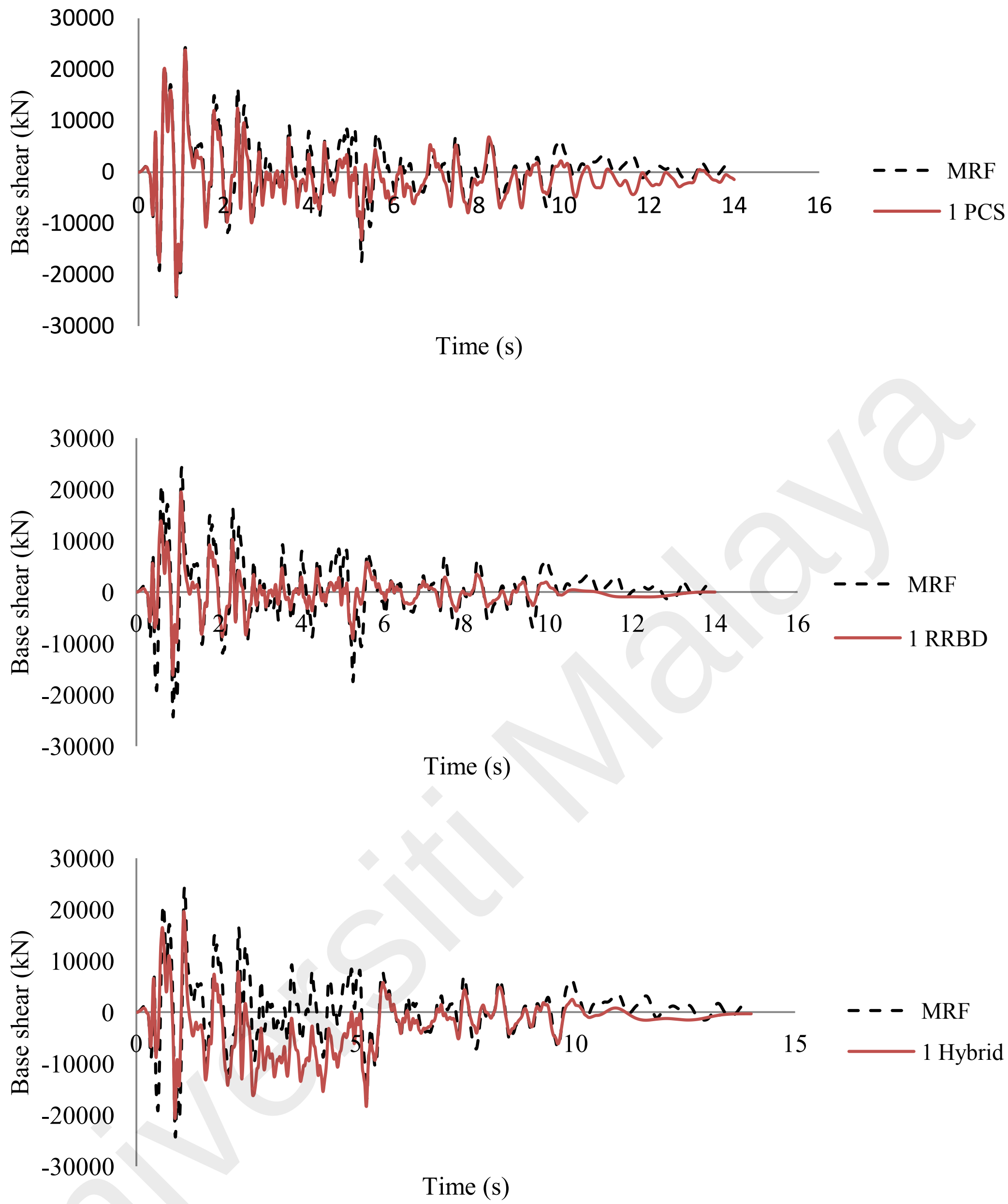

(a) El Centro

Figure 5. 31: Base Shear Response History

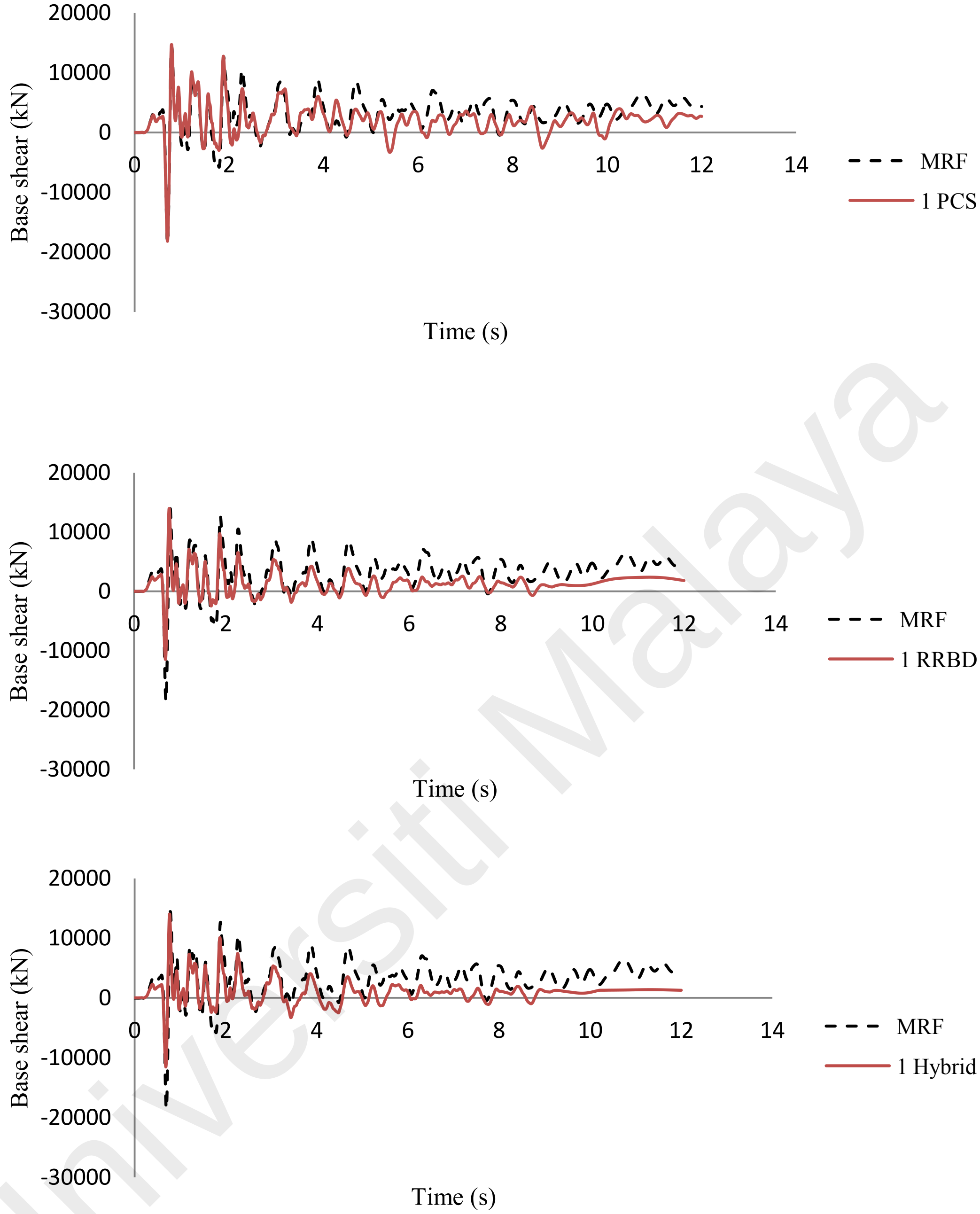

(b) Northridge

Figure 5. 31: Base Shear Response History (Cont.)

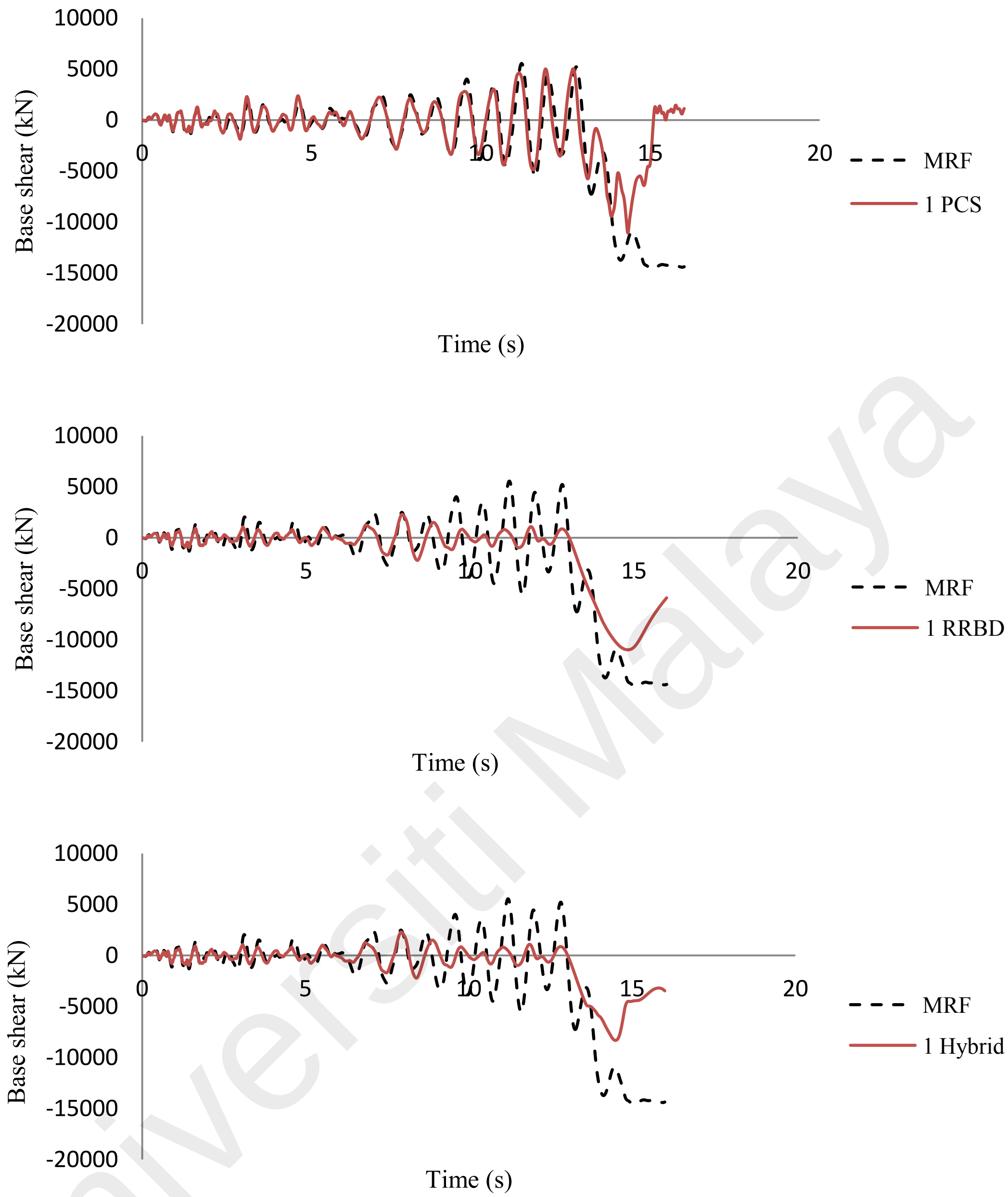

(c) Kobe

Figure 5. 31: Base Shear Response History (Cont.)

Results of the conducted nonlinear static pushover analysis are presented in Figure 5.32. The BF with typical linear elastic behavior up to the yield point showed a good amount of ductility with nearly 4% for roof drift. In addition, BF experienced the lowest initial stiffness which was found to be in contrast with that of the HPCS and RRBS-equipped frame. Application of the retrofitting systems apparently led to an increased strength level provided to the frames and consequently higher yielding moment values. Speaking of the phased mechanism of the proposed hybrid system, the yield of the cables cannot be specified since the additional stiffness of the VE rubber dampers is still present. In addition, the graphs show the initially lower stiffness which is increased as the cables engage. It has to be mentioned that analysis of the frames could continue up to formation of collapse mechanism beyond which the frame became unstable and therefore the analysis could not progress. This is why the respective plot did not show a descending branch.

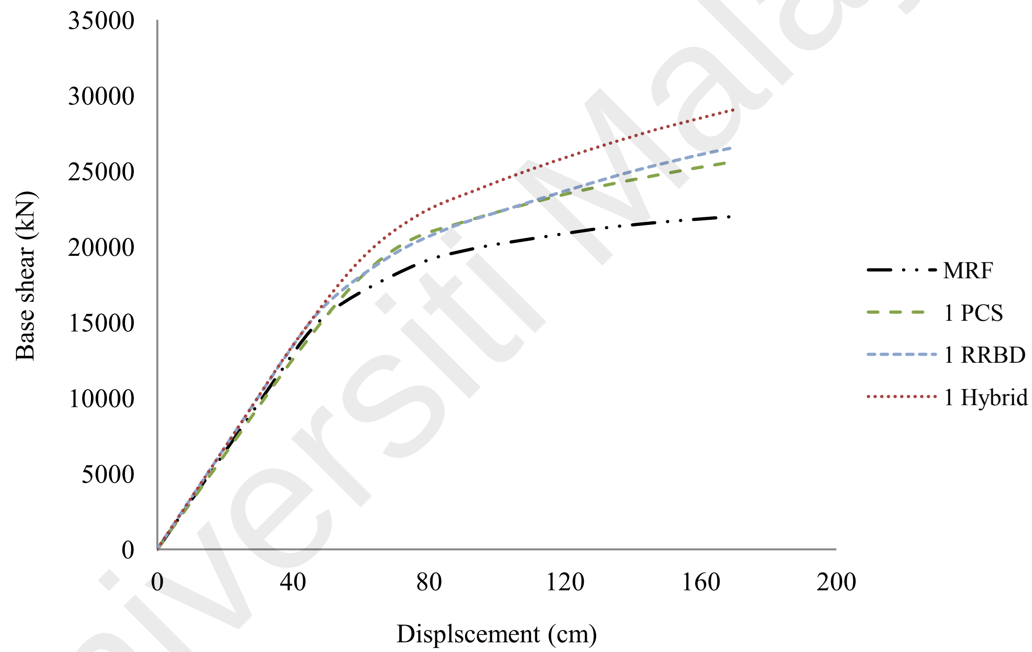

Figure 5. 32: Static Pushover Plot

5.13.2 Two retrofit systems per storey

This section interprets the results of the considered nine-storey steel moment frame equipped with different systems arrangement. Improvements of the structural performance of the frame retrofitted by one proposed system per storey were discussed and superiority of the HPCS over other retrofitting systems was highlighted. This section, however, focuses on another arrangement of the considered proposed systems to investigate the possibility of optimizing the devices effect on the response of the SMRF. This arrangement applied two systems at each storey and then frames were subjected to the aforementioned seismic excitations and response history results were then compared with the BF. Figures 5.33 through 5.40 depict the time history analysis results.

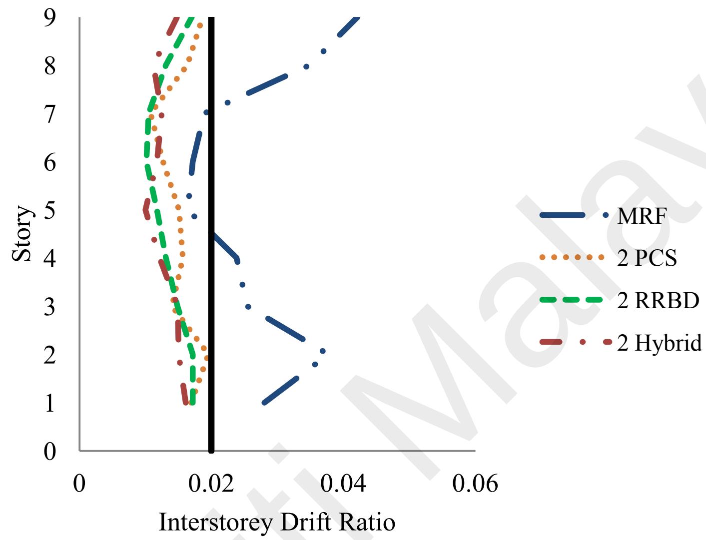

(a) El Centro

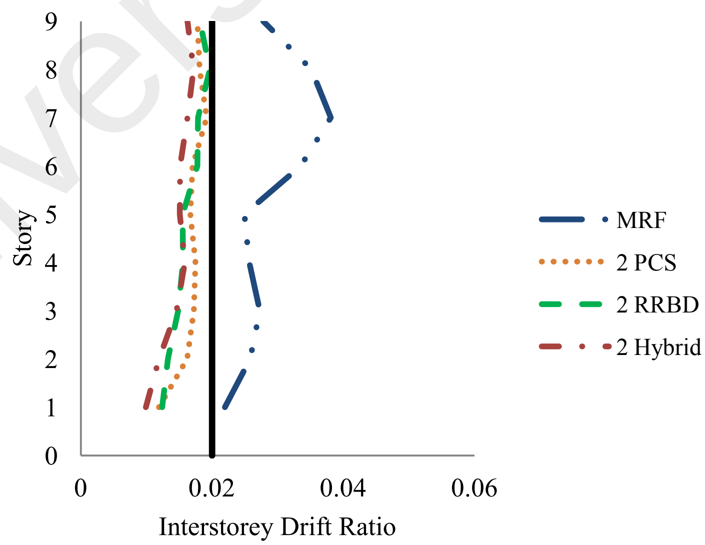

(b) Northridge

Figure 5. 33: Maximum Storey Drifts

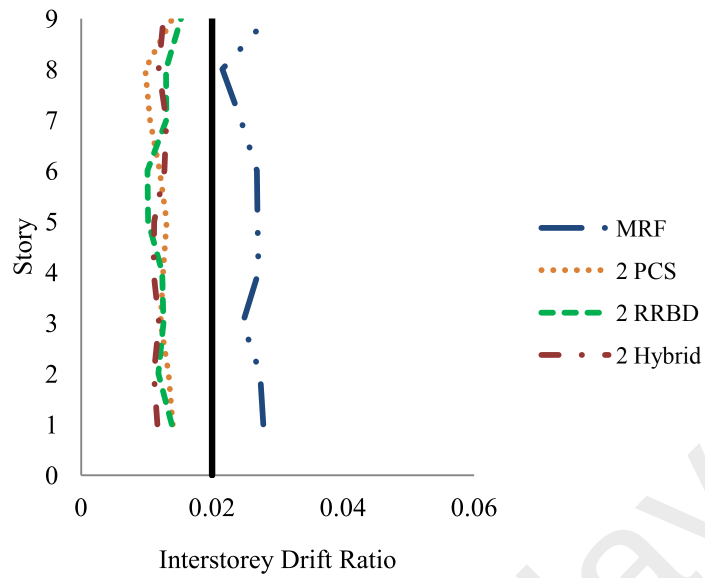

(c) Kobe

Figure 5. 33: Maximum Storey Drifts (Cont.)

Results showed that the base-line BF case experienced the greatest drift values at roof level while it was outperformed by other frames especially frame with HPCS which possessed the first place for maximum drift reduction. Values of roof drift for all cases were found below the maximum values of the codes. Observations of the storey drift trace along the height of frames concluded almost similar trends where frame with RRBD experienced moderately higher values yet well below the maximum allowable value given in the codes.

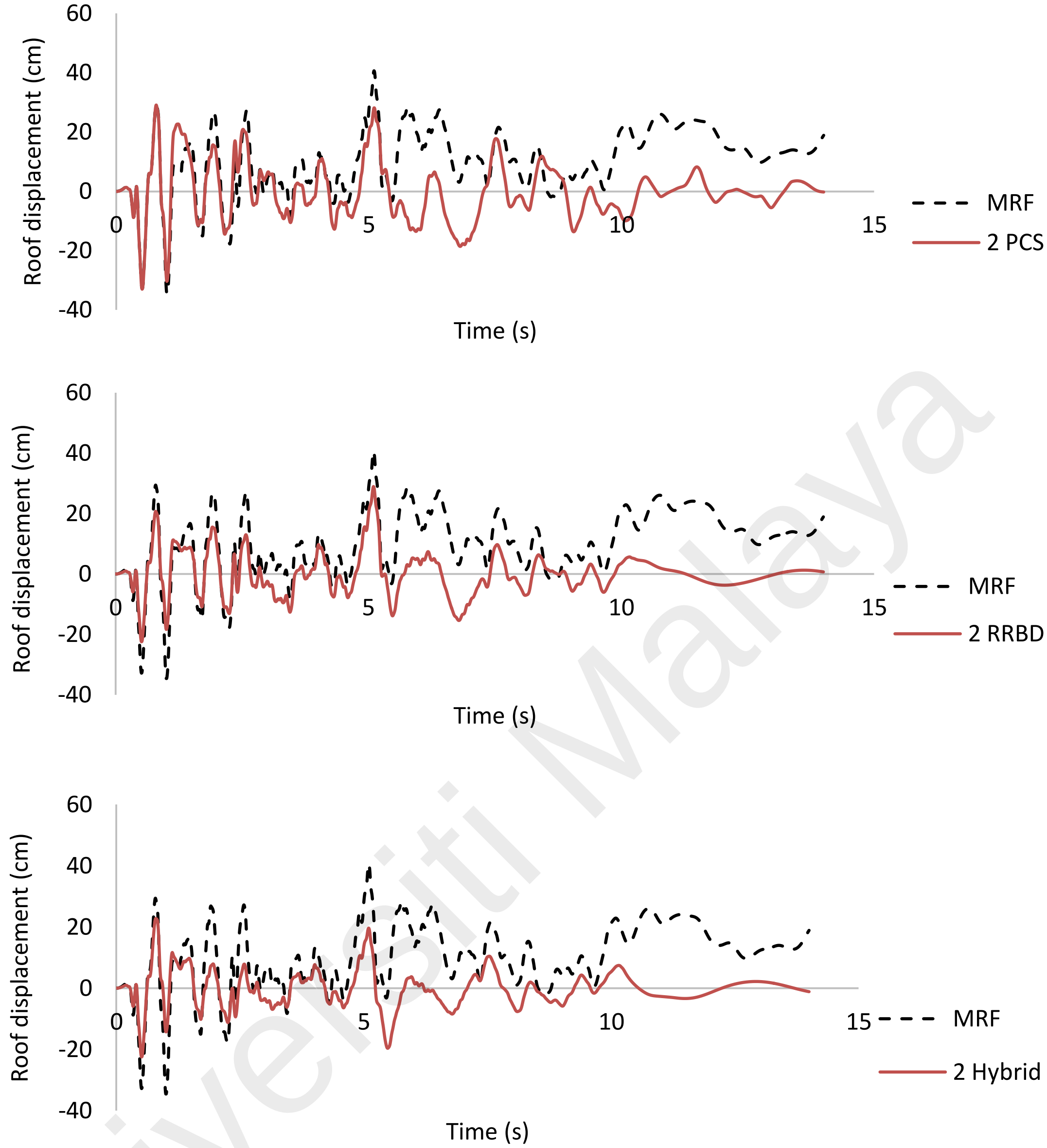

(a) El Centro

Figure 5. 34: Roof displacement

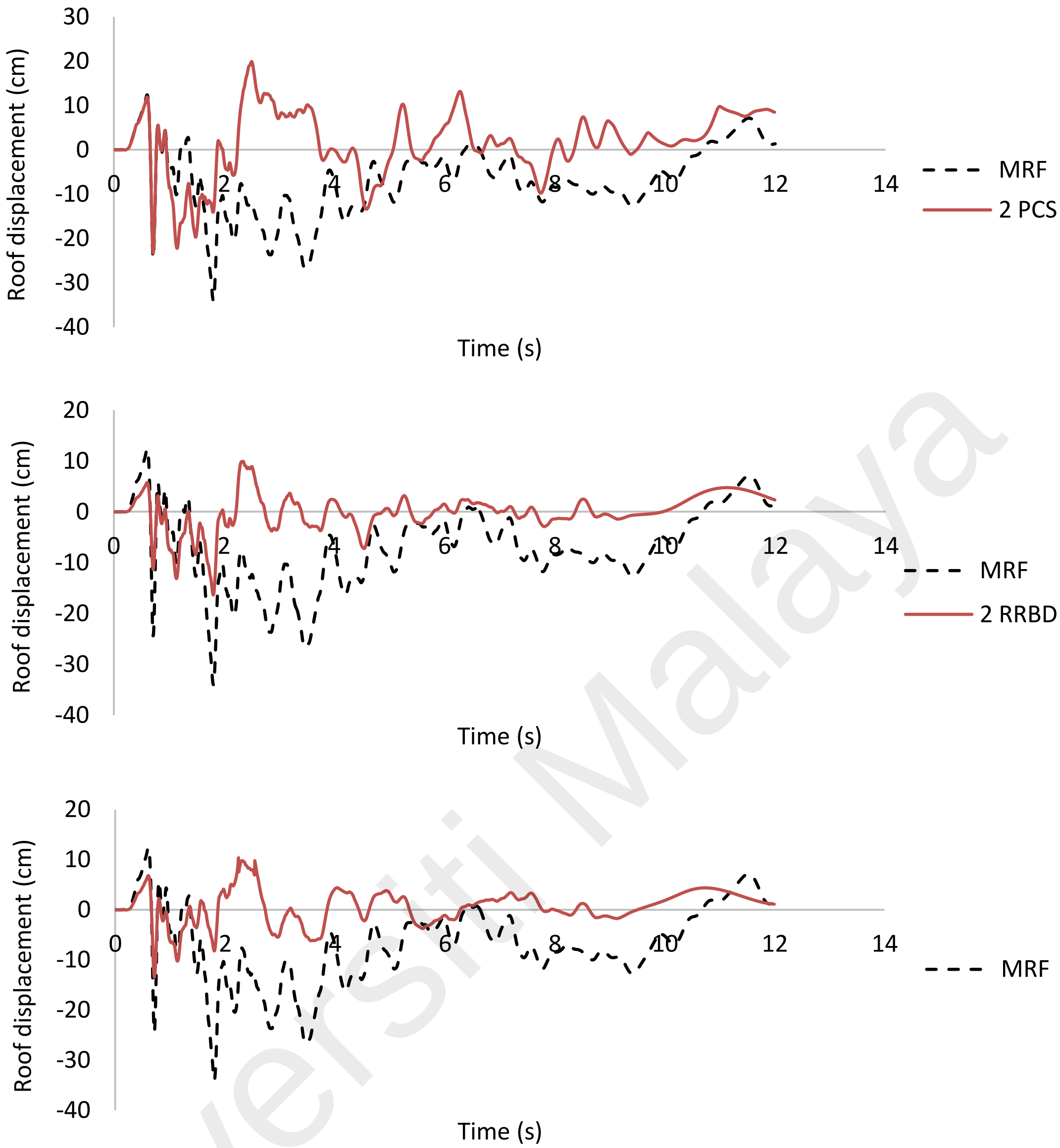

(b) Northridge

Figure 5. 34: Roof displacement (Cont.)

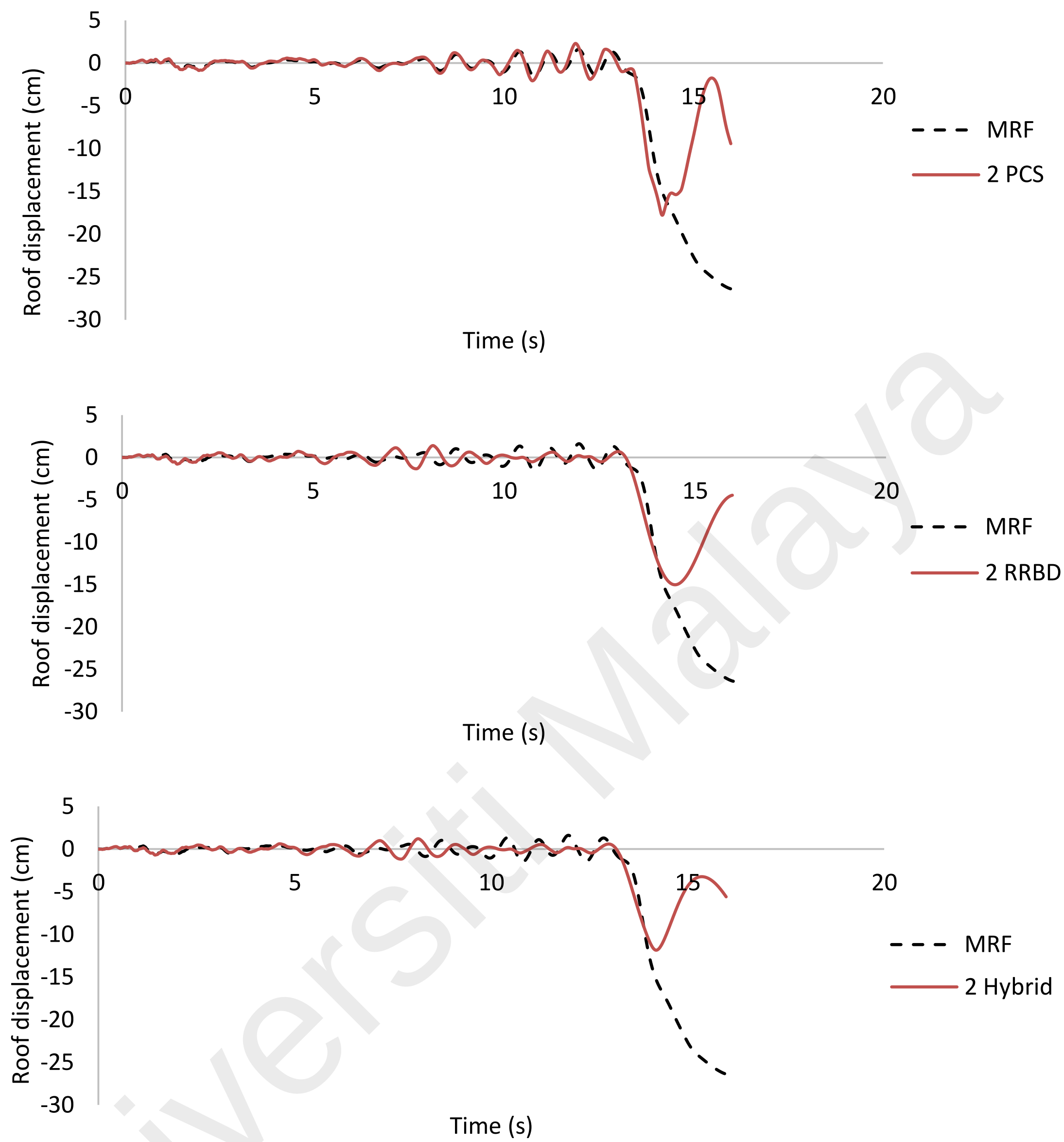

(c) Kobe

Figure 5. 34: Roof displacement (Cont.)

Frame with PCS system results are grouped with the other systems in maximum roof displacement and were found to be the worst case for roof acceleration while RRBD system resulted in well performance of the frame for roof acceleration response. Generally speaking, the proposed hybrid system led to an improved seismic behavior of the frame in terms of roof drift, displacement and distributed drift reduction owing to the hyperelastic behavior of the rubber material that has higher stiffness at higher displacement.

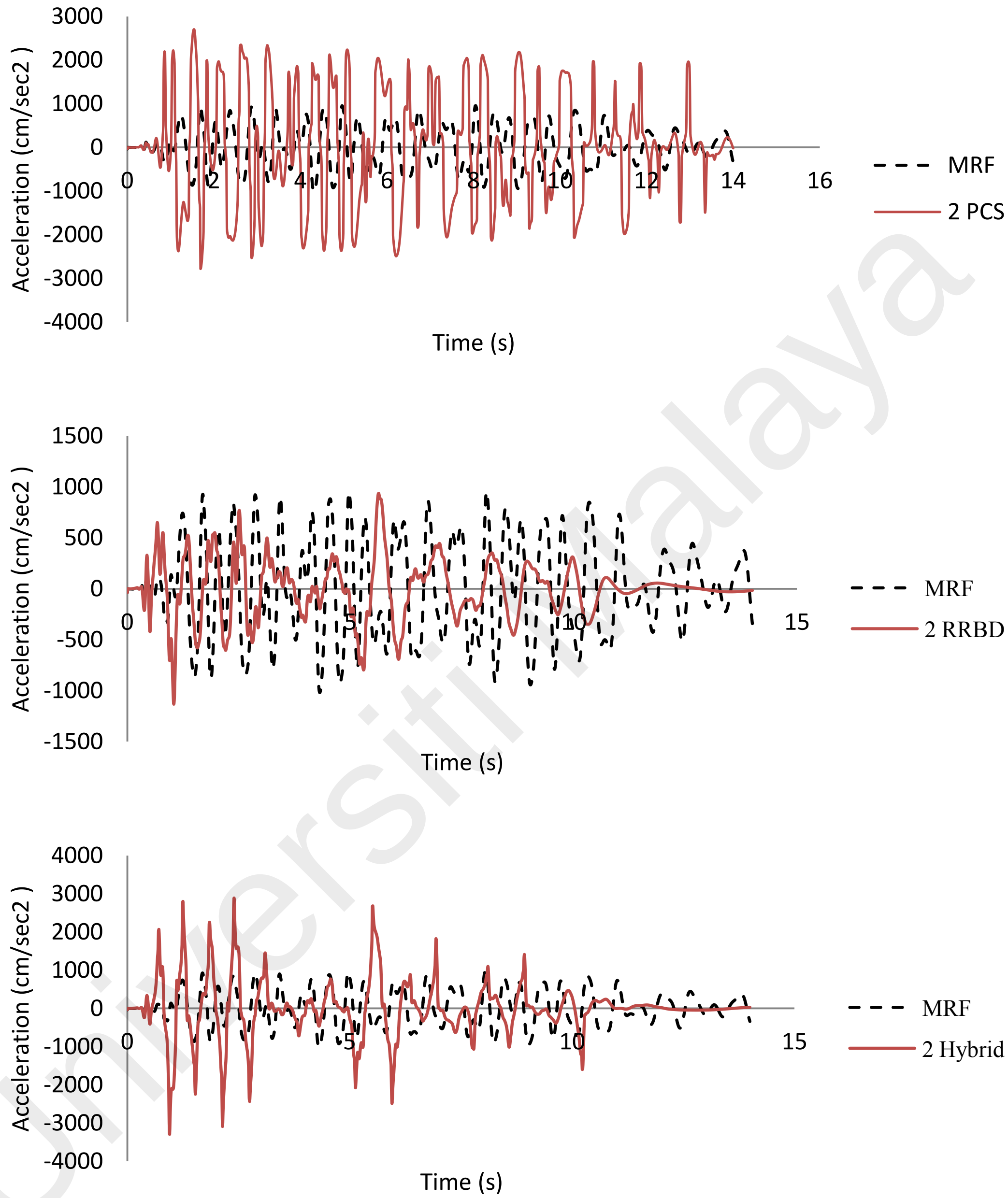

Figure 5. 35: Roof acceleration: El Centro

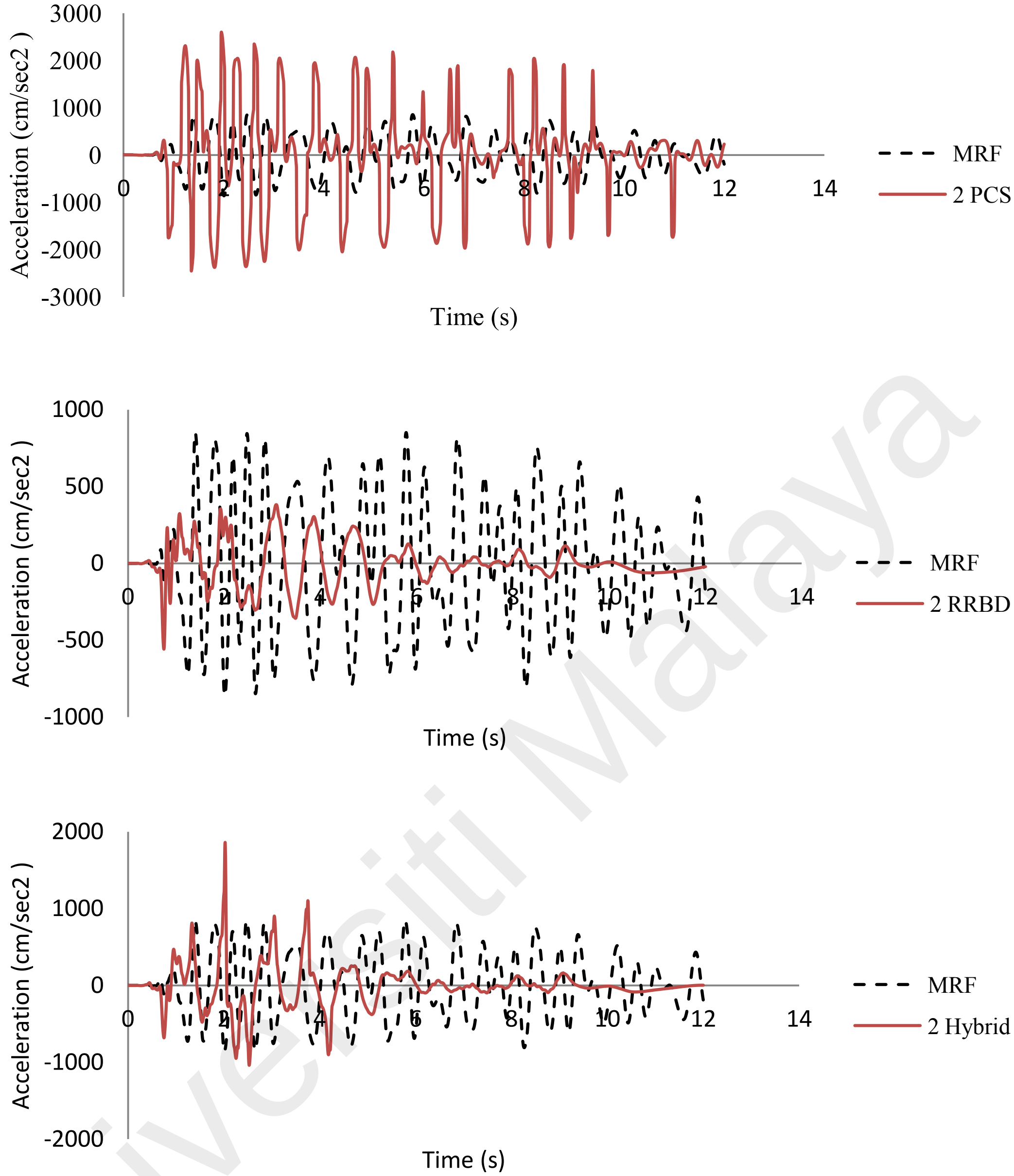

Figure 5. 36: Roof acceleration: Northridge

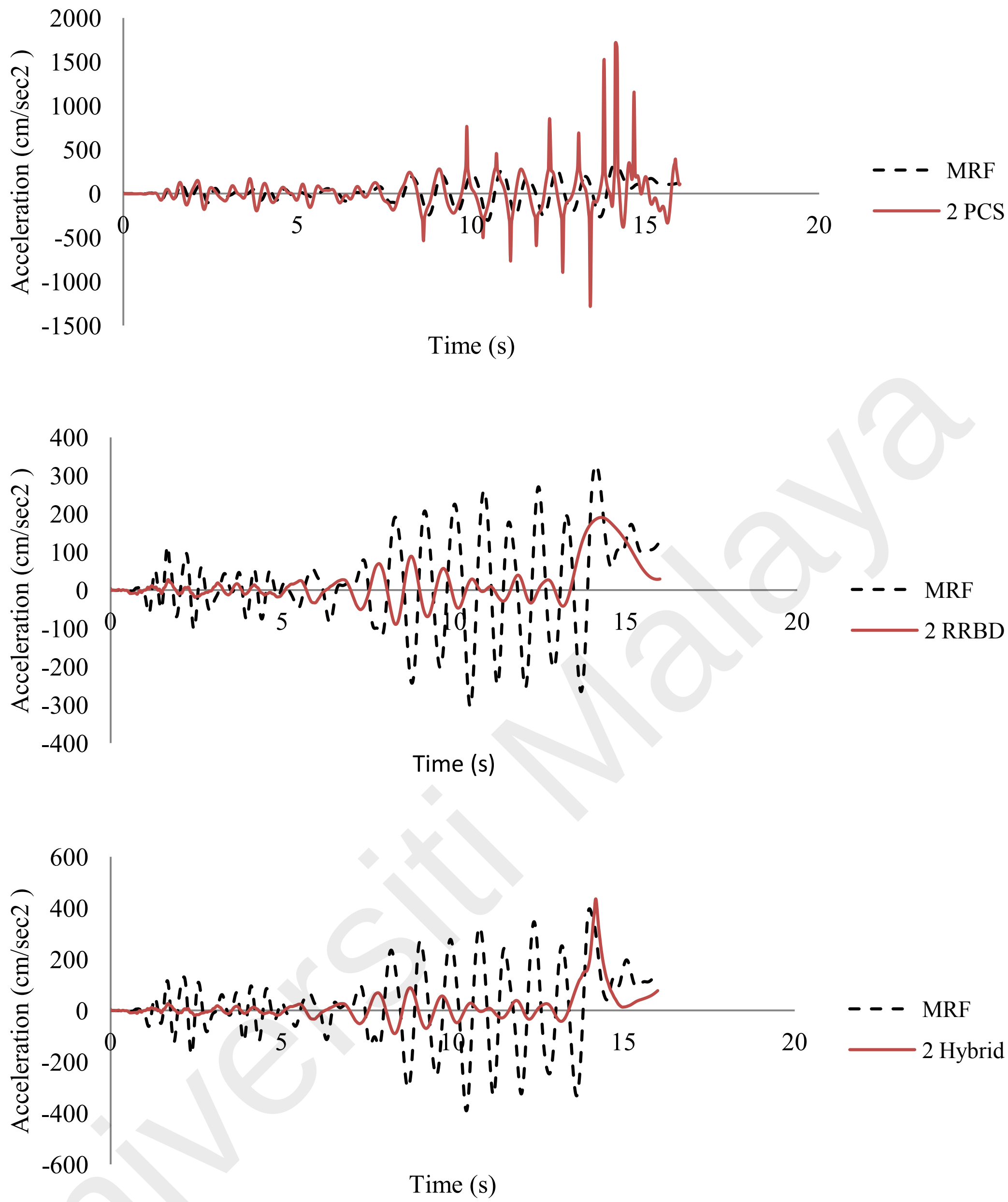

Figure 5. 37: Roof acceleration: Kobe

Residual displacements are depicted in Figure 5.38. Significant residual drift were observed along the height of the BF while HPCS led to very well performance of the frame with little residual deformations which was found similar to the case of one device per storey. The RRBD- and PCS-retrofitted frames had larger residual drifts compared to the frame with the HPCS. PCS frame experienced large residual displacement especially when subjected to Northridge ground motion. Plots of residual displacements associated with the three ground motions for RRBD and HPCS cases were found similar although those caused by El Centro record were greater. The common point noted among the resultant residual deformations was that lower portions of the frames experienced the majority of the residual deformations and that is in agreement with larger drift ratios at lower levels. At 3rd or 4th floors occurrence of crossover was observed.

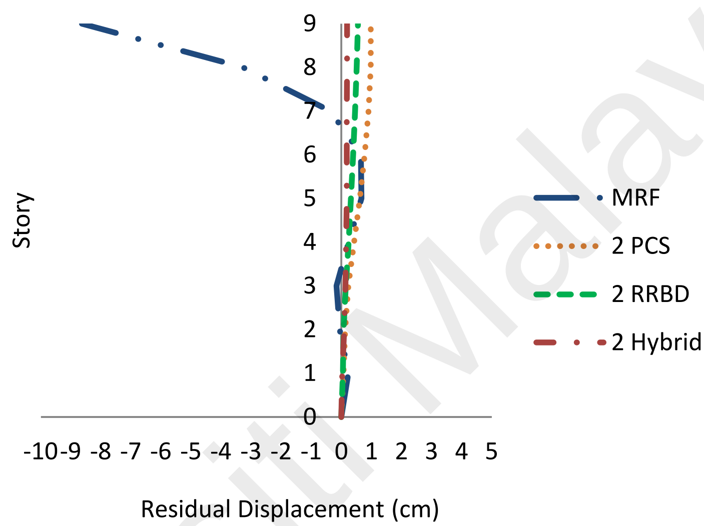

(a) El Centro

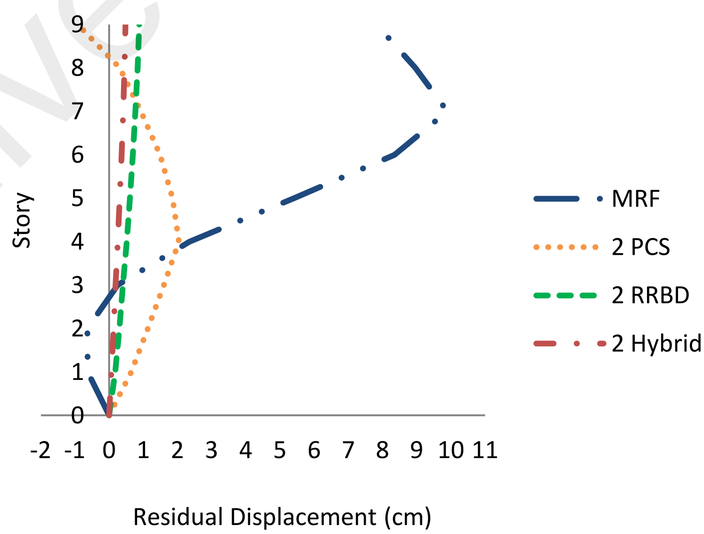

(b) Northridge

Figure 5. 38: Residual displacement

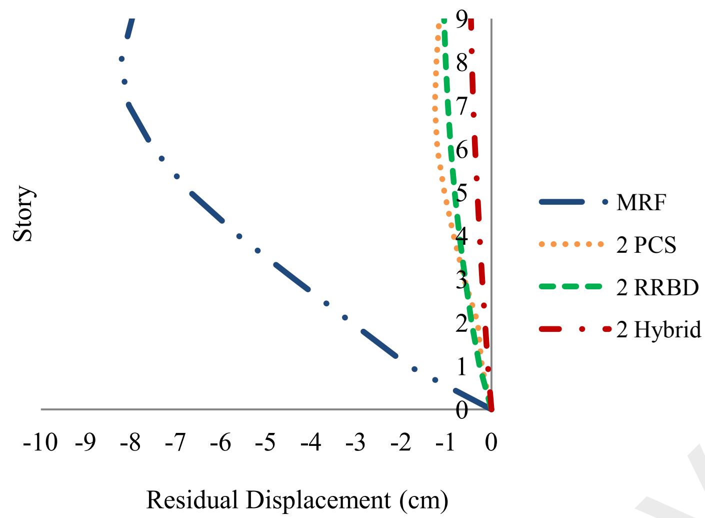

(c) Kobe

Figure 5. 38: Residual displacement (Cont.)

Figure 5.39 depicts the results of the nonlinear static analysis. Interpretation of the obtained curves showed that BF yielded at the end of a linear curve with maximum yielding point (base shear) around 15200 kN which is more than the structural strength. This clarifies the yielding during the dynamic analysis. This value rose up to 17000 kN for RRBD-equipped frame which was revealed to be less than that of the PCS-equipped frame. Case of HPCS-retrofitted structure, however, revealed even higher yielding point upon reaching damper lockout which can provide larger stiffness up until the cables are completely straightened. For the HPCS model, since the dampers were not locked out, they were able to keep withstanding greater load. By additional stiffness provided to the structure through the hybrid system, the structural yielding force can rise up to nearly two times of the BF strength. Meanwhile, the respective plot depicts the phasing mechanism of the hybrid device during the analysis.

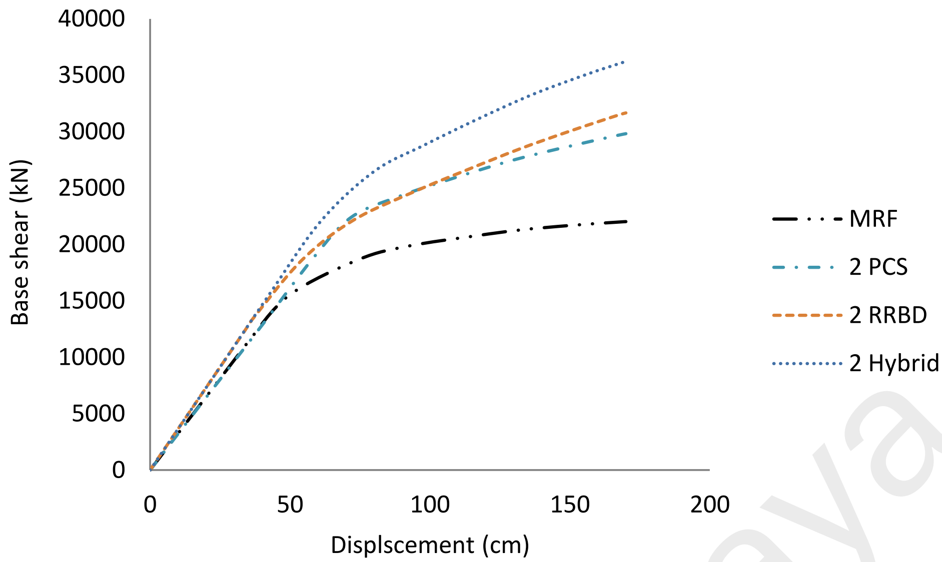

Figure 5. 39: Static Pushover Plot

Histories of base shear response of the BF, RRBD- and PCS- and HPCS-equipped frames are plotted in Figure 5.40. Accordingly, results obtained from HPCS and RRBD showed similar base shear during the initial pulse of the seismic force. The RRBD-retrofitted frame clearly provided damping against the loads and frame with HPCS demonstrated a high ability to stand against high lateral displacement. Further benefit of the HPCS was revealed to be not just in reduction of magnitude of cycles but also in attenuation of number of cycles. This influence was more pronounced for the Northridge ground motion.

Owning to the action mechanism of HPCS, higher stiffness can be provided to the system since the rubber damper of the HPCS does not lockout. This also reflects in base shear magnitude and shortened period. As long as displacement is less than the gap level and cables are not engaged, resultant variation of base shear of HPCS-retrofitted frame is nearly identical with that of RRBD-equipped frame.

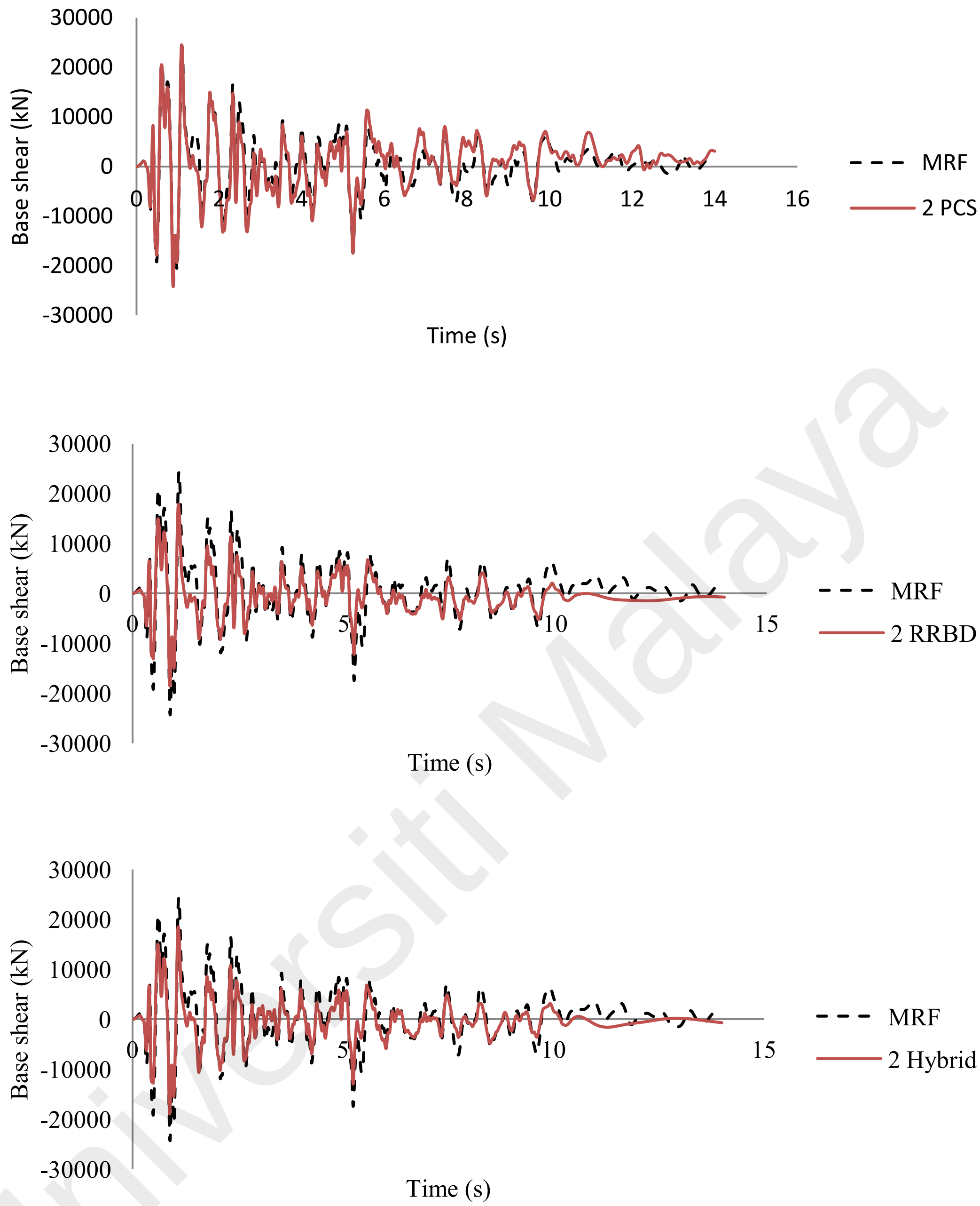

(a) El Centro

Figure 5. 40: Base Shear Response History

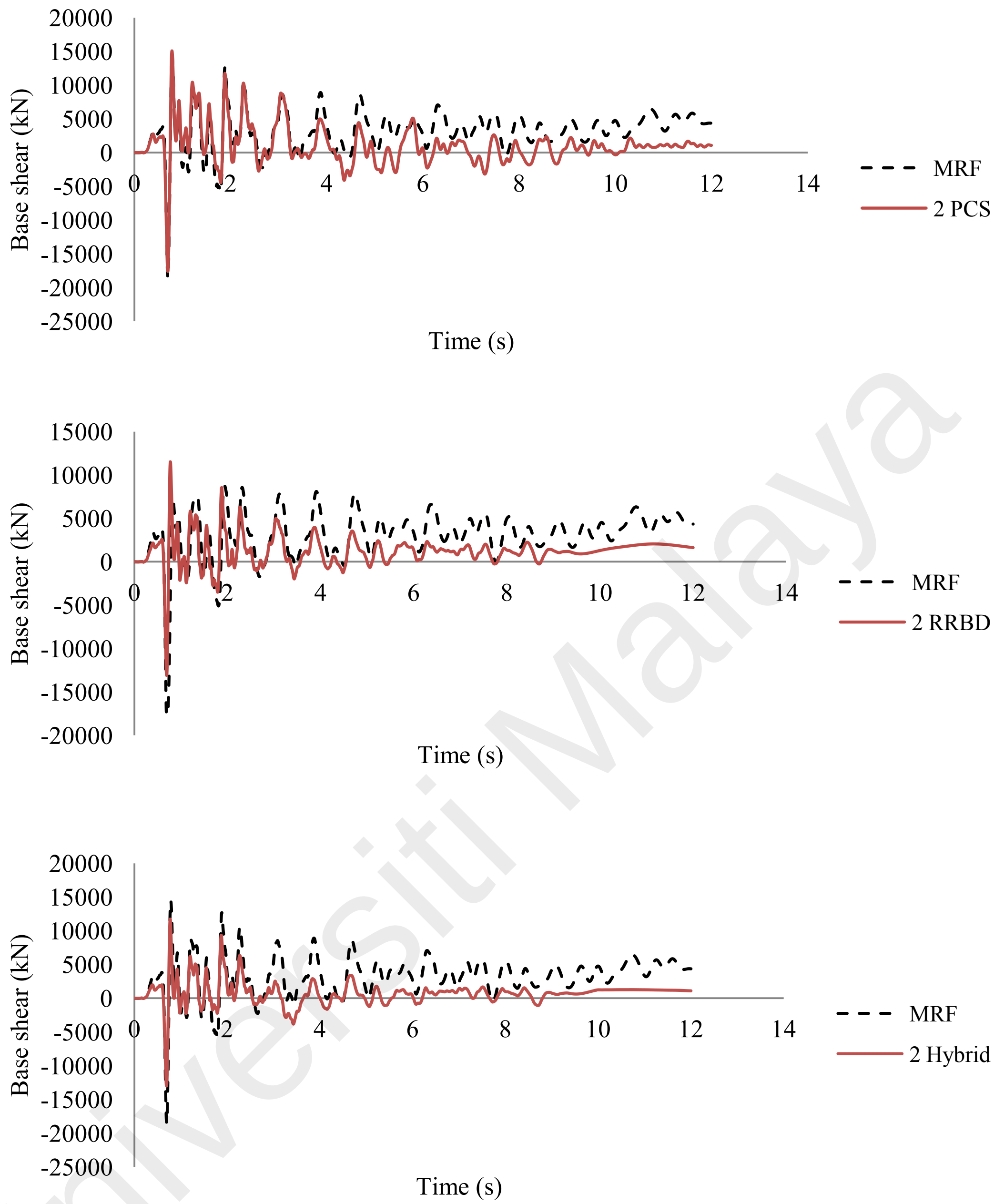

(b) Northridge

Figure 5. 40: Base Shear Response History (Cont.)

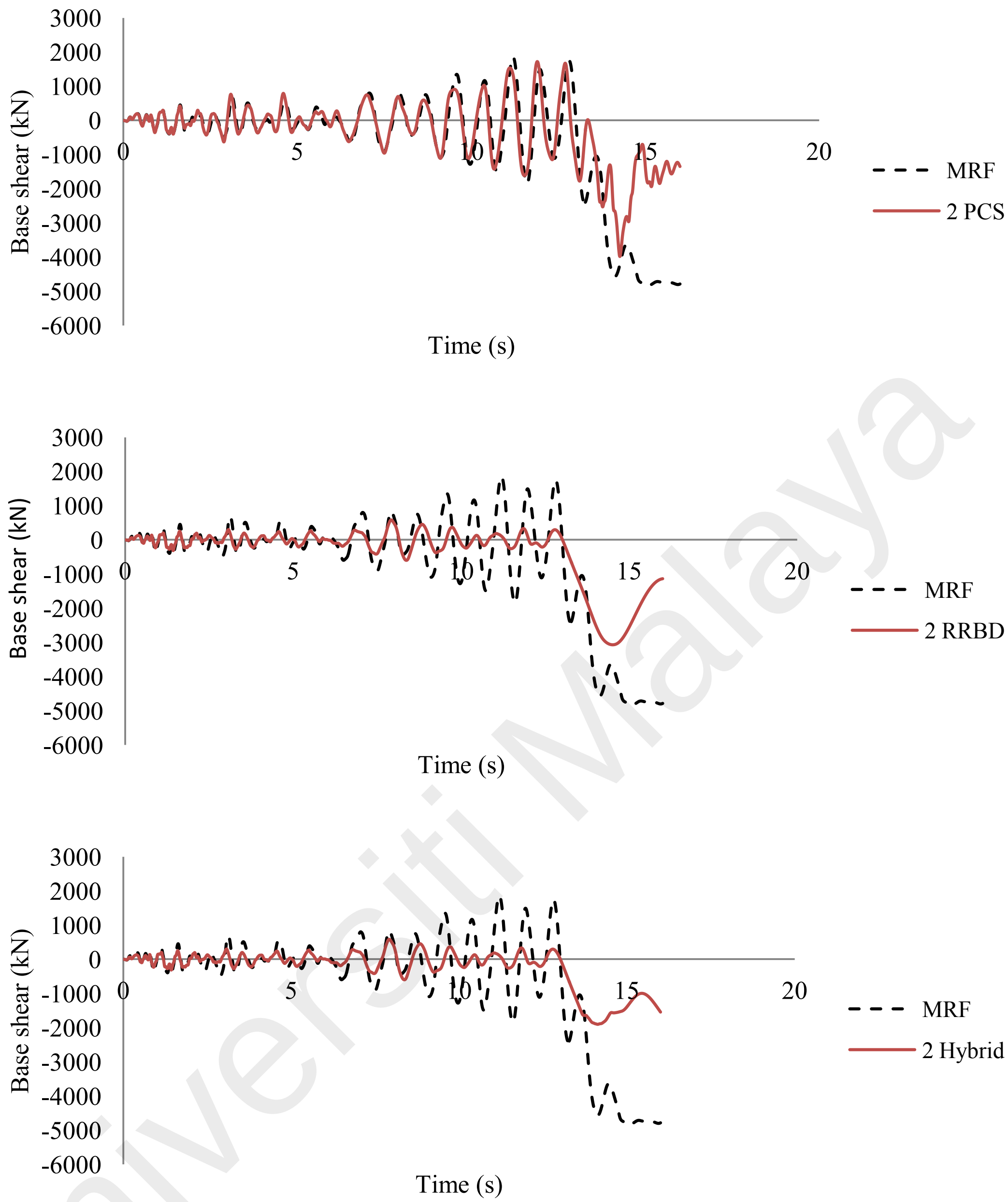

(c) Kobe

Figure 5. 40: Base Shear Response History (Cont.)

Considering two different arrangements of the proposed systems showed that seismic performance of multi-storey structure can be optimized through a carefully selected arrangement. This thesis discussed only two arrangements and available options are not limited, nevertheless one of governing factors in this regard is the economical cost. Since elements of the proposed systems are made of readily available materials, thus cost of optimum number of devices to be attached is not expected to be high.

5. 14 Concluding Remark

A comprehensive analytical study was presented in this chapter and three different passive systems PCS, RRBD and HPCS were subjected to FEA through modeling single and multi-storey frames. Analyses contained both dynamic time-history and push-over analyses. Results led to comprehensive discussion about performance of considered frames and parametric study revealed superiority of the proposed HPCS over other systems when subjected to the ground motions.

The passive RRBD with controllable factors showed its ability for dissipating energy through many design parameters which can optimize its performance.

Conducted analyses showed that attachment of RRBD damping device in the single-storey single-bay and the nine-storey five-bay structures led to considerable attenuation of structural response when subjected to real records of El Centro, Kobe and Northridge earthquakes. Moreover, an experimental test was conducted on the VEM and resultant graphs highlighted a fine energy dissipation capacity obtained through smooth and plump ellipses of the hysteresis curves which continued to incline more when excitation rate was increased under fixed displacement amplitude. This indicates positive correlation of VEM stiffness with excitation rate.

Application of RRBD in the frames disclosed addition of stiffness and damping to the structure which resulted in significant reduction of structural displacement. This proposed damper has other advantages such as being inexpensive, easy to build and easy to install.

Efficiency of the PCS cable bracing system was also discussed and enhancement of structural response in terms of attenuation of structural movement and inter-storey drift were observed upon attaching this system to the frame. One installation-related benefit of the PCS is that interference to structural and non-structural elements is limited. In addition, ease of installation minimizes the construction time. Owing to the action mechanism of PCS and its direct relation to frame's lateral displacement, this system does not provide a constant stiffness. Other two advantages of PCS are first, contribution of both cables to the lateral structural stiffness and second, removal of the impulse caused by cable loosening. These advantages originate from pre-compressed status of the spring. The energy dissipation capacity observed from PCS was significant, owing to the delay of the brace action. The nonlinear time-history analysis showed enhanced structural performance through degradation of inter-storey drift along with lowering down possibility of soft storey formation. This outcome is in debt of stable hysteretic performance with greater stiffness created at both original and deflected position of frame. Increasing ductility and elimination of the risk of brittle failure in the brace elements are other benefits of PCS system.

The respective concept of the hybrid passive control system (HPCS) was first analytically studied and then it was applied to a 9-storey frame structure to investigate pros and cons when attached to the frame. Performance of the HPCS along with the structure was rated according to condition of the structure after the ground motion was exerted by monitoring maximum storey drifts and accelerations, residual displacements and applied seismic ground motions. One of the challenges in application of retrofitting systems is that sensitive equipment and non-structural components are considerably vulnerable in confronting large externally exerted accelerations. Although the best solution is reduction of all seismic-performance aspects and quantities of structures, nevertheless this may not be feasible at low cost.

Time history analysis executed for the 9-storey moment frames revealed several advantages of the proposed HPCS;

- Compared to the BF with SMRF system, almost all the performance measurements and quantities were reduced.
- Considerable degradation in magnitude and number of base shear cycles were observed associated with the late part of the applied seismic record; bearing in mind that there is a high risk of severe structural damages at late part of earthquake particularly those associated with aftershocks.
- Improvement of structural seismic behaviour in terms of induced maximum storey drift and residual drift when compared to PCS- and RRBD-retrofitted frames; comparisons showed that PCS plays its role mostly in prevention of extra lateral displacement against high acceleration amplitudes by providing larger stiffness while RRBD was found to have energy dissipation potential at all levels of vibration. The HPCS, however, was found superior to the other two lateral resisting systems.
- Improved structural behavior with HPCS in degradation of accelerations can considerably enhance safety of the occupants and lower down the probability of damaging of sensitive equipments placed inside the building in case of large accelerations.
- Action mechanism of HPCS took advantage of an inherent tendency to re-centre right after loading was finished.

CHAPTER 6: CONCLUSIONS

6.1 Introduction

This thesis presented an innovative multi-stage strategy for seismic retrofitting which is primarily for steel structures. The proposed hybrid passive-control damping system with two-phase mechanism is proved to have response characteristics under seismic load and benefits from reduced installation effort and minimal social environmental impact. The first phase can provide damping for all levels of vibration while functionality of the second phase provides an increase in stiffness to prevent large storey displacement. Development of the proposed system included verification analysis, design of prototype, development of design procedure and test to prove the concept which consists of the combination of the two proposed systems: Rotary Rubber Brace Damper (RRBD) and pre-compressed spring (PCS) cable bracing.

6.2 Conclusions

This study comes up with conclusions which are presented in the following subsections. The first subsection discusses the testing, analysis and application of high damping rubber (HDR) and performance and experimental testing of RRBD against dynamic loads. The second subsection talks about the performance and experimental testing of PCS cable bracing system. The last subsection presents conclusions generated by the proposed hybrid system response.

6.2.1 Rotary Rubber Brace Damper

The RRBD takes advantage of hyperelastic and viscoelastic (VE) properties of rubber and readily accessible materials. This energy dissipating device was studied experimentally under varied dynamic loads and the generated force-deformation relations showed that this damper can perform efficiently in displacement and acceleration reduction against various levels of excitation. In addition, at higher levels of deformation the hyperelastic behavior of RRBD was even more pronounced. Performance of RRBD under cyclic excitation revealed that increment of excitation rates results in increment of inclination angle of the hysteresis loops while displacement amplitude is fixed. This shows the positive correlation of VEM stiffness and excitation rate. On the other hand, increment of displacement amplitude caused reduction of angle and subsequently larger hysteresis loops were appeared. Increase in the area of the hysteresis curves highlights the energy dissipation capacity of the device.

Effectiveness of this energy dissipating device was shown through comparing the seismic performance of the retrofitted frame with that of bare frame. This comparison highlighted significant reduction of the displacement, acceleration and structural response due to higher stiffness and damping provided by the device.

6.2.2 Pre-compressed spring cable bracing system

The PCS bracing system takes advantage of the pre-compressed force of the spring to provide an impulse-free mechanism, i.e. no cable loosening exists, and also simultaneous utilization of cables so that both cables can contribute to the lateral stiffness of the structure by recompressing the spring when frame comes back to its original place during seismic oscillation. This mechanism provides further stiffness for structural performance.

Analyses revealed large energy dissipation capacity of the proposed PCS bracing system. Mechanism followed a delayed brace action which caused greater structural ductility in addition to significant influence of the PCS system on the energy-displacement relationship of the frame especially when frame was at its original position. Moreover, the stable hysteretic performance of the PCS bracing system in the nonlinear cyclic analysis provided greater magnitude of stiffness in initial and deflected position of the frame and therefore attenuated both the inter-storey drift and the possibility of soft storey formation.

6.2.3 Hybrid passive control System

In order to enhance the strengths of a structural system and offsets the weaknesses, the proposed HPCS uses a two-phase technique that benefits from a VE solid damper made of synthetic rubber material in the first phase of its mechanism and a PCS cable bracing system in the second phase of the mechanism. The first phase is desirably assigned to withstand against all levels of deformation like wind events and minor earthquakes specifically targeting at elimination of probable structural repair. The second stage is designed to dissipate significant energy by applying delayed-action brace so that the VED can efficiently dissipate the seismic energy and simultaneously raise the lateral stiffness of the moment frame. This phase is in charge of preventing instability by reducing displacements and it is only engaged against major earthquakes. The function mechanism of the second phase is such that the permanent damage imposed by major seismic load is transferred and focused into cable elements so that it can be replaced while the core structure is immune from the damage. A nine-storey steel model structure was chosen to be retrofitted by the proposed HPCS to evaluate its effectiveness.

Results of the cyclic test showed a multi-phased behavior with significant energy dissipation capacity against significant seismic events in addition to relatively constant performance of the damper with relatively unchanged loss factor and dynamic stiffness over the typically applicable range of frequencies and deformation levels. Moreover, storey drift was very well controlled within the specified range associated with severe seismic motions. Performance of the hybrid system takes advantage of re-centering effect on the vibration center and has deformation dispersion effect along the height.

6.3 Future work

The future study of the proposed seismic retrofitting strategy involving the RRBD and PCS systems will have direct links to the concepts developed in this dissertation. The associated improvement requires evolution and validation of ideas to become a practical option in structural design and construction. Further improvements of the RRBD-PCS system might be associated with the following ideas:

- Since variety of rubber compounds exist with different high-damping characteristics and mechanical properties like modulus of elasticity, tensile strength, and elongation at break, they have to be compared so that the one with proper energy dissipation can be selected. Such selection is normally conducted via uniaxial, biaxial tension-compression and relaxation shear tests. Cost of the rubber compound is another aspect to be considered.
- Effectiveness of a proper rubber material with a high damping mechanism requires a comprehensive and comparative study that includes variables such as type of structural system, structure height and dynamic loading. Such comparison is better to involve other types of energy dissipating dampers like viscous, friction and hysteretic steel dampers.
- Application and effectiveness of hybrid damping systems have to be further subjected to detailed and rigorous analytical study starting from a single degree of freedom system so that influence of variables on performance of the damping system will be easier to be evaluated. This analytical study should contain both PCS size (gap size), amount of damping and economic feasibility of the system.

- Various hybrid damping systems consisting of PCS cable bracing, friction, metallic and viscous dampers can be developed and different stages of PCS engagement can be analyzed.
- The proposed retrofitting methods can be promoted with cost-benefit analysis. Such analysis should include installation cost, required installation time and amount of saved materials. Furthermore, it has to be highlighted that application of a selected hybrid system leads to limited usage of heavy construction equipment and consequently reduction of initial investment.
- Distribution and placement of HPCS, i.e. vertical distribution and effective number of HPCSs, building typologies including building heights, number of bays, and span lengths should be subjected to further investigation. Moreover, various intensity levels of ground motions are suggested to be considered to monitor the performance of the proposed systems.

REFERENCES

Abaqus, F. E. A. (2017). Abaqus Inc. Providence, Rhode Island, United States.

Ahn, S. K., Min, K. W., Park, J. H., Lee, S. H., Lee, D. G., Oh, J. K., ... & Lee, S. K. (2008). Practical issues and solutions on installation of viscoelastic dampers in a 46-story reinforced concrete building structure. *The Structural Design of Tall and Special Buildings*, *17*(1), 231-243.

Aiken, I. D. and Kelly, J. M., (1990). "Earthquake Simulator Testing and Analytical Studies of Two Energy-Absorbing Systems for Multistorey Structures," Report No.UCB/EERC-90/03, Earthquake Engineering Research Center, University of California at Berkeley, Berkeley, CA.

Aiken, I. D., Nims, D. K., Whittaker, A. S., & Kelly, J. M. (1993). Testing of Passive Energy Dissipation Systems. *Earthquake Spectra, 9*(3), 335-370. doi:10.1193/1.1585720

American Society of Civil Engineers. (2013). Minimum Design Loads for Buildings and Other Structures (ASCE/SEI 7-10). American Society of Civil Engineers.

ANSI, A. (2005). AISC 341-05: Seismic provisions for structural steel buildings. American Institute of Steel Construction Inc, American Institute of Steel Construction, Chicago, IL.

ASCE. (1997). Structural applications of steel cables for buildings. ASCE Standard 19–96, 4.

Banisheikholeslami, A., Behnamfar, F., & Ghandil, M. (2016). A beam-to-column connection with visco-elastic and hysteretic dampers for seismic damage control. *Journal of Constructional Steel Research, 117*, 185-195. doi:https://doi.org/10.1016/j.jcsr.2015.10.016

Bartera, F., & Giacchetti, R. (2004). Steel dissipating braces for upgrading existing building frames. *Journal of Constructional Steel Research*, *60*(3-5), 751-769.

Bartera, F., Dezi, L., & Giacchetti, R. (2004). Cyclic behaviour of a reinforced concrete braced frame with high damping rubber devices. *WIT Transactions on The Built Environment*, *73*.

Bergman, D. M., & Goel, S. C. (1987). Evaluation of cyclic testing of steel plate device for added damping and stiffness. Report no. UMCE 87-10, The University of Michigan. *Ann Arbor, MI*.

Bergström, J. S., & Boyce, M. C. (1998). Constitutive modeling of the large strain time-dependent behavior of elastomers. Journal of the Mechanics and Physics of Solids, 46(5), 931-954.

Bergström, J. S., & Boyce, M. C. (2000). Large strain time-dependent behavior of filled elastomers. Mechanics of materials, 32(11), 627-644.

Bergström, J. S., & Boyce, M. C. (2001). Constitutive modeling of the time-dependent and cyclic loading of elastomers and application to soft biological tissues. Mechanics of materials, 33(9), 523-530.

Cardone, D., & Dolce, M. (2009). SMA-based tension control block for metallic tendons. *International Journal of Mechanical Sciences, 51*(2), 159-165. doi:https://doi.org/10.1016/j.ijmecsci.2008.12.002

CEN, E. (2005). 1-1-Eurocode 3: Design of steel structures-Part 1-1: General rules and rules for buildings. European Committee for Standardization, Brussels.

Chan, R. W. K., & Albermani, F. (2008). Experimental study of steel slit damper for passive energy dissipation. *Engineering Structures, 30*(4), 1058-1066. doi:https://doi.org/10.1016/j.engstruct.2007.07.005

Chang, K. C., & Lin, Y. Y. (2004). Seismic response of full-scale structure with added viscoelastic dampers. *Journal of Structural Engineering*, *130*(4), 600-608.

Chang, K. C., Chen, S. J., & Lai, M. L. (1996). Inelastic behavior of steel frames with added viscoelastic dampers. *Journal of Structural Engineering*, *122*(10), 1178-1186.

Chang, K. C., Lai, M. L., Soong, T. T., Hao, D. S., & Yeh, Y. C. (1993). Seismic behavior and design guidelines for steel frame structures with added viscoelastic dampers.

Chang, K. C., Soong, T. T., Oh, S. T., & Lai, M. L. (1995). Seismic behavior of steel frame with added viscoelastic dampers. *Journal of structural engineering*, *121*(10), 1418-1426.

Chen, W.-F., & Scawthorn, C. (2003). Earthquake Engineering Handbook. CRC Press LLC.

Cheng, F. Y., Jiang, H., & Lou, K. (2008). *Smart structures: innovative systems for seismic response control*. CRC press.

Chowdhury, M. A., Rahmzadeh, A., Moradi, S., & Alam, M. S. (2017). Cyclic behavior of post tensioned steel beam column connections with reduced length strands. In *CSCE 6th international conference on engineering mechanics and materials*.

Chowdhury, M. A., Rahmzadeh, A., Moradi, S., & Alam, M. S. (2019). Feasibility of using reduced length superelastic shape memory alloy strands in post-tensioned steel beam–column connections. *Journal of Intelligent Material Systems and Structures*, *30*(2), 283-307.

Christenson, R. E., & Spencer, B. F. (2001). *Semiactive control of civil structures for natural hazard mitigation: analytical and experimental studies* (Doctoral dissertation, directed by B. F. Spencer, Jr. for the Department of Civil Engineering and Geological Sciences.University of Notre Dame).

Christenson, R. E., & Spencer, B. F. (2001). *Semiactive control of civil structures for natural hazard mitigation: analytical and experimental studies* (Doctoral dissertation, directed by B. F. Spencer, Jr. for the Department of Civil Engineering and Geological Sciences.University of Notre Dame).

Ciampi, V. (1995). Research and development of passive energy dissipation techniques for civil buildings in Italy. In *International Post—SMIRT Conference Seminar on Seismic Isolation, Passiver Energy Dissipation and Control of Vibration of Structures* (pp. 1-15).

Ciampi, V., & Ferretti, A. S. (1990). Energy dissipation in buildings using special bracing systems. In *Proceedings of the 10th International Earthquake Conference*.

Ciampi, V., Arcangeli, M., & Perno, S. (1993). Characterization of the low-cycle fatigue life of a class of energy dissipating devices. *Structural Dynamic—Eurodyn'93*, 137-144.

Constantinou, M. C., Soong, T. T., & Dargush, G. F. (1998). Passive energy dissipation systems for structural design and retrofit.

Construction, A. (2002). Seismic provisions for structural steel buildings. American Institute of Steel Construction.

Costello, G. A. (1997). Theory of wire rope. Springer Science & Business Media.

Cruz Cháidez, S. T. D. L. (2003). *Contribution to the assessment of the efficiency of friction dissipators for seismic protection of buildings*. Universitat Politècnica de Catalunya.

Deng, K., Pan, P., Li, W., & Xue, Y. (2015). Development of a buckling restrained shear panel damper. *Journal of Constructional Steel Research*, *106*, 311-321.

Deng, K., Pan, P., Nie, X., Xu, X., Feng, P., & Ye, L. (2015). Study of GFRP steel buckling restraint braces. *Journal of Composites for Construction*, *19*(6), 04015009.

Deng, K., Pan, P., Sun, J., Liu, J., & Xue, Y. (2014). Shape optimization design of steel shear panel dampers. *Journal of Constructional Steel Research*, *99*, 187-193.

Derham, C. J., Kelly, J. M., & Thomas, A. G. (1985). Nonlinear natural rubber bearings for seismic isolation. *Nuclear Engineering and Design*, *84*(3), 417-428.

Derham, C. J., Kelly, J. M., & Thomas, A. G. (1985). Nonlinear natural rubber bearings for seismic isolation. Nuclear Engineering and Design, 84(3), 417-428.

Dicleli, M., & Mehta, A. (2007). Efficient energy dissipating steel-braced frame to resist seismic loads. *Journal of Structural Engineering*, *133*(7), 969-981.

Dolce, M., & Cardone, D. (2001). Mechanical behaviour of shape memory alloys for seismic applications 2. Austenite NiTi wires subjected to tension. *International journal of mechanical sciences*, *43*(11), 2657-2677.

Dong, H., Du, X., & Han, Q. (2019). Seismic responses of steel frame structures with self-centering energy dissipation braced on shape memory alloy cables. *Advances in Structural Engineering*, 1369433219834752.

Donnet, J. B. (Ed.). (1993). Carbon black: science and technology. CRC Press.

Fang, C., Zheng, Y., Chen, J., Yam, M. C., & Wang, W. (2019). Superelastic NiTi SMA cables: Thermal-mechanical behavior, hysteretic modelling and seismic application. *Engineering Structures*, *183*, 533-549.

Filiatrault, A., & Cherry, S. (1987). Performance Evaluation of Friction Damped Braced Steel Frames Under Simulated Earthquake Loads. *Earthquake Spectra, 3*(1), 57-78. doi:10.1193/1.1585419

Filiatrault, A., & Cherry, S. (1989). Efficient numerical modelling for the design of friction damped braced steel plane frames. *Canadian Journal of Civil Engineering, 16*(3), 211-218. doi:10.1139/l89-046

Filiatrault, A., Tremblay, R., & Wanitkorkul, A. (2001). Performance Evaluation of Passive Damping Systems for the Seismic Retrofit of Steel Moment-Resisting Frames Subjected to Near-Field Ground Motions. *Earthquake Spectra, 17*(3), 427-456. doi:10.1193/1.1586183

Franklin Y Cheng, Hongping Jiang, and Kangyu Lou. Smart structures: innovative systems for seismic response control. CRC Press, 2010.

Freakley, P. K., & Payne, A. R. (1978). Theory and practice of engineering with rubber. Applied Science Publishers.

Fuller, K. N. G. (1996b). High damping natural rubber seismic bearings: longevity and modelling. In *Proc. ASME PVP Conf.*(Vol. 341, p. 71).

Fuller, K., Gough, J., & Pond, T. (1996a). High damping natural rubber compounds for seismic isolators: Properties and specifications. In *1st European conference on structural control*(p. 288).

Gemme, M. C. (2009). *Seismic retrofitting of deficient Canadian buildings* (Doctoral dissertation, Massachusetts Institute of Technology).

Gent, A. N. (2012). Engineering with rubber: how to design rubber components. Carl Hanser Verlag GmbH Co KG.

Gupta, A., & Krawinkler, H. (1998). Seismic demands for the performance evaluation of steel moment resisting frame structures (Doctoral dissertation, Stanford University).

Han, Q., Jia, J., Xu, Z., Bai, Y., & Song, N. (2014). Experimental evaluation of hysteretic behavior of rhombic steel plate dampers. *Advances in Mechanical Engineering*, *6*, 185629.

Higgins, C. P. (2001). Hysteretic dampers for wood frame shear walls. *Structures 2001- A Structural Engineering Odyssey*.

Higgins, C., & Kasai, K. (1998). Experimental and analytical simulation of wind response for a full-scale VE-damped steel frame. *Journal of Wind Engineering and Industrial Aerodynamics*, *77*, 297-313.

Hou, X., & Tagawa, H. (2009). Displacement-restraint bracing for seismic retrofit of steel moment frames. *Journal of Constructional Steel Research*, *65*(5), 1096-1104.

Ibrahim, Y. E., Marshall, J., & Charney, F. A. (2007). A visco-plastic device for seismic protection of structures. *Journal of Constructional Steel Research*, *63*(11), 1515-1528.

Ikeda, Y. (2009). Active and semi-active vibration control of buildings in Japan—Practical applications and verification. Structural Control and Health Monitoring: The Official Journal of the International Association for Structural Control and Monitoring and of the European Association for the Control of Structures, 16(7-8), 703-723.

Inoue, K., Chang, P., Mine, T., Hukuyama, K., & Inoue, K. (1993). Stiffening design of the precast concrete panels to prevent the steel flat braces from buckling. *Annual technical papers of steel structures*, *1*, 195-202.

Isoda, K., Mase, S., Terada, T., & Satake, N. (2001). Development of unbonded brace damper restrained by channel section steel. In *Summaries of technical papers of annual meeting* (Vol. 3, pp. 663-8).

JACSON, C. (1972). 55-Nitinol-the alloy with a memory: its physical metallurgy, properties and applications. *NASA-SP-5110*, *15*.

Judd, J. P., & Charney, F. A. (2016). Seismic collapse prevention system for steel-frame buildings. *Journal of Constructional Steel Research*, *118*, 60-75.

Kamiya, M., Simokawa, H., Morino, S., Kawaguchi, J., Manabe, N., & Itoh, S. (1997). Elasto-plastic behavior of flat-bar brace stiffened by square steel tube. In *Summaries of Technical Papers of Annual Meeting, AIJ* (pp. 789-792).

Kareem, A., Kijewski, T., & Tamura, Y. (1999). Mitigation of motions of tall buildings with specific examples of recent applications. *Wind and structures*, *2*(3), 201-251.

Kelly, J. M. (1997). Earthquake-resistant design with rubber Springer.

Kelly, J. M. (1999). Analysis of fiber-reinforced elastomeric isolators. *Journal of Seismology and Earthquake Engineering*, *2*(1), 19-34.

Kelly, J. M., & Takhirov, S. M. (2001). Analytical and experimental study of fiber-reinforced elastomeric isolators. PEER Report 2001/11, Pacific Earthquake Engineering Research Center. *University of California, Berkeley, Calif*.

Khodaverdian, A., Ghorbani-Tanha, A. K., & Rahimian, M. (2012). An innovative base isolation system with Ni–Ti alloy and its application in seismic vibration control of Izadkhast Bridge. *Journal of Intelligent Material Systems and Structures*, *23*(8), 897-908.

Kim, J., & Shin, H. (2017). Seismic loss assessment of a structure retrofitted with slit-friction hybrid dampers. Engineering Structures, 130, 336-350.

Kim, J., Ryu, J., & Chung, L. (2006). Seismic performance of structures connected by viscoelastic dampers. *Engineering Structures, 28*(2), 183-195. doi:https://doi.org/10.1016/j.engstruct.2005.05.014

Koetaka, Y., Chusilp, P., Zhang, Z., Ando, M., Suita, K., Inoue, K., & Uno, N. (2005). Mechanical property of beam-to-column moment connection with hysteretic dampers for column weak axis. *Engineering structures*, *27*(1), 109-117.

Koh, C. G., & Kelly, J. M. (1988). A simple mechanical model for elastomeric bearings used in base isolation. *International journal of mechanical sciences*, *30*(12), 933-943.

Kruep, S.J. (2007) Using incremental dynamic analysis to visualize the effects of viscous fluid dampers on steel moment frame drift.

Kuwahara, S., Tada, M., Yoneyama, T., & Imai, K. (1993). Study on stiffening capacity of double-tube members. Niju kokan no hogo seino ni kansuru kenkyu.

Lafortune, P., McCormick, J., DesRoches, R., & Terriault, P. (2007). Testing of Superelastic Recentering Pre-Strained Braces for Seismic Resistant Design. *Journal of Earthquake Engineering, 11*(3), 383-399. doi:10.1080/13632460601031326

Lai, M. L., Chang, K. C., Soong, T. T., Hao, D. S., & Yeh, Y. C. (1995). Full-scale viscoelastically damped steel frame. *Journal of Structural Engineering*, *121*(10), 1443-1447.

Leblouba, M. (2007, October). Combined systems for seismic protection of buildings. In *International Symposium on Strong Vrancea Earthquakes and Risk Mitigation* (pp. 363-373). Oct.

Lee, J., Kang, H., & Kim, J. (2017). Seismic performance of steel plate slit-friction hybrid dampers. *Journal of Constructional Steel Research*, *136*, 128-139.

Lee, K. S., Sause, R., Ricles, J., Ab-Malek, K., & Lu, L. W. (2004). Non-linear rate-dependent hysteresis model for structural dampers made from ultra-high damping natural rubber. *Journal of Rubber Research*, *7*(2), 79-103.

Li, H. N., & Li, G. (2007). Experimental study of structure with “dual function” metallic dampers. *Engineering Structures*, *29*(8), 1917-1928.

Lin, T. K., Chang, K. C., Chang, C. Y., and Chen, C. H. (2006). "Application of Viscoelastic Dampers in a Multi-Purpose Vibration Prevention System." 8th US National Conference on Earthquake Engineering, Earthquake Engineering Research Institute, San Francisco, CA.

Love, J. S., Tait, M. J., & Toopchi-Nezhad, H. (2011). A hybrid structural control system using a tuned liquid damper to reduce the wind induced motion of a base isolated structure. *Engineering Structures*, *33*(3), 738-746.

Lu, H., Han, L. H., & Zhao, X. L. (2009). Analytical behavior of circular concrete-filled thin-walled steel tubes subjected to bending. Thin-Walled Structures, 47(3), 346-358.

M. S. Speicher, “Cyclic Testing and Assessment of Shape Memory Alloy Recentering Systems.”

Makris, N. (1997). “Vibration control of structures during urban earthquakes.” Proc., American Control Conference, AACC, Albuquerque, NM, 3957-3961.

Maleki, S., & Mahjoubi, S. (2013). Dual-pipe damper. *Journal of Constructional Steel Research*, *85*, 81-91.

Marshall, J. D. (2008). *Development, analysis and testing of a hybrid passive control device for seismic protection of framed structures* (Doctoral dissertation, Virginia Tech).

Marshall, J. D., & Charney, F. A. (2010). A hybrid passive control device for steel structures, I: Development and analysis. *Journal of Constructional Steel Research*, *66*(10), 1278-1286.

Martinez-Romero, E. (1993). Experiences on the use of supplementary energy dissipators on building structures. *Earthquake spectra*, *9*(3), 581-625.

Mase, S., & Yabe, Y. (1995). Elasto-plastic damper using unbonded brace of low yield-point steel (part 2 low cyclefatigue test). In *Summaries of technical papers of annual meeting* (Vol. 3, pp. 409-10).

McCormick, J., Tyber, J., DesRoches, R., Gall, K., & Maier, H. J. (2007). Structural engineering with NiTi. II: mechanical behavior and scaling. *Journal of Engineering Mechanics*, *133*(9), 1019-1029.

Min, K.-W., Kim, J., and Lee, S.-H. (2004). "Vibration Tests of 5-Storey Steel Frame with Viscoelastic Dampers." Engineering Structures, 26(6), 831-839.

Ming-Hsiang, S., Wen-pei, S., & Cheer-Germ, G. O. (2004). Investigation of newly developed added damping and stiffness device with low yield strength steel. *Journal of Zhejiang University-SCIENCE A*, *5*(3), 326-334.

Miyamoto, H. K., Determan, L., Gilani, A., & Hanson, R. (2003). Seismic rehabilitation of historic concrete structure with fluid viscoelastic dampers. In Proc of 72nd Annual Structural Engineers Association of California Convention.

Moliner, E., Museros, P., & Martínez-Rodrigo, M. D. (2012). Retrofit of existing railway bridges of short to medium spans for high-speed traffic using viscoelastic dampers. *Engineering Structures*, *40*, 519-528.

Montgomery, M. 2011. "Fork configuration dampers (FCDs) for enhanced dynamic performance of high-rise buildings." Ph.D. dissertation, Dept. of Civil Engineering, Univ. of Toronto.

Moon, B. Y., Kang, G. J., Kang, B. S., & Kelly, J. M. (2002). Design and manufacturing of fiber reinforced elastomeric isolator for seismic isolation. *Journal of Materials Processing Technology*, *130*, 145-150.

Mordini, A., & Strauss, A. (2008). An innovative earthquake isolation system using fibre reinforced rubber bearings. *Engineering Structures*, *30*(10), 2739-2751.

Motamedi, M., & Nateghi-A, F. (2018). Study on mechanical characteristics of accordion metallic damper. *Journal of Constructional Steel Research*, *142*, 68-77.

Muhr, A. H. (2005). Modeling the stress-strain behavior of rubber. Rubber chemistry and technology, 78(3), 391-425.

Mullins, L. (1969). Softening of rubber by deformation. Rubber chemistry and technology, 42(1), 339-362.

Myslimaj, B., Midorikawa, M., Iiba, M., & Ikenaga, M. (2002). Seismic behavior of a newly developed base isolation system for houses. *Journal of Asian Architecture and Building Engineering*, *1*(2), 2_17-24.

Naderzadeh, A. (2009). Application of seismic base isolation technology in Iran. *Menshin*, (63), 40-47.

Naeim, F, Kelly, JM. Design of Seismic Isolated Structures - From Theory to Practice. John Wiley and Sons, New York, 1999.

Naeim, F., & Kelly, J. M. (1999). *Design of seismic isolated structures: from theory to practice*. John Wiley & Sons.

Nagao, T., Mikuriya, K., Matsumoto, Y., & Takahashi, S. (1988). An experimental study on the elastoplastic behavior of unbonded composite bracing (part 1–4). In *Summaries of technical papers of annual meeting* (Vol. 2, pp. 1329-26).

Narihara, H., Tsujita, O., & Koeteka, Y. (2000). The experimental study on buckling restrained braces (Part 1: Experiment on pin connection type). In *Summaries of technical papers of annual meeting* (Vol. 9, pp. 911-912). Tokyo: Architectural Institute of Japan.

Nashif, A. D., Jones, D. I., & Henderson, J. P. (1985). Vibration damping. John Wiley & Sons.

Nateghi-E, F., Motamedi, M., & Izadi-Z, E. (2008). Experimental behavior of the seismic filled accordion metallic dampers, famd. In *14th World Conference on Earthquake Engineering. Beijing, China, Paper* (No. 2264).

Nguyen, Q. H., Choi, S. B., & Park, Y. G. (2012). An analytical approach to optimally design of electrorheological fluid damper for vehicle suspension system. Meccanica, 47(7), 1633-1647.

Otsuka, K., & Wayman, C. M. (1998). Shape Memory Materials, Cambridge Uni. *Press, New York*.

Palacios Quiñonero, F., Rossell Garriga, J. M., Rodellar Benedé, J., & Pons López, R. (2010). Passive-active vibration control for connected multi-building structures. In *Proceedings of the 8th International Conference on Structural Dynamics, EURODYN 2011: Leuven, Belgium, 4-6 July 2011* (pp. 1931-1938).

Pall, A. (2004, August). Performance-based design using pall friction dampers-an economical design solution. In 13th World Conference on Earthquake Engineering, Vancouver, BC, Canada (Vol. 70, pp. 576-571).

Pall, A. S. and Marsh, C., (1982). "Response of Friction Damped Braced Frames," Journal of Structural Engineering, 108(ST6), 1313-1323

Pall, A. S., & Pall, R. (1996, June). Friction-dampers for seismic control of buildings–a Canadian experience. In Eleventh World Conference on Earthquake Engineering, Acapulco, Mexico.

Perry, C. L., Fierro, E. A., Sedarat, H., & Scholl, R. E. (1993). Seismic upgrade in San Francisco using energy dissipation devices. *Earthquake Spectra*, *9*(3), 559-579.

Phocas, M. C., & Pocanschi, A. (2003). Steel frames with bracing mechanism and hysteretic dampers. *Earthquake engineering & structural dynamics*, *32*(5), 811-825.

Pimiento, J., Salas, A., & Ruiz, D. (2015). Seismic performance of frames with passive energy dissipation steel slit plates. Revista Ingeniería de Construcción, 29(3), 283-298.

Prestandard, F. E. M. A. (2000). commentary for the seismic rehabilitation of buildings (FEMA356). Washington, DC: Federal Emergency Management Agency, 7.

Raut, S. N., Majumder, R., Jain, A., & Mehta, V. (2019). Analysis of the Behavior of High-Rise Structures with Viscoelastic Dampers Installed at Various Locations. In *Innovations in Infrastructure* (pp. 183-194). Springer, Singapore.

Renzi, E., Perno, S., Pantanella, S., & Ciampi, V. (2007). Design, test and analysis of a light-weight dissipative bracing system for seismic protection of structures. *Earthquake engineering & structural dynamics*, *36*(4), 519-539.

Roh, J. E., Hur, M. W., Choi, H. H., & Lee, S. H. (2018). Development of a multiaction hybrid damper for passive energy dissipation. *Shock and Vibration*, *2018*.

Sabelli, R. (2001). *Research on improving the design and analysis of earthquake-resistant steel-braced frames* (Vol. 12). Oakland: EERI.

Sahoo, D. R., Singhal, T., Taraithia, S. S., & Saini, A. (2015). Cyclic behavior of shear-and-flexural yielding metallic dampers. *Journal of Constructional Steel Research*, *114*, 247-257.

Sarno, L. D., & Elnashai, A. S. (2003). Special metals for seismic retrofitting of steel buildings. *Progress in Structural Engineering and Materials*, *5*(2), 60-76.

Sause, R., Lee, K. S., Ricles, J., Ab-Malek, K., & Lu, L. W. (2001). Non-linear hysteresis models for ultra-high damping NR structural dampers. *Journal of Rubber Research*, *4*(4), 222-244.

Sepúlveda, J., Boroschek, R., Herrera, R., Moroni, O., & Sarrazin, M. (2008). Steel beam–column connection using copper-based shape memory alloy dampers. *Journal of Constructional Steel Research*, *64*(4), 429-435.

Shen, K. L., Soong, T. T., Chang, K. C., & Lai, M. L. (1995). Seismic behaviour of reinforced concrete frame with added viscoelastic dampers. *Engineering Structures*, *17*(5), 372-380.

Shimizu, T., Fujisawa, K., Uemura, K., & Inoue, K. (1997). Design method to prevent buckling of low yield strength steel tube brace and fracturing of joints (Part 1: design method and test plan of braced braces). In *Summaries of Technical Papers of Annual Meeting, Architectural Institute of Japan* (Vol. 9, pp. 781-782).

Silwal, B., Michael, R. J., & Ozbulut, O. E. (2015). A superelastic viscous damper for enhanced seismic performance of steel moment frames. *Engineering Structures*, *105*, 152-164.

Spencer Jr, B. F., & Nagarajaiah, S. (2003). State of the art of structural control. *Journal of structural engineering*, *129*(7), 845-856.

Spencer Jr, B. F., Dyke, S. J., & Deoskar, H. S. (1997). Benchmark problem in structural control. In Proceeding of the ASCE Structural Congress XV (Vol. 2, pp. 1265-1269).

STANDARD, B. (1995). Physical Testing of Rubber: Method for Determination of Tensile Stress Properties.

Suzuki, N., Kono, R., Higasibata, Y., Sasaki, T., & Segawa, T. (1994). Experimental study on the H-section steel brace encased in RC or steel tube. In *Summaries of technical papers of annual meeting* (pp. 1621-1622).

Symans, M. D., & Constantinou, M. C. (1999). Semi-active control systems for seismic protection of structures: a state-of-the-art review. *Engineering structures*, *21*(6), 469-487.

Symans, M. D., Charney, F. A., Whittaker, A. S., Constantinou, M. C., Kircher, C. A., Johnson, M. W., & McNamara, R. J. (2008). Energy dissipation systems for seismic applications: current practice and recent developments. Journal of structural engineering, 134(1), 3-21.

Symans, M. D., Charney, F. A., Whittaker, A. S., Constantinou, M. C., Kircher, C. A., Johnson, M. W., & McNamara, R. J. (2008). Energy dissipation systems for seismic applications: current practice and recent developments. *Journal of structural engineering*, *134*(1), 3-21.

Symans, M. D., Cofer, W. F., & Fridley, K. J. (2002). Base isolation and supplemental damping systems for seismic protection of wood structures: Literature review. *Earthquake Spectra*, *18*(3), 549-572.

Tagawa, H., Yamanishi, T., Takaki, A., & Chan, R. W. (2016). Cyclic behavior of seesaw energy dissipation system with steel slit dampers. *Journal of Constructional Steel Research*, *117*, 24-34.

Tan, X. M., Ko, J. M., Fang, E. H., & Qian, J. R. (1997). Vibration control with viscoelastic dampers in a high-rise building. In *Proceedings of the 15th International Modal Analysis Conference* (Vol. 3089, p. 935).

Tehranizadeh, M. (2001). Passive energy dissipation device for typical steel frame building in Iran. *Engineering Structures*, *23*(6), 643-655.

TENA-COLUNGA, A. R. T. U. R. O., & VERGARA, A. (1997). Comparative study on the seismic retrofit of a mid-rise steel building: steel bracing vs energy dissipation. *Earthquake engineering & structural dynamics*, *26*(6), 637-655.

Toopchi-Nezhad, H., Tait, M. J., & Drysdale, R. G. (2008, October). A novel elastomeric base isolation system for seismic mitigation of low-rise buildings. In *Proceedings of the 14th world conference on earthquake engineering. Beijing* (pp. 12-18).

Toopchi-Nezhad, H., Tait, M., & Drysdale, R. G. (2007b). Experimental study on carbon fiber-reinforced square seismic isolators. *Ninth Canadian Conference on Earthquake Engineering*, (pp. 26-29). Ottawa, Ontario, Canada.

Towashiraporn, P., Park, J., Goodno, B. J., & Craig, J. I. (2002). Passive control methods for seismic response modification. *Progress in Structural Engineering and Materials*, *4*(1), 74-86.

Treloar, L. R. G. (1975). *The physics of rubber elasticity*. Oxford University Press, USA.

Tsai, C. S., & Lee, H. H. (1993). Applications of viscoelastic dampers to high-rise buildings. *Journal of structural engineering*, *119*(4), 1222-1233.

Tsai, C. S., & Tsai, K. C. (1995). TPEA device as seismic damper for high-rise buildings. *Journal of engineering mechanics*, *121*(10), 1075-1081.

Tsai, C. S., Lee, G. H., Chen, W. S., & Hsu, L. T. (2005, January). Experimental Tests of Longitudinal Added Damping and Stiffness Device. In *ASME 2005 Pressure Vessels and Piping Conference* (pp. 101-107). American Society of Mechanical Engineers.

Tsai, C. S., Wei, T. T., & Chen, W. S. (2003, January). Experimental Study for Highly Plastic Material Damper. In *ASME 2003 Pressure Vessels and Piping Conference* (pp. 97-102). American Society of Mechanical Engineers.

Tsai, K. C., & Huang, Y. C. (2002). Experimental responses of large scale BRB frames. *Center for Earthquake Engineering Research*.

Tsai, K. C., Chen, H. W., Hong, C. P., and Su, Y. F. (1993). "Design of Steel Triangular Plate Energy Absorbers for Seismic-Resistant Construction." Earthquake Spectra, 9(3), 505-528.

Tyber, J., McCormick, J., Gall, K., DesRoches, R., Maier, H. J., & Abdel Maksoud, A. E. (2007). Structural engineering with NiTi. I: basic materials characterization. *Journal of Engineering Mechanics*, *133*(9), 1009-1018.

Tyler, R. G. (1985). Further notes on a steel energy-absorbing element for braced frameworks. *Bulletin of the New Zealand National Society for Earthquake Engineering*, *18*(3), 270-279.

Uang, C. M., & Bertero, V. V. (1988). *Use of energy as a design criterion in earthquake-resistant design* (Vol. 88, No. 18). Berkeley, California: Earthquake Engineering Research Center, University of California.

Usami, T., & Kaneko, H. (2001). Strength of H-shaped brace constrained flexural buckling having unconstrained area at both ends. Both ends simply supported. *Journal of Structural and Construction Engineering*, (542), 171-177.

Vatanshenas, A., Rohanimanesh, M. S., & Mohammadiha, E. (2018). Ivestigating the Performance of Viscoelastic Dampers (VED) Under Nearfield Earthquakes with Directivity Feature. *Civil and Environmental Engineering*, *14*(1), 21-27.

Verma, R. K., P. N. Dubey, and G. R. Reddy. "Determination of Effectiveness of Viscoelastic Dampers in Controlling the Seismic Response of Piping System by Shake Table Testing." *Advances in Structural Integrity*. Springer, Singapore, 2018. 493-501.

Vincent, J. (2012). Structural biomaterials. Princeton University Press.

Roland, C. M. (2011). Viscoelastic behavior of rubbery materials. OUP Oxford.

Wakabayashi, M., Nakamura, T., Katagihara, A., Yogoyama, H., & Morisono, T. (1973). Experimental study on the elastoplastic behavior of braces enclosed by precast concrete panels under horizontal cyclic loading—Parts 1 & 2. In *Summaries of technical papers of annual meeting* (Vol. 6, pp. 121-128). Architectural Institute of Japan.

Wang, B., Zhu, S., Qiu, C. X., & Jin, H. (2019). High-performance self-centering steel columns with shape memory alloy bolts: Design procedure and experimental evaluation. *Engineering Structures*, *182*, 446-458.

Wang, G., Wang, Y., Yuan, J., Yang, Y., & Wang, D. (2017). Modeling and experimental investigation of a novel arc-surfaced frictional damper. *Journal of Sound and Vibration, 389*, 89-100. doi:https://doi.org/10.1016/j.jsv.2016.11.019

Watanabe, A., Hitomi, Y., Saeki, E., Wada, A., & Fujimoto, M. (1988, August). Properties of brace encased in buckling-restraining concrete and steel tube. In *Proceedings of ninth world conference on earthquake engineering* (Vol. 4, pp. 719-724).

Weinert, K., & Petzoldt, V. (2004). Machining of NiTi based shape memory alloys. *Materials Science and Engineering: A*, *378*(1-2), 180-184.

Welch, P. (1967). The use of fast Fourier transform for the estimation of power spectra: a method based on time averaging over short, modified periodograms. IEEE Transactions on audio and electroacoustics, 15(2), 70-73.

Whittaker, A. S., Bertero, V. V., Thompson, C. L., and Alonso, L. J. (1991). "Seismic Testing of Steel Plate Energy Dissipation Devices." Earthquake Spectra, 7(4), 563-604.

Wu, B., Ou, J. P., & Soong, T. T. (1997). Optimal placement of energy dissipation devices for three-dimensional structures. Engineering Structures, 19(2), 113-125.

Wu, B., Zhang, J., Williams, M. S., & Ou, J. (2005). Hysteretic behavior of improved Pall-typed frictional dampers. *Engineering Structures, 27*(8), 1258-1267. doi:https://doi.org/10.1016/j.engstruct.2005.03.010

Xie, Q. (2005). State of the art of buckling-restrained braces in Asia. *Journal of constructional steel research*, *61*(6), 727-748.

Xu, L., Yao, S., & Sun, Y. (2019). Development and validation tests of an assembly self-centering energy dissipation brace. *Soil Dynamics and Earthquake Engineering*, *116*, 120-129.

Xu, Y. L., & Zhang, W. S. (2001). Modal analysis and seismic response of steel frames with connection dampers. *Engineering Structures, 23*(4), 385-396. doi:https://doi.org/10.1016/S0141-0296(00)00062-6

Xu, Z. D. (2007). Earthquake mitigation study on viscoelastic dampers for reinforced concrete structures. Journal of Vibration and Control, 13(1),

Yan, S., Song, G., Huo, L., & Gu, H. (2007). *Seismic response control of frame structure braced with SMA tendons* (Vol. 6529): SPIE.

Yao, J. T. (1972). Concept of structural control. Journal of the Structural Division, 98(st 7).

Yoshino, T., & Karino, Y. (1971). Experimental study on shear wall with braces: Part 2. In *Summaries of technical papers of annual meeting* (Vol. 11, pp. 403-404). Architectural Insti

LIST OF PUBLICATIONS

Mehrabi, M. H., Ibrahim, Z., Ghodsi, S. S., & Suhatril, M. (2019). Seismic characteristics of X-cable braced frames bundled with a pre-compressed spring. *Soil Dynamics and Earthquake Engineering*, *116*, 732-746. (ISI)

Mehrabi, M. H., Suhatril, M., Ibrahim, Z., Ghodsi, S. S., & Khatibi, H. (2017). Modeling of a viscoelastic damper and its application in structural control. PloS one, 12(6), e0176480. (ISI)

Mehrabi, M. H., Ghodsi, S. S., Ibrahim, Z., & Suhatril, M. (2017). Performance of Steel Frame with a Viscoelastic Damper Device under Earthquake Excitation. *World Academy of Science, Engineering and Technology, International Journal of Civil, Environmental, Structural, Construction and Architectural Engineering*, *11*(10), 1372-1375.